Universiteit
Leiden
The Netherlands

Coiled-coil biomaterials for biological applications

Shen, M.

Citation
Shen, M. (2021, November 24). *Coiled-coil biomaterials for biological applications*. Retrieved from https://hdl.handle.net/1887/3243305

Version:	Publisher's Version
License:	Licence agreement concerning inclusion of doctoral thesis in the Institutional Repository of the University of Leiden
Downloaded from:	https://hdl.handle.net/1887/3243305

Note: To cite this publication please use the final published version (if applicable).

Coiled-coil biomaterials for biological applications

Proefschrift

ter verkrijging van
de graad van doctor aan de Universiteit Leiden,
op gezag van rector magnificus prof.dr.ir. H. Bijl,
volgens besluit van het college voor promoties
te verdedigen op woensdag 24 november 2021
klokke 11:15 uur

door

Mengjie Shen

geboren op 14 Juli 1988 te Shandong, P.R.China

Promotiecommissie

Promotor: Prof.dr. A. Kros

Copromotor: Dr. A.L. Boyle

Overige leden:

Prof.dr. H.S. Overkleeft (voorzitter)

Dr. G.F. Schneider (secretaris)

Dr. R.E. Kieltyka

Prof.dr. D. Claessen

Prof.dr. H.A. Santos

Prof.dr. J.N.H. Reek

PhD Thesis, Leiden University, 2021

Title: Coiled-coil biomaterials for biological applications

Cover design and thesis layout: Mengjie Shen

Print: printsupport4u

This thesis was financed by the Chinese Scholarship Council (Grant No.201606360129) and Leiden University.

Life may not be as perfect as you expected, nor as bad as you worried. Your fragile and strengths are beyond your imagination. Sometimes, you could be so vulnerable that even a word could bring tears to your eyes. Sometimes, you may suddenly realize that you have been persistent walking in adversity for such a long distance.

生活可能不像你想象得那么好，但是也不会像你想象得那么糟。人的脆弱和坚强都超乎自己的想象。有时后，可能脆弱得一句话就泪流满面；有时后，你发现自己咬着牙已经走过了很长的路。

Table of contents

Chapter 1

Introduction: Coiled-coil Peptides Based Biomaterials and Membrane Fusion

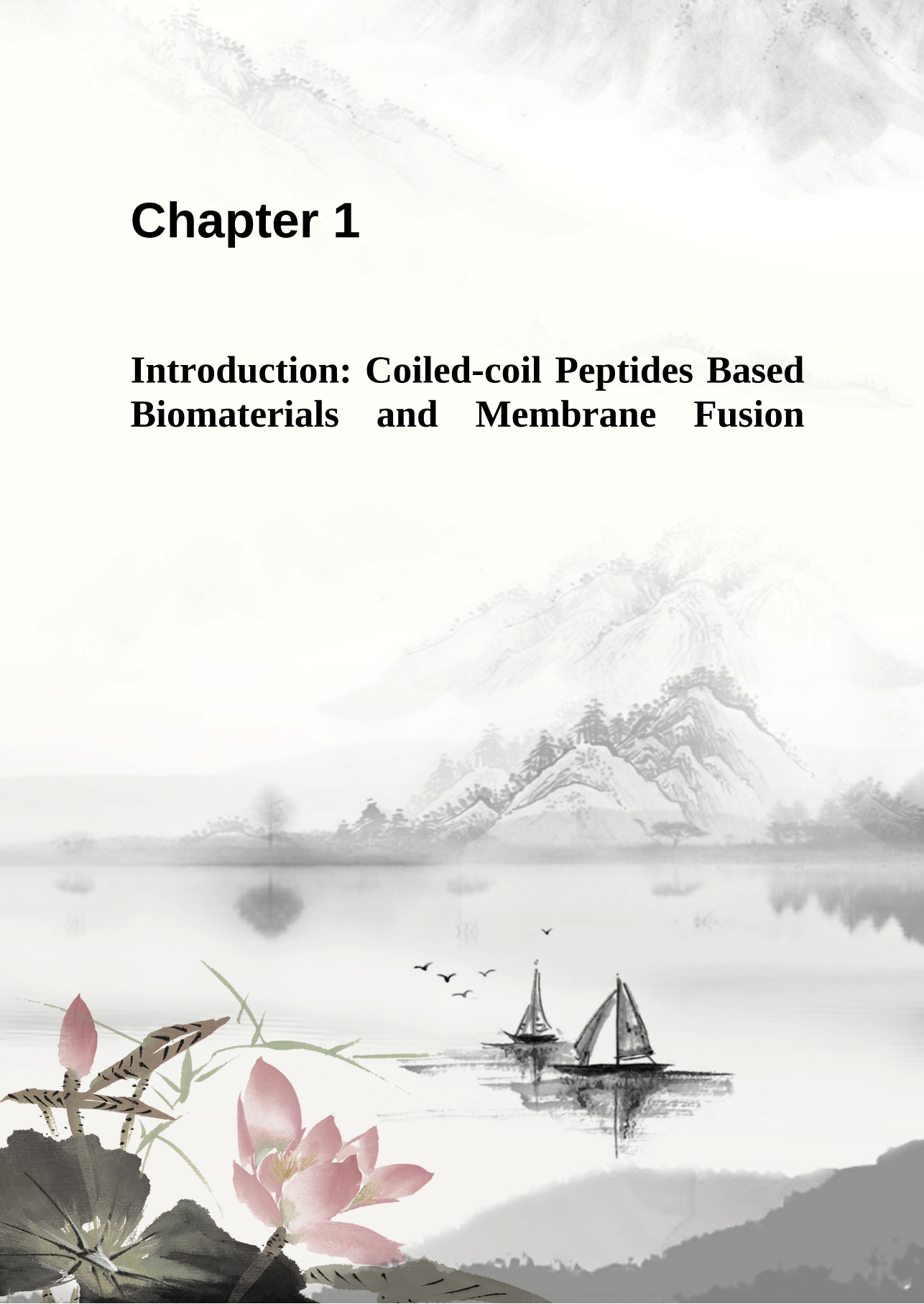

1.1 Coiled-coil peptides

The coiled-coil motif was first named and described by Crick,[1-2] and Linus Pauling,[3] independently in 1953. After more than 60 years of research, the coiled-coil still arouses the interest of many researchers and has become more and more popular, for both fundamental and applied research.[4-5] The coiled-coil is a common structural motif in proteins,[6] with about 3-5% of amino acids in proteins forming such structures.[7] This motif is especially common in a large class of fibrous proteins like tropomyosin,[8-9] myosin,[10-11] intermediate filaments,[12-13] and prokaryotic surface proteins,[14-15] where the coiled-coil has been described as the main structural element.

A coiled-coil contains two or more α-helices which wrap around each other and form a left-handed supercoil. Crick described the structure as having "knobs-into-holes" packing since the α-helices twist, at an angle of around 20°, with respect to each other, which interlocks the side chains of the amino acids on neighbouring peptide chains.[6-7] The reason for this twist is that, in α-helices, each complete turn of a helix usually contains 3.6 residues, while in a coiled-coil there is a lower number of residues in each turn - 3.5. A repeat of seven residues, which is known as a heptad repeat, is common in many coiled coils. In that case, each heptad in a coiled-coil contains two helical turns. This heptad repeat is usually denoted as $\mathbf{(\mathit{abcdefg})_n}$ where each letter represents each position of the coiled-coil and '**n**' is the number of repeats. Heptad repeats can be shown using a helical wheel diagram (Figure 1).

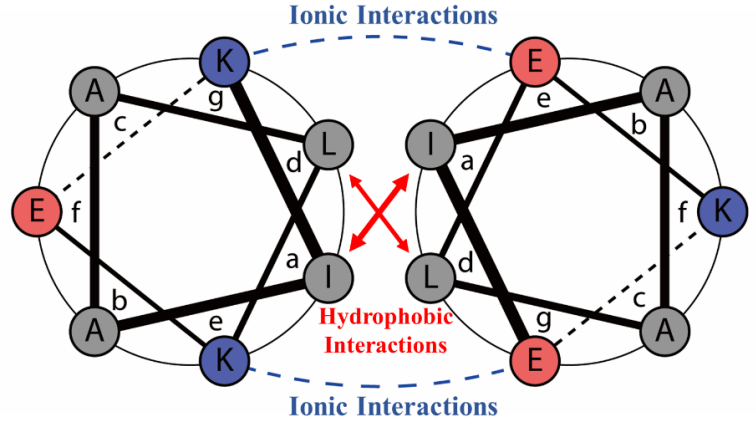

Figure 1. Helical wheel diagram of a parallel heterodimeric coiled-coil.

Figure 1 shows an example of a parallel heterodimeric coiled-coil. In such a structure, positions ***a*** and ***d*** usually contain hydrophobic amino acids, thus forming the non-polar core of the α-helix. Therefore, hydrophobic interactions and van der Waals interactions could induce coiled-coil formation in an aqueous solution. Positions ***e*** and ***g*** normally have amino acids containing complementary charged side chains and then the coiled-coil structure can be stabilized by interhelical electrostatic interactions. Since positions ***b***, ***c*** and ***f*** are exposed to the solvent, hydrophilic amino acids are preferred to increase the solubility of the peptide. Previously, these positions were thought to be less important for defining the properties of the coiled-coil, however, some recent studies have shown that ***b***, ***c*** and ***f*** residues can affect coiled-coil specificity and stability.[16-17]

Most coiled coils, both from nature or developed via artificial design, contain two to four helices and these structures have cyclic or dihedral symmetry. [18] However, coiled coils containing five or more helices have also been reported in numerous studies.[18-21] Figures 2A-2D show helical wheel diagrams of different structures of coiled coils; those with different oligomeric states or orientations.[5] All of these structures present 'knobs-in-holes' interactions (figure 2E & 2F).

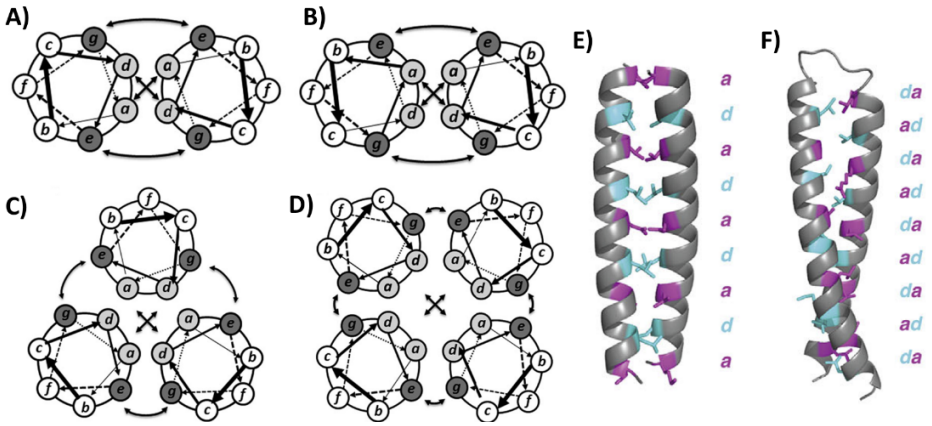

Figure 2. Differently structured coiled-coils: (A) parallel dimeric coiled-coil; (B) antiparallel dimeric coiled-coil; (C) parallel trimeric coiled-coil; (D) parallel tetrameric coiled-coil. The 'knobs-in-holes' arrangement of a parallel coiled-coil (E) and an antiparallel coiled-coil (F). The parallel coiled-coil contains *a* and *d* layers while the antiparallel coiled-coil has mixed *ad* layers in its 'knobs-in-holes' arrangement. Figures are adapted from references.[4-5]

Many structural features can influence the stability of coiled coils.[7, 22] For example, by introducing more hydrophobic residues in the ***a*** and ***d*** **positions,** coiled-coil

stability can be increased. Additionally, the salt bridges between residues in ***g/e'*** positions can also influence the coiled-coil stability. Most importantly, increasing the length of the coiled-coil forming peptides can not only increase the area of the coiled-coil hydrophobic core but will also increase the number of salt bridges. Many studies have shown that increasing the length of the coiled-coil forming peptides is a facile way to increase the stability of coiled coil.[7, 22-25] Therefore, coiled-coil stability can be tuned by changing the length of the coiled-coil peptides.

1.2 Coiled coils for use in biomaterials

Peptide- and protein-based biomaterials have seen rapid development over the last two decades because such biomaterials not only have potential applications in biotechnology but they can also help researchers to learn how natural biomaterials work in biology.[26] Coiled coils have become one of the most attractive building blocks for peptide- and protein-based biomaterials due to their excellent self-assembly properties, in addition to their specific recognition and responsiveness. The coiled-coil building block is widely used in drug delivery, protein purification, protein labeling, nanoparticle self-assembly, biosensing, and hydrogel formation, amongst others (Figure 3).[5]

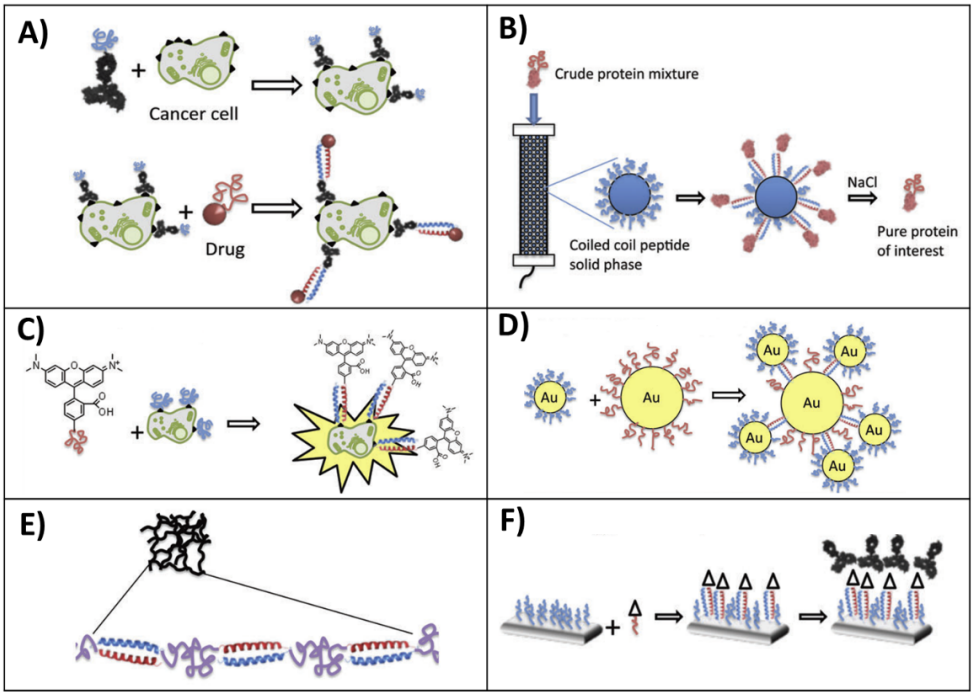

Figure 3. Examples of coiled-coil peptide-based biomaterials: A) drug delivery; B) peptide purification; C) protein labelling; D) nanoparticle self-assembly; E) hydrogel formation, and; F) biosensing. The figure is adapted from reference.[5]

The E/K coiled coil, is a *de novo* designed parallel heterodimeric coiled-coil, developed by Hodges and coworkers.[22, 27-29] The coiled-coil forming peptides that make up this assembly were named peptide E and peptide K, because they are rich in glutamic acid and lysine respectively. This heterodimer, and others which are similar, have become very popular in a multitude of applications because of its stability and specificity. For example, a two-stage drug-free macromolecular therapeutic system has been developed by Wu *et al.*[30] In this work, the coiled-coil forming peptides E and K, were separately modified with the 1F5 anti-CD20 antibody and an HPMA polymer, respectively. The therapeutic process contains two stages. In the first stage, peptide E modified antibodies selectively bind to CD20 on the surface of Raji B cells. Next, coiled coil formation between peptides K and E crosslinks CD20 receptors due to the action of the HPMA copolymer, resulting in apoptosis. In another study, coiled-coil motifs were used to develop a drug delivery system using the pH-sensitive nature of the K_3/E_3 coiled coil.[31] Here, peptides E_3 and K_3 were attached to either a synthetic polymer or a drug/dye. By forming a coiled-coil, a polymer drug conjugate was formed which entered cells

via endocytosis. Next, these drugs could be released from the polymer complex due to the lower pH in endosomes/lysosomes compared to the rest of the cell. The pH change results in the dissociation of the K_3/E_3 coiled coil and concomitant drug release.

The coiled-coil motif has also has been used in various hydrogels.[32-37] Hill and coworkers designed a thermo-responsive hydrogel using coiled-coil domains as physical crosslinks.[32] Due to the reversible self-assembly properties of coiled-coil peptides, the formation and dissociation of the hydrogel can be easily controlled by adjusting the temperature. These hydrogel biomaterials can be used to control small molecule release, which also has potential applications for drug delivery.

1.3 Membrane fusion

Membrane fusion is a fundamental and essential process in life.[38-42] It occurs between cellular plasma membranes, intracellular compartments, cellular membranes and intracellular compartments, and lipid-covered vesicles and cellular membranes.[43] Neurotransmitter release,[44-45] fertilization,[46-47] endocrine hormone secretion,[48-49] and enveloped virus infection[50-51] are examples of biological processes that require membrane fusion. The process of membrane fusion can be described using the fusion-through-hemifusion pathway model, which is shown in Figure 4.[52] This process starts from a pre-fusion contact, (i), in which two lipid membranes are forced close to each other. Because of the energy barrier caused by the hydration repulsion between the proximal leaflets of the membranes, a point-like membrane protrusion state, (ii), is formed which can lower the energy barrier for the transition into the hemifusion stalk state, (iii). The hemifusion stalk state represents the two outer leaflets fused while the inner leaflets are still unfused. The fusion pore can then either directly form from the hemifusion stalk or go through a hemifusion diaphragm state (iv) obtained by hemifusion stalk expansion. After the fusion pore, (v), is formed, complete membrane fusion is achieved. During hemifusion-stalk to fusion pore formation and expansion, high energy barriers exist because of the necessary membrane curvature deformations. Studies have shown that lipid composition influences the curvature of the lipid membrane and assists membrane deformation, thus reducing the energy barrier and facilitating membrane fusion.[53-57] Lipids with short and unsaturated fatty acids can increase the fluidity of the lipid membrane and a higher membrane fluidity has a positive effect on membrane fusion.[58-60] Therefore, the lipid composition is a very important parameter in membrane fusion.

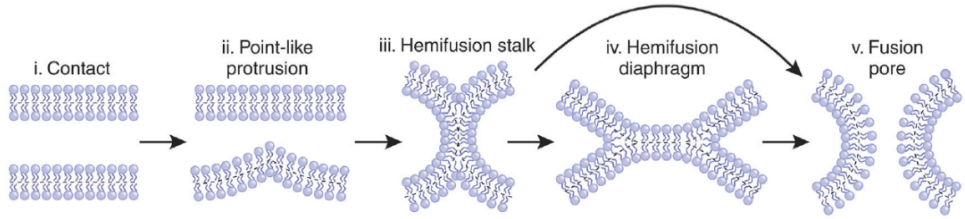

Figure 4. Lipid membrane fusion via the fusion-through-hemifusion pathway. The figure is adapted from reference.[52]

1.4 SNARE assisted membrane fusion

SNARE (soluble N-ethylmaleimide-sensitive factor attachment protein receptors) proteins play a key role in mediating membrane fusion in eukaryotic cells.[61-62] SNARE proteins were first characterized in the late 1980s, and these SNAREs were found to mediate a variety of intracellular trafficking processes.[63-64] For instance, efficient membrane fusion between synaptic vesicles and presynaptic plasma membranes, a process induced by SNARE proteins, allows fast neurotransmitter release and thus efficient synaptic transmission.[44-45, 65] The SNARE complex contains two parts: the transport vesicle SNARE (v-SNARE) and target membrane SNARE (t-SNARE). Usually, the SNARE complex contains one v-SNARE with two or three t-SNAREs. The first identified structure of a SNARE complex in the presynaptic neuron was composed of vesicle-associated membrane protein (VAMP), syntaxin 1 and SNAP-25.[66] VAMP is located on the synaptic vesicle and therefore acts as the v-SNARE while syntaxin and SNAP-25 are located on the presynaptic plasma membrane and are known as t-SNAREs. VAMP and syntaxin contain transmembrane domains (TMD), which anchor them into the lipid membrane, while SNAP-25 is connected to membranes via covalent bonds between palmitoyl side chains of the membrane and multiple cysteine side chains of the protein. Some studies have shown that the TMD of the SNARE proteins within the complex could reduce the energy barrier and facilitate fusion pore formation.[67] By forming a four-helix coiled-coil structure (Figure 5), the v-SNARE and t-SNAREs could interact with each other and bridge two membranes thus facilitating fusion. Other SNARE proteins have similar structures and mediate membrane fusion in quite similar manners.

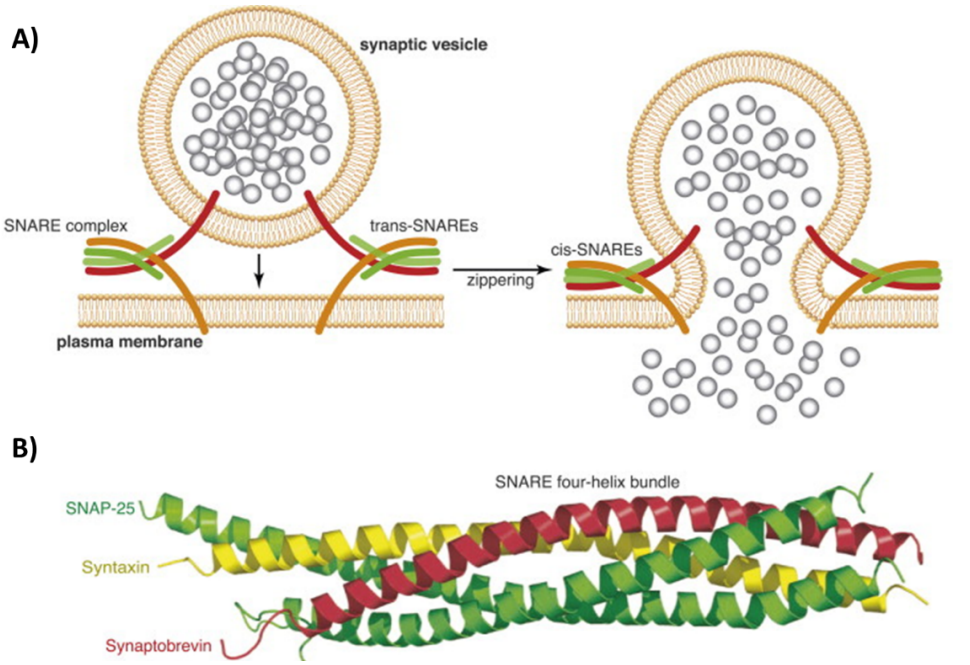

Figure 5. A) Membrane fusion induced by a SNARE complex which contains a tetrameric coiled-coil motif formed by syntaxin, and SNAP-25 on target membrane and synaptobrevin (also known as VAMP) on the synaptic vesicle. The fusion pore is formed by the coiled-coil complex 'zipping up' from the N- to the C-terminus and dragging the two membranes into close proximity. B) The tetramer coiled-coil complex of the SNARE protein. The figure is adapted from reference.[68]

1.5 Membrane fusion triggered by lipid-anchored coiled coils

In our group, we have designed a coiled-coil peptide mediated membrane fusion system inspired by SNARE proteins.[69-70] A lipid anchor was conjugated to the coiled-coil forming peptides K and E by a short poly(ethylene glycol) (PEG) spacer (Figure 6). In one study examining the effect of the lipid anchor, cholesterol was found to be the best anchor as it triggers liposome membrane fusion with the highest efficiency.[71] The spacer length has also been investigated and the results show that short coiled-coil peptides prefer a longer spacer in order to reach each other and form a coiled-coil interaction, while longer coiled-coil peptides do not need such a long spacer.[72] The length of coiled-coil peptides was also found to play an important role in fusogenicity: four heptad coiled coils can trigger both liposome-liposome and cell-liposome membrane fusion while three heptad coiled-coils can only induce liposome-liposome membrane fusion.[71, 73-74] The K/E coiled-coil triggered membrane fusion system was also found to have potential

applications in drug delivery.[74-76]

Mechanistic studies show that the stability of the coiled-coil and the membrane affinity of peptide K are two crucial factors that affect fusogenicity.[77-79] As previously mentioned, several energy barriers exist during the membrane fusion process. A more stable coiled-coil can bind the two separate membranes more tightly and overcome these energy barriers more easily. Furthermore, peptide K interacts with membranes and induces a positive curvature, thereby destabilizing the membrane, lowering the energy barrier for fusion pore formation.[77]

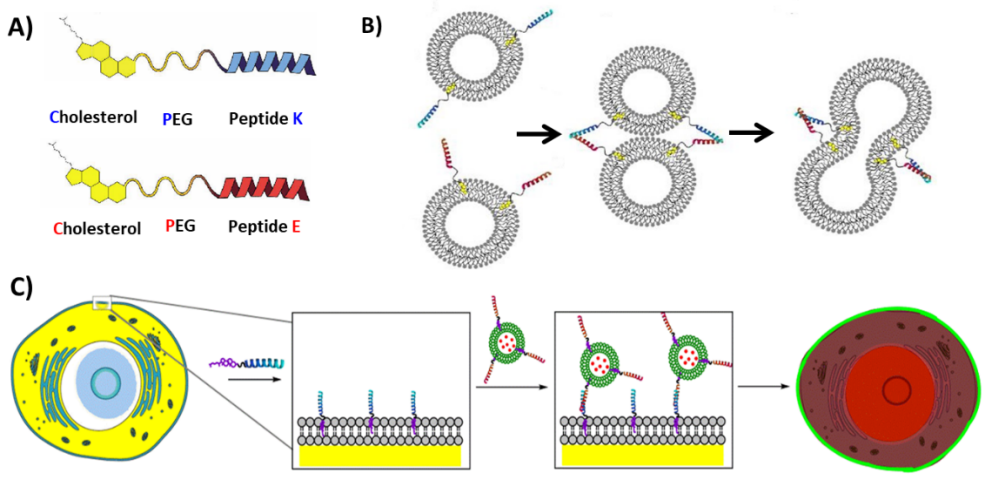

Figure 6. Cartoon pictures illustrating A) the structure of CPK and CPE, B) liposome membrane fusion triggered by CPK and CPE, C) cell-liposome membrane fusion triggered by CPK_4 and CPE_4.

1.6 Aim and outline of this thesis

In this thesis, we used the K/E coiled-coil motifs to facilitate various novel applications.

In **chapter 2**, a magnetic-activated cell sorting (MACS) system based on the K_3/E_3 coiled-coil is described. For this project, iron oxide particles (IOPs) were functionalized with coiled-coil forming peptides and coiled-coil formation on the IOPs surface was demonstrated. Using these coiled-coil forming peptide-functionalized IOPs and an external magnetic field, cell sorting assays were performed with three different cell lines, showing that coiled-coil decorated cells can be separated from non coiled-coil decorated cells. Finally, we will show that cells that express peptide K_3 on the cell membrane can be enriched using this

approach.

In **chapter 3**, we compare the fusogenicity of different coiled-coil pairs formed by different lengths of K and E peptides. Using circular dichroism (CD) spectroscopy and dynamic light scattering (DLS), the secondary structure and stability of the individual K and E peptides, together with their coiled-coil complexes has been studied in order to probe the relationship between coiled-coil length and stability. We subsequently investigated the fusogenicity of these coiled coils by performing lipid-mixing and content-mixing assays using liposomes. After demonstrating their fusogenicity in liposome systems, we prove that all K-lipopeptides can be used to decorate cell membranes, and we subsequently performed liposome-cell docking and evaluated the docking efficiency by flow cytometry. Finally, we selected the coiled-coil pairs which exhibited good liposome-cell docking and used them for cell-liposome membrane fusion studies. These studies showed that liposome-loaded propidium iodide (PI) can be released into cells, and the cell-liposome fusion efficiency can be obtained by comparing the PI fluorescence intensity inside the cells.

The membrane affinity of peptide K is crucial for coiled-coil triggered membrane fusion because it can induce positive curvature of the lipid membrane, which lowers the energetic barrier and thus facilitates fusion pore formation. In **chapter 4**, we describe a membrane fusion system comprising different dimeric K_4 peptides, which interact with E_4 peptides resulting in membrane fusion. The secondary structure of three different K_4 dimers, and their self-assembly with E_4, was investigated. These K_4 dimers form either temperature-dependent aggregates or concentration-dependent homodimers in buffered solutions. Furthermore, all K_4 dimers are capable of forming coiled coils with E_4. The membrane affinity of these three K_4 dimers was studied by performing a tryptophan fluorescence titration assay, before the fusogenicity of different K_4 dimer-E_4 coiled coils was examined by liposome fusion assays. Finally, we studied cell-liposome membrane fusion triggered by these coiled coils.

Since a K_4 dimer-E_4 coiled-coil shows enhanced fusogenicity for both liposome-liposome and cell-liposome membrane fusion (**chapter 4**), in **chapter 5** we used this coiled-coil complex to trigger l-form cell-cell membrane fusion. L-forms are cell wall-deficient bacteria that can survive without their original cell wall.[80-81] Therefore, the study of l-form fusion may be a novel tool to study the origin of life questions.[82] Two phenotypes of l-forms containing different fluorescence markers

and different antibiotic resistance markers were produced. We studied the possibility of decorating l-form membranes with E_4 via a membrane labelling assay. Then, l-form cell-cell fusion was performed using the K_4 dimer-E_4 coiled-coil pair and the fusion efficiency was determined. In order to obtain stable l-forms expressing double markers, a fused l-form enrichment protocol was developed. After enrichment, more than 97% of double marker expressing l-forms were obtained in the total l-form population. Finally, we investigated the fused l-form cell division in medium and chromosome segregation in the solid-state.

In **chapter 6**, the main results and conclusions of the studies described in this thesis are summarized and future perspectives of coiled-coil based biomaterials are discussed.

REFERENCES

(1) Crick, F. The packing of α-helices: simple coiled coils. *Acta crystallographica* **1953,** *6*, 689.

(2) Crick, F. H. The Fourier transform of a coiled-coil. *Acta crystallographica* **1953,** *6*, 685.

(3) Pauling, L.; Corey, R. B. Compound helical configurations of polypeptide chains: structure of proteins of the α-keratin type. *Nature* **1953,** *171*, 59.

(4) Truebestein, L.; Leonard, T. A. Coiled-coils: The long and short of it. *Bioessays* **2016,** *38*, 903.

(5) Apostolovic, B.; Danial, M.; Klok, H. A. Coiled-coils: attractive protein folding motifs for the fabrication of self-assembled, responsive and bioactive materials. *Chem Soc Rev* **2010,** *39*, 3541.

(6) Lupas, A. N.; Bassler, J. Coiled-coils - A Model System for the 21st Century. *Trends Biochem Sci* **2017,** *42*, 130.

(7) Mason, J. M.; Arndt, K. M. Coiled-coil domains: stability, specificity, and biological implications. *Chembiochem* **2004,** *5*, 170.

(8) McLachlan, A.; Stewart, M. Tropomyosin coiled-coil interactions: evidence for an unstaggered structure. *Journal of molecular biology* **1975,** *98*, 293.

(9) Parry, D. Analysis of the primary sequence of α-tropomyosin from rabbit skeletal muscle. *Journal of molecular biology* **1975,** *98*, 519.

(10) Root, D. D.; Yadavalli, V. K.; Forbes, J. G.; Wang, K. Coiled-coil nanomechanics and uncoiling and unfolding of the superhelix and α-helices of myosin. *Biophysical journal* **2006,** *90*, 2852.

(11) Zhou, G.-P. The structural determinations of the leucine zipper coiled-coil domains of the cGMP-dependent protein kinase Iα and its interaction with the myosin binding subunit of the myosin light chains phosphase. *Protein and peptide letters* **2011,** *18*, 966.

(12) Parry, D. A.; Steven, A. C.; Steinert, P. M. The coiled-coil molecules of intermediate filaments consist of two parallel chains in exact axial register. *Biochemical and biophysical research communications* **1985,** *127*, 1012.

(13) Steinert, P. The two-chain coiled-coil molecule of native epidermal keratin intermediate

filaments is a type I-type II heterodimer. *Journal of Biological Chemistry* **1990,** *265*, 8766.

(14) Söderholm, N.; Javadi, A.; Flores, I. S.; Flärdh, K.; Sandblad, L. Affinity to cellulose is a shared property among coiled-coil domains of intermediate filaments and prokaryotic intermediate filament-like proteins. *Scientific reports* **2018,** *8*, 1.

(15) Soppa, J. Prokaryotic structural maintenance of chromosomes (SMC) proteins: distribution, phylogeny, and comparison with MukBs and additional prokaryotic and eukaryotic coiled-coil proteins. *Gene* **2001,** *278*, 253.

(16) Kaplan, J. B.; Reinke, A. W.; Keating, A. E. Increasing the affinity of selective bZIP-binding peptides through surface residue redesign. *Protein Sci* **2014,** *23*, 940.

(17) Drobnak, I.; Gradisar, H.; Ljubetic, A.; Merljak, E.; Jerala, R. Modulation of Coiled-Coil Dimer Stability through Surface Residues while Preserving Pairing Specificity. *J Am Chem Soc* **2017,** *139*, 8229.

(18) Rhys, G. G.; Wood, C. W.; Lang, E. J. M.; Mulholland, A. J.; Brady, R. L.; Thomson, A. R.; Woolfson, D. N. Maintaining and breaking symmetry in homomeric coiled-coil assemblies. *Nat Commun* **2018,** *9*, 4132.

(19) Zaccai, N. R.; Chi, B.; Thomson, A. R.; Boyle, A. L.; Bartlett, G. J.; Bruning, M.; Linden, N.; Sessions, R. B.; Booth, P. J.; Brady, R. L.; Woolfson, D. N. A de novo peptide hexamer with a mutable channel. *Nat Chem Biol* **2011,** *7*, 935.

(20) Thomas, F.; Dawson, W. M.; Lang, E. J. M.; Burton, A. J.; Bartlett, G. J.; Rhys, G. G.; Mulholland, A. J.; Woolfson, D. N. De Novo-Designed alpha-Helical Barrels as Receptors for Small Molecules. *ACS Synth Biol* **2018,** *7*, 1808.

(21) Dawson, W. M.; Martin, F. J. O.; Rhys, G. G.; Shelley, K. L.; Brady, R. L.; Woolfson, D. N. Coiled-coils 9-to-5: rational de novo design of α-helical barrels with tunable oligomeric states. *Chemical Science* **2021,** *12*, 6923.

(22) Litowski, J. R.; Hodges, R. S. Designing heterodimeric two-stranded alpha-helical coiled-coils. Effects of hydrophobicity and alpha-helical propensity on protein folding, stability, and specificity. *J Biol Chem* **2002,** *277*, 37272.

(23) Kwok, S. C.; Hodges, R. S. Effect of chain length on coiled-coil stability: decreasing stability with increasing chain length. *Biopolymers* **2004,** *76*, 378.

(24) Sadeghi, S.; Emberly, E. Length-dependent force characteristics of coiled-coils. *Phys Rev E Stat Nonlin Soft Matter Phys* **2009,** *80*, 061909.

(25) Fairman, R.; Chao, H. G.; Mueller, L.; Lavoie, T. B.; Shen, L.; Novotny, J.; Matsueda, G. R. Characterization of a new four-chain coiled-coil: Influence of chain length on stability. *Protein Science* **1995,** *4*, 1457.

(26) Woolfson, D. N. Building fibrous biomaterials from alpha-helical and collagen-like coiled-coil peptides. *Biopolymers* **2010,** *94*, 118.

(27) Chao, H.; Bautista, D. L.; Litowski, J.; Irvin, R. T.; Hodges, R. S. Use of a heterodimeric coiled-coil system for biosensor application and affinity purification. *Journal of chromatography. B, Biomedical sciences and applications* **1998,** *715*, 307.

(28) Tripet, B.; Yu, L.; Bautista, D. L.; Wong, W. Y.; Irvin, R. T.; Hodges, R. S. Engineering a de

novo designed coiled-coil heterodimerization domain for the rapid detection, purification and characterization of recombinantly expressed peptides and proteins. *Protein Eng* **1997,** *10*, 299.

(29) Chao, H.; Houston, M. E.; Grothe, S.; Kay, C. M.; O'Connor-McCourt, M.; Irvin, R. T.; Hodges, R. S. Kinetic study on the formation of a de novo designed heterodimeric coiled-coil: use of surface plasmon resonance to monitor the association and dissociation of polypeptide chains. *Biochemistry* **1996,** *35*, 12175.

(30) Wu, K.; Liu, J.; Johnson, R. N.; Yang, J.; Kopecek, J. Drug-free macromolecular therapeutics: induction of apoptosis by coiled-coil-mediated cross-linking of antigens on the cell surface. *Angew Chem Int Ed Engl* **2010,** *49*, 1451.

(31) Apostolovic, B.; Deacon, S. P.; Duncan, R.; Klok, H.-A. Hybrid polymer therapeutics incorporating bioresponsive, coiled-coil peptide linkers. *Biomacromolecules* **2010,** *11*, 1187.

(32) Hill, L. K.; Meleties, M.; Katyal, P.; Xie, X.; Delgado-Fukushima, E.; Jihad, T.; Liu, C.-F.; O'Neill, S.; Tu, R. S.; Renfrew, P. D. Thermoresponsive protein-engineered coiled-coil hydrogel for sustained small molecule release. *Biomacromolecules* **2019,** *20*, 3340.

(33) Jing, P.; Rudra, J. S.; Herr, A. B.; Collier, J. H. Self-assembling peptide-polymer hydrogels designed from the coiled-coil region of fibrin. *Biomacromolecules* **2008,** *9*, 2438.

(34) Wang, C.; Stewart, R. J.; KopeČek, J. Hybrid hydrogels assembled from synthetic polymers and coiled-coil protein domains. *Nature* **1999,** *397*, 417.

(35) Wang, C.; Kopeček, J.; Stewart, R. J. Hybrid hydrogels cross-linked by genetically engineered coiled-coil block proteins. *Biomacromolecules* **2001,** *2*, 912.

(36) Fletcher, N. L.; Lockett, C. V.; Dexter, A. F. A pH-responsive coiled-coil peptide hydrogel. *Soft Matter* **2011,** *7*, 10210.

(37) Hellmund, K. S.; Von Lospichl, B.; Böttcher, C.; Ludwig, K.; Keiderling, U.; Noirez, L.; Weiß, A.; Mikolajczak, D. J.; Gradzielski, M.; Koksch, B. Functionalized peptide hydrogels as tunable extracellular matrix mimics for biological applications. *Peptide Science* **2021,** *113*, e24201.

(38) Wickner, W.; Schekman, R. Membrane fusion. *Nature structural & molecular biology* **2008,** *15*, 658.

(39) Blumenthal, R.; Clague, M. J.; Durell, S. R.; Epand, R. M. Membrane fusion. *Chemical Reviews* **2003,** *103*, 53.

(40) Jahn, R.; Lang, T.; Südhof, T. C. Membrane fusion. *Cell* **2003,** *112*, 519.

(41) White, J. M. Membrane fusion. *Science* **1992,** *258*, 917.

(42) Wickner, W.; Schekman, R. Membrane fusion. *Nat Struct Mol Biol* **2008,** *15*, 658.

(43) Martens, S.; McMahon, H. T. Mechanisms of membrane fusion: disparate players and common principles. *Nat Rev Mol Cell Biol* **2008,** *9*, 543.

(44) Scheller, R. H. In search of the molecular mechanism of intracellular membrane fusion and neurotransmitter release. *Nature medicine* **2013,** *19*, 1232.

(45) Yang, Z.; Gou, L.; Chen, S.; Li, N.; Zhang, S.; Zhang, L. Membrane Fusion Involved in Neurotransmission: Glimpse from Electron Microscope and Molecular Simulation. *Front Mol Neurosci* **2017,** *10*, 168.

(46) Primakoff, P.; Myles, D. G. Cell-cell membrane fusion during mammalian fertilization. *FEBS Lett* **2007,** *581*, 2174.

(47) Wassarman, P. M.; Litscher, E. S. Mammalian fertilization is dependent on multiple membrane fusion events. *Cell Fusion* **2008,** *475*, 99.

(48) Lang, J. Molecular mechanisms and regulation of insulin exocytosis as a paradigm of endocrine secretion. *European journal of biochemistry* **1999,** *259*, 3.

(49) Jena, B. P. Cell secretion and membrane fusion. *Domestic animal endocrinology* **2005,** *29*, 145.

(50) Harrison, S. C. Viral membrane fusion. *Virology* **2015,** *479*, 498.

(51) Harrison, S. C. Viral membrane fusion. *Nature structural & molecular biology* **2008,** *15*, 690.

(52) Chernomordik, L. V.; Kozlov, M. M. Mechanics of membrane fusion. *Nat Struct Mol Biol* **2008,** *15*, 675.

(53) Irie, A.; Yamamoto, K.; Miki, Y.; Murakami, M. Phosphatidylethanolamine dynamics are required for osteoclast fusion. *Sci Rep* **2017,** *7*, 46715.

(54) Harayama, T.; Riezman, H. Understanding the diversity of membrane lipid composition. *Nat Rev Mol Cell Biol* **2018,** *19*, 281.

(55) Meher, G.; Chakraborty, H. Membrane Composition Modulates Fusion by Altering Membrane Properties and Fusion Peptide Structure. *J Membr Biol* **2019,** *252*, 261.

(56) Casares, D.; Escribá, P. V.; Rosselló, C. A. Membrane lipid composition: Effect on membrane and organelle structure, function and compartmentalization and therapeutic avenues. *International journal of molecular sciences* **2019,** *20*, 2167.

(57) Hamai, C.; Yang, T.; Kataoka, S.; Cremer, P. S.; Musser, S. M. Effect of average phospholipid curvature on supported bilayer formation on glass by vesicle fusion. *Biophys J* **2006,** *90*, 1241.

(58) Carlini, E.; Palmerini, C. A.; Cosmi, E. V.; Arienti, G. Fusion of sperm with prostasomes: effects on membrane fluidity. *Archives of biochemistry and biophysics* **1997,** *343*, 6.

(59) Prives, J.; Shinitzky, M. Increased membrane fluidity precedes fusion of muscle cells. *Nature* **1977,** *268*, 761.

(60) Howell, J.; Ahkong, Q.; Cramp, F. Membrane fluidity and membrane fusion. *J. Pathol* **1972,** *104*, 115.

(61) Jahn, R.; Scheller, R. H. SNAREs--engines for membrane fusion. *Nat Rev Mol Cell Biol* **2006,** *7*, 631.

(62) Bock, J. B.; Scheller, R. H. SNARE proteins mediate lipid bilayer fusion. *Proceedings of the National Academy of Sciences* **1999,** *96*, 12227.

(63) Wang, T.; Li, L.; Hong, W. SNARE proteins in membrane trafficking. *Traffic* **2017,** *18*, 767.

(64) Jung, J. J.; Inamdar, S. M.; Tiwari, A.; Choudhury, A. Regulation of intracellular membrane trafficking and cell dynamics by syntaxin-6. *Biosci Rep* **2012,** *32*, 383.

(65) Ramakrishnan, N. A.; Drescher, M. J.; Drescher, D. G. The SNARE complex in neuronal and sensory cells. *Mol Cell Neurosci* **2012,** *50*, 58.

(66) Sutton, R. B.; Fasshauer, D.; Jahn, R.; Brunger, A. T. Crystal structure of a SNARE complex

involved in synaptic exocytosis at 2.4 Å resolution. *Nature* **1998,** *395*, 347.

(67) Smirnova, Y. G.; Risselada, H. J.; Müller, M. Thermodynamically reversible paths of the first fusion intermediate reveal an important role for membrane anchors of fusion proteins. *Proceedings of the National Academy of Sciences* **2019,** *116*, 2571.

(68) Zucker, R. S.; Kullmann, D. M.; Kaeser, P. S. Release of neurotransmitters. In *From Molecules to Networks*; Elsevier: 2014; pp 443.

(69) Robson Marsden, H.; Kros, A. Self-assembly of coiled-coils in synthetic biology: inspiration and progress. *Angew Chem Int Ed Engl* **2010,** *49*, 2988.

(70) Robson Marsden, H.; Korobko, A. V.; Zheng, T.; Voskuhl, J.; Kros, A. Controlled liposome fusion mediated by SNARE protein mimics. *Biomater Sci* **2013,** *1*, 1046.

(71) Versluis, F.; Voskuhl, J.; van Kolck, B.; Zope, H.; Bremmer, M.; Albregtse, T.; Kros, A. In situ modification of plain liposomes with lipidated coiled-coil forming peptides induces membrane fusion. *J Am Chem Soc* **2013,** *135*, 8057.

(72) Daudey, G. A.; Zope, H. R.; Voskuhl, J.; Kros, A.; Boyle, A. L. Membrane-fusogen distance is critical for efficient coiled-coil-peptide-mediated liposome fusion. *Langmuir* **2017,** *33*, 12443.

(73) Zope, H. R.; Versluis, F.; Ordas, A.; Voskuhl, J.; Spaink, H. P.; Kros, A. In vitro and in vivo supramolecular modification of biomembranes using a lipidated coiled-coil motif. *Angewandte Chemie International Edition* **2013,** *52*, 14247.

(74) Yang, J.; Bahreman, A.; Daudey, G.; Bussmann, J.; Olsthoorn, R. C.; Kros, A. Drug Delivery via Cell Membrane Fusion Using Lipopeptide Modified Liposomes. *ACS Cent Sci* **2016,** *2*, 621.

(75) Yang, J.; Shimada, Y.; Olsthoorn, R. C.; Snaar-Jagalska, B. E.; Spaink, H. P.; Kros, A. Application of Coiled-coil Peptides in Liposomal Anticancer Drug Delivery Using a Zebrafish Xenograft Model. *ACS Nano* **2016,** *10*, 7428.

(76) Kong, L.; Askes, S. H.; Bonnet, S.; Kros, A.; Campbell, F. Temporal control of membrane fusion through photolabile PEGylation of liposome membranes. *Angewandte Chemie* **2016,** *128*, 1418.

(77) Rabe, M.; Aisenbrey, C.; Pluhackova, K.; de Wert, V.; Boyle, A. L.; Bruggeman, D. F.; Kirsch, S. A.; Bockmann, R. A.; Kros, A.; Raap, J.; Bechinger, B. A Coiled-Coil Peptide Shaping Lipid Bilayers upon Fusion. *Biophys J* **2016,** *111*, 2162.

(78) Rabe, M.; Schwieger, C.; Zope, H. R.; Versluis, F.; Kros, A. Membrane interactions of fusogenic coiled-coil peptides: implications for lipopeptide mediated vesicle fusion. *Langmuir* **2014,** *30*, 7724.

(79) Zheng, T.; Voskuhl, J.; Versluis, F.; Zope, H. R.; Tomatsu, I.; Marsden, H. R.; Kros, A. Controlling the rate of coiled-coil driven membrane fusion. *Chem Commun (Camb)* **2013,** *49*, 3649.

(80) Errington, J. L-form bacteria, cell walls and the origins of life. *Open Biol* **2013,** *3*, 120143.

(81) Errington, J.; Mickiewicz, K.; Kawai, Y.; Wu, L. J. L-form bacteria, chronic diseases and the origins of life. *Philosophical Transactions of the Royal Society B: Biological Sciences* **2016,** *371*, 20150494.

(82) Shitut, S.; Bergman, G. Ö.; Kros, A.; Rozen, D. E.; Claessen, D. Use of permanent wall-deficient cells as a system for the discovery of new-to-nature metabolites. *Microorganisms* **2020,** *8*, 1897.

Chapter 2

Magnetic-activated Cell Sorting using Coiled-coil Peptides

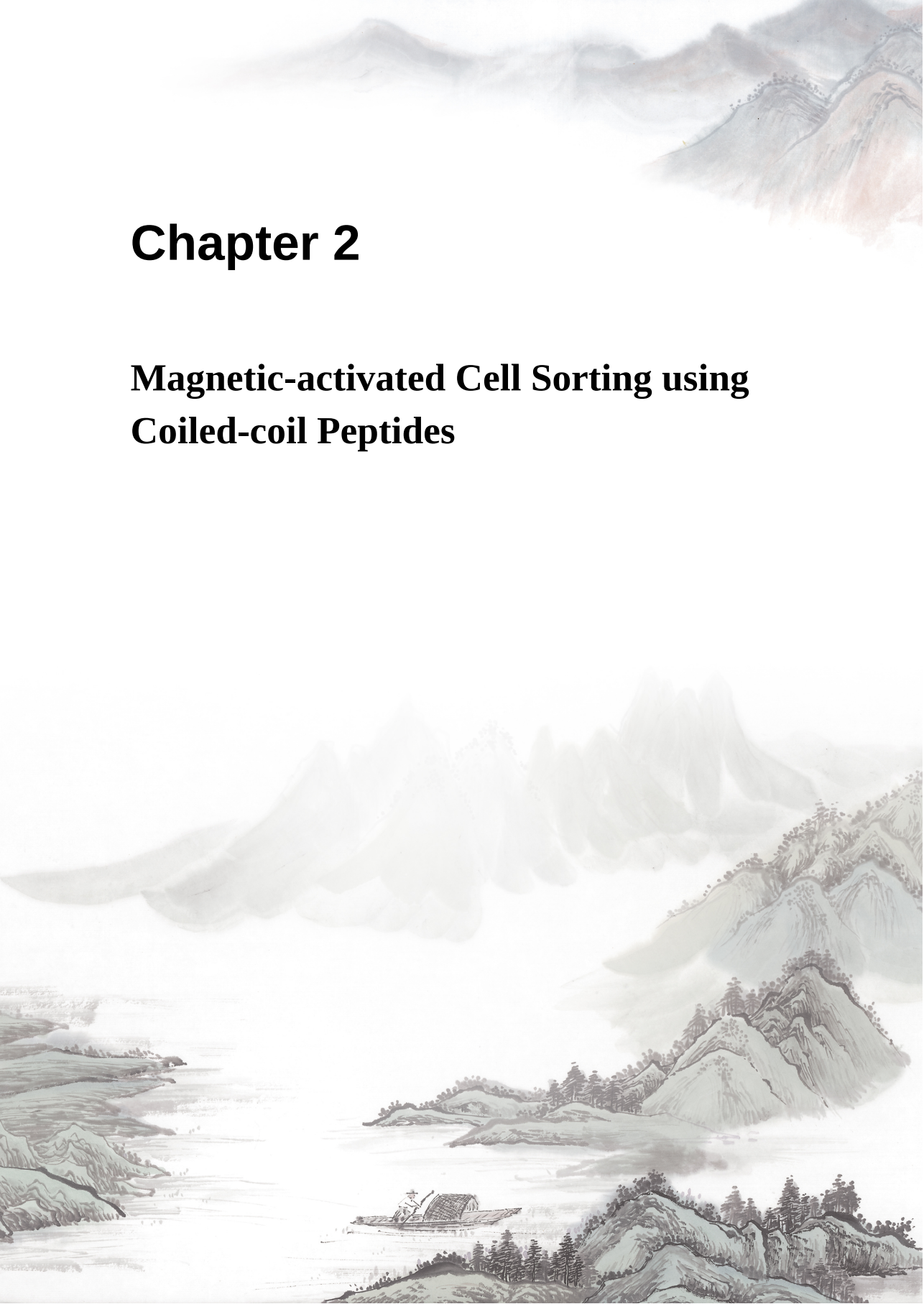

ABSTRACT

Magnetic-activated cell sorting (MACS) is an affinity-based technique used to separate cells according to the presence of specific markers. Current MACS systems generally require an antigen to be expressed at the cell surface; these antigen-presenting cells subsequently interact with antibody-labelled magnetic particles, facilitating separation. Here, we present an alternative MACS method based on coiled-coil peptide interactions. We demonstrate that HeLa, CHO and NIH3T3 cells can either incorporate a lipid-modified coiled-coil-forming peptide into their membrane, or that the cells can be transfected with a plasmid containing a gene encoding a coiled-coil-forming peptide. Iron oxide particles are functionalized with the complementary peptide and, upon incubation with the cells, labelled cells are facilely separated from non-labeled populations. In addition, the resulting cells and particles can be treated with trypsin to facilitate detachment of the cells from the particles. Therefore, our new MACS method promotes efficient cell sorting of different cell lines, without the need for antigen presentation, and enables simple detachment of the magnetic particles from cells after the sorting process. Such a system can be applied to rapidly developing, sensitive, research areas, such as the separation of genetically modified cells from their unmodified counterparts.

INTRODUCTION

The sorting of specific cells from complex mixtures is necessary for a variety of applications, ranging from cancer research,[1-4] to assisted reproduction,[5] and cell-based therapies,[6-7] in addition to the selection of genetically modified cells.[8-9] Two of the primary affinity-based techniques used for cell sorting are fluorescence-activated cell sorting (FACS) and magnetic-activated cell sorting (MACS).[10-11] Whilst FACS has several advantages: analysis is rapid and multiple parameters can be simultaneously analyzed, the disadvantages include the fact that expensive, specialist equipment is needed and cells must be modified to display a fluorescent moiety. MACS can circumvent these disadvantages: no specialist equipment is required and no fluorescent labels are needed. Instead, MACS employs magnetic particles that can be functionalized to enable binding to a subset of cells in a mixture, facilitating separation.[12-15] Usually, the particles are functionalized with an antibody, which is specific for antigens expressed on the surface of cells of interest. The beads and the cells are incubated and subsequently placed in a magnetic field. Cells that do not express the antigen of interest are not retained in the magnetic field, whereas cells that do display the antigen of interest bind to the beads and are retained. Once the magnetic field is removed, the cells of interest can be eluted. However, MACS does have disadvantages: functionalization of the iron oxide particles (IOPs) with antibodies is not trivial, and such antibodies are typically expensive. Indeed, one study highlighted that, when MACS was used to select for induced pluripotent stem cells from a cell mixture, the antibody comprised 65% of the purification cost.[16] MACS systems can also suffer from low cell purity after separation due to non-specific binding between the cells and the functionalized magnetic particles.[17-18] In addition, it is not trivial to separate the cells from the magnetic particles, which can lead to adverse effects. For example, magnetic particles can influence the phenotype and function of some cells,[19-20] in addition to affecting cell viability.[21-22]

Therefore, there is a need to design and synthesize functionalized magnetic particles that possess a high specificity for the cells of interest and are facile to dissociate from the cells after separation. Such a system would benefit multiple areas of cell biology and medicine, for example facilitating the separation, and subsequent enrichment, of genetically modified cells.

Coiled coils are a protein-folding motif comprising two or more alpha-helices that interact to form a left-handed supercoil.[23] Different oligomer states, orientations of

helices, and both homomeric and heterodimeric assemblies are possible.[24] Moreover, rules exist for the programmable design of such structures,[25-26] which has enabled synthetic coiled-coil systems to be designed and employed in a variety of applications.[27-30] We were motivated to determine whether coiled-coil peptides could be used to separate cells in a MACS-based approach. Therefore, we designed a MACS system based on interactions between magnetic beads and cells that were functionalized with complementary coiled-coil forming peptides, (Figure 1). We employed a heteromeric coiled-coil system, dubbed E_3/K_3.[31] Nanometer-sized iron oxide magnetic particles (IOPs) were coated with dextran-divinyl sulfone (dextran-DVS) and subsequently functionalized with E_3 to yield IOPs-E_3. HeLa, CHO and NIH3T3 cells were incubated with a lipidated K_3 derivative, (CPK), which is known to spontaneously incorporate into the cell membrane.[32] When the cells and the functionalized IOPs were mixed, cells that displayed K_3 on their surface bound to the IOPs-E_3 via the formation of a coiled-coil. Subsequent application of an external magnetic field facilitated isolation of these cells with high efficiency and specificity, (Figure 1A). Another advantage of this system is that the coiled-coil peptides could be degraded by trypsin, which made the dissociation of the cells from the IOPs facile and efficient. We subsequently demonstrate that HeLa, NIH3T3, and CHO cells can be transfected with a plasmid containing K_3. These cells express K_3 on their membrane and we show that these cells could be separated, (Figure 1B), and subsequently enriched, from non-transfected cells. These results demonstrate that our coiled-coil based MACS system can facilitate cell separation, and subsequent enrichment of transfected cells, with high specificity and efficiency.

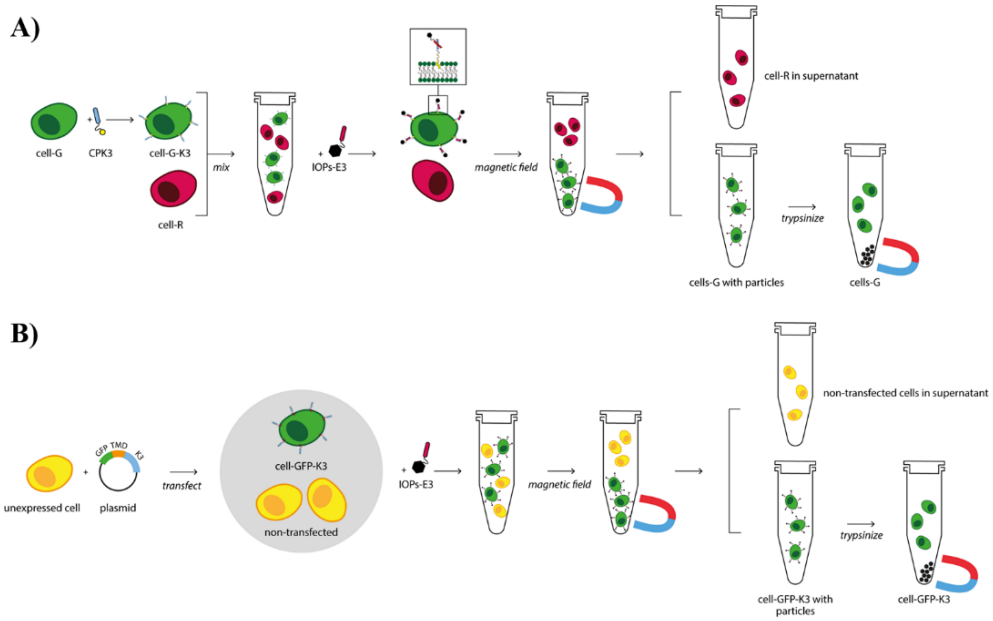

Figure 1. Coiled-coil-based MACS. Cells are either functionalized with a coiled-coil forming peptide (A) or transfected with a K_3-containing plasmid (B); low transfection rates mean not all cells express the K_3 peptide. IOPs bearing the complementary peptide are added and separation is facilitated by coiled-coil formation and application of a magnetic field. Post-separation, cells are separated from the IOPs *via* trypsinization.

RESULTS AND DISCUSSION

Design and synthesis of peptide-functionalized IOPs

Functionalized magnetic particles suitable for cell sorting need to possess several properties including: specificity for the cells of interest; high binding and separation efficiency, and; effective dissociation. To fulfil these criteria a coiled-coil-functionalized IOP system was designed. Two complementary peptides are known as K_3, $(KIAALKE)_3$, and E_3, $(EIAALEK)_3$, named for the prevalence of lysine and glutamic acid residues in their respective sequences, were employed.[31] These two peptides interact to form a heterodimeric coiled coil with a micromolar dissociation constant. This tight binding enables peptide-functionalized IOPs to bind to the complementary peptide with high efficiency, (Figure 2A).

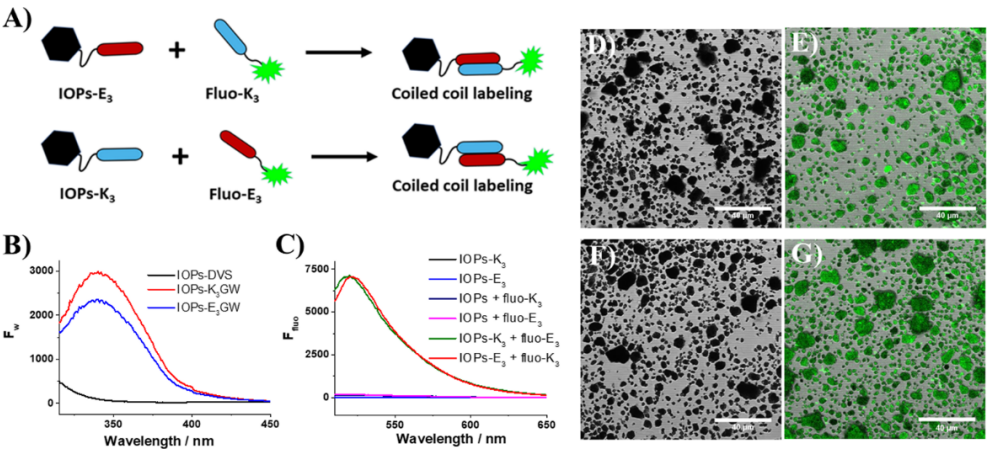

Figure 2. Coiled-coil-functionalized magnetic particles. A) Schematic of fluorescent labelling of the IOPs: coiled-coil functionalized IOPs are incubated with the complementary fluorescent peptide. B) Tryptophan fluorescence spectrum of functionalized IOPs, indicating attachment of the peptides to the particles. C) Fluorescein fluorescence spectrum of fluorescently-labeled IOPs; a fluorescein spectrum is only observed when the IOPs are labeled with the complementary peptide. D-G) Confocal microscopy images of: IOPs-DVS treated with fluo-K_3 (D); IOPs-E_3 treated with fluo-K_3 (E); IOPs-DVS treated with fluo-E_3 (F), and; IOPs-K_3 treated with fluo-E_3 (G). Scale bar: 40 µm.

IOPs need to be coated to reduce non-specific interactions with cells and to facilitate functionalization with a moiety specific to the cells of interest. In this study, IOPs were synthesized and coated with a dextran-divinyl sulfone (Dex-DVS) polymer in a one-pot reaction. The DVS functionality facilitates labelling of the IOPs with any compound containing a free sulfhydryl group *via* a Michael addition. An added advantage is that the number of DVS groups can be adjusted by synthesizing Dex-DVS with differing degrees of substitution, allowing for control over the number of functional groups displayed on the surface of the IOPs.

Conjugation of the coiled coil-forming peptides to the IOPs was facilitated by modifying the peptides to include a free sulfhydryl group. To this end, Ac-E_3GW-PEG_4-Cys and Ac-K_3GW-PEG_4-Cys were designed, these peptides incorporate a cysteine (Cys, C) at their C-terminus. A polyethylene glycol (PEG) spacer was included between the cysteine and the rest of the peptide sequence to minimize potential steric hindrance, which may impact coiled-coil formation. A tryptophan (Trp, W) was included to facilitate detection and quantification of the peptide.

To demonstrate the peptide-functionalized IOPs were successfully synthesized, fluorescence spectroscopy was employed. IOPs functionalized with the coiled-coil-forming peptides exhibit a fluorescence spectrum corresponding to that of Trp, (Figure 2B), which indicates the peptides were successfully conjugated to the IOPs.

Coiled-coil formation was subsequently confirmed using a fluorescence labelling assay. The fluorescein conjugated peptides, fluo-K_3 and fluo-E_3, were mixed with either non-functionalized IOPs or IOPs bearing the complementary peptide. Figure 2C shows that a fluorescein fluorescence spectrum is only observed when the peptides are mixed with IOPs functionalized with the complementary peptides. This indicates coiled-coil formation and demonstrates that no non-specific binding between fluo-E_3 or fluo-K_3 and non-functionalized IOPs occurs. The results were verified by confocal microscopy imaging, (Figure 2D-G). The unmodified IOPs did not exhibit fluorescence after incubation with fluo-K_3 or fluo-E_3, (Figure 2D&F), whereas peptide-modified IOPs have a green fluorescent surface after labelling with the complementary peptide, *i.e.* IOPs-E_3 + fluo-K_3, (Figure 2E) or IOPs-K_3 + fluo-E_3, (Figure 2G).

MACS for lipopeptide-decorated cells

We have previously employed the lipopeptides CPK and CPE to facilitate membrane fusion.[33-34] These lipopeptides comprise the K and E peptides, with a PEG spacer that connects the peptide to a cholesterol anchor. This anchor enables the insertion of the lipopeptide into the lipid bilayer of a cell membrane. By functionalizing specific cells with these lipopeptides and adding IOPs functionalized with the complementary coiled-coil forming peptide, cells can be separated from others in a mixture.

To confirm that the lipopeptides synthesized for this study are capable of inserting into the cell membrane and subsequently forming a coiled-coil, a cell membrane labelling assay was performed. The fluo-K_3 or fluo-E_3 peptides were added to cells decorated with the complementary lipopeptide. Using confocal microscopy, it was determined that the lipopeptide-decorated cells exhibited a fluorescently-labelled membrane, while no fluorescent labelling was observed on non-decorated cell membranes, (Figure S1).

After it was confirmed that coiled-coil forming peptides could be used to functionalize IOPs and cell membranes, and that coiled-coil formation occurred, a proof-of-principle coiled-coil-mediated MACS experiment was designed. Separate

HeLa cell populations were stained with either CellTracker™ Green or CellTracker™ Red. Green cells were incubated with CPK_3 for one hour, before being mixed with the same number of red cells. IOPs-E_3 were subsequently added to the cell mixture. It was anticipated that the IOPs-E_3 would selectively bind to the CPK_3 decorated green cells via coiled-coil formation. Through the application of an external magnetic field, cells attached to the magnetic particles could be isolated. The IOP-attached cells could subsequently be treated with trypsin to dissociate the magnetic particles before an external magnetic field could again be used to separate the IOPs from the detached HeLa cells.

Confocal imaging was performed directly after MACS; the results are shown in Figure 3. Before MACS, the cell population contained CPK_3 decorated green cells and undecorated red cells (Figure 3A). After MACS, only red cells were found in the supernatant (Figure 3B) and cells attached to the IOPs were almost exclusively green (Figure 3C). This demonstrates that the K_3/E_3 coiled-coil-based MACS system can be used to efficiently separate cell populations. To demonstrate that the cells can be cleaved from the IOPs, they were incubated with trypsin and then separated from the IOPs using an external magnetic field. Figure 3D shows the image of the cells after dissociation: most of the cells exhibit green fluorescence. The cell-IOPs dissociation is efficient: no cells were observed to remain attached to the IOPs (Figure 3E). After MACS, the cells were allowed to grow for 24 h before imaging again to demonstrate that both the cells from the supernatant, (Figure 3F) and the cells detached from the IOPs, (Figure 3G) remain viable. The same study was then performed using CHO and NIH3T3 cells to illustrate the broad applicability of this MACS system, (Figures S2-S3).

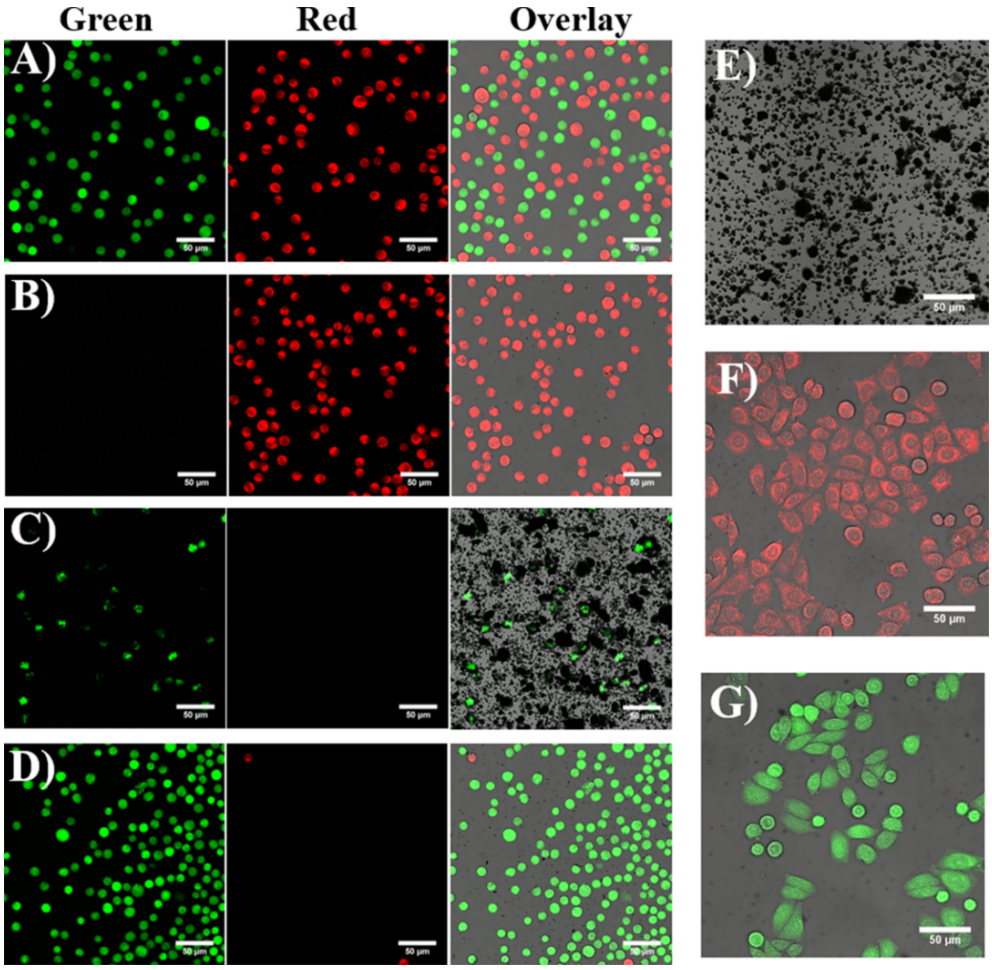

Figure 3. Coiled-coil-facilitated MACS of HeLa cells. A) CPK_3 modified HeLa cells stained with CellTracker™ green mixed with non-functionalized HeLa cells stained with CellTracker™ red; B) cells in the supernatant after MACS; C) IOP-attached cells after MACS; D) cells detached from the IOPs after trypsinization; E) no visible cells remain attached to the IOPs after trypsinization; cells from the supernatant (F) and those detached from IOPs (G) show signs of recovery and growth after 24 hours. Scale bar: 50 µm.

Whilst confocal imaging provides a qualitative impression of the efficiency of this system, quantification of cell separation is desirable. Therefore, flow cytometry was employed for all three cell lines. Before MACS, the flow cytometry data shows the cells are mixed in an approximately 1:1 ratio, as designed, Table 1. After one round of MACS, the cells were demonstrated to be highly efficiently separated as, for all three cells lines tested, more than 99% of the cells in the

supernatant were red cells and more than 94% of cells detached from the IOPs were green cells (Table 1, Figures S4-S6).

Table 1. FACS quantification of cell populations before and after MACS.

Cell line	Before MACS (%)		After MACS: Supernatant (%)		After MACS: IOP detached cells (%)	
	Red	Green	Red	Green	Red	Green
Hela	51.5	47.2	**99.2 (0.2)** [a]	0.5 (0.2)	4.9 (1.5)	**94.8 (1.3)**
CHO	44.5	55	**99.7 (0.0)**	0.3 (0.0)	4.3 (0.1)	**95.7 (0.1)**
NIH3T3	48.5	51.5	**100 (0.0)**	0 (0.0)	0.7 (0.2)	**99.3 (0.2)**

[a] Error is calculated as the standard deviation from the average of at least two independent measurements.

Alternative IOP Functionalization

Cell membranes are usually negatively charged. For this reason, IOPs were functionalized with E_3 and not K_3 as it was hypothesized that IOPs-K_3 could non-specifically interact with the negatively charged cell membrane. To verify this hypothesis, an experiment was performed using Hela cells modified with CPE_3 and IOPs functionalized with K_3, (Figure S7). The CPE_3 decorated green cells were mixed with red cells in a 1:1 ratio (Figure S7A). The cell mixture was incubated with IOPs-K_3 and after MACS, only red cells were found in the supernatant (Figure S7B). However, a mixture of red and green cells were found to be attached to the IOPs, (Figures S7C); this is more evident after trypsinization, (Figure S7D). In addition, FACS analysis was performed and this revealed that the cells detached from the IOPs have almost equal populations of green and red cells (Figure S7E & S8).

Combined, these experiments reveal that coiled-coil-forming peptide-functionalized IOPs can be used to efficiently sort cells bearing the complementary coiled-coil-forming peptide from a mixture. This system can be applied to a variety of different cell lines. The data also indicates that the charge of the peptide which is conjugated to the IOPs makes a significant difference to the efficiency of the cell sorting process.

MACS with GFP-K3 expressed cells

For the proof-of-principle experiment, cells have to be manually decorated with K_3 before cell sorting; this process limits the potential applications of the MACS system. To fully benefit from using coiled coils as a cell-surface marker, cells that express K_3 on their membranes were employed, (Figure 1B): such a system has been used previously in our lab.[34] The K_3 peptide was fused to a signal sequence and a transmembrane domain (TMD) from the platelet-derived growth factor receptor beta (PDGFRB). The presence of this signaling sequence and the TMD ensures that the K_3 peptide is transported to, and anchored in, the cell membrane. In addition, GFP was included to act as a fluorescent marker to illustrate the expression of the K_3-TMD-GFP construct after transfection. GFP can also be used as a fluorescent label for FACS quantification before and after MACS.

After cell transfection and two weeks of antibiotic selection, approximately 10% of all transfected cells successfully expressed the K_3-TMD-GFP construct. A cell-labelling experiment was subsequently performed using a Cy5-conjugated E_3 peptide to confirm that the K_3 peptide was successfully expressed on the cell membrane, (Figure 4A).

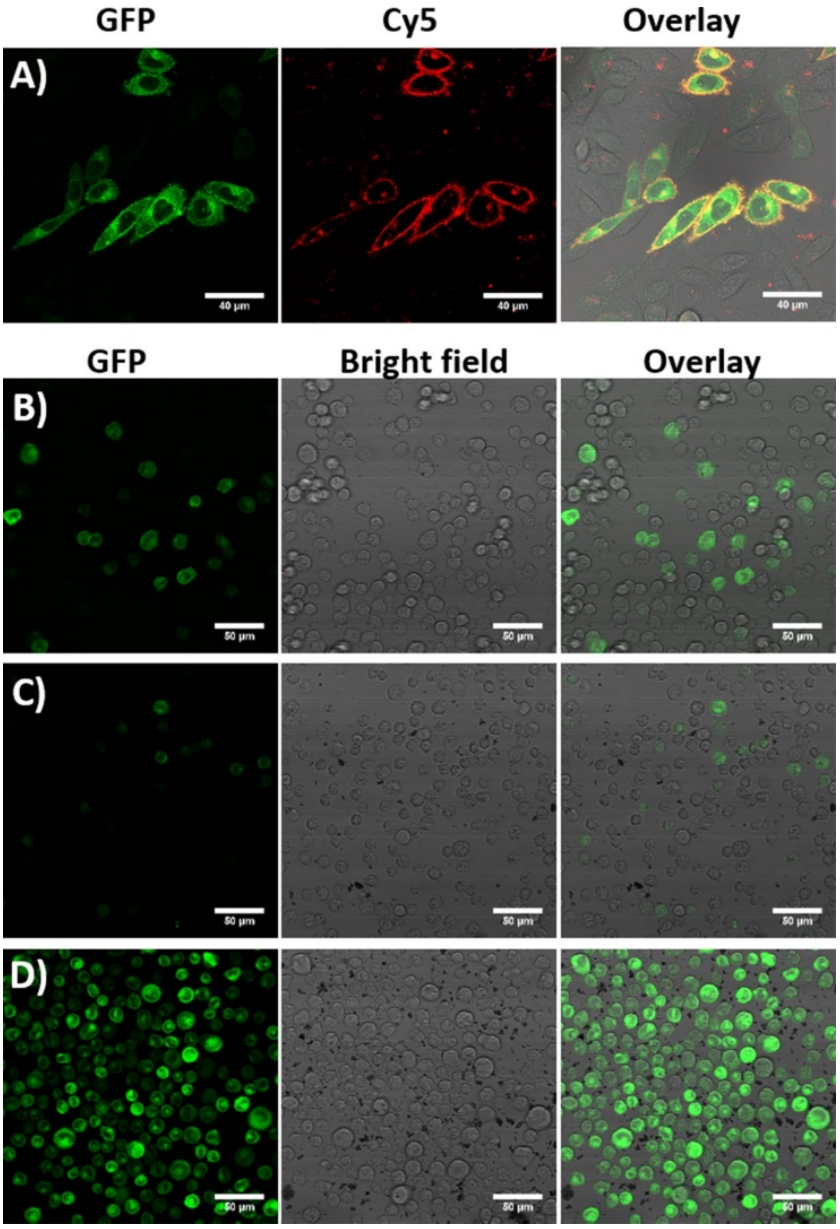

Figure 4. HeLa cell membrane labelling and cell sorting. A) HeLa cells were transfected with a plasmid containing the K_3-TMD-GFP gene. The transfected cells were subsequently incubated with Cy5-E_3 to demonstrate successful expression of K_3 at the cell surface. Green channel: GFP, Red channel: Cy5. Scale bar: 40 µm. Transfected cells were then subjected to MACS: (B) before MACS; C) cells from the supernatant after MACS; D) cells detached from IOPs after MACS. Green channel: GFP. Scale bar: 50 µm.

As the K_3 peptide was indeed expressed on the cell membrane, it was possible to use it as a selection marker for cell sorting. As GFP is co-expressed in the K_3-expressing cells, confocal microscopy can be employed to track the cell sorting process. Before MACS, a low percentage of green cells were found in cell mixture due to the low transfection efficiency (Figure 4B). IOPs-E_3 were added to the cells and an external magnetic field was applied. After MACS, few green cells were observed in the supernatant, (Figure 4C), whereas cells retained in the magnetic field and then detached from the IOPs were GFP-expressing cells, (Figure 4D). This shows that the coiled-coil peptide-based MACS system is capable of selective separation of K_3-expressing cells from non-transfected cells. Although some cells that expressed GFP were found in the supernatant, the fluorescence level was low, indicating that the expression level of K_3 could also affect the separation. The cells were subsequently cultured for two days: Figure 5A shows that the GFP positive cells could be enriched to a high level after coiled-coil based MACS. FACS quantification showed only 17.4% of GFP positive cells in the transfected cell mixture before MACS, (Table 2, and Figure S9), but after MACS selection, 94.3% of GFP positive cells were obtained. These results confirm that GFP-K_3 expressed cells can be effectively enriched by this MACS system.

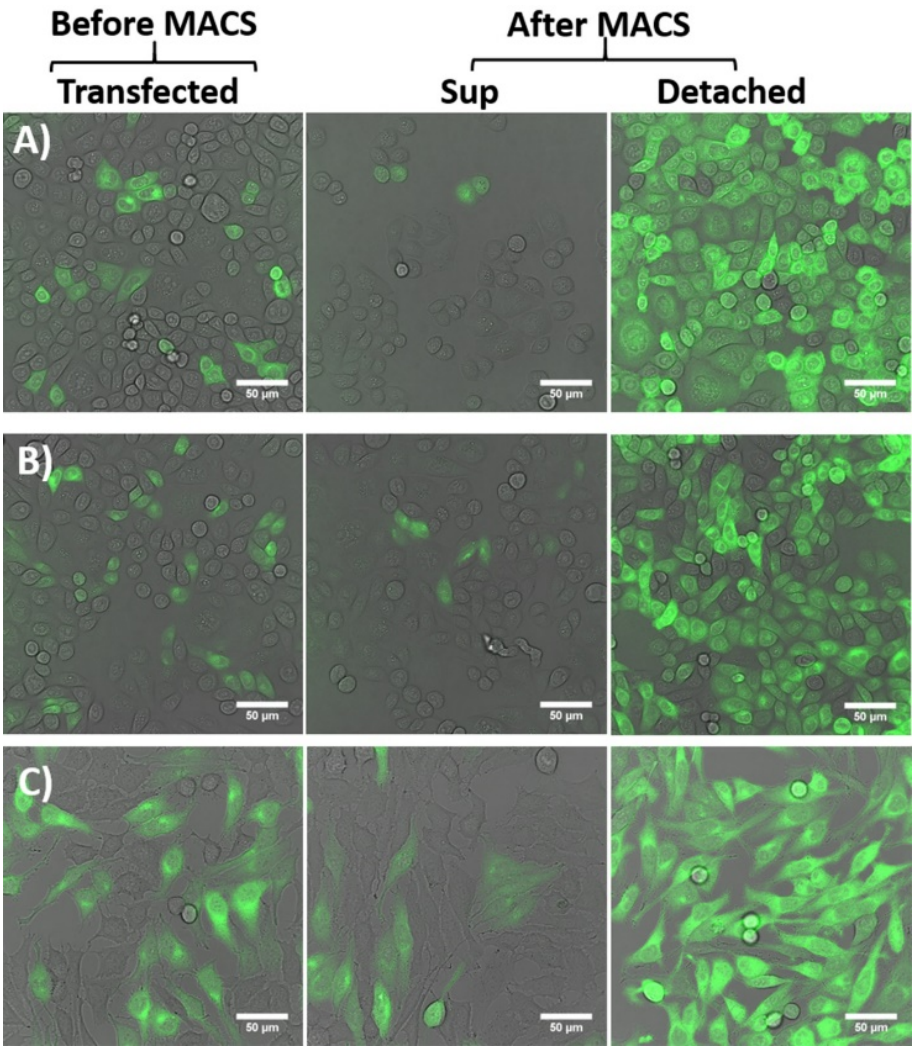

Figure 5. Imaging of K_3-TMD-GFP cells before and after MACS. A) Hela-K_3 cells, B) CHO-K_3 cells, C) NIH3T3-K_3 cells. The left column shows transfected cells before MACS, the middle column shows cells in the supernatant after MACS and cells detached from IOPs after MACS are on the right. All images are an overlay of bright field and fluorescence microscopy images. Scale bar: 50µm.

To demonstrate the wider applicability of the transfected MACS system for cell sorting and enrichment, CHO and NIH3T3 cell lines were again employed, (Figure 5B & C). Cells were analyzed using FACS after separation, (Figures S10 & 11). For CHO cells, an enrichment from 14.8% to 76% of GFP-expressing cells could be obtained after MACS. This system is even more successful for NIH3T3 cells;

the FACS data shows that 24.2% of GFP-K_3 expressing NIH3T3 cells could be enriched to 95.6% after MACS.

Table 2. FACS quantification of GFP positive cells before and after MACS.

Cell line	Before MACS (%)	After MACS (%)	
		Supernatant	Detached
Hela	17.4	11.7 (0.6) [a]	**94.3 (2.2)**
CHO	14.8	12.2 (8.1)	**76.0 (2.5)**
NIH3T3	24.2	19.8 (0.1)	**95.6 (0.4)**

[a] Errors are calculated as the standard deviation from the average of at least two independent measurements.

Both the qualitative and quantitative data show that the GFP-K_3 expressing cells from different cell lines can be efficiently isolated from a cell mixture using IOPs-E_3. These results demonstrate that the coiled-coil-mediated MACS system can be applied to enrich cell populations. For this study, GFP was co-expressed with K_3 to facilitate both imaging and quantification by FACS. However, MACS itself doesn't require the cells to express GFP or indeed any fluorophore, which is beneficial for studies where fluorescent proteins are detrimental and therefore FACS is not possible. Additionally, the GFP could be replaced by any protein of interest and a single round of coiled-coil-mediated MACS will separate the cells expressing this protein with high specificity and efficiency.

CONCLUSIONS

In this study, we have taken advantage of coiled-coil peptide interactions and designed a new MACS system based on this non-covalent interaction. This MACS system facilitates efficient, facile cell sorting. A particularly attractive feature of this system is that the isolated cells can be easily dissociated from the IOPs by trypsinization, meaning the magnetic particles do not remain attached to the cells. This system may not be suitable for all cell types, particularly those isolated from tissues, due to the need to incorporate an extrinsic selection marker. However, the fact that the K_3 peptide can be employed as a selection marker for transfected cells means that this approach has the potential to become an alternative method for transfected cell selection, eliminating the need for FACS or antibiotics. Moreover, the plasmid can be modified to include any gene of interest, either as a fusion with

K_3 or by including cleavage sites. Such a system could therefore have applications in a wide range of biomedical areas that require cell separation.

EXPERIMENTAL SECTION

Chemicals

All chemicals were purchased from Sigma unless otherwise stated. Amino acids and HCTU were purchased from Novabiochem. Tentagel HL RAM resin was purchased from Iris Biotech GmbH. Piperidine, trifluoroacetic acid, acetic anhydride and all other solvents were purchased from Biosolve. Oxyma pure was purchased from Carl Roth GmbH. Dextran 70 was supplied by Pharmacosmos. CellTracker™ red and green, lipofectamine 3000 and 2 KDa MWCO dialysis membrane were purchased from Thermo Fisher. Confocal Chambered Coverslips (µ-Slide 8 Well) were purchased from Ibidi. All cell culture supplies were purchased from Starstedt. Carbon/Formvar grids for transmission electron microscopy were purchased from Agar Scientific.

Peptide synthesis

For the synthesis of CPE_3 and CPK_3, peptides K_3 $(KIAALKE)_3$ and E_3 $(EIAALEK)_3$ were synthesized using Fmoc chemistry on a CEM Liberty Blue microwave-assisted peptide synthesizer. DIC was used as the activator and Oxyma as the activator base. Fmoc deprotection was performed with 20% piperidine in DMF. The peptide was synthesized on a Tentagel HL RAM resin (0.39 mmol/g). Once synthesis of the peptide was complete, two eqv. N_3-PEG_4-COOH (synthesized as described elsewhere),[35] were manually coupled to the peptides on resin, using three eqv. HCTU and five eqv. DIPEA in DMF. The resin was washed with DMF after three hours. Five eqv. trimethylphosphine (1M in toluene) in a dioxane:H_2O (6:1) mixture were added to the resin to reduce the azide. After three hours, the resin was washed with dioxane followed by DMF before cholesteryl hemisuccinate (three eqv.) was coupled to the N-terminus of the PEG linker using three eqv. HCTU and five eqv. DIPEA in DMF. After overnight coupling, the resin was washed with DMF followed by DCM and the resulting CPK_3 or CPE_3 construct was cleaved from the resin by adding 5 ml of a TFA:triisopropylsilane (97.5:2.5%) mixture and shaking for 45 mins. The crude peptide was precipitated by pouring into 45 mL cold diethyl ether and isolated by centrifugation. The

peptide pellet was dissolved in 20 mL H_2O with 10% acetonitrile and freeze-dried to yield a white powder.

The fluo-E_3 and fluo-K_3 peptides were synthesized in a similar manner. Two additional glycine residues were coupled to the N-terminus of the K_3 and E_3 peptides. 5(6)-carboxyfluorescein (three eqv.) was subsequently manually coupled to the peptides using four eqv. HCTU and six eqv. DIPEA in DMF. After an overnight reaction, the resin was washed using DMF and the fluorophore-labelled peptides, flu-K_3 and flu-E_3, were cleaved from the resin using 5 mL TFA:triisopropylsilane:H_2O (95%:2.5%:2.5%) for one hour. The peptide was precipitated into diethyl ether, centrifuged, redissolved in H_2O and MeCN and freeze-dried.

For the Ac-E_3GW-PEG_4-Cys and Ac-K_3GW-PEG_4-Cys peptides, cysteine was coupled to Tentagel HL RAM resin before N_3-PEG_4-COOH was coupled to the cysteine using the procedure described above. After three hours, the resin was washed and the azide was reduced. The resin was transferred to the peptide synthesizer and either E_3: $(EIAALEK)_3GW$ or K_3: $(KIAALKE)_3GW$ was synthesized. Upon completion of the synthesis, the resin was manually acetylated by adding 3 mL of an acetic anhydride:pyridine:DMF (5%:6%:89%) solution. After one hour, the resin was washed with DMF and DCM, before the peptide was cleaved from the resin by adding 5 mL TFA:TIPS:EoDT:H_2O (92.5:2.5%:2.5%:2.5%). After two hours, the peptide was precipitated into diethyl ether, centrifuged, redissolved and freeze-dried.

Cy5-E_3 was synthesized for labelling GFP-K_3 expressing cells. E_3 was synthesized using the method described above. After the synthesis, three eqv. 4-pentynoic acid, four eqv. HCTU and six eqv. DIPEA in 2 mL DMF were added to the E_3 peptide, on the resin, to facilitate coupling of an alkyne to the N-terminus. After one hour, the resin was washed (DMF followed by DCM) and the peptide was cleaved. The Alkyne-E_3 peptide was purified using HPLC (see below) before coupling to Azide-Cy5. This coupling was performed by dissolving 1.55 mg (9.7 nmol) $CuSO_4$ in 1 mL H_2O. 19 mg (97 nmol) of L-ascorbic acid was subsequently added and the color of the solution became brown, before turning light yellow. 21 mg (48.5 nmol) Tris(3-hydroxypropyltriazolylmethyl)amine was dissolved in 150 µL DMSO and added to solution, which was stirred for 3 min at 500 rpm before 1 mg (0.97 nmol) Azide-Cy5 in 500 µL H_2O was added, followed by 11.5 mg (4.85 nmol) Alkyne-E_3 in 500 µL H_2O. The reaction was stirred for 2 hours before being dialyzed

overnight using a 2 KDa MWCO membrane. The resulting Cy5-E3 peptide was purified using HPLC.

Peptide Purification

Peptide and lipopeptide purification was performed using reversed-phase HPLC on a Shimazu system with two LC-8A pumps and an SPD-20A UV-Vis detector.

Lipopeptide (CPK_3 and CPE_3) purification was performed with a Vydac C4 column (22 mm diameter, 250 mm length, 10 μm particle size). A linear gradient from 20% to 80% acetonitrile (with 0.1% TFA) in water (with 0.1% TFA) was performed over 36 mins, with a flow rate of 12 mL/min.

Peptides Ac-K_3GW-PEG_4-Cys, Ac-K_3GW-PEG_4-Cys, fluo-E_3, fluo-K_3, E_3, and Cy5-E_3 were purified using a Kinetix Evo C18 column (21.2 mm diameter, 150 mm length, 5 μm particle size). A linear gradient from 20% to 55% acetonitrile (with 0.1% TFA) and water (0.1% of TFA) was used for the HPLC method: the running time was 28 mins, and the flow rate was 12 mL/min.

After purification, the collected fractions of all lipopeptides and peptides were assessed using LC-MS (Figures S12-S15, Table S1). Fractions that were deemed to be >95% pure were combined and lyophilized.

Modification of Dextran with DVS

The synthesis of Dextran-DVS was performed according to a previously reported protocol.[36] Briefly, 10 g (61.7 mmol) of Dextran 70 was dissolved in 300 mL of a 0.1 M NaOH solution in an ice bath. Afterwards, 23 mL (229 mmol) divinyl sulfone was added under vigorous stirring (1000 rpm). The reaction was left for 65 s before 5 mL of 6 M HCl was added to acidify the solution to pH 5.0. Dextran-DVS precipitation was achieved after 300 mL cold isopropanol was added. The gel-like precipitate was dissolved in H_2O and dialyzed using 2 KDa MWCO dialysis tubing; the dialysis solution was changed every 12 hours, and the dialysis was left for three days. The resulting dextran-DVS solution was concentrated to a final volume of 100 mL by overnight exposure to an N_2 stream. The solution was dried and 7.5 g (yield = 74%) of lyophilized powder was obtained. A schematic detailing the entire synthesis process is shown in Figure S16.

The degree of substitution (DS) of dextran can be defined as the number of vinyl sulfone groups per 100 glucopyranose residues. The calculated DS of dextran

which has been used for coating IOPs in this work is 4.6 and the calculation is based on ^{1}H NMR (Figure S17). The DS can be controlled by altering the reaction time, therefore it is possible to obtain dextran-DVS with a higher DS. However, the solubility of DVS-modified dextran was found to negatively correlate with the DS, therefore it was determined that dextran-DVS with a DS of 4.6 offered the optimal balance between solubility and functional group density.

Dextran-DVS coated magnetic IOPs synthesis (IOPs-DVS)

0.88 g (5.4 mmol) $FeCl_3$ and 0.55 g (2.7 mmol) $FeCl_2 \cdot 4H_2O$ were dissolved in 50 mL degassed water and heated to 80 °C under N_2. 10 ml, 17.5% $NH_3 \cdot H_2O$ was quickly added to the flask while stirring at 800 rpm. The reaction was left for 1 hour at 80 °C before 2 g of Dex-DVS was added. The solution was left to stir overnight before the resulting IOPs-DVS particles were purified by washing with water whilst using a magnet to minimize particle loss. The particles were dried under a flow of N_2 gas.

Synthesis of E_3 or K_3 conjugated magnetic particles (IOPs-E_3/IOPs-K_3)

Ac-E_3GW-PEG_4-Cys or Ac-K_3GW-PEG_4-Cys was dissolved in PBS (pH 7.4) to a final concentration of 1 mM (as determined by UV-Vis) and then added to 100 mg of IOPs-DVS. The mixture was shaken at 600 rpm at room temperature overnight. The peptide solution was collected under an external magnetic field and the concentration of unreacted peptide was measured by UV-Vis (Figure S18). The difference in peptide concentration before and after the reaction can be used to calculate the amount of peptide conjugated to the magnetic IOPs, (for further details, see the Supporting Information). It was determined that 5.5 nmol peptide E_3 and 5.8 nmol peptide K_3 were conjugated to 1 mg of IOPs. The peptide-functionalized IOPs were purified by washing with H_2O under an external magnetic field. The mass of particles was clearly visible to the naked eye, (Figure S19A) and TEM analysis revealed them to be nanometer sized, (Figure S19B). Particles were stored in 75% EtOH to minimize bacterial growth. Before cell experiments, the particles were washed with PBS and diluted to a final concentration of 2 mg/mL, which equates to 11 µM E_3 in IOPs-E_3 suspension or 11.6 µM K_3 in IOPs-K_3 suspension.

Lipopeptide-decorated cell sorting

Cells were seeded in a six-well plate (1 x 10^6 cells per well) and incubated overnight. Before trypsinization from the plate, cells were stained with CellTracker™ Green (5 µg/ml) or CellTracker™ Red (10 µg/ml) for 30 min. 3 x 10^5 green cells were incubated with 1 mL, 10 µM CPK_3 for one hour and washed three times before mixing with the same amount of non-functionalized red cells. 100 µL of IOPs-E_3 was subsequently added to 1 mL cell mixture to facilitate the formation of a coiled-coil between K_3-functionalized cells and the magnetic IOPs. A magnet was used to separate the cells which were connected to the IOPs from the remainder of the cell mixture. The cells in the supernatant were collected and cells connected to the IOPs were then washed three times with PBS before trypsin was added to digest the peptides, (Figure S20 & 21) and dissociate the cells from the IOPs. After detachment, the cells were separated from the IOPs by application of an external magnetic field. Both cell populations were washed twice with PBS before being analyzed. To probe the utility of IOPs functionalized with K_3, the process above was repeated, but cells were decorated with CPE_3 and IOPs were labelled with K_3 in the same manner as described above.

Fluorescence spectroscopy

Fluorescence measurements were performed using a Tecan Infinite M1000 plate reader. All spectra were collected with 200 µL, 2mg/mL IOPs at room temperature in black 96-well plates. For tryptophan fluorescence measurements, excitation was performed at 275nm and emission was recorded from 450 to 310 nm.

In the IOPs fluorescent labeling assay, 200µL, 10 µM fluo-E_3 or fluo-K_3 were added to non-functionalized IOPs or IOPs with a complimentary coiled-coil-forming peptide. After a one minute incubation, the IOPs were thoroughly washed and resuspended in PBS. The IOPs were transferred to a black 96-well plate and a spectrum was recorded. Excitation was performed at 488 nm and the emission spectrum was recorded between 650 and 510 nm.

Confocal microscopy

Cell imaging was performed using a Leica SPE laser scanning confocal microscope. Cells expressing GFP, or stained with CellTracker™ Green or labelled with fluo-K_3/E_3 were excited with a 488 nm laser and the emission signal was detected from 495 to 530 nm. Cells stained with CellTracker™ Red were excited

with a 532 nm laser and emission was detected between 560-600 nm. Cells labelled with Cy5-E_3 were excited with a 635 nm laser and emission was detected from 650-690 nm.

Flow cytometry

All flow cytometry measurements were performed with a Guava® EasyCyte 12HT Benchtop Flow Cytometer and the data was analyzed using FlowJo v10. The cells were suspended in PBS containing 2 mM EDTA at a concentration of approximately 500 cells/µL. 5000 events in duplicate were collected for each measurement. A manual gating strategy can be founding in supporting information (Figures S4-S6 & S8-S11). Quadrant gates were used to quantify the fluorescence of Cell Tracker Red (RED-B) *versus* Cell Tracker Green (GRN-B) or GFP expression (GRN-B) *versus* cell size (FSC-A). No compensation was required for the fluorophores used.

Plasmid Constructs

A DNA fragment coding for a signal peptide sequence from the mouse IgK gene and the K_3 peptide fused to a transmembrane domain from PDGFRB, and EGFP was purchased from BaseClear (Leiden, NL) and cloned into an Acc65I and NotI digested pEBMulti-Hyg vector (Wako Pure Chemical Ind, Osaka, Japan) as described previously.[37] The DNA sequence is shown in the Supporting Information (Figure S22).

Cell transfection and antibiotics selection

HeLa and NIH3T3 cells were seeded in a 12-well plate and grown to 80% confluency. 1 µg of plasmid (0.2 µg/µL) and 8 µg of PEI were used per well. The cells were incubated with the DNA/PEI complex for 5 hours at 37 ℃ and then washed with DMEM three times.

CHO cells were transfected using Lipofectamine 3000. Cells were seeded in a 24-well plate and allowed to grow to 80% confluency. 0.5 µg of plasmid DNA (0.2 µg/ µL) and 1.5 µL of Lipofectamine 3000 were used per well. Cells were incubated at 37 ℃ for 5 hours before washing the cells with DMEM three times.

After transfection, all cells were grown for three days. Hygromycin B was used to enrich successfully transfected cells. After two weeks of antiobiotic selection, the percentage of GFP-positive cells was found to stop increasing, presumably because

the cells acquired resistance to the antibiotic. At this point, the GFP-expressing cells comprised approximately 10% of the total cell population.

MACS with GFP-K_3 expressed cells

Before MACS, GFP-K_3 expressing cells were subcultured for at least two generations. The cells were subsequently detached from the cell culture plate using EDTA (2 mM in PBS) and dispersed by thorough pipetting. Cell sorting was performed by utilizing 1 mL cell suspension containing 1 x 10^6 GFP-K_3 expressing cells. 100 μL of IOPs-E_3 suspension was subsequently added to enable coiled-coil formation between the K_3 peptide on the cell membrane and the E_3 peptide attached to the IOPs. A magnet was then used to separate the cells which were connected to the IOPs from the other cells in the mixture. Cells connected to the IOPs were washed with PBS three times and trypsin was then added to dissociate the cells from the IOPs. After detachment, the cells and IOPs were separated by application of an external magnetic field.

Transmission Electron Microscopy

A 10 μL droplet of the IOPs was placed on a Forvar/Carbon grid (200 mesh) and left for ten minutes. The excess solution was blotted off and the grid was left to air dry. Images were obtained used a JEM1400 plus (JEOL) microscope, operating at 80 kV. The microscope was fitted with a CCD camera.

REFERENCES

(1) Chen, P.; Huang, Y. Y.; Hoshino, K.; Zhang, X. Multiscale immunomagnetic enrichment of (1) Chen, P.; Huang, Y. Y.; Hoshino, K.; Zhang, X. Multiscale immunomagnetic enrichment of circulating tumor cells: from tubes to microchips. *Lab Chip* **2014,** *14*, 446.

(2) Di Corato, R.; Bigall, N. C.; Ragusa, A.; Dorfs, D.; Genovese, A.; Marotta, R.; Manna, L.; Pellegrino, T. Multifunctional nanobeads based on quantum dots and magnetic nanoparticles: synthesis and cancer cell targeting and sorting. *Acs Nano* **2011,** *5*, 1109.

(3) Geens, M.; Van de Velde, H.; De Block, G.; Goossens, E.; Van Steirteghem, A.; Tournaye, H. The efficiency of magnetic-activated cell sorting and fluorescence-activated cell sorting in the decontamination of testicular cell suspensions in cancer patients. *Hum Reprod* **2007,** *22*, 733.

(4) Saliba, A. E.; Saias, L.; Psychari, E.; Minc, N.; Simon, D.; Bidard, F. C.; Mathiot, C.; Pierga, J. Y.; Fraisier, V.; Salamero, J.; Saada, V.; Farace, F.; Vielh, P.; Malaquin, L.; Viovy, J. L. Microfluidic sorting and multimodal typing of cancer cells in self-assembled magnetic arrays. *Proc Natl Acad Sci U S A* **2010,** *107*, 14524.

(5) Gil, M.; Sar-Shalom, V.; Melendez Sivira, Y.; Carreras, R.; Checa, M. A. Sperm selection using magnetic activated cell sorting (MACS) in assisted reproduction: a systematic review and meta-analysis. *J Assist Reprod Genet* **2013,** *30*, 479.

(6) Fong, C. Y.; Peh, G. S.; Gauthaman, K.; Bongso, A. Separation of SSEA-4 and TRA-1-60 labelled undifferentiated human embryonic stem cells from a heterogeneous cell population using magnetic-activated cell sorting (MACS) and fluorescence-activated cell sorting (FACS). *Stem Cell Rev Rep* **2009,** *5*, 72.

(7) Schriebl, K.; Lim, S.; Choo, A.; Tscheliessnig, A.; Jungbauer, A. Stem cell separation: a bottleneck in stem cell therapy. *Biotechnol J* **2010,** *5*, 50.

(8) Kim, H.; Kim, M. S.; Wee, G.; Lee, C. I.; Kim, H.; Kim, J. S. Magnetic separation and antibiotics selection enable enrichment of cells with ZFN/TALEN-induced mutations. *PLoS One* **2013,** *8*, e56476.

(9) Ren, C.; Xu, K.; Segal, D. J.; Zhang, Z. Strategies for the Enrichment and Selection of Genetically Modified Cells. *Trends Biotechnol* **2019,** *37*, 56.

(10) Bacon, K.; Lavoie, A.; Rao, B. M.; Daniele, M.; Menegatti, S. Past, Present, and Future of Affinity-based Cell Separation Technologies. *Acta Biomater* **2020,** *112*, 29.

(11) Plouffe, B. D.; Murthy, S. K.; Lewis, L. H. Fundamentals and application of magnetic particles in cell isolation and enrichment: a review. *Rep Prog Phys* **2015,** *78*, 016601.

(12) Miltenyi, S.; Muller, W.; Weichel, W.; Radbruch, A. High gradient magnetic cell separation with MACS. *Cytometry* **1990,** *11*, 231.

(13) Molday, R. S.; Yen, S. P.; Rembaum, A. Application of magnetic microspheres in labelling and separation of cells. *Nature* **1977,** *268*, 437.

(14) Moore, L. R.; Zborowski, M.; Sun, L.; Chalmers, J. J. Lymphocyte fractionation using immunomagnetic colloid and a dipole magnet flow cell sorter. *J Biochem Biophys Methods* **1998,** *37*, 11.

(15) Schmitz, B.; Radbruch, A.; Kummel, T.; Wickenhauser, C.; Korb, H.; Hansmann, M. L.; Thiele, J.; Fischer, R. Magnetic activated cell sorting (MACS)--a new immunomagnetic method for megakaryocytic cell isolation: comparison of different separation techniques. *Eur J Haematol* **1994,** *52*, 267.

(16) Weil, B. D.; Jenkins, M. J.; Uddin, S.; Bracewell, D. G.; Wellings, D.; Farid, S. S.; Veraitch, F. An integrated experimental and economic evaluation of cell therapy affinity purification technologies. *Regen Med* **2017,** *12*, 397.

(17) Chalmers, J. J.; Xiong, Y.; Jin, X.; Shao, M.; Tong, X.; Farag, S.; Zborowski, M. Quantification of non-specific binding of magnetic micro- and nanoparticles using cell tracking velocimetry: Implication for magnetic cell separation and detection. *Biotechnol Bioeng* **2010,** *105*, 1078.

(18) Moore, D. K.; Motaung, B.; du Plessis, N.; Shabangu, A. N.; Loxton, A. G.; Consortium, S.-I. Isolation of B-cells using Miltenyi MACS bead isolation kits. *PLoS One* **2019,** *14*, e0213832.

(19) Farrell, E.; Wielopolski, P.; Pavljasevic, P.; van Tiel, S.; Jahr, H.; Verhaar, J.; Weinans, H.; Krestin, G.; O'Brien, F. J.; van Osch, G.; Bernsen, M. Effects of iron oxide incorporation for long term cell tracking on MSC differentiation in vitro and in vivo. *Biochem Biophys Res Commun* **2008,**

369, 1076.

(20) Meinhardt, K.; Kroeger, I.; Abendroth, A.; Muller, S.; Mackensen, A.; Ullrich, E. Influence of NK cell magnetic bead isolation methods on phenotype and function of murine NK cells. *J Immunol Methods* **2012,** *378*, 1.

(21) Mahmoudi, M.; Azadmanesh, K.; Shokrgozar, M. A.; Journeay, W. S.; Laurent, S. Effect of nanoparticles on the cell life cycle. *Chem Rev* **2011,** *111*, 3407.

(22) Van de Walle, A.; Perez, J. E.; Abou-Hassan, A.; Hémadi, M.; Luciani, N.; Wilhelm, C. Magnetic nanoparticles in regenerative medicine: what of their fate and impact in stem cells? *Materials Today Nano* **2020,** *11*, 100084.

(23) Crick, F. H. C. Is α-Keratin a Coiled Coil? *Nature* **1952,** *170*, 882.

(24) Woolfson, D. N. The design of coiled-coil structures and assemblies. *Adv Protein Chem* **2005,** *70*, 79.

(25) Fletcher, J. M.; Boyle, A. L.; Bruning, M.; Bartlett, G. J.; Vincent, T. L.; Zaccai, N. R.; Armstrong, C. T.; Bromley, E. H.; Booth, P. J.; Brady, R. L.; Thomson, A. R.; Woolfson, D. N. A basis set of de novo coiled-coil peptide oligomers for rational protein design and synthetic biology. *ACS Synth Biol* **2012,** *1*, 240.

(26) Harbury, P. B.; Zhang, T.; Kim, P. S.; Alber, T. A switch between two-, three-, and four-stranded coiled coils in GCN4 leucine zipper mutants. *Science* **1993,** *262*, 1401.

(27) Apostolovic, B.; Danial, M.; Klok, H. A. Coiled coils: attractive protein folding motifs for the fabrication of self-assembled, responsive and bioactive materials. *Chemical Society Reviews* **2010,** *39*, 3541.

(28) Beesley, J. L.; Woolfson, D. N. The de novo design of alpha-helical peptides for supramolecular self-assembly. *Current Opinion in Biotechnology* **2019,** *58*, 175.

(29) Marsden, H. R.; Kros, A. Self-Assembly of Coiled Coils in Synthetic Biology: Inspiration and Progress. *Angewandte Chemie-International Edition* **2010,** *49*, 2988.

(30) Wu, Y. Y.; Collier, J. H. alpha-Helical coiled-coil peptide materials for biomedical applications. *Wiley Interdisciplinary Reviews-Nanomedicine and Nanobiotechnology* **2017,** *9*.

(31) Litowski, J. R.; Hodges, R. S. Designing heterodimeric two-stranded alpha-helical coiled-coils. Effects of hydrophobicity and alpha-helical propensity on protein folding, stability, and specificity. *J Biol Chem* **2002,** *277*, 37272.

(32) Zope, H. R.; Versluis, F.; Ordas, A.; Voskuhl, J.; Spaink, H. P.; Kros, A. In vitro and in vivo supramolecular modification of biomembranes using a lipidated coiled-coil motif. *Angew Chem Int Ed Engl* **2013,** *52*, 14247.

(33) Versluis, F.; Voskuhl, J.; van Kolck, B.; Zope, H.; Bremmer, M.; Albregtse, T.; Kros, A. In situ modification of plain liposomes with lipidated coiled coil forming peptides induces membrane fusion. *J Am Chem Soc* **2013,** *135*, 8057.

(34) Yang, J.; Bahreman, A.; Daudey, G.; Bussmann, J.; Olsthoorn, R. C. L.; Kros, A. Drug Delivery via Cell Membrane Fusion Using Lipopeptide Modified Liposomes. *ACS Central Science* **2016,** *2*, 621.

(35) Crone, N. S. A.; Kros, A.; Boyle, A. L. Modulation of Coiled-Coil Binding Strength and Fusogenicity through Peptide Stapling. *Bioconjug Chem* **2020,** *31*, 834.

(36) Yu, Y.; Chau, Y. One-step "click" method for generating vinyl sulfone groups on hydroxyl-containing water-soluble polymers. *Biomacromolecules* **2012,** *13*, 937.

(37) Yang, J.; Shimada, Y.; Olsthoorn, R. C.; Snaar-Jagalska, B. E.; Spaink, H. P.; Kros, A. Application of Coiled Coil Peptides in Liposomal Anticancer Drug Delivery Using a Zebrafish Xenograft Model. *ACS Nano* **2016,** *10*, 7428.

APPENDIX 2

Cell Labelling Experiments

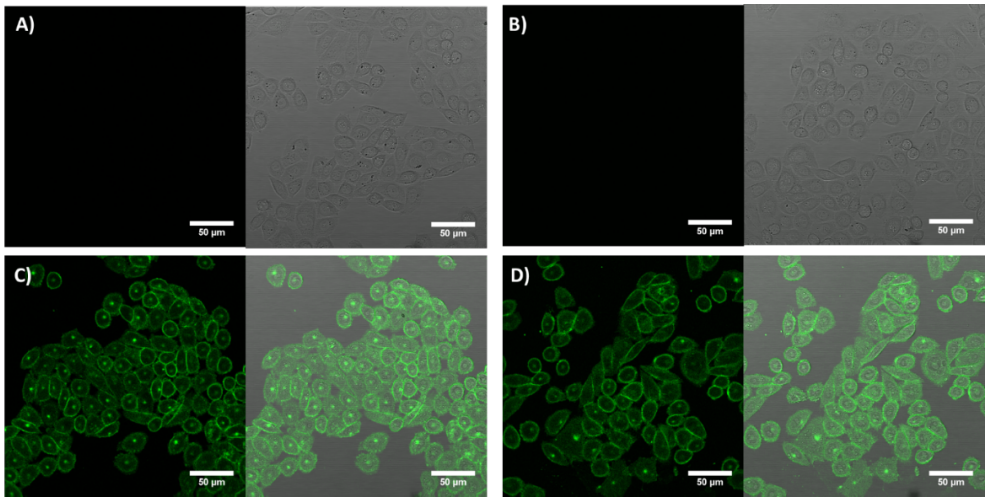

Figure S1. Cell labeling assay with HeLa cells. A) Non-labeled cells incubated with fluo-K_3, B) non-labeled cells incubated with fluo-E_3, C) CPE_3 decorated cells incubated with fluo-K_3, D) CPK_3 decorated cells incubated with fluo-E_3. Green: fluorescein. Scale bar: 50 µm.

MACS with CHO and NIH3T3 cells—CPK_3 decorated cells

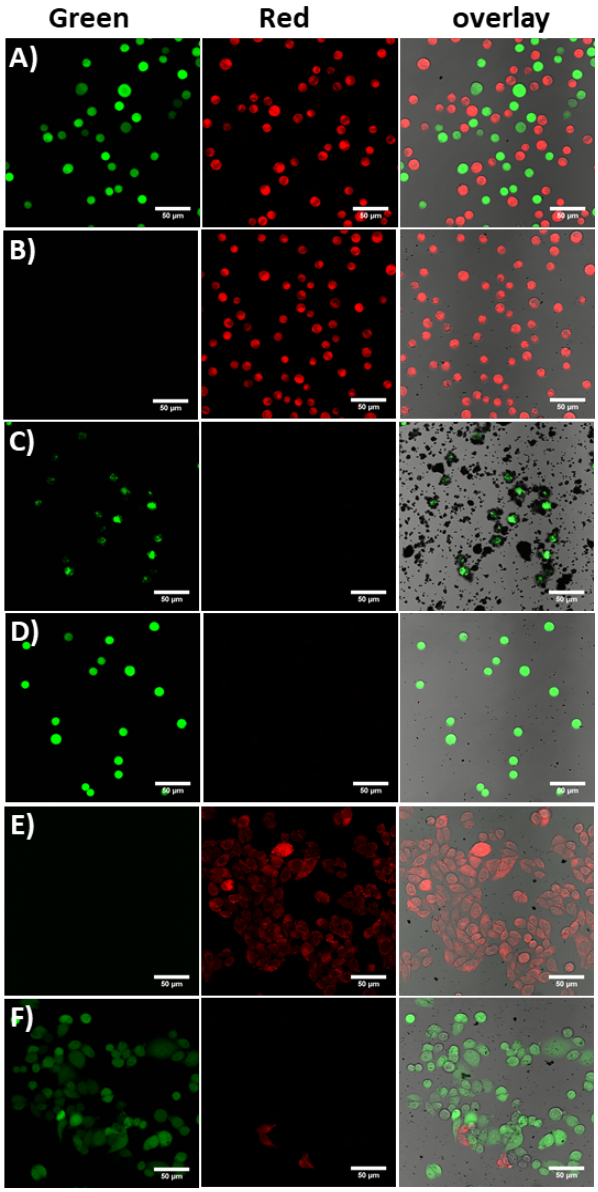

Figure S2. CHO cell sorting using IOPs-E_3 A) Green cells were decorated with CPK_3 and mixed with the same number of red cells. (B) Cells in the supernatant after MACS. (C) Cells attached to IOPs after MACS. (D) Cells detached from IOPs by trypsinization. (E) Cells in the supernatant 24 hours after MACS and (F) cells detached from the IOPs 24 hours after MACS. Cells were stained with CellTracker Green or CellTracker Red. Scale bar 50µm.

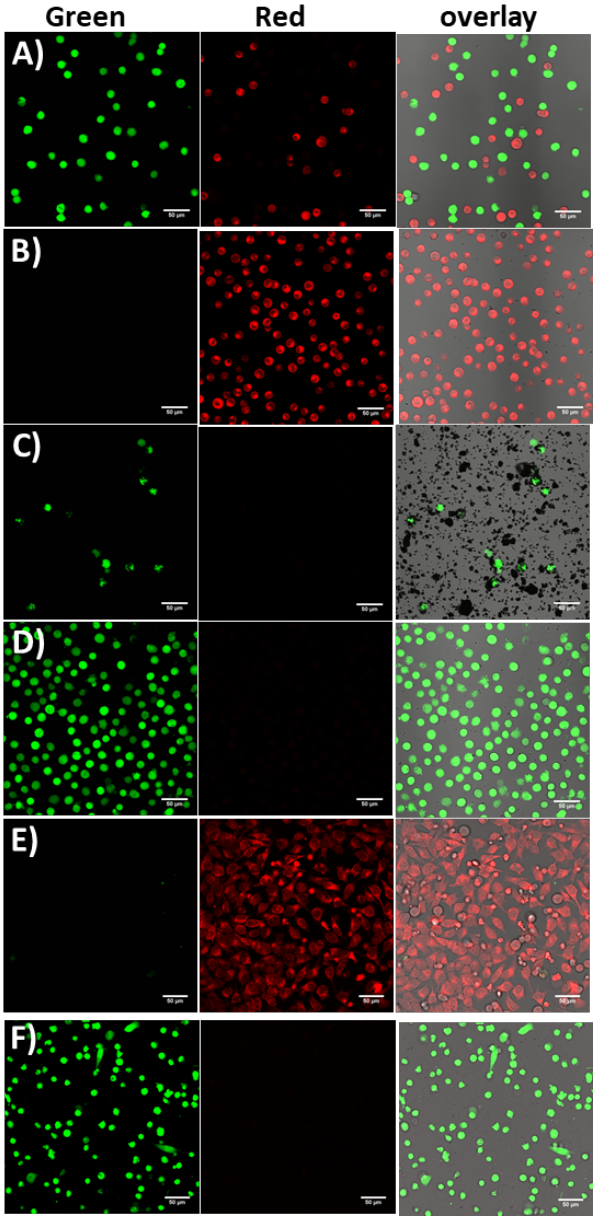

Figure S3. NIH3T3 cell sorting using IOPs-E_3 A) Green cells were decorated with CPK_3 and mixed with the same number of red cells. (B) Cells in the supernatant after MACS. (C) Cells attached to IOPs after MACS. (D) Cells detached from IOPs by trypsinization. (E) Cells in the supernatant 24 hours after MACS and (F) cells detached from the IOPs 24 hours after MACS. Cells were stained with CellTracker Green or CellTracker Red. Scale bar 50µm.

FACS analysis of cell population after MACS with CPK_3 decorated cells

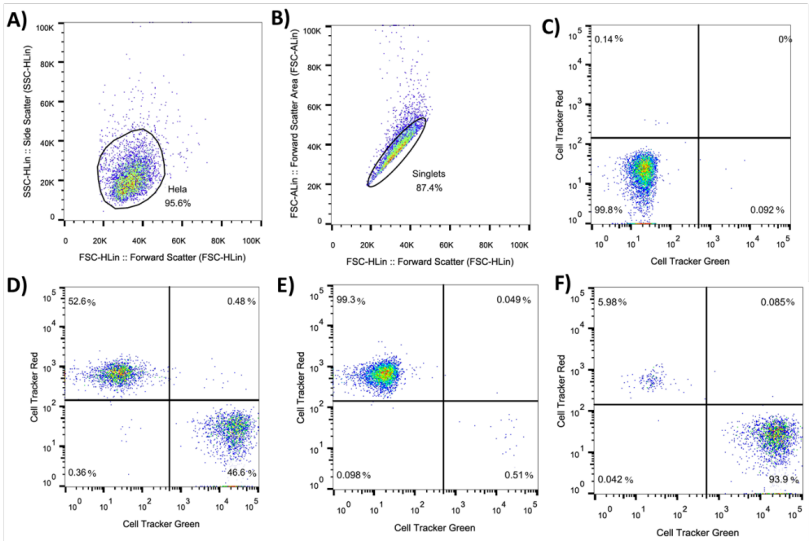

Figure S4. HeLa cell sorting using IOPs-E3. A) Hela cell population gated by FSC-H *vs.* SSC-H, B) cell singlets gated by FSC-A *vs.* FSC-H, C) HeLa cells without staining, D) HeLa cells mixture: green-CPK_3 and red cells, E) cells in supernatant after MACS, F) cells detached from IOPs after MACS. Cell tracker Green: GRN-B, cell tracker Red: RED-B.

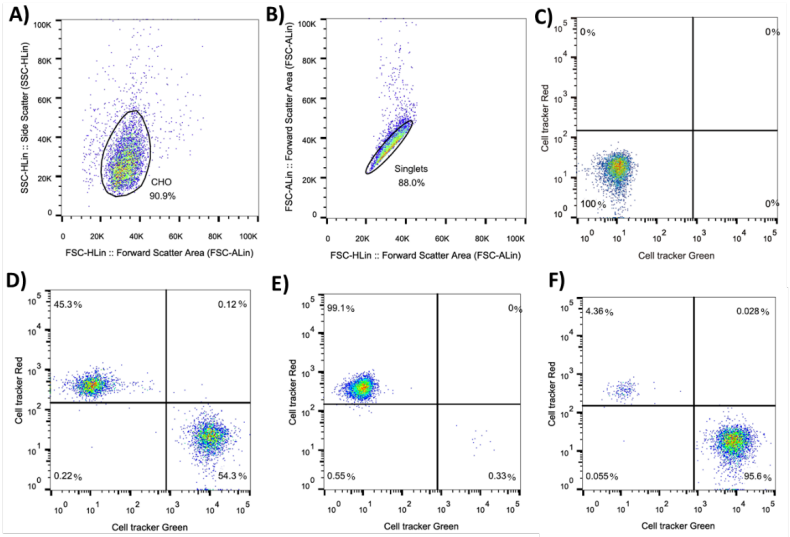

Figure S5. CHO cell sorting using IOPs-E3. A) CHO cell population gated by FSC-H *vs.* SSC-H, B) cell singlets gated by FSC-A *vs.* FSC-H, C) CHO cell without staining, D) CHO cells mixture: green-CPK_3 and red cells, E) cells in supernatant after MACS, F) cells detached from IOPs after MACS. Cell tracker Green: GRN-B, cell tracker Red: RED-B.

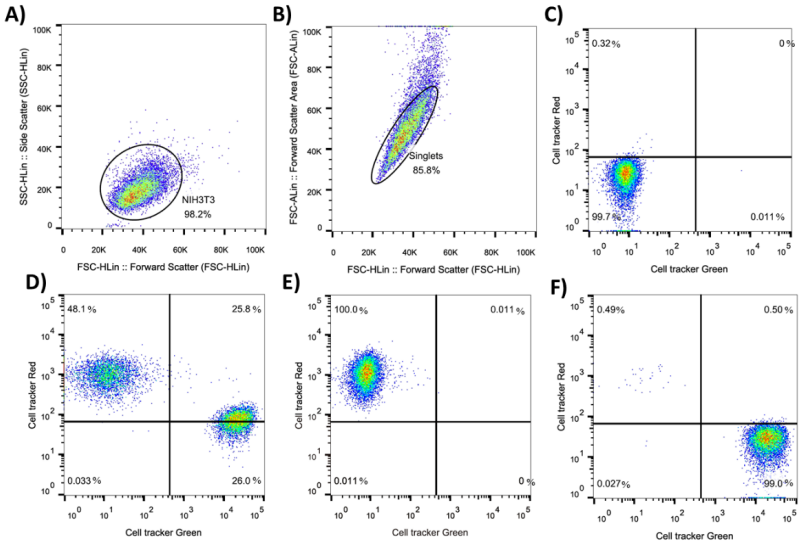

Figure S6. NIH3T3 cell sorting using IOPs-E3. A) NIH3T3 cell population gated by FSC-H *vs.* SSC-H, B) cell singlets gated by FSC-A *vs.* FSC-H, C) NIH3T3 cell without staining, D) NIH3T3 cells mixture: green-CPK_3 and red cells, E) cells in supernatant after MACS, F) cells detached with IOPs after MACS. Cell tracker Green: GRN-B, cell tracker Red: RED-B.

MACS with peptide K_3 functionalized IOPs

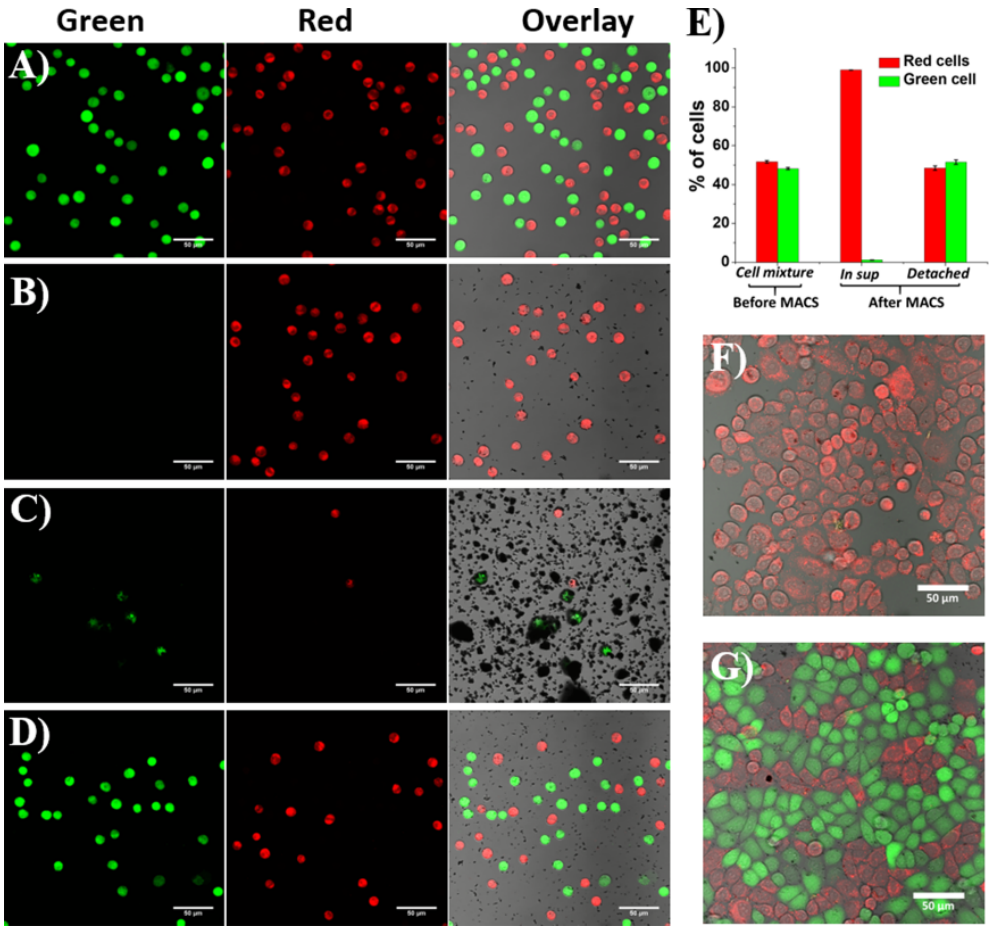

Figure S7. Coiled-coil-assisted MACS of HeLa cells. A) CPE_3-modified HeLa cells stained with CellTracker™ green were mixed with HeLa cells stained with CellTracker™ red; B) cells in the supernatant after MACS; C) IOP-attached cells after MACS; D) detached cells after MACS. Scale bar: 50 µm. E) The bar chart illustrates cell quantification, *via* FACS, before and after MACS. Cells from the supernatant (F) and those detached from the IOPs (G) show signs of recovery and growth after 24 hours. Scale bar: 50 µm.

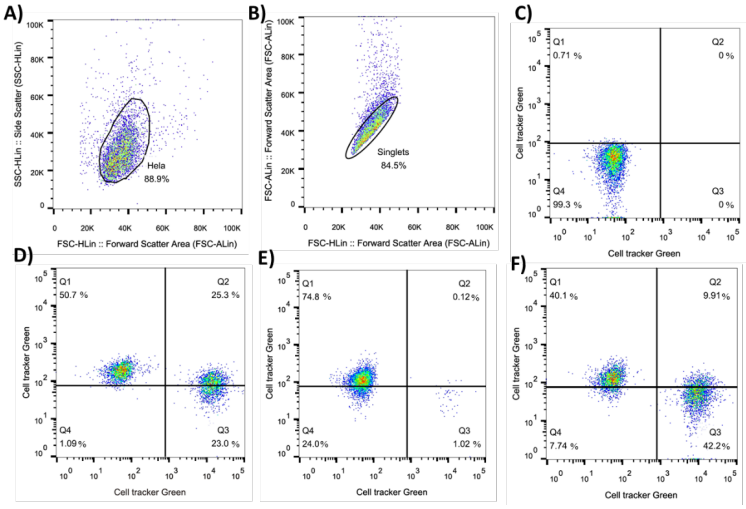

Figure S8. HeLa cell sorting using IOPs-K_3. A) Hela cell population gated by FSC-H *vs.* SSC-H, B) cell singlets gated by FSC-A *vs.* FSC-H, C) HeLa cell without staining, D) HeLa cells mixture: green-CPE_3 and red cells, E) cells in supernatant after MACS, F) cells detached with IOPs after MACS. Cell tracker Green: GRN-B, cell tracker Red: RED-B.

FACS analysis of cell population after MACS with K_3 membrane expressed cells

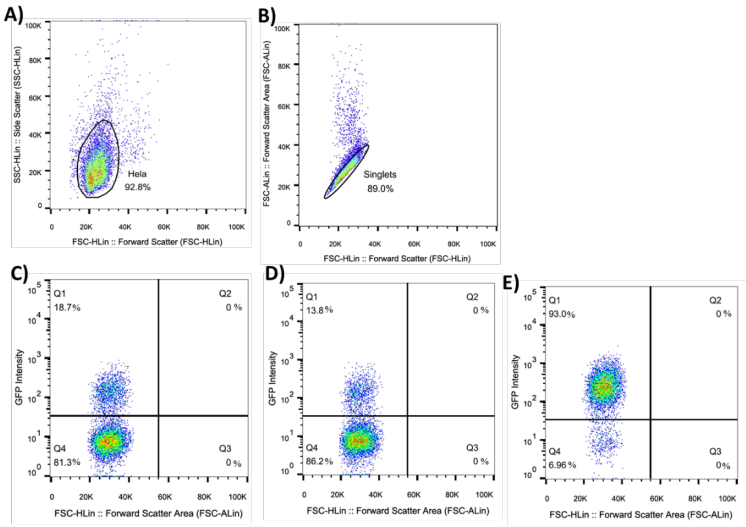

Figure S9. Hela-GFP-K_3 cells enrichment by MACS. A) Hela-GFP-K_3 cell population gated by FSC-H *vs.* SSC-H, B) cell singlets gated by FSC-A *vs.* FSC-H, C) Cells after transfection and two weeks antibiotics selection. D) Cells in supernatant after MACS, E) cells detached from IOPs after MACS. GFP: GRN-B.

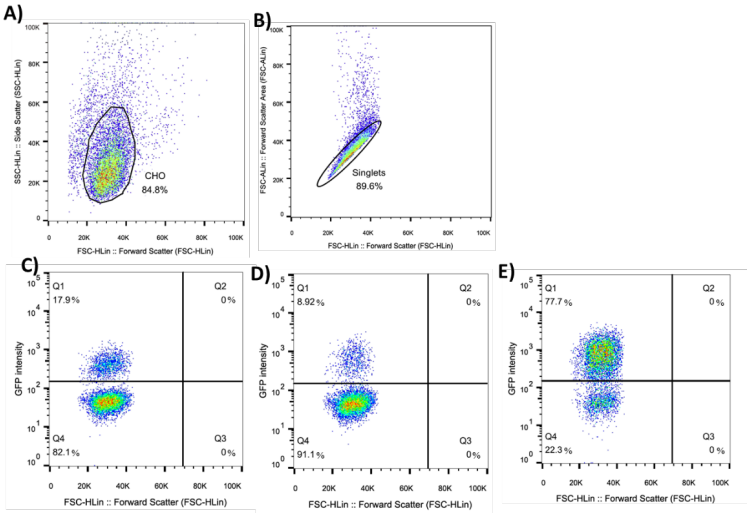

Figure S10. CHO-GFP-K3 cells enrichment by MACS. A) CHO-GFP-K_3 cell population gated by FSC-H *vs.* SSC-H, B) cell singlets gated by FSC-A *vs.* FSC-H, C) Cells after transfection and two weeks antibiotics selection. D) Cells in supernatant after MACS, E) cells detached from IOPs after MACS. GFP: GRN-B.

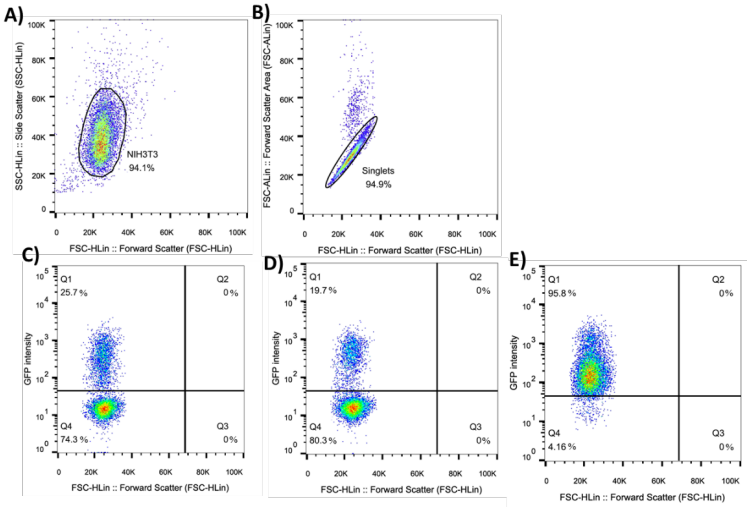

Figure S11. NIH3T3-GFP-K3 cells enrichment by MACS. A) NIH3T3-GFP-K_3 cell population gated by FSC-H *vs.* SSC-H, B) cell singlets gated by FSC-A *vs.* FSC-H, C) Cells after transfection and two weeks antibiotics selection. D) Cells in supernatant after MACS, E) cells detached from IOPs after MACS. GFP: GRN-B.

LCMS data for the synthesized peptides.

Table S1. Calculated mass and found mass via LC-MS of all peptides

peptide	Mass (calcd.)	Mass (found)
CPK_3	2978.0	2977.7
CPE_3	2980.8	2981.2
Ac-K_3GW-PEG_4-Cys	2898.7	2899.2
Ac-E_3GW-PEG_4-Cys	2901.5	2901.2
Fluo-K_3	2969.6	2969.6
Fluo-E_3	2972.5	2972.0
Cy5-E_3	3305.8	3306.8

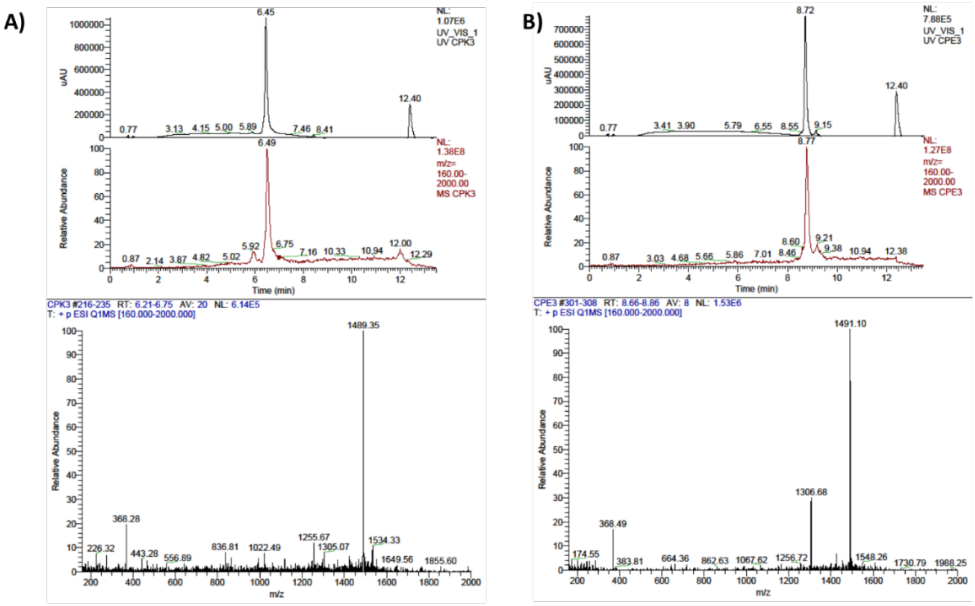

Figure S12. LC-MS of: A) CPK_3 and B) CPE_3.

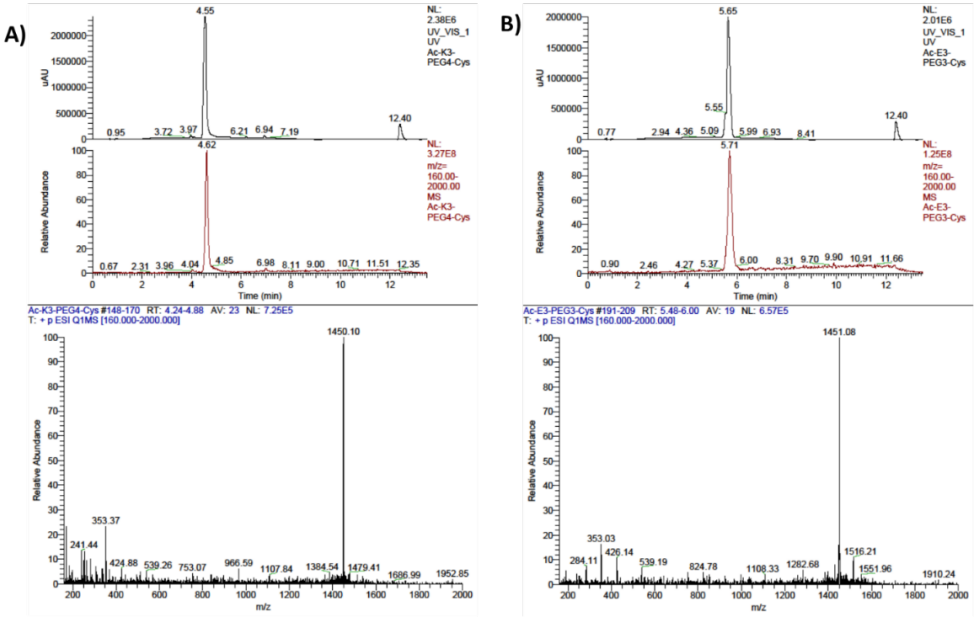

Figure S13. LC-MS of: A) Ac-K_3GW-PEG4-Cys and B) Ac-E_3GW-PEG4-Cys.

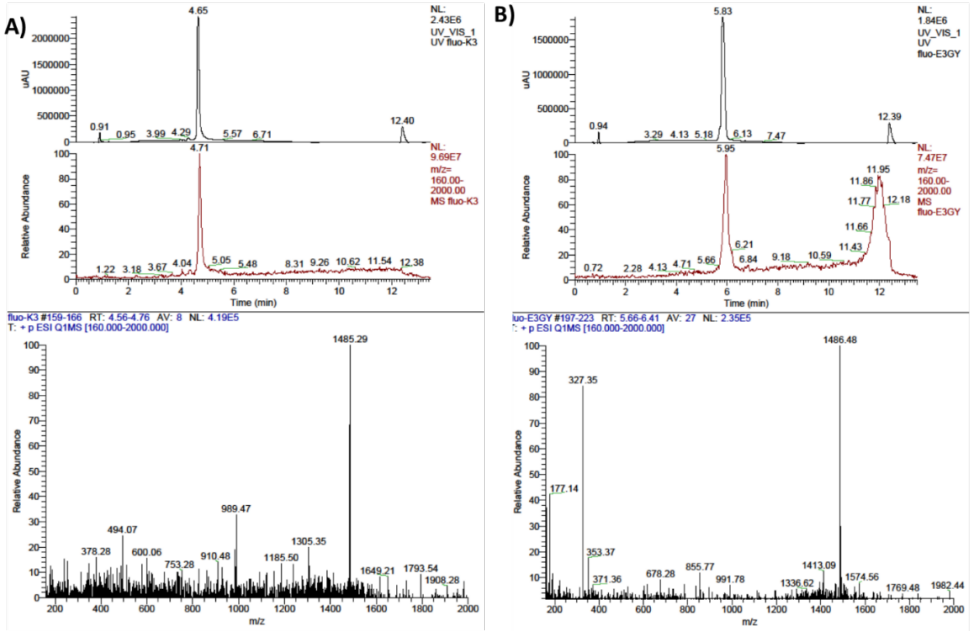

Figure S14. LC-MS of: A) fluo-K_3 and B) fluo-E_3.

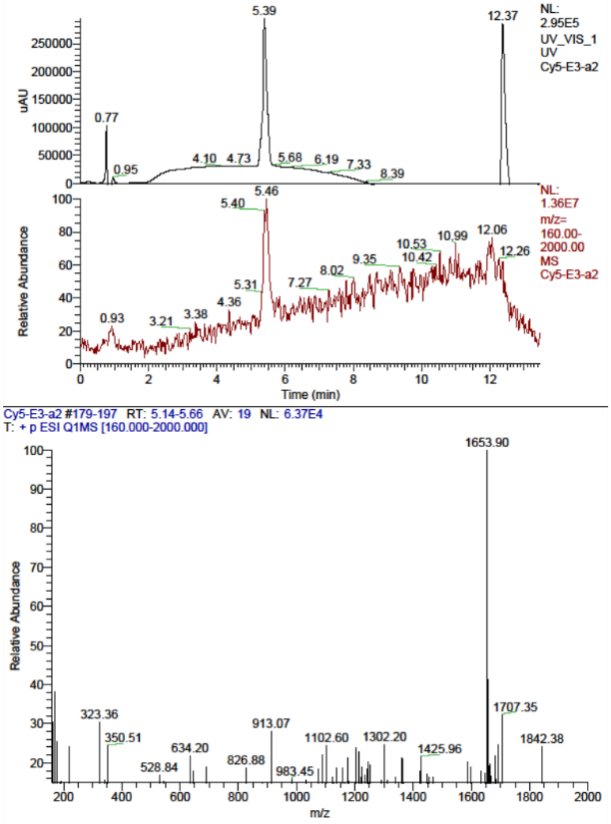

Figure S15. LC-MS of Cy5-E_3.

Synthetic, coating and functionalize IOPs

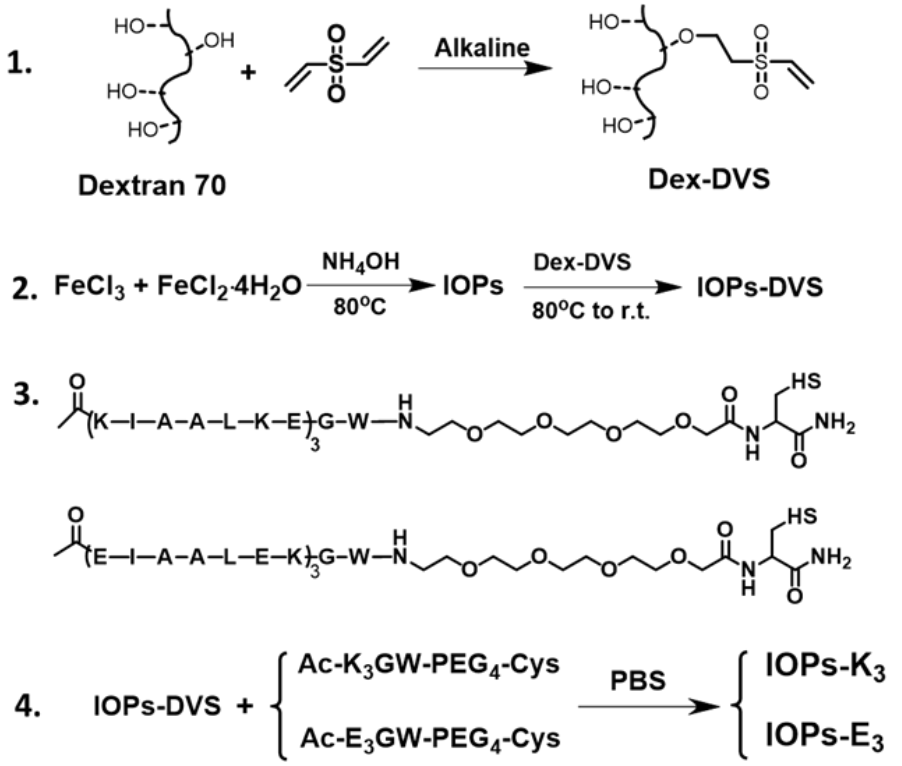

Figure S16. Synthetic route to coiled-coil functionalized magnetic particles: 1. Synthesis of Dex-DVS, the NMR data of Dex-DVS can be seen in Figure S16. 2. Synthesis of micron-sized IOPs and surface coating. 3. Chemical structure of Ac-K_3-PEG_4GW-Cys and Ac-E_3GW-PEG_4-Cys, 4. IOPs-DVS functionalization, coiled coil peptide conjugated to the IOPs-DVS by Michael addition between vinyl sulfone group on dextran-DVS and sulfhydryl group on cysteine.

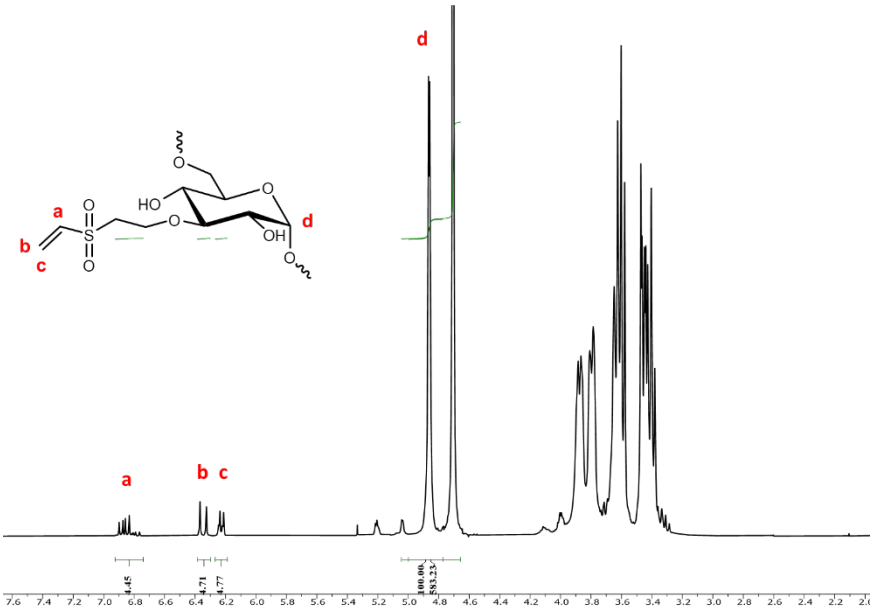

Figure S17. ^{1}H NMR of Dex-DVS used to coat IOPs. ^{1}H NMR (400MHz, D_2O): δ 3.2-4.2 (m, dextran glucosidic protons) 4.9 (s, dextran anomeric proton), 6.8-6.9 (m, -SO_2CH=CH_2), 6.2 (d, -SO_2CH=CH_2), 6.4 (d, -SO_2CH=CH_2). The integral of peak 'd' can be used to define the total number of d-glucopyranose repeating units in dextran. The integrals of peaks 'a' 'b' or 'c' can be used to define the number of vinyl sulfone modified d-glucopyranose repeating units. Here, the integral of peak 'd' has been defined as 100, then the average integral of peaks 'a' 'b' and 'c' can be calculated and this corresponds to the degree of substitution (DS). The DS of the Dex-DVS used in this study is 4.6.

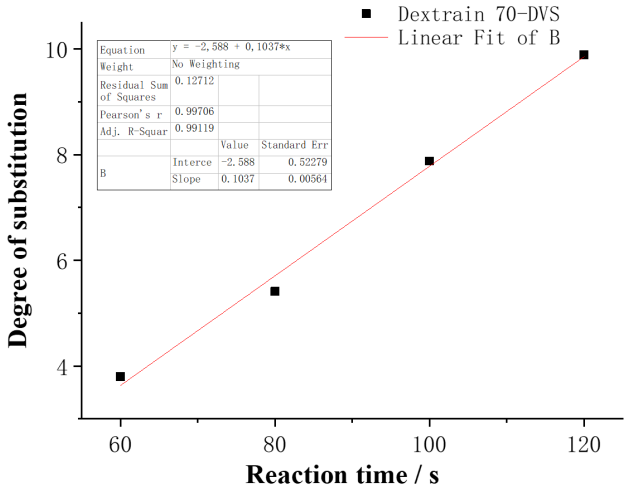

Figure S18. The linear fit which used determine the DS of dextran-DVS with reaction time.

Determination of peptide concentration attached to the IOPs.

The density of peptides conjugated to the IOPs can be calculated using equation 1.

$$\rho = \Delta A \cdot V_1 \cdot 10^6/(\varepsilon \cdot l \cdot m_1) \quad (1)$$

ρ is the density of peptide on the IOPs (nmol/mg), ΔA is the difference in UV-Vis absorption at 280nm before and after IOPs functionalization, V_1 is the volume of peptide solution reacted with IOPs (mL), ε is the molar absorption coefficient of tryptophan at 280nm (M^{-1} cm^{-1}), l is path length of cuvette (cm), m_1 is the mass of IOPs reacted with peptide (mg).

Since the concentrations of peptide used to functionalize IOPs are too high to directly measure, both peptide Ac-E_3GW-PEG_4-Cys and Ac-E_3GW-PEG_4-Cys have been diluted four times before the UV-Vis measurement was performed. The calculated ρ for IOPs-E_3 is 5.5 nmol/mg and for IOPs-K_3 is 5.8 nmol/mg.

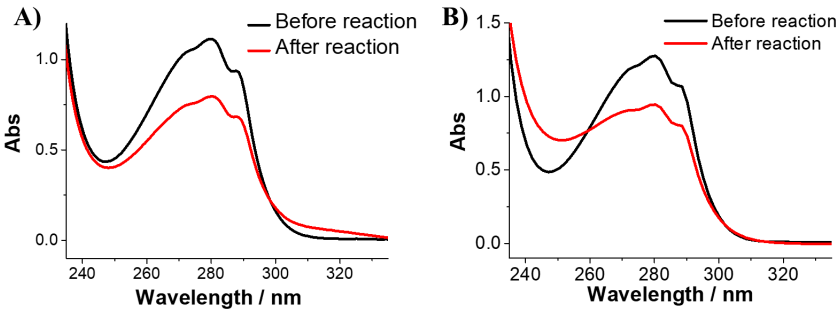

Figure S19. UV-Vis spectra of Ac-E_3GW-PEG_4-Cys A) and Ac-K_3GW-PEG_4-Cys B) before and after reacting with IOPs-DVS.

9. Images of IOPs-E_3

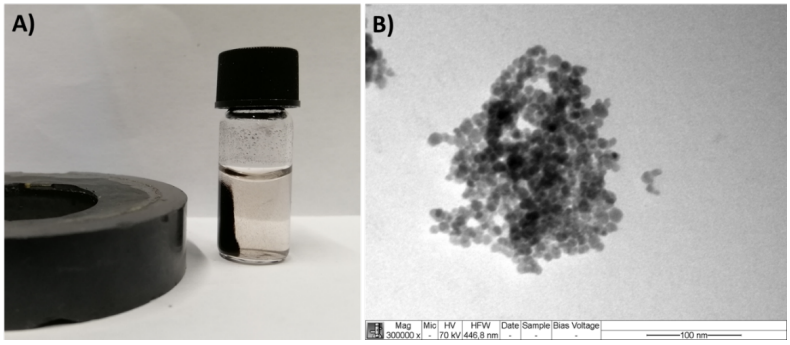

Figure S20. A) Image of IOPs-E_3 with an external magnetic field applied. B) TEM image of IOPs-E_3.

10. Trypsin degradation of peptide Ac-K$_3$GW-PEG$_4$-Cys and Ac-E$_3$GW-PEG$_4$-Cys

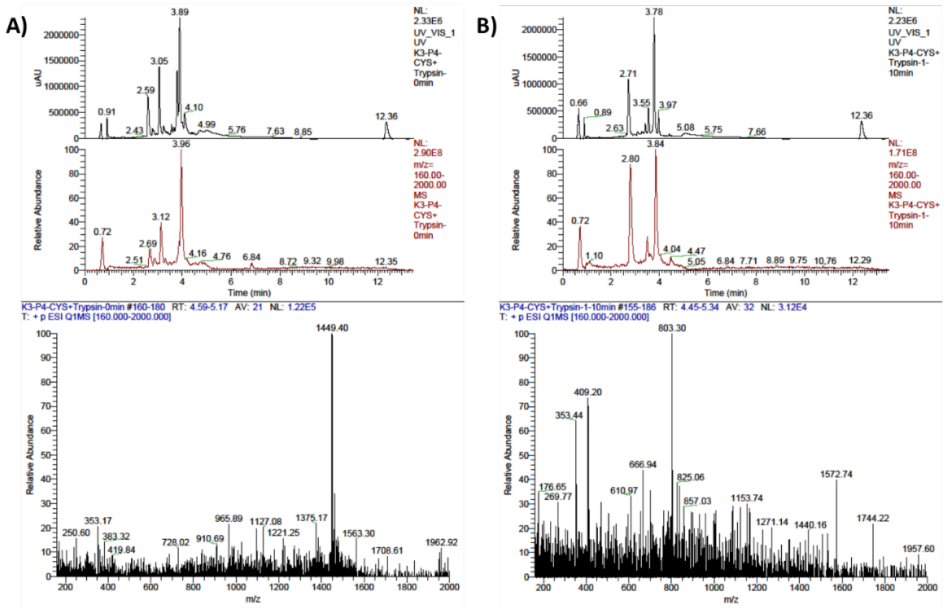

Figure S21. LC-MS of Ac-K$_3$GW-PEG4-Cys digested by trypsin. Ac-K$_3$GW-PEG4-Cys was incubated with trypsin for: A) 0 min and B) 10 min at 37 ℃.

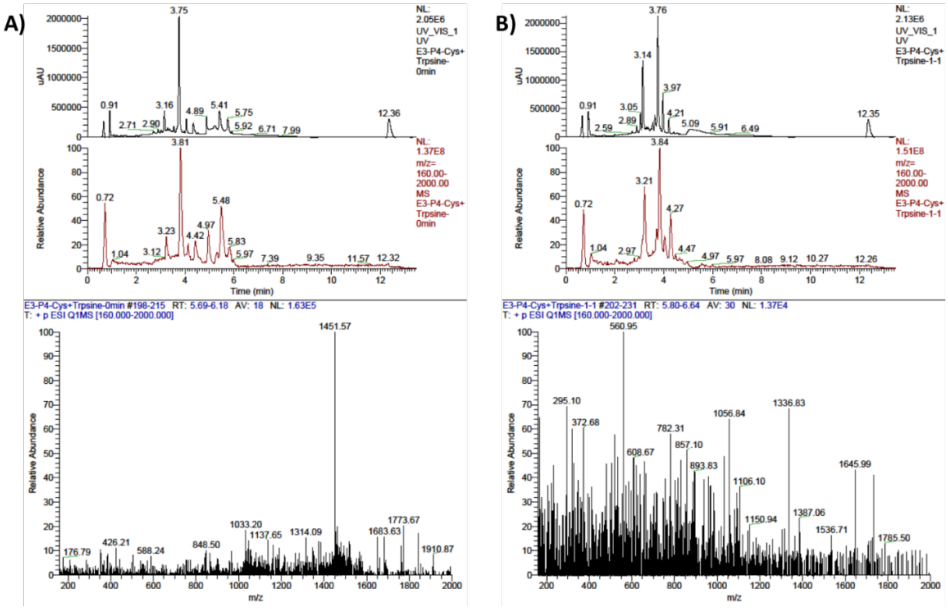

Figure S22. LC-MS of Ac-E$_3$GW-PEG4-Cys digested by trypsin. Ac-E$_3$GW-PEG4-Cys incubated with trypsin for: A) 0 min and B) 10 min at 37 ℃.

11. DNA sequence of the K3-TMD-GFP gene

ggtaccGCCACCATGGAGACAGACACACTCCTGCTATGGGTACTGCTGC
TCTGGGTTCCAGGTTCCACTGGTGACGGTGGgtcgactAAAATAGCCGC
ACTGAAGGAAAAAATCGCTGCGCTGAAGGAGAAGATTGCTGCACTC
AAGGAGgtgaccAACGCTGTGGGCCAGGACACGCAGGAGGTCATCGTG
GTGCCACACTCCTTACCGGTTAAGGTGGTGGTGATCTCAGCCATCCT
GGCCCTGGTGGTGCTCACCATCATCTCCCTTATCATCCTCATCATGCT
TTGGCAGAAGAAGCCACGTGGTGGAtgtacaGTGAGCAAGGGCGAAGA
GCTGTTCACCGGGGTGGTGCCCATCCTGGTCGAGCTGGACGGCGACG
TAAACGGCCACAAGTTCAGCGTGTCCGGCGAGGGCGAGGGCGATGC
CACCTACGGCAAGCTGACCCTGAAGTTCATCTGCACCACCGGCAAGC
TGCCCGTGCCCTGGCCCACCCTCGTGACCACCCTGACCTACGGCGTG
CAGTGCTTCAGCCGCTACCCCGACCACATGAAGCAGCACGACTTCTT
CAAGTCCGCCATGCCCGAAGGCTACGTCCAAGAGCGCACCATCTTCT
TCAAGGACGACGGCAACTACAAGACCCGCGCCGAGGTGAAGTTCGA
GGGCGACACCCTGGTGAACCGCATCGAGCTGAAGGGCATCGACTTC
AAGGAGGACGGCAACATCCTGGGGCACAAGCTGGAGTACAACTACA
ACAGCCACAACGTCTATATCATGGCCGACAAGCAGAAGAACGGCAT
CAAGGTGAACTTCAAGATCCGCCACAACATCGAGGACGGCAGCGTG
CAGCTCGCCGACCACTACCAGCAGAACACCCCCATCGGCGACGGCC
CCGTGCTGCTGCCCGACAACCACTACCTGAGCACCCAGTCCGCCCTG
AGCAAAGACCCCAACGAGAAGCGCGATCACATGGTCCTGCTGGAGT
TCGTGACCGCCGCCGGGATCACTCTCGGCATGGACGAGCTGTATAAG
TAActcgagattaatgcggccgc

Figure S23. The DNA sequence of the K_3-TMD-GFP gene comprises a signal sequence from the mouse IgK gene (yellow), the K_3 peptide (red), a transmembrane domain from PDGFRB (blue), and EGFP (green).

Chapter 3

Investigating the Effect of Peptide Length on Coiled-Coil Stability, Self-Assembly, and Fusogenicity

ABSTRACT

Developing efficient drug delivery methods is challenging, as many rely on the endocytosis pathway to deliver drugs into cells. Unfortunately, the drug release efficiency is often low due to poor lysosomal/endosomal escape. Previously, we developed an efficient drug delivery system based on membrane fusion triggered by coiled-coil peptides to ensure cytosolic delivery of drugs. In this chapter, we investigate the effects of altering the lengths of the coiled-coil forming peptides K_n $(KIAALKE)_n$ and E_n $(EIAALEK)_n$ on membrane fusion. The secondary structure of the peptides was studied and it was found that long peptides (*i.e.* four or five heptads) tend to form homodimers. Also, K_5 and E_5 were found to form higher-order assemblies. Thermal stability studies showed that longer peptides, in both homo- and hetero-assemblies, are more stable than shorter peptides. Liposome membrane fusion assays revealed that the K_4/E_5 coiled-coil pair was optimal in triggering both lipid and content-mixing. Cell-liposome fusion experiments suggested that the K_4/E_4 coiled-coil pair was the most efficient at delivering the model drug propidium iodide (PI) into the cytosol of cells. In summary, this work studied the relationship between coiled-coil stability and peptide fusogenicity and provided further insights into the coiled coil-based membrane fusion system, which may have applications in drug delivery.

INTRODUCTION

Membrane fusion systems have potential applications in drug delivery.[1-3] Traditional drug delivery systems often rely on endosomal escape pathways and an inherent weakness is that the majority of the drug is either degraded or cleared after cell uptake due to lysosomal recycling pathways.[4-6] Therefore the membrane fusion pathway, which permits the direct delivery of molecules into cells, is considered a superior method as it avoids lysosomal pathways resulting in enhanced drug delivery efficiency.[3]

Membrane fusion is a fundamental, widespread process occurring in all cells. Full membrane fusion is characterized by both lipid mixing of the two opposing membranes and content mixing. The process usually contains the following steps: the opposing membranes are forced in close proximity by a given driving force, followed by a 'stalk' intermediate, after which hemifusion occurs resulting in lipid mixing. Finally, a fusion pore is formed resulting in content mixing.[7] Many processes such as embryogenesis,[8-10] *in vivo* vesicular transport,[11-12] and enveloped virus infection[13-15] rely on the occurrence of membrane fusion. As scientists have learned from these natural processes, many artificial membrane fusion systems have been designed which are able to achieve vesicle-vesicle membrane fusion.[16-18] However, very few of these artificial membrane systems are capable of achieving cell-vesicle membrane fusion and are able to deliver molecules into cells.[3, 19]

Coiled coils, a common folding motif in proteins, are widely used in biomaterial design.[20-24] A coiled coil consists of two or more α-helical peptides that are wrapped around each other to form a left-handed supercoil. Due to their folding properties and responsiveness, coiled coil-based building blocks are attractive for developing self-assembling, responsive, and bioactive materials.[21, 25-28]

In previous studies from our group, a coiled coil driven membrane fusion system has been designed.[29-30] The complementary coiled-coil forming peptides K and E were modified with a cholesterol membrane anchor connected via a PEG spacer, (denoted CPK and CPE), which readily insert into a synthetic or biological lipid membrane. By mixing CPK- and CPE-containing liposomes, efficient membrane fusion was achieved. A previous study showed that the liposome membrane fusion efficiency is correlated to coiled-coil stability.[31] For example, cell-liposome membrane fusion assays show that full membrane fusion can be achieved using four-heptad lipopeptides CPK_4 and CPE_4, while only cell-liposome docking was

achieved using three-heptad lipopeptides CPK_3 and CPE_3.[3, 32-34] Therefore, a more stable coiled-coil comprised of peptides with an additional heptad repeat unit may have an even better capacity to induce membrane fusion. Here, we have designed and synthesized the five heptad coiled-coil forming peptides K_5 and E_5. Using circular dichroism (CD) spectroscopy and dynamic light scattering (DLS), we studied the secondary structure, thermostability, and self-assembly of these coiled-coil forming peptides. The membrane fusion efficiency was evaluated by performing lipid and content mixing assays. A cell membrane labelling assay proved that all of these 'K_n' lipopeptides, CPK_3, CPK_4 and CPK_5 can be used to decorate cell membranes. Moreover, we quantitively studied the cell membrane docking efficiency and selected coiled-coil pairs that may induce efficient cell membrane-liposome fusion. For this, the efficiency of delivery of propidium iodide (PI) into cells and nitrobenzoxadiazole (NBD) incorporation in the cell membrane was quantified. We studied the relevance between coiled-coil stability and membrane fusion efficiency, providing a method for predicting and selecting coiled coils which have the greatest potential for membrane fusion and drug delivery.

RESULTS AND DISCUSSION

1. Secondary structure determination and self-assembly of coiled-coil forming peptides K and E

The two complementary peptides used in this study are based on original designs from the Hodges group.[35] These two peptides are rich in lysine and glutamic acid and were named peptide K and peptide E respectively. Peptides K_n $(KIAALKE)_n$ and E_n $(EIAALKE)_n$ were designed to form a heterodimeric coiled-coil, by virtue of the residues that make up the hydrophobic core and their opposing charges.

In this study, we used either three, four or five heptads in E_n/K_n. All the peptides have a 'GW' extension at the C-terminus to facilitate accurate concentration determination (see methods). The sequences of all peptides used in this study are listed in Table 1. All lipopeptides used in this study do not contain the 'GW' tail at the C-terminus and so their concentration was calculated based on their weight.

Table 1. Coiled-coil forming peptides used in this study.

Peptides	Sequence						
	ef	*gabcdef*	*gabcdef*	*gabcdef*	*gabcdef*	*gabcdef*	*ga*
K_3		KIAALKE	KIAALKE	KIAALKE	GW		
E_3		EIAALEK	EIAALEK	EIAALEK	GW		
K_4		KIAALKE	KIAALKE	KIAALKE	KIAALKE	GW	
E_4		EIAALEK	EIAALEK	EIAALEK	EIAALEK	GW	
K_5		KIAALKE	KIAALKE	KIAALKE	KIAALKE	KIAALKE	GW
E_5		EIAALEK	EIAALEK	EIAALEK	EIAALEK	EIAALEK	GW
Flu-K_4[a]	Fluo-GG	KIAALKE	KIAALKE	KIAALKE	KIAALKE	GW	
Flu-E_4[a]	Fluo-GG	EIAALEK	EIAALEK	EIAALEK	EIAALEK	GW	

[a]Fluo-K_4 and Fluo-E4: 5(6)-Carboxyfluorescein conjugated peptide K_4 and peptide E_4.

CD spectroscopy was employed to study the secondary structure of the different coiled-coil forming peptides. In line with the previous study,[31] K_3 and E_3 adopt an unfolded secondary structure, while four and five heptad peptides show a typical helical structure (Figure 1A and Table 2). This is somewhat surprising because the peptides are designed to be unfolded on their own as the presence of charged residues means self-association is disfavored. However, for the longer peptides, the stabilization gained by burying the hydrophobic residues appears to outweigh the destabilizing effects of the repulsive electrostatic interactions. A previous study also showed that both peptides K and E are prone to form homodimers, inducing these peptides to form a helical structure.[36]

The ellipticity ratio between the minima at 222/208 nm can be used to determine whether isolated helices (<0.9) or coiled-coil (>1) structures are formed.[37-38] For all the four and five heptad peptides, the ellipticity ratios at 222/208 nm were > 1.15, suggesting homodimer formation.

Figure 1B shows the thermal melting curves of all peptides. As expected, longer peptides are more stable when heated from 5 to 90°C, reflecting the higher melting temperature (T_m) (Table 2). When comparing peptides with the same number of heptads, the K_4/K_5 peptides are more stable than E_4/E_5 peptides, which is in line with the previous observation that peptide K forms more stable homodimers than peptide E.[39]

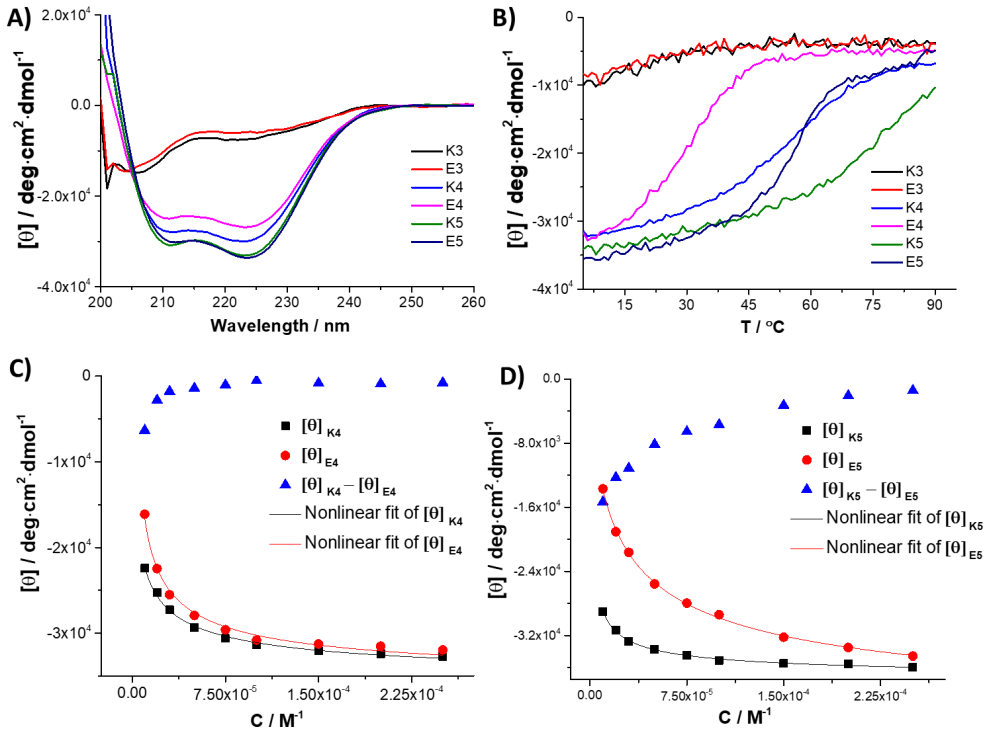

Figure 1. (A) CD spectra of peptides K_n and E_n. (B) Thermal melting curves for the different peptides. (C) Concentration-dependent CD titration of peptides K_4 and E_4. (D) Concentration-dependent CD titration of peptides K_5 and E_5. The non-linear fit curves were obtained based on equation 6. All measurements were performed in PBS (pH 7.2). [Peptide] = 10 μM. All measurements except the melting curve were recorded at 20 °C.

Table 2 Characteristics of peptides K and E with differing numbers of heptads as measured by CD spectroscopy.

	K_3	E_3	K_4	E_4	K_5	E_5
Helicity / % [a]	26	22	89	80	95	96
$[\theta]_{222}$ / $[\theta]_{208}$	0.55	0.50	1.20	1.15	1.22	1.30
Helicity decline / %	62	53	78	85	70	86
T_m / °C [b]	-	-	50	34	77	55

[a]The helicity of all peptides was calculated using equation 5. [b] The T_m was obtained by calculating the first-order derivative of the melting curve using the JASCO spectra analysis software, in which the melting temperature corresponds to the peak maximum of the first-order derivative.

To study homodimer formation of four and five heptad peptides, a titration assay

was performed using CD spectroscopy. Figure 1C shows the CD titration results for the four heptad peptides K_4 and E_4. A non-linear correlation between peptide molar ellipticity and concentration was obtained,[40] revealing that the homodimer is formed in a concentration-dependent manner. The difference in molar ellipticity between peptides K_4 and E_4, as a function of concentration, is remarkable at low concentrations (Figure 1C), while there is almost no difference at high concentrations. This suggests that peptide K_4 forms a homodimer more readily than E_4 at low peptide concentrations. At high peptide concentrations, both peptides tend to homodimerize. For K_5 and E_5, the same trend was observed (Figure 1D). The molar ellipticity of peptide K_5 is consistent at different concentrations, suggesting that homodimer formation occurs at all measured concentrations. In contrast, the helicity of peptide E_5 is strongly concentration-dependent. At high peptide concentrations, peptides K_5 and E_5 have a similar molar ellipticity, suggesting that both peptides are fully homodimerized with a helicity of ~96%. It should be noted that, although the non-linear curve fitting (obtained by equation 14) matches well to the CD data (Figure 1C & 1D), the dissociation constant (K_d) of these peptides could not be determined as the peptides are not fully unfolded even at very low concentrations.

2. Concentration-dependent thermal stability of peptides K_5 and E_5

The thermal stability and concentration-dependent CD titration studies suggest homodimer formation of peptides K_5 and E_5. To further study this, temperature-dependent CD measurements were performed to evaluate the thermal stability of peptides K_5 and E_5 at different concentrations (Figure 2A and 2B). The melting temperature (T_m) was calculated based on the first-order derivative of the melting curve (Figure 2C). For K_5, the T_m increases by 10 °C when the peptide concentration increases from 3 μM to 9 μM, suggesting concentration-dependent thermal stability. Surprisingly, the T_m decreased 5 °C when the peptide concentration was increased further to 12 μM. To investigate whether this could be caused by peptide aggregation, we performed DLS measurements. Indeed, with increasing temperature, the derived count rate (DCR) increased, suggestive of peptide K_5 aggregates at high temperatures. A higher peptide concentration is likely to contribute to the peptide aggregate formation, leading to the apparent T_m decrease of K_5 at a higher concentration. For peptide E_5, a continuous, yet small T_m increase was obtained when the peptide concentration was increased from 3 μM to 12 μM. Since the DCR remained stable as the temperature was increased, it

suggests that E_5 does not aggregate.

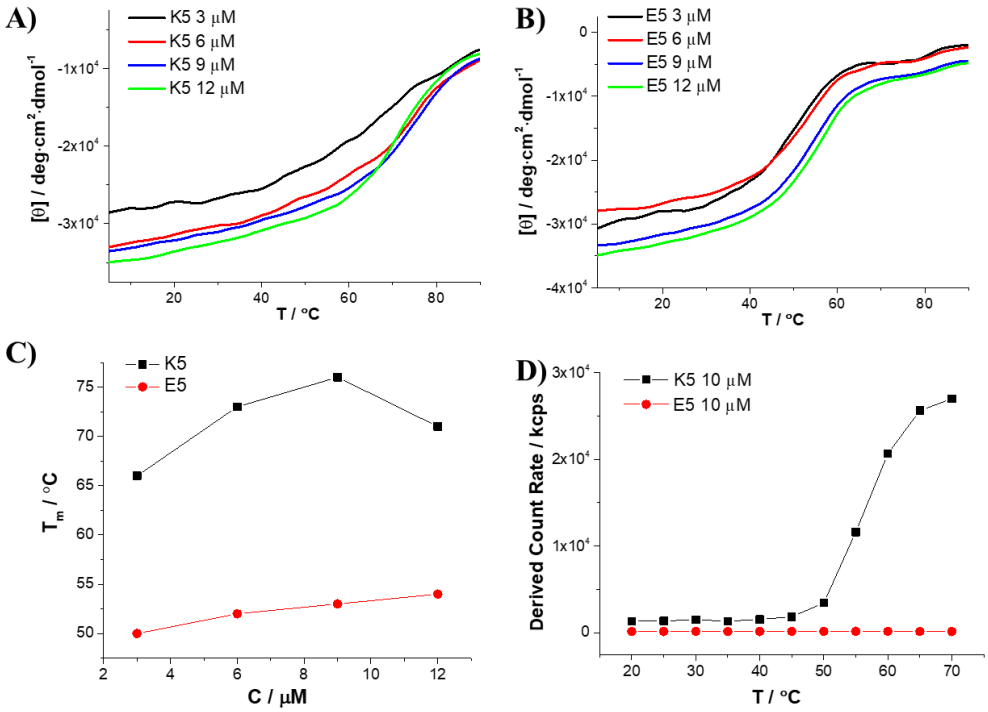

Figure 2. Melting curves of peptide K_5 (A) and E_5 (B) at a different peptide concentration, (C) correlation of peptide melting temperature (T_m) to the peptide concentration, (D) temperature-dependent DCR of peptide K_5 and E_5, measured by DLS. All measurements were recorded in PBS (pH 7.2).

3. Thermal stability of peptides K_5 and E_5 in the presence of GdnHCl

Both K_5 and E_5 were found to be highly thermally stable. To further understand the stability of peptides K_5 and E_5, guanidine hydrochloride (GdnHCl) was used to study the peptide folding stability. GdnHCl is a commonly used protein denaturing reagent of which the mechanism of denaturation is still controversial.[41-43] The generally accepted theory is that GdnHCl affects electrostatic interactions.

Different concentrations of GdnHCl were added to the peptides and the melting curves were measured by CD spectroscopy. It should be noted that the high UV-Vis absorption of GdnHCl can influence the CD spectra at wavelengths < 215 nm (Figure S1), fortunately, the typical α-helix maximum at 222 nm is not affected (Figure S2), which makes monitoring of the peptide unfolding possible. The results show that increasing the concentration of GdnHCl indeed impacts the thermal

stability of both K_5 and E_5, as evidenced by the shift in T_m. Interestingly, in the presence of 1M and 3M GdnHCl the T_m of both K_5 and E_5 increased (Figure 3A & 3B) with the highest T_m for both peptides was found at 1M GdnHCl. For K_5, the T_m decreased (relative to the peptide in the absence of GdnHCl) only when 5M GdnHCl was present. Remarkably, even in 5 M GdnHCl, E_5 is still more stable than in the absence of this reagent. One explanation for this behavior is that at a low concentration of GdnHCl, the Gdn^+ can bind to the negatively charged glutamic acid residues eliminating the charge interactions between peptides. Such a result could contribute to homodimer formation and increase the thermostability of peptides K_5 and E_5. At high concentrations, GdnHCl acts as a classical denaturant that unfolds and destabilizes the peptides, which results in a decrease of the T_m for both peptides. In addition, temperature-dependent K_5 peptide aggregation was not observed in the presence of GdnHCl (Figure 3D).

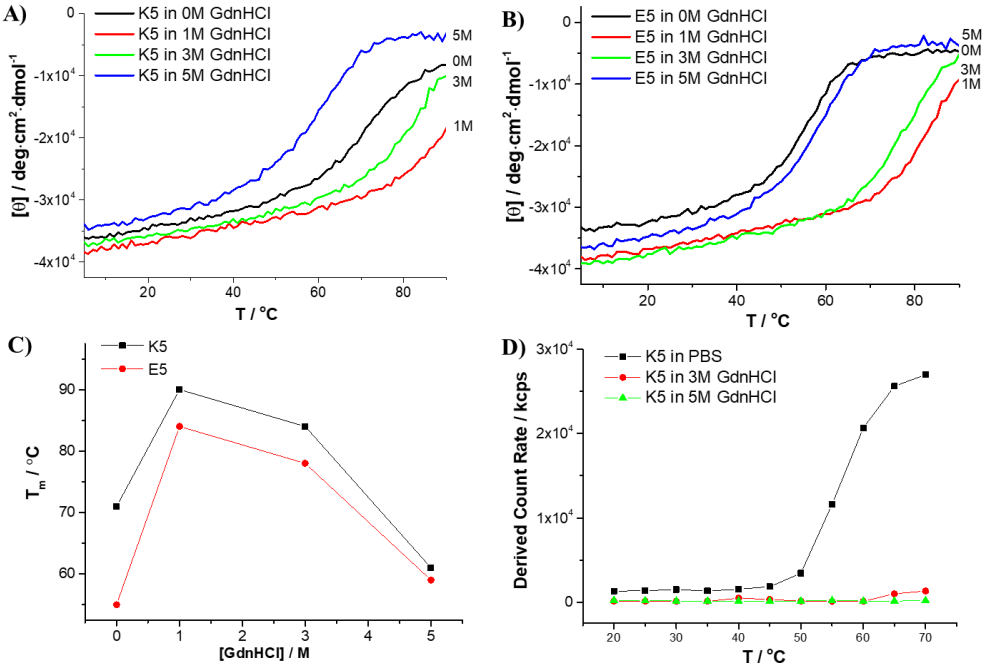

Figure 3. CD melting curves of K_5 (A) and E_5 (B) in the presence of GdnHCl at different concentrations. (C) Correlation of peptide melting temperature (T_m) to GdnHCl concentration. (D) Temperature-dependent DLS study of the effect of GdnHCl on K_5 peptide aggregation formation. Spectra were recorded in PBS (pH 7.2). [Peptide] = 10 μM.

This study shows that GdnHCl influences the thermostability of both peptide K_5 and E_5, possibly by influencing the electrostatic interactions between peptides,

impacting homodimer formation. To study homodimer formation of K_5 and E_5 in the presence of GdnHCl, thermal unfolding experiments were performed at different peptide concentrations in the presence of 3 M or 5 M GdnHCl (Figure 4A & 4B). Next, the T_m was calculated for each melting curve (Figure 4C & 4D). The T_m increased with increasing peptide concentration, suggesting that homodimer formation is still possible in presence of GdnHCl. This suggests that the hydrophobic interactions may not be influenced by the addition of GdnHCl. Moreover, GdnHCl at 3 M seems to decrease the electrostatic interactions between peptides or reduce the repulsion between peptides (for peptide E_5) thus contributing to the stability of the homodimeric coiled-coil.

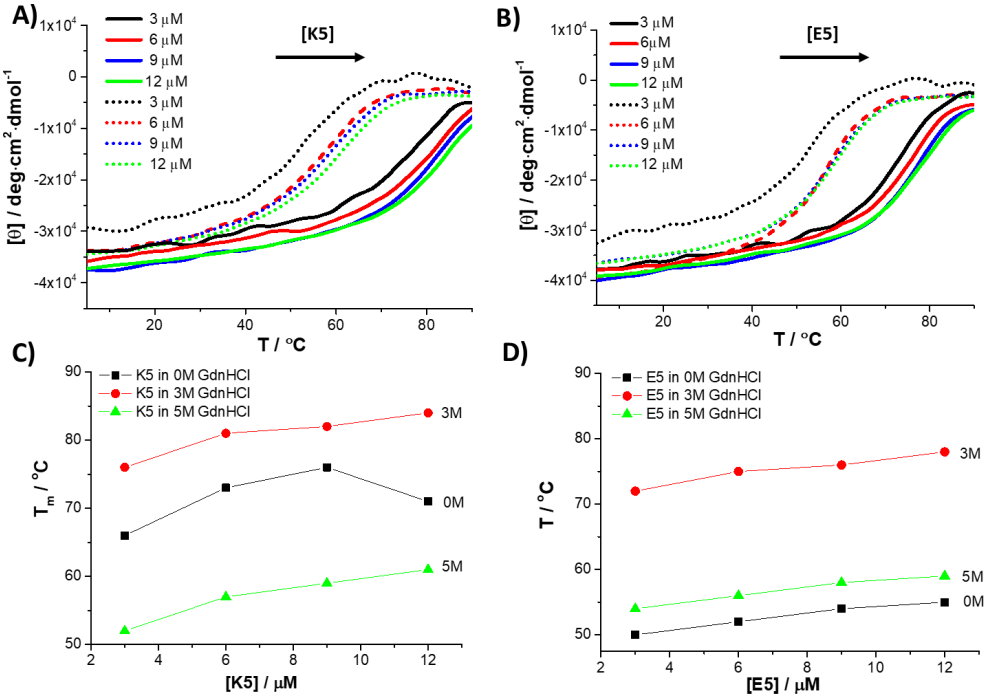

Figure 4. CD melting curves for different concentrations of K_5 (A) and E_5 (B) in presence of 3 M (solid lines) or 5 M (dotted lines) GdnHCl. (C) Correlation of T_m for K_5 (C) and E_5 (D) to peptide concentration with 0 M, 3 M and 5 M GdnHCl. Spectra were recorded in PBS (pH 7.2).

4. E/K coiled coils: thermal stability and self-assembly

Heterodimeric coiled-coil formation of three-, four- and five-heptad peptides was also studied and evaluated by CD spectroscopy (Figure 5A and Table 3). Upon mixing, the unfolded K_3 and E_3 form a helical structure with a high overall helicity

and T_m indicating the peptides form a heterodimeric coiled-coil. A helicity increase was also obtained for the K_4/E_4 mixture, indicating coiled-coil formation. However, no helicity increase was obtained when peptides K_5 and E_5 were mixed because these peptides were nearly fully helical already. An increase in the 222/208 nm ellipticity ratio was achieved, which suggests coiled-coil formation. Support for this comes from the thermal melting experiment of K_5/E_5 as the thermostability increased (Figure 5B).

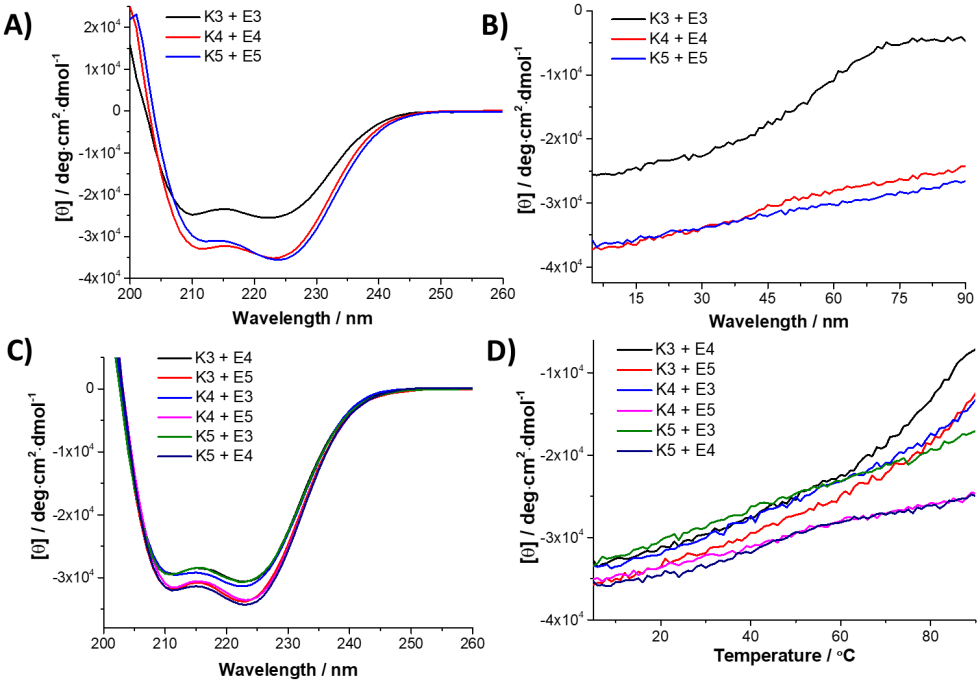

Figure 5. CD spectra of symmetric (A) and asymmetric (C) coiled-coil peptide pairs. CD melting curves of symmetric (B) and asymmetric (D) coiled-coil peptide pairs. All measurements were performed in PBS (pH 7.2) with [peptide] = 10 μM at 20 °C.

Table 3. Characteristics of coiled coils formed by combining E and K peptides of different lengths.

Entry	K_3-E_3	K_4-E_4	K_5-E_5	K_3-E_4	K_3-E_5	K_4-E_3	K_4-E_5	K_5-E_3	K_5-E_4
Helicity / %	72	96	95	85	99	87	91	85	93
$[\theta]_{222}$ / $[\theta]_{208}$	1.10	1.21	1.40	1.16	1.19	1.19	1.23	1.15	1.21
Helicity Decline / %	82	35	26	78	66	60	30	49	29
T_m / °C	58	> 90	> 90	77	> 90	> 90	> 90	> 90	> 90

Asymmetric coiled-coil pairs were also evaluated (Figure 5C and Table 3). Generally, a higher total number of heptad repeats results in a higher helicity of the coiled-coil complex. The thermal stability study reveals that all these coiled-coils have a high thermostability which correlated to the total number of heptad repeats (Figure 5D).

To determine whether high-order assemblies were formed in a mixture of K_5/E_n mixture, DLS experiments were performed to determine the DCR (Figure 6A). For all the individual peptides and all coiled-coil pairs (except for K_5), a low DCR was observed indicative of the absence of large aggregates. Peptide K_5 and K_5/E_n coiled-coils showed only a threefold increase of the DCR in comparison to other peptide monomers, revealing that they tend to form self-assembled peptide aggregates in solution. However, a > 100 fold in the DCR was observed for the K_5/E_5 coiled-coil pair. UV-Vis measurements also indicated particle formation of the K_5-E_5 coiled-coil pair (Figure S3). We speculate that a mismatched, or 'slipped' structure may form in the K_5/E_5 complex due to the long hydrophobic face, resulting in exposed hydrophobic residues inducing the formation of large assemblies. Next, a temperature-dependent DLS assay was performed. The DCR decreased upon increasing the temperature, revealing that K_5/E_5 assemblies are temperature sensitive (Figure 6B). Interestingly, no DCR increase was obtained when the solution was cooled from 90 °C back to 20 °C, indicating that these larger assemblies are kinetic products. We, therefore, hypothesize that large assemblies are formed as a result of slipped coiled-coil formation. However, these assemblies are less stable than an aligned heterodimeric assembly. By increasing the temperature, these kinetically trapped assemblies dissolve and the thermodynamically stable blunt-ended coiled-coil is obtained.

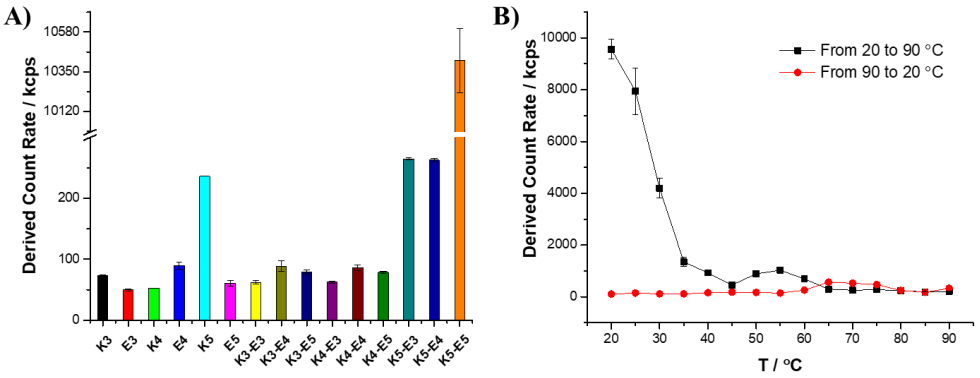

Figure 6. (A) DCR determined by DLS measurements to probe the self-assembly of different peptides and coiled coils at 20 °C. (B) Temperature-dependent DCR of K_5-E_5. The temperature changes at a rate of 1 °C/min and the measurement of each data point takes ~5 minutes. All measurements were recorded in PBS (pH 7.2) with a peptide concentration of 10 µM.

Next, the thermal stability of E_5/K_5 was determined in the presence of GdnHCl. With increasing concentrations of GdnHCl, the thermostability of the coiled-coil complex decreases gradually, as anticipated (Figure 7A & 7B). Due to the high thermal stability of the E_5/K_5 pair, the T_m cannot be accurately determined and was estimated when the GdnHCl concentration was lower than 4 M. The unfolded state of the E_5/K_5 complex was reached only in the presence of 5 M GdnHCl. This differs from the monomer peptides K_5 or E_5 which showed optimal thermal stability at a low GdnHCl concentration (*i.e.* 1 M and 3 M). This further verified our hypothesis that GdnHCl mainly influences the electrostatic interactions between lysines and glutamic acids in heterodimeric coiled coils, thus decreasing the thermal stability.

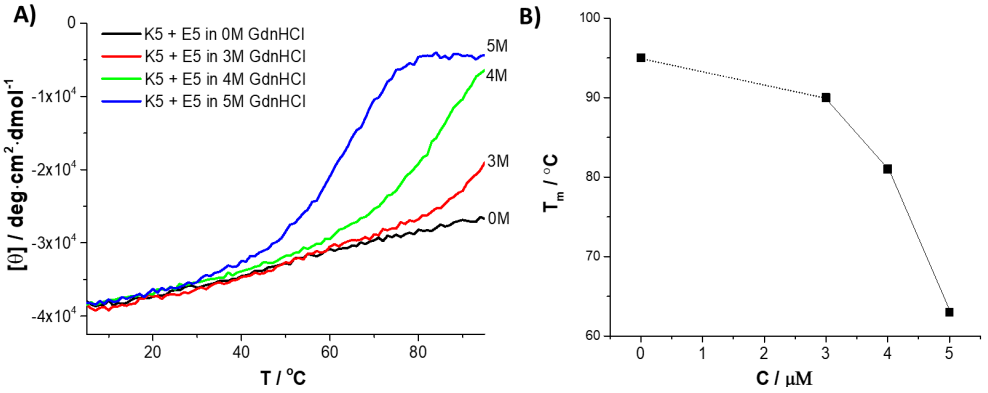

Figure 7. (A) CD melting curves of the K_5-E_5 coiled coil with different concentrations of GdnHCl. (B) Correlation of the K_5-E_5 coiled coil T_m to GdnHCl concentration. All measurements were recorded in PBS (pH 7.2). [K_5 + E_5] = 5 µM + 5 µM.

5. Lipid mixing and content mixing using lipopeptides CPK_n and CPE_n

Liposome membrane fusion represents the process where two vesicles are forced to be close to each other, and then adopt a hemifusion state where lipid mixing occurs, following by content mixing as the final step. Previous studies have shown that the efficiency of K/E induced membrane fusion is related to many factors, including coiled-coil stability.[30-31, 40, 44] The K_5/E_5 coiled-coil pair is more stable than the previously tested pairs and therefore the fusogenicity was studied by performing lipid-mixing and content-mixing assays.

A lipid mixing assay was performed using the Förster resonance energy transfer (FRET) pair of NBD/lissamine rhodamine B (LrB).[30, 40] The NBD-PE and LrB-PE dyes were incorporated into liposomes. Before lipid mixing, the NBD (donor) and LrB (acceptor) fluorophores are in close proximity resulting in FRET and thus a weak NBD emission. When fusion occurs with plain liposomes (*i.e.* liposomes without fluorophores), the average distance between NBD and LrB increases, with concomitant NBD emission increase. Here, nine symmetrical and non-symmetrical coiled-coil combinations were investigated for their ability to promote lipid mixing (Figure 8A-C). The four and five heptad coiled-coil pairs show a higher lipid mixing efficiency than coiled coils containing three heptad peptides, indicating that membrane fusion efficiency is related to coiled-coil stability. Interestingly, the K_5-E_4 coiled coil showed the highest lipid mixing efficiency while the K_5-E_5 coiled coil shows only the fourth-highest lipid mixing efficiency, which suggests that coiled-coil stability is not the only factor determining fusogenicity. Further analysis

of the lipid mixing efficiency (Figure S4A) revealed that by increasing the length of peptide K, lipid mixing also increased. These results support the theory that peptide K plays a crucial role in membrane fusion, whilst the E peptide plays more of a supporting role.[45-46]

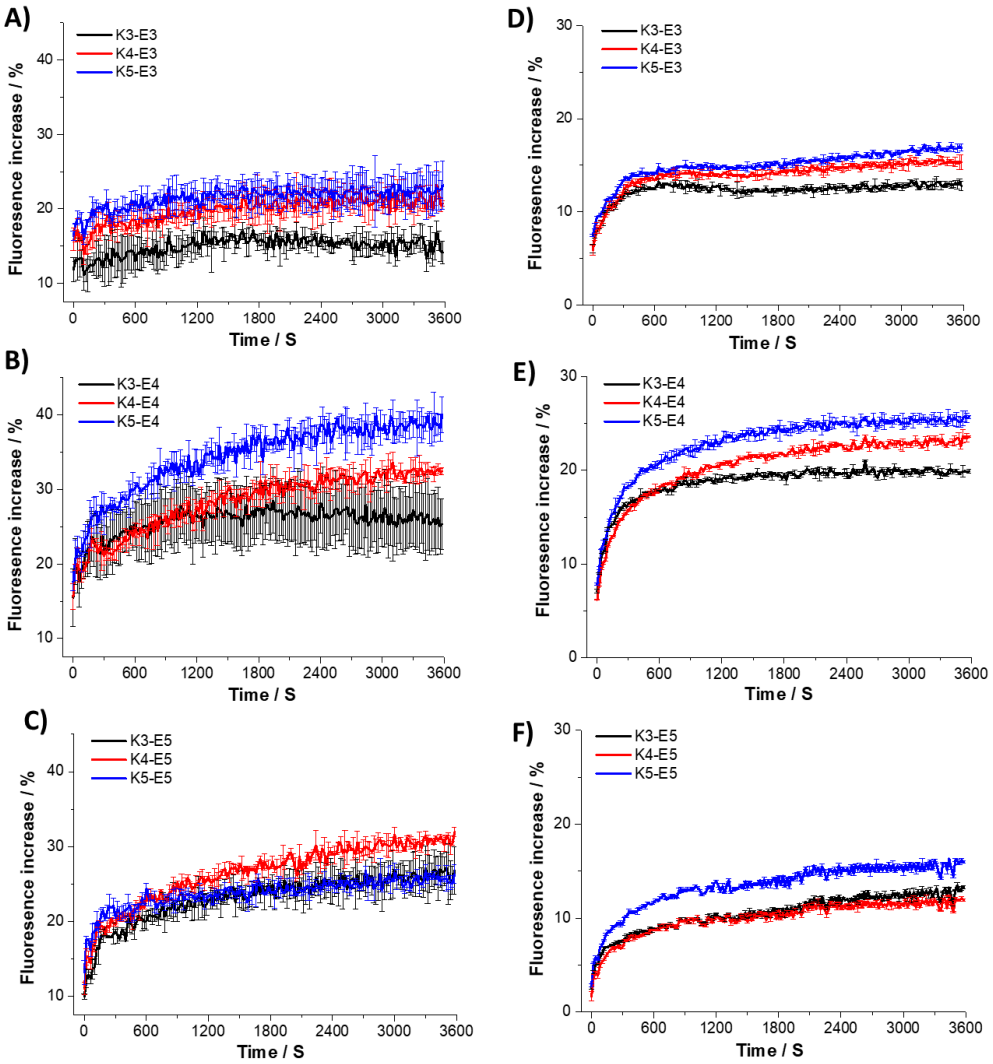

Figure 8. Lipid mixing assays triggered by K_n-E_3 (A), K_n-E_4 (B) and K_n-E_5 (C) coiled-coil pairs (n=3-5). Content mixing assay performed using K_n-E_3 (D), K_n-E_4 (E) and K_n-E_5 (F) coiled-coil pairs.

Efficient content mixing is the hallmark of membrane fusion. For content mixing assays, Sulforhodamine B (SrB) at self-quenching concentrations was encapsulated

into liposomes. Upon fusion with plain liposomes, the SrB will be diluted resulting in a fluorescence increase (Figure 8D-F). The highest amount of membrane fusion was obtained with K_5-E_4, in line with the lipid mixing assay. The total content mixing efficiency analysis (Figure S4B) shows that the content mixing efficiency also increases when using the longer peptide K. For peptide E, the four heptad variant yielded the highest membrane fusion efficiency, while E_5 had the lowest efficiency. This might be due to the fact that peptide E_5 forms a stable homodimer, resulting in a low effective E_5 concentration available to interact with peptide K, resulting in a fusion efficiency decrease.

The overall results of lipid mixing and content mixing show that optimal membrane fusion was obtained using the K_5-E_4 pair. Together with the coiled-coil stability study, it can be concluded that although coiled-coil stability is important for membrane fusion, other factors such as the stability of homodimers and the presence of higher-order assemblies also influence liposome fusion efficiency.

6. Cell Membrane labelling

CPK_3 and CPK_4 were previously used to decorate cell membranes[3, 32] To determine whether CPK_5 is also able to modify cell membranes, a membrane labeling assay was performed. Cells were decorated with CPK_n and the binding of fluorescein labelled E_4 (fluo-E_4) through coiled-coil formation at the cell membrane was studied. As expected, all CPK_n were able to decorate cell membranes and interact with fluo-E_4 (Figure 9). The fluorescence intensity on the cell membrane increased when the cells were decorated with longer CPK_n, revealing the correlation with coiled-coil stability of K_n/E_n (Table 3).

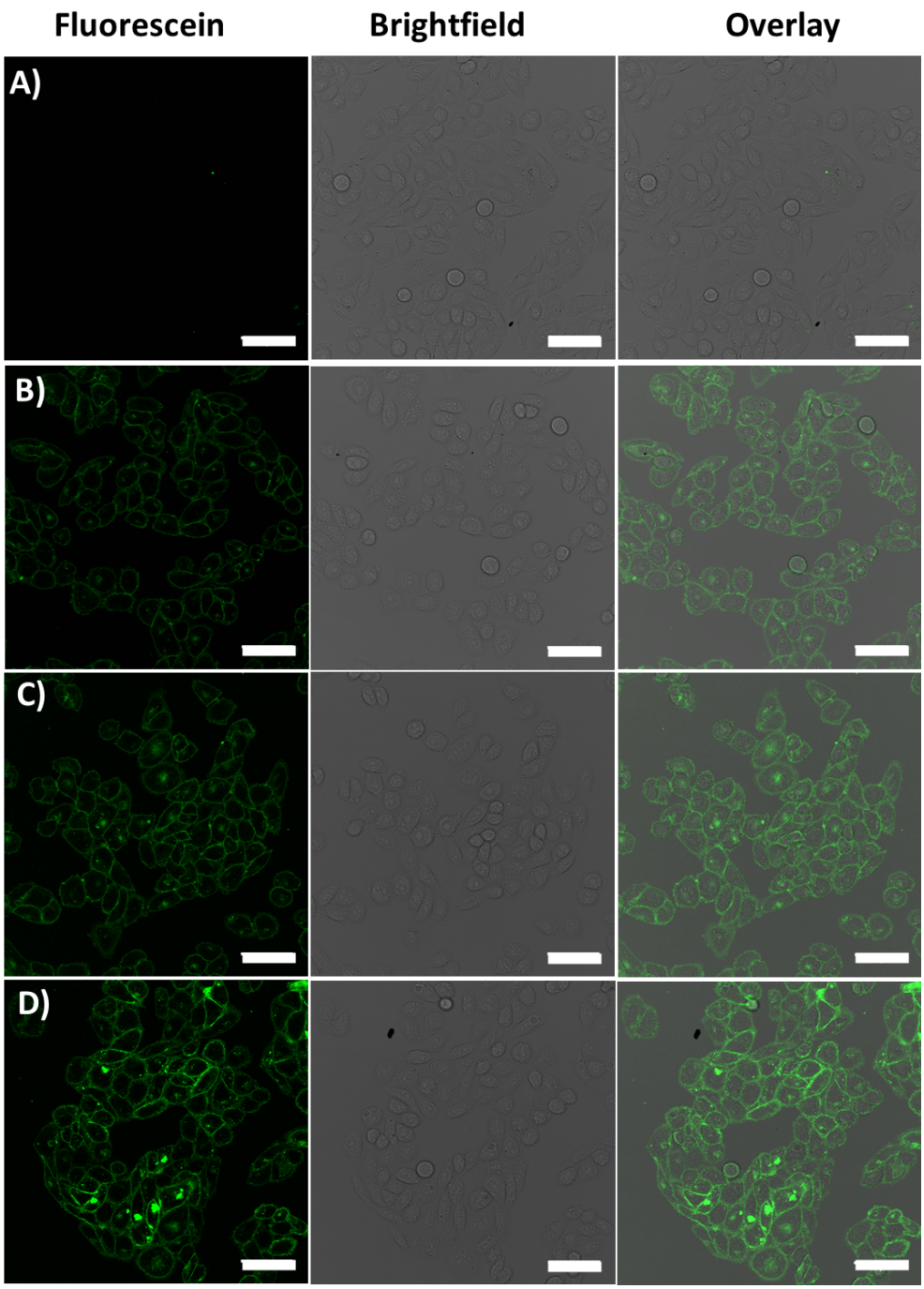

Figure 9. Cell membrane labelling assay. Non-CPK decorated cells incubated with fluo-E_4 (A). Cells incubated with 10 μM CPK_3 (B), CPK_4 (C) or CPK_5 (D) for two hours, following by incubated with fluo-E_4 (20 μM) for 10 minutes. Scale bar: 50 μm. Green: fluorescein.

7. Cell-liposome docking

To investigate cell-liposome membrane fusion triggered by the different coiled-coil pairs, cell-liposome docking was studied as a first step before full membrane fusion was performed.

Hela cells were decorated with CPK_n of varying lengths and treated with CPE_n liposomes labelled with NBD-PE. Cell-liposome docking was quantified using FACS and we determined both the percentage of fluorescent cells and also the mean fluorescence intensity per cell. Efficient fluorescent-labelling of cells with all coiled-coil pairs was observed (Figure 10A). In the absence of CPK_n, < 5% of cells were fluorescently labelled. The mean fluorescence intensity was also measured, showing that the cell-liposome docking efficiency is dependent on the coiled coil used (Figure 10B). Coiled-coils pairs formed by four- and five-heptad peptides exhibit higher mean fluorescence intensities. This might be because the three heptad peptides are shorter, thus coiled-coil formation is hindered due to steric hindrance, or because longer peptides form more stable coiled coils.

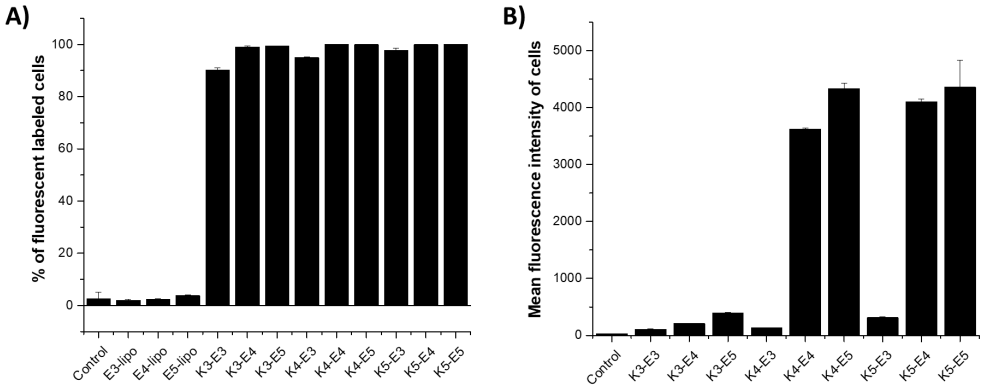

Figure 10. FACS analysis of cells in the cell-liposome docking assay induced by different coiled-coil pairs. (A) Analysis of fluorescent cells (A) and mean fluorescence intensity of fluorescent cells (B).

8. Cell-liposome membrane fusion

The liposome-cell docking assay illustrates that the four and five heptad peptides are most efficient at inducing liposome docking on cell membranes. Next, we investigated the fusogenicity of the coiled-coil pairs which achieved the highest cell-liposome docking. The K_3-E_3 coiled-coil pair was used as a reference. Propidium iodide (PI) is a membrane-impermeable dye, therefore it is a suitable

dye for studying cell-liposome membrane fusion as it cannot enter cells spontaneously.[3] Hela cells were decorated with CPK_n lipopeptides and treated with CPE_n liposomes containing PI. Upon fusion, the nucleus will be stained red. As expected, the CPK_3-CPE_3 coiled-coil pair led to low cell-liposome membrane fusion efficiency as only a weak fluorescence was observed on both the cell membrane and in the nucleus (Figure 11A). Optical cell-liposome fusion was obtained with CPK_n decorated cells and CPE_n liposomes (Figure 11B). Homogenously NBD-labelled cell membranes and a PI-stained cytosol and nucleus were observed. The CPK_4/CPE_5 pair also showed good delivery of PI to the cells (Figure 11C). In contrast, both CPK_5/CPE_4 and CPK_5/CPE_5 coiled-coil pairs showed strong NBD labelling of the cell membrane but weak PI staining (Figure 11D & 11E), resulting in efficient cell-liposome docking but low membrane fusion. Thus CPK_5 decorated cells are able to capture CPE_n modified liposomes efficiently (Figure 11D & 11E), but have limitations in completing fusion and releasing liposomal contents into cells. The CPE_4-modified liposomes did display an advantage over CPE_5-modified liposomes as more homogenous docking on the cell membrane was observed (Figure 11B *vs* 11C and 11D *vs* 11E). This might be due to the fact that CPE_5-modified liposomes contain more negative charges resulting in more repulsion with the negatively charged cell membrane.

The control experiments show that without CPK decoration on the cell membrane or CPE modification on the liposomes, neither cell-liposome docking nor cell-liposome fusion occurred (Figure S5 & S6). Because the lipid composition of a cell membrane is more complex than the liposome membrane, the final cell-liposome membrane fusion efficiency is not the same as the liposome-liposome membrane fusion. In summary, the K_4-E_4 coiled coil is optimal for cell-liposome fusion, while the K_5/E_4 pair is the best choice for liposome-liposome fusion.

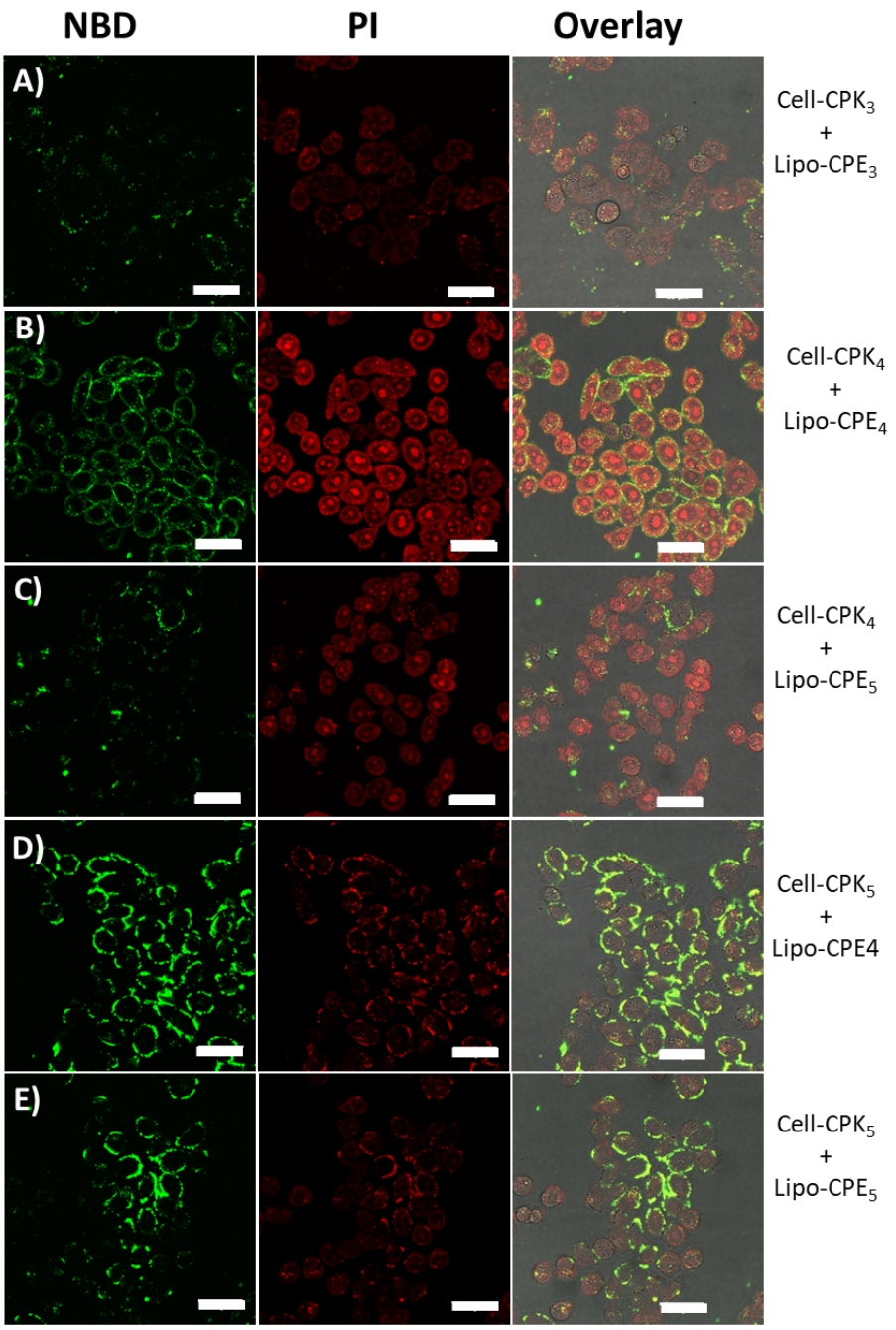

Figure 11. Cell-liposome fusion assay using CPK_n and CPE_n. Cells were treated with CPK_n lipopeptides (10 μM), followed by incubation with different CPE_n-modified liposomes (200 μM) which contained PI inside and NBD-PE on the lipid membrane. Scale bar: 50 μm. Green: NBD, red: PI.

CONCLUSION

In this work, six coiled-coil forming peptides with different numbers of heptad repeat units were designed, synthesized and evaluated. Using CD spectroscopy, the secondary structure of these individual peptides, as well as the heterodimeric coiled coils were studied. As expected, the longer peptides tend to be more helical. We also found that peptide K_5 self-assembles to form peptide aggregates at high temperatures but is soluble at low temperatures. In contrast, an equimolar E_5/K_5 mixture aggregates at low temperatures and becomes soluble at elevated temperatures. These results suggest a complicated self-assembly process for K_5 and the E_5/K_5 coiled coils. Thermal melting curves reveal that both K_5 and E_5 have concentration-dependent unfolding behavior, suggesting possible homodimer formation. The thermostability of K_5 and E_5 increases in the presence of 1M GdnHCl and decreases at higher GdnHCl concentrations. The stability of the E_5/K_5 coiled coil decreases as the GdnHCl concentration increases. This study suggests that GdnHCl may be able to weaken electrostatic interactions between amino acid side chains and influence peptide stability in this manner.

Six lipopeptides with different peptide lengths have been synthesized and membrane fusion assays were performed. The results show that the K_5-E_4 coiled-coil pair is optimal for inducing efficient lipid and content mixing. Cell membrane labeling assays prove that all CPK_n lipopeptides can decorate cell membranes and form coiled coils with the complimentary peptide E_4. By performing cell-liposome docking assays, we found that used of E_n/K_n (n = 4 or 5) coiled-coil pairs resulted in efficient membrane docking. A PI delivery assay suggests that the cell-liposome fusion efficiency was optimal using CPE_4/CPK_4. These results reveal that coiled-coil stability is relevant to membrane fusion, but the fusogenicity of coiled-coil peptides is also influenced by peptide self-assembly and membrane-peptide interactions.

Together, this data provides insights into the most effective coiled-coil pairs for membrane fusion, which may ultimately have applications in drug delivery.

EXPERIMENTAL SECTION

Chemical and Materials

All chemicals were supplied by Sigma and used without further purification unless otherwise stated. Amino acids were purchased from Novabiochem. Tentagel HL RAM resin was obtained from Iris Biotech GmbH. All solvents, as well as piperidine, trifluoroacetic acid, and acetic anhydride, were purchased from Biosolve. Oxyma pure was purchased from Carl Roth GmbH. All lipids were supplied by Avanti Polar Lipids. The Chambered Coverslips for confocal microscopy were purchased from Ibidi (µ-Slide 8 Well). Ultrapure water was obtained by a Milli-Q^{TM} purification system from Millipore (Amsterdam, the Netherlands).

Peptide synthesis

All peptides were synthesized on a CEM Liberty Blue microwave-assisted peptide synthesizer using Fmoc chemistry. 20% piperidine in DMF was used as the deprotection agent. During coupling, DIC was applied as the activator and Oxyma as the base. All peptides were synthesized on a Tentagel S RAM or HL RAM resin (0.39 mmol/g for K_3 and E_3, 0.22 mmol/g for K_4 and E_4, 0.19 mmol/g for K_5 and E_5). The resin was swollen for at least 15 min before use. For each amino acid coupling step, 5 equivalents of the Fmoc protected amino acid (2.5 mL in DMF), DIC (1 mL in DMF) and Oxyma (0.5 mL in DMF) were added to the resin in the reaction vessel and heated to 90 ℃ for 4 minutes. For each deprotection step, 20% of piperidine (4 mL in DMF) was used and heated to 90 ℃ for 1 minute. Between the deprotection and peptide coupling steps, the resin was washed three times using DMF. For the three heptad and four heptad peptides, a single coupling method was used for the synthesis. For five heptad peptides, the single coupling method was used for the first four heptads and a triple coupling method was used for the last heptad.

For peptides used in CD and DLS studies, the N-terminus of the peptides was manually acetylated. To the 0.1 mmol resin-loaded peptide, 3 mL DMF containing 5% acetic anhydride and 6% pyridine was added and shaken for 1 hour at room temperature.

For synthesis of fluo-K_4 and fluo-E_4, two additional glycine residues were coupled to the N-terminus of the peptides on resin, before fluorescein was manually

coupled by the addtion of 0.2 mmol 5(6)-carboxyfluorescein, 0.4 mmol HCTU and 0.6 mmol DIPEA in 3 mL DMF. The reaction was shaken at room temperature overnight.

For lipopeptide synthesis, a poly(ethylene glycol) $(PEG)_4$ linker and cholesterol were coupled manually to the peptide on-resin. To 0.1 mmol of resin-loaded peptide was added 0.2 mmol of N_3-PEG_4-COOH, 0.4 mmol of HCTU and 0.6 mmol of DIPEA in 3 mL DMF. The reaction was performed at room temperature for 5 hours. After thorough washing, 3 mL of 0.5 mmol trimethylphosphine in a 1,4-dioxane:H_2O (6:1) mixture was added to the resin (overnight reaction). Next, the peptide was reacted for 3 hours with cholesteryl hemisuccinate (0.3 mmol) in 3 mL DMF by the addition of HCTU (0.4 mmol) and DIPEA (0.6 mmol).

All peptides were cleaved from the resin using 3 mL of a TFA:triisopropylsilane: H_2O (95:2.5:2.5%) mixture and shaken for 1.5 hours. The peptides were precipitated by pouring the reaction mixture into 45 mL cold diethyl ether (-20 ℃) and isolated by centrifugation. The crude peptides were redissolved in H_2O (20 mL) and lyophilized.

For lipopeptide cleavage from the resin, 3 mL of a TFA:triisopropylsilane (97.5:2.5%) mixture was added and shaken for one hour. The crude lipopeptides were precipitated by pouring the reaction mixture into 45 ml of cold diethyl ether: n-hexane (1:1) and isolated by centrifugation. The pellet of the lipopeptides was redissolved in H_2O (20 mL) containing 10% acetonitrile and freeze-dried to yield a white powder.

Peptide purification

All peptides were purified with reversed-phase HPLC on a Shimazu system with two LC-8A pumps and an SPD-20A UV-Vis detector. A Kinetix Evo C18 column (21.2 mm diameter, 150 mm length, 5 μm particle size) was used for purification of all peptides. For the K_3, K_4, and K_5 peptides, a linear gradient from 20 to 45% acetonitrile in water (with 0.1% TFA) with a 12 mL/min flow rate over 28 mins was used. For the E_3, E_4, E_5 and fluo-E_4 peptides, a linear gradient from 20 to 55% was used. For lipopeptide purification, a Vydac C4 column (22 mm diameter, 250 mm length, 10 μm particle size) was used. All CPK lipopeptides were purified using a linear gradient from 20 to 65 % acetonitrile in water (with 0.1% TFA) with a 12 mL/min flow rate over 36 mins. All CPE lipopeptides were purified using a linear gradient from 20 to 75 % acetonitrile in water (with 0.1% TFA) with a 12

mL/min flow rate over 36 mins.

After HPLC purification, peptides were lyophilized yielding a white powder. The purity of all peptides was determined by LC-MS (Figure S7-S12, Table S1). The LC-MS results of CPK_3 and CPE_3 are shown in **chapter 2** of this thesis.

LC-MS analysis

LC-MS analysis was performed on a Thermo Scientific TSQ quantum access MAX mass detector connected to Ultimate 3000 liquid chromatography system fitted with a 50x4.6 mm Phenomenex Gemini 3 μm C18 column. LC-MS spectra were recorded using a linear gradient of 10-90% acetonitrile in H_2O with 0.1% TFA.

CD Spectroscopy

All CD measurements were performed on a JASCO J-815 CD spectrometer equipped with a Peltier temperature controller. All peptide stock solutions and measurement solutions were prepared in PBS. An 8 M GdnHCl stock solution was prepared in PBS. Unless otherwise specified, all CD measurements were performed at 20 ℃ in a 2 mm path length quartz cuvette. Datapoints were recorded from 190 nm to 260 nm wavelength with a 1 second response time and 2 nm bandwidth. The scanning speed was 200 nm/min and an average of five sequential spectra was recorded. For the concentration-dependent CD titration assay, the measurements were performed using a low sensitivity setting. Samples were prepared in a 1 mm path length quartz cuvette. All other parameters were the same as above. The initial concentration of each peptide was 250 μM and was diluted stepwise to 10 μM. For temperature-dependent CD measurements, the ellipticity at 222 nm was recorded from 5 ℃ to 90 ℃ at a rate of 60 ℃/h. Data points were recorded every 1 ℃ with a delay time of 3 seconds. The T_m was obtained by calculating the first-order derivative of the melting curve using the JASCO spectra analysis software, in which the melting temperature corresponded to the peak maximum of the first-order derivative of the melting curve.

All the spectra and melting curves were normalized to mean residue ellipticity using equation 1:

$$[\theta] = (1000 \times [\theta]_{obs})/(cnl) \quad (1)$$

Where $[\theta]$ represents the mean residue ellipticity in deg·cm^2·dmol^{-1}, $[\theta]_{obs}$ is the observed ellipticity in mdeg, c represents the peptide concentration in mM, n is the

number of amino acids in the peptide sequence and l represents the path length of the cuvette in mm.

The percentage of helicity of the peptides (F_{helix}) was calculated by equations 2 to 5:[47]

$$[\theta]_{max} = [\theta]_{\infty}(n - x)/n \quad (2)$$

$$[\theta]_{\infty} = (-44000 + 250T) \quad (3)$$

$$[\theta]_0 = 2220 - 53T \quad (4)$$

$$F_{helix} = 100\% \, ([\theta]_{222} - [\theta]_0) / ([\theta]_{max} - [\theta]_0) \quad (5)$$

In equation 2, $[\theta]_{max}$ is the maximum theoretical mean residue ellipticity, n is the number of the amino acids in the peptide sequence, x is the empirical constant which represents the number of amino acids that cannot contribute to the helicity due to the end fraying effect (usually between 2.4 to 4), for this work, x is 4. $[\theta]_{\infty}$ is the theoretical helicity of an infinite α-helix which can be calculated with equation (3). T is the temperature in ℃. $[\theta]_0$ is the mean residue ellipticity of the peptide when the peptide is in an entirely random coil conformation. $[\theta]_{\infty}$ and $[\theta]_0$ are temperature-dependent. $[\theta]_{222}$ represents the mean residue molar ellipticity of peptide at 222 nm.

The temperature-dependent CD was performed with the same instrument, using the same cuvette. Melting curves of all peptides were obtained by recording the ellipticity at 222 nm from 5 ℃ to 95 ℃ with a 1 ℃ data pitch and with a 60 ℃/h temperature ramp. The delay time for each data point was 2 seconds.

CD concentration-dependent titrations

Peptide monomers were dissolved in PBS at 250 μM and diluted gradually to lower concentrations (200 μM, 150 μM, 100 μM, 75 μM, 50 μM, 30 μM, 20 μM, 10 μM). Concentration-dependent CD spectra were recorded and the molar ellipticity at 222 nm was measured to calculate the helicity.

The nonlinear fitting and the peptide homodimerization calculation was obtained by employing the following equations:[40]

$$2P_m \leftrightarrow P_d \quad (6)$$

$$K_a = \frac{1}{K_d} \quad (7)$$

$$\mathrm{K_d} = \frac{[\mathrm{P_m}]^2}{[\mathrm{P_d}]} \quad (8)$$

$$[\mathrm{P_t}] = [\mathrm{P_m}] + 2[\mathrm{P_d}] \quad (9)$$

$$[\mathrm{P_t}] = [\mathrm{P_m}] + \frac{[\mathrm{P_m}]^2}{\mathrm{K_d}} \quad (10)$$

$$[P_m] = \frac{K_d}{4}\left(-1 + \sqrt{1 + \frac{8[P_t]}{K_d}}\right) \quad (11)$$

where $[\mathrm{P_m}]$ and $[\mathrm{P_d}]$ is the concentration of the monomeric and homodimeric peptide in mol/L. $[\mathrm{P_t}]$ is the total concentration of peptide in mol/L and $\mathrm{K_d}$ is the dissociation constant.

$$[\theta] = \frac{[\mathrm{P_m}][\theta_\mathrm{m}] + 2[\mathrm{P_d}][\theta_\mathrm{d}]}{\mathrm{P_t}} \quad (12)$$

$$[\theta] = \frac{[\mathrm{P_m}][\theta_\mathrm{m}] + \frac{2[\mathrm{P_m}]^2}{\mathrm{K_d}}[\theta_\mathrm{d}]}{\mathrm{P_t}} \quad (13)$$

$$[\theta] = \frac{\mathrm{K_d}\left(-1+\sqrt{1+\frac{8[\mathrm{P_t}]}{\mathrm{K_d}}}\right)\{2[\theta_\mathrm{m}] + \left(-1+\sqrt{1+\frac{8[\mathrm{P_t}]}{\mathrm{K_d}}}\right)[\theta_\mathrm{d}]\}}{8[\mathrm{P_t}]} \quad (14)$$

The normalized mean residue molar ellipticity can be calculated by equation 14, where $[\theta]$ represents the total normalized mean residue molar ellipticity at 222 nm wavelength, $[\theta_m]$ represents the normalized mean residue molar ellipticity contributed by the monomeric peptide and $[\theta_d]$ is the normalized mean residue molar ellipticity contributed by the homodimeric peptide. The non-linear binding curve can be fitted based on equation 14.

DLS

DLS measurements were recorded on a Zetasizer Nano S (Malvern Instruments, Malvern, UK) fitted with a green laser (532 nm). The derived count rate (DCR) measurements were performed using the non-invasive backscatter mode (automatic mode), detecting the scattered light at 175°. Room temperature measurements were recorded in a low volume cuvette (Brand, Wertheim, Germany) while temperature-dependent measurements were performed in a PCS8507 glass cuvette (Malvern). Temperature-dependent DLS data were collected from 20 ℃ to 90 ℃ and then

reversed from 90 ℃ to 20 ℃ at a rate of 1 ℃/min. Data points were recorded every 5 ℃ and all measurements were performed in duplicate.

UV-Vis

UV-Vis spectra were measured on an Agilent cary 300 spectrophotometer fitted with an Agilent temperature controller. Spectra were measured at 20 ℃ in a 1 cm quartz low-volume cuvette, using a scanning speed of 100 nm/min. Baseline correction was performed using the same solvent for sample preparation. The concentration of peptides for spectroscopy measurements are determined by using equation 15:

$$c = (A_{280} \times 10^6)/(5689 \times l) \quad (15)$$

Where c represents the concentration of mearsured peptide in μM, A_{280} represents the UV-Vis absorption at 280 nm, l is the path length of the cuvette in cm.

Lipid mixing and content mixing assays

Lipid mixing and content mixing assays were performed in black 96-well plates and the fluorescence change was recorded using a TECAN Infinite M1000 Pro microplate reader. A 10 mM lipid stock containing DOPC/DOPE/cholesterol (2:1:1) in $CHCl_3$/MeOH (1:1) was used for all liposome membrane fusion assays. All lipopeptides were dissolved in $CHCl_3$/MeOH (1:1) with a final concentration of 100 μM. DOPE-Nitrobenzoxadiazole (DOPE-NBD) and DOPE-Lissamine rhodamine B (DOPE-LrB) were dissolved in $CHCl_3$ with a final concentration of 1 mM.

For lipid mixing assays, four different batches of liposomes were prepared. Liposomes were prepared in 20 mL glass vials at [lipid] = 500 μM and 1 mL volume. For the first batch, a lipid film containing 99% lipids and 1% of lipopeptide K (CPK_3, CPK_4, and CPK_5) was used. For the second batch, the lipid film contained 98% lipids, 0.5% DOPE-NBD, 0.5% DOPE-LrB and 1% lipopeptide E (CPE_3, CPE_4 and CPE_5). The third batch contained 99.5% lipids, 0.25% DOPE-NBD and 0.25% DOPE-LrB. Plain liposomes were also prepared as a control sample. All lipid films were dried under N_2 for 2 hours, followed by

vacuum desiccation for 30 mins. Lipid films were rehydrated with 1 mL PBS, vortexed for 30 seconds and sonicated at 55 ℃ for 3 mins in a Branson 2510 bath sonicator. The quality of the liposomes (size and polydispersity) was assessed by DLS. Liposome with a hydrodynamic diameter of 100 nm with a PDI < 0.3 were used in the lipid- and content-mixing assays. All liposomes were diluted to [total lipid] = 200 μM before use.

For the lipid-mixing assays, 100 μL of liposomes from batch 1 were mixed with 100 μL of liposomes from batch 2 and the NBD emission at 530 nm was measured over time immediately after mixing. 200 μL of liposomes from batch 3 were used as the positive control, which contains the same amount of NBD/LrB but in double the amount of liposomes. The negative control for the assay was prepared by mixing 100 μL of liposomes from batch 2 with 100 μL of free liposomes. The experiment was performed in triplicate with liposomes from the same batch and repeated at least twice with liposomes from different batches. The lipid mixing efficiency was calculated using equation 16.

$$\%F_t = 100\% \times (F_t - F_0)/(F_{max} - F_0) \quad (16)$$

Where F_t represents the real-time fluorescence intensity, F_0 and F_{max} are the fluorescence intensity from the negative control and positive control respectively at the same time point.

Content mixing was performed in a similar manner. Three batches of liposomes were prepared. Batch 1 liposomes contained 99% lipid and 1% CPK_n. Batch 2 liposomes contained 99% lipid and 1% CPE_n and these are loaded with 20 mM Sulforhodamine B (SrB) . Batch 3 liposomes contained 99% lipid and 1% CPE_n and these were loaded with 10 mM Srb. Plain liposomes were prepared for control experiments. All batches of liposomes were prepared using the sonication method at [total lipid] = 500 μM. SRb liposomes were purified using a Illustra NAP-25 size-exclusion column to remove the non-encapsulated dye. All liposomes were diluted to [lipid] = 200 μM before use. The assay was performed by mixing 100 μL of liposomes from batch 1 and 100 μL of liposomes from batch 2 while measuring SRb emission at 585 nm. Batch 3 liposomes were used as the positive control. As negative control, 100 μL of liposomes from batch 2 were mixed with 100 μL of plain liposomes. The experiment was performed in triplicate with liposomes from the same batch and repeated at least twice with liposomes from different batches. The content mixing efficiency was calculated with equation 15.

Membrane labelling

100 μL CPK_n (100 μM in $CHCl_3$/MeOH (1:1) was transferred to a 20 mL glass vial and dried to a film under an N_2 flow, followed by drying in a vacuum desiccator for 30 mins. 1 mL of DMEM (with 10% of FCS) was added and sonicated for five minutes, resulting in lipopeptide micelles.

Hela cells were seeded in an μ-Slide 8 Well with a cell number of $5x10^4$ cells per well for 20 hours. CPK_n micelles (200 μM) were added to each well and incubated at 37 ℃ for 1.5 h. The cells were washed with DMEM three times before 200 μL of fluo-E_4 (10 μM in DMEM) was added and incubated at 37 ℃ for 10 min. A well of non-lipopeptide K treated cells was also incubated with fluo-E_4 as the negative control. After incubation, free fluo-E_4 was removed and the cells were washed at least three times with DMEM before imaging. Cell imaging was performed with a Leica SP8 confocal microscopy. A 488nm laser was used for excitation and the emission signal was collected from 500 nm to 550 nm.

Membrane Docking

Hela cells were seeded in a 48-well plate with a cell number of $1x10^5$ cells per well and incubated at 37 ℃ for 20 h. CPK_n micelles in DMEM were prepared using the same method as above. 400 μL of each micelle solution was added to each well plate and incubated with the cells at 37 ℃ for 1.5 h. 500 μM of liposomes containing 1% CPE_n and 1% DOPE-NBD were prepared. For the control experiment, plain liposomes containing 1% DOPE-NBD were used. The liposomes were diluted to [total lipid] = 200 μM in DMEM before addition to cells. After 15 minutes of incubation, the cells were washed three times with DMEM, followed by the addition of 400 μL liposome solution with CPE_n. Control experiment: CPK decorated cells with non-CPE liposomes and non-CPK decorated cells with CPE-modified liposomes were used. Cells were incubated with the liposomes for 15 min at 37 ℃ before thoroughly washing with PBS. Cells were trypsinized and transferred to Eppendorf tubes, washed with PBS and centrifuged. The cells were resuspended in PBS (supplemented with 2 mM EDTA) to a density of $5x10^5$ cells/mL and transferred to a 96-well plate for FACS measurements using a Guava® EasyCyte 12HT Benchtop Flow Cytometer. The data were analyzed using FlowJo v10. For each measurement, 10,000 events in duplicate were collected. No compensation was required for the fluorophores used.

PI-NBD delivery through membrane fusion

$5x10^4$ Hela cells were seeded in each well of two µ-Slide 8 Well plates and incubated at 37 ℃ for 20 hours. A 10 µM solution of CPK_n in DMEM was prepared as described above. A lipid film ([Total lipid] = 1 mmol) containing 1% CPE_n and 1% DOPE-NBD was rehydrated with 1 mL of a PI (10 mg/mL) solution in PBS and sonicated five minutes at 55 ℃ to obtain liposomes. Non-encapsulated PI was removed using an Illustra NAP-25 size-exclusion column. For comparison, liposomes containing DOPE-NBD and PI but without CPE were also prepared. All liposomes were diluted with DMEM to a final lipid concentration of 200 µM. 200 µL of CPK_n micelles (10 µM) were added to the cells and incubated for 1.5 h at 37 ℃. After thorough washing, liposomes (200 µL) were added to the cells for 15 mins. Control experiments: liposomes without CPE + cells decorated with CPK, and liposomes with CPE + cells without CPK were used. After incubation, excess liposomes were removed and the cells were washed with DMEM. The cells were covered with fresh DMEM and incubated at 37 ℃ for another 20 mins before imaging.

Cell imaging was performed using a Leica SP8 confocal microscope. A 488 nm laser was applied for excitation and NBD emission was observed in the range from 500 to 550 nm. For PI observation, a 535 nm laser was used for excitation and emission was measured from 600 nm to 700 nm.

REFERENCES

(1) Elsharkasy, O. M.; Nordin, J. Z.; Hagey, D. W.; de Jong, O. G.; Schiffelers, R. M.; Andaloussi, S. E.; Vader, P. Extracellular vesicles as drug delivery systems: Why and how? *Adv Drug Deliv Rev* **2020,** *159*, 332.

(2) Su, Y.-Y.; Li, C.-Y.; Li, D. Progress in Membrane Fusion and Its Application in Drug Delivery. *Chinese Journal of Analytical Chemistry* **2019,** *47*, 1871.

(3) Yang, J.; Bahreman, A.; Daudey, G.; Bussmann, J.; Olsthoorn, R. C.; Kros, A. Drug Delivery via Cell Membrane Fusion Using Lipopeptide Modified Liposomes. *ACS Cent Sci* **2016,** *2*, 621.

(4) Brock, D. J.; Kustigian, L.; Jiang, M.; Graham, K.; Wang, T. Y.; Erazo-Oliveras, A.; Najjar, K.; Zhang, J.; Rye, H.; Pellois, J. P. Efficient cell delivery mediated by lipid-specific endosomal escape of supercharged branched peptides. *Traffic* **2018,** *19*, 421.

(5) Gilleron, J.; Querbes, W.; Zeigerer, A.; Borodovsky, A.; Marsico, G.; Schubert, U.; Manygoats, K.; Seifert, S.; Andree, C.; Stoter, M.; Epstein-Barash, H.; Zhang, L.; Koteliansky, V.; Fitzgerald, K.; Fava, E.; Bickle, M.; Kalaidzidis, Y.; Akinc, A.; Maier, M.; Zerial, M. Image-based analysis of lipid

nanoparticle-mediated siRNA delivery, intracellular trafficking and endosomal escape. *Nat Biotechnol* **2013,** *31*, 638.

(6) Sahay, G.; Querbes, W.; Alabi, C.; Eltoukhy, A.; Sarkar, S.; Zurenko, C.; Karagiannis, E.; Love, K.; Chen, D.; Zoncu, R.; Buganim, Y.; Schroeder, A.; Langer, R.; Anderson, D. G. Efficiency of siRNA delivery by lipid nanoparticles is limited by endocytic recycling. *Nat Biotechnol* **2013,** *31*, 653.

(7) Chernomordik, L. V.; Kozlov, M. M. Mechanics of membrane fusion. *Nat Struct Mol Biol* **2008,** *15*, 675.

(8) Byrne, R. D.; Veeriah, S.; Applebee, C. J.; Larijani, B. Conservation of proteo-lipid nuclear membrane fusion machinery during early embryogenesis. *Nucleus* **2014,** *5*, 441.

(9) Jantsch-Plunger, V.; Glotzer, M. Depletion of syntaxins in the early Caenorhabditis elegans embryo reveals a role for membrane fusion events in cytokinesis. *Current biology* **1999,** *9*, 738.

(10) Paululat, A.; Holz, A.; Renkawitz-Pohl, R. Essential genes for myoblast fusion in Drosophila embryogenesis. *Mechanisms of development* **1999,** *83*, 17.

(11) Scales, S. J.; Chen, Y. A.; Yoo, B. Y.; Patel, S. M.; Doung, Y.-C.; Scheller, R. H. SNAREs contribute to the specificity of membrane fusion. *Neuron* **2000,** *26*, 457.

(12) Wang, Y.; Li, L.; Hou, C.; Lai, Y.; Long, J.; Liu, J.; Zhong, Q.; Diao, J. SNARE-mediated membrane fusion in autophagy. *Semin Cell Dev Biol* **2016,** *60*, 97.

(13) Harrison, S. C. Viral membrane fusion. *Nat Struct Mol Biol* **2008,** *15*, 690.

(14) Tang, T.; Bidon, M.; Jaimes, J. A.; Whittaker, G. R.; Daniel, S. Coronavirus membrane fusion mechanism offers a potential target for antiviral development. *Antiviral Res* **2020,** *178*, 104792.

(15) Harrison, S. C. Viral membrane fusion. *Virology* **2015,** *479-480*, 498.

(16) Whitehead, S. A.; McNitt, C. D.; Mattern-Schain, S. I.; Carr, A. J.; Alam, S.; Popik, V. V.; Best, M. D. Artificial Membrane Fusion Triggered by Strain-Promoted Alkyne-Azide Cycloaddition. *Bioconjug Chem* **2017,** *28*, 923.

(17) Ma, M.; Bong, D. Controlled fusion of synthetic lipid membrane vesicles. *Accounts of chemical research* **2013,** *46*, 2988.

(18) Stengel, G.; Simonsson, L.; Campbell, R. A.; Höök, F. Determinants for membrane fusion induced by cholesterol-modified DNA zippers. *The Journal of Physical Chemistry B* **2008,** *112*, 8264.

(19) Sun, L.; Gao, Y.; Wang, Y.; Wei, Q.; Shi, J.; Chen, N.; Li, D.; Fan, C. Guiding protein delivery into live cells using DNA-programmed membrane fusion. *Chem Sci* **2018,** *9*, 5967.

(20) Mason, J. M.; Arndt, K. M. Coiled coil domains: stability, specificity, and biological implications. *Chembiochem* **2004,** *5*, 170.

(21) Apostolovic, B.; Danial, M.; Klok, H. A. Coiled coils: attractive protein folding motifs for the fabrication of self-assembled, responsive and bioactive materials. *Chem Soc Rev* **2010,** *39*, 3541.

(22) Conticello, V.; Hughes, S.; Modlin, C. Biomaterials made from coiled-coil peptides. *Fibrous Proteins: Structures and Mechanisms* **2017,** 575.

(23) Wu, Y.; Collier, J. H. α‐Helical coiled‐coil peptide materials for biomedical applications. *Wiley Interdisciplinary Reviews: Nanomedicine and Nanobiotechnology* **2017,** *9*, e1424.

(24) Woolfson, D. N. Building fibrous biomaterials from alpha-helical and collagen-like coiled-coil peptides. *Biopolymers* **2010,** *94*, 118.

(25) Fletcher, N. L.; Lockett, C. V.; Dexter, A. F. A pH-responsive coiled-coil peptide hydrogel. *Soft Matter* **2011,** *7*, 10210.

(26) Wu, Y.; Collier, J. H. alpha-Helical coiled-coil peptide materials for biomedical applications. *Wiley Interdiscip Rev Nanomed Nanobiotechnol* **2017,** *9*.

(27) Hill, L. K.; Meleties, M.; Katyal, P.; Xie, X.; Delgado-Fukushima, E.; Jihad, T.; Liu, C. F.; O'Neill, S.; Tu, R. S.; Renfrew, P. D.; Bonneau, R.; Wadghiri, Y. Z.; Montclare, J. K. Thermoresponsive Protein-Engineered Coiled-Coil Hydrogel for Sustained Small Molecule Release. *Biomacromolecules* **2019,** *20*, 3340.

(28) Lin, Y.; An, B.; Bagheri, M.; Wang, Q.; Harden, J. L.; Kaplan, D. L. Electrochemically Directed Assembly of Designer Coiled-Coil Telechelic Proteins. *ACS Biomater Sci Eng* **2017,** *3*, 3195.

(29) Marsden, H. R.; Tomatsu, I.; Kros, A. Model systems for membrane fusion. *Chemical Society Reviews* **2011,** *40*, 1572.

(30) Versluis, F.; Voskuhl, J.; van Kolck, B.; Zope, H.; Bremmer, M.; Albregtse, T.; Kros, A. In situ modification of plain liposomes with lipidated coiled coil forming peptides induces membrane fusion. *J Am Chem Soc* **2013,** *135*, 8057.

(31) Zheng, T.; Voskuhl, J.; Versluis, F.; Zope, H. R.; Tomatsu, I.; Marsden, H. R.; Kros, A. Controlling the rate of coiled coil driven membrane fusion. *Chem Commun (Camb)* **2013,** *49*, 3649.

(32) Zope, H. R.; Versluis, F.; Ordas, A.; Voskuhl, J.; Spaink, H. P.; Kros, A. In vitro and in vivo supramolecular modification of biomembranes using a lipidated coiled-coil motif. *Angew Chem Int Ed Engl* **2013,** *52*, 14247.

(33) Yang, J.; Shimada, Y.; Olsthoorn, R. C.; Snaar-Jagalska, B. E.; Spaink, H. P.; Kros, A. Application of Coiled Coil Peptides in Liposomal Anticancer Drug Delivery Using a Zebrafish Xenograft Model. *ACS Nano* **2016,** *10*, 7428.

(34) Kong, L.; Askes, S. H.; Bonnet, S.; Kros, A.; Campbell, F. Temporal control of membrane fusion through photolabile PEGylation of liposome membranes. *Angewandte Chemie* **2016,** *128*, 1418.

(35) Litowski, J. R.; Hodges, R. S. Designing heterodimeric two-stranded alpha-helical coiled-coils. Effects of hydrophobicity and alpha-helical propensity on protein folding, stability, and specificity. *J Biol Chem* **2002,** *277*, 37272.

(36) Rabe, M.; Boyle, A.; Zope, H. R.; Versluis, F.; Kros, A. Determination of oligomeric states of peptide complexes using thermal unfolding curves. *Biopolymers* **2015,** *104*, 65.

(37) Paulucci, A. A.; Hicks, L.; Machado, A.; Miranda, M. T.; Kay, C. M.; Farah, C. S. Specific sequences determine the stability and cooperativity of folding of the C-terminal half of tropomyosin. *J Biol Chem* **2002,** *277*, 39574.

(38) Crooks, R. O.; Rao, T.; Mason, J. M. Truncation, randomization, and selection: generation of a reduced length c-Jun antagonist that retains high interaction stability. *J Biol Chem* **2011,** *286*, 29470.

(39) Kumar, P.; van Son, M.; Zheng, T.; Valdink, D.; Raap, J.; Kros, A.; Huber, M. Coiled-coil formation of the membrane-fusion K/E peptides viewed by electron paramagnetic resonance. *PLOS ONE* **2018,** *13*, e0191197.

(40) Crone, N. S. A.; Kros, A.; Boyle, A. L. Modulation of Coiled-Coil Binding Strength and Fusogenicity through Peptide Stapling. *Bioconjug Chem* **2020,** *31*, 834.

(41) Monera, O. D.; Kay, C. M.; Hodges, R. S. Protein denaturation with guanidine hydrochloride or urea provides a different estimate of stability depending on the contributions of electrostatic interactions. *Protein Science* **1994,** *3*, 1984.

(42) Lim, W. K.; Rosgen, J.; Englander, S. W. Urea, but not guanidinium, destabilizes proteins by forming hydrogen bonds to the peptide group. *Proc Natl Acad Sci U S A* **2009,** *106*, 2595.

(43) Huerta-Viga, A.; Woutersen, S. Protein Denaturation with Guanidinium: A 2D-IR Study. *J Phys Chem Lett* **2013,** *4*, 3397.

(44) Daudey, G. A.; Zope, H. R.; Voskuhl, J.; Kros, A.; Boyle, A. L. Membrane-Fusogen Distance Is Critical for Efficient Coiled-Coil-Peptide-Mediated Liposome Fusion. *Langmuir* **2017,** *33*, 12443.

(45) Rabe, M.; Schwieger, C.; Zope, H. R.; Versluis, F.; Kros, A. Membrane interactions of fusogenic coiled-coil peptides: implications for lipopeptide mediated vesicle fusion. *Langmuir* **2014,** *30*, 7724.

(46) Rabe, M.; Aisenbrey, C.; Pluhackova, K.; de Wert, V.; Boyle, A. L.; Bruggeman, D. F.; Kirsch, S. A.; Bockmann, R. A.; Kros, A.; Raap, J.; Bechinger, B. A Coiled-Coil Peptide Shaping Lipid Bilayers upon Fusion. *Biophys J* **2016,** *111*, 2162.

(47) de Araujo, A. D.; Hoang, H. N.; Kok, W. M.; Diness, F.; Gupta, P.; Hill, T. A.; Driver, R. W.; Price, D. A.; Liras, S.; Fairlie, D. P. Comparative α‐Helicity of Cyclic Pentapeptides in Water. *Angewandte Chemie International Edition* **2014,** *53*, 6965.

APPENDIX 3

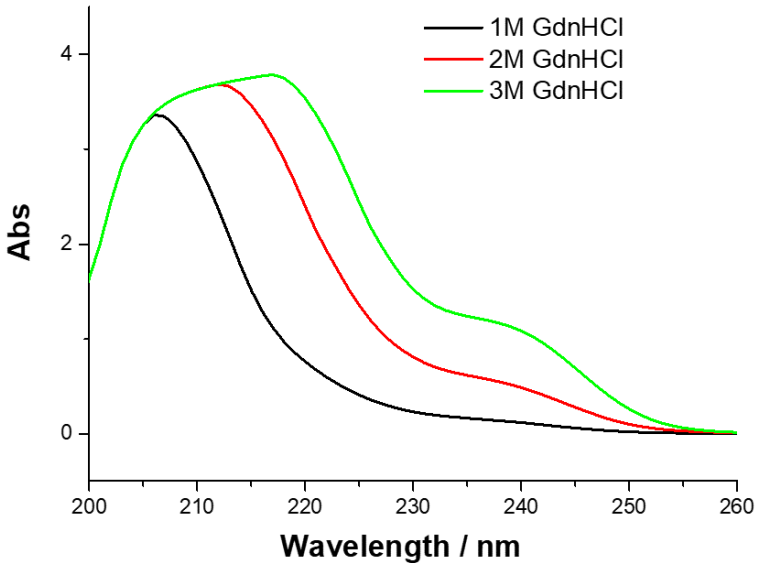

Figure S1. UV-Vis spectra of different concentrations of GdnHCl in PBS.

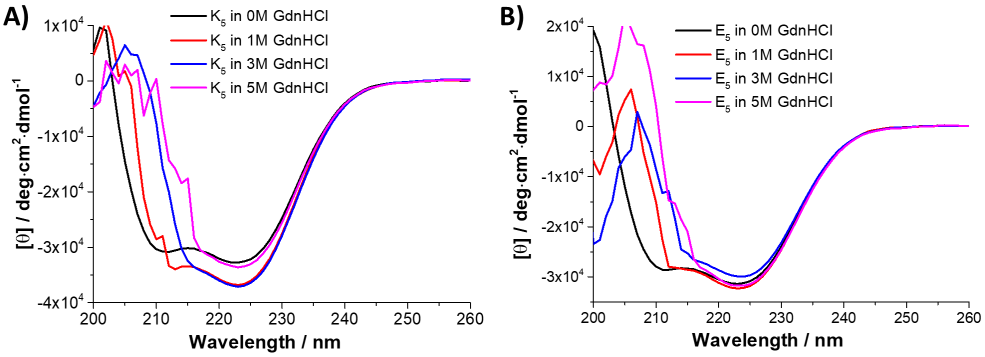

Figure S2. CD spectra of peptides K_5 (A) and E_5 (B) with different concentrations of GdnHCl. Peptide: 10 μM, temperature: 20 °C.

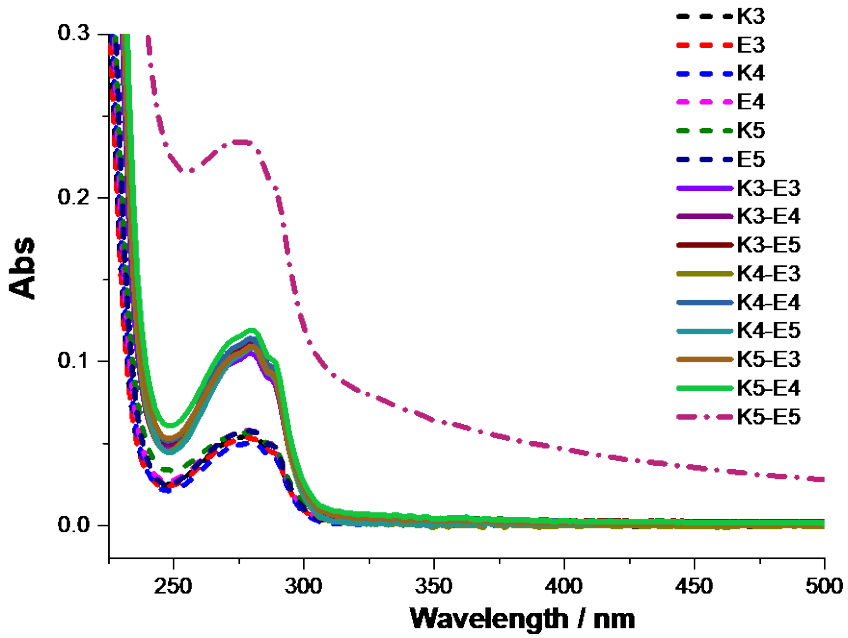

Figure S3. UV-Vis spectra of different coiled-coil forming peptides and coiled-coil pairs. A baseline shift was obtained for the K_5-E_5 coiled coil pair, indicative of aggregation. All measurements were recorded in PBS (pH 7.2) at 20 °C. Peptide: 10 µM.

A) Lipid mixing:

Lipid mixing efficiency with reference to peptide E:

K5E4 > K4E4 > K4E5 > K5E5 = K3E4 = K3E5 > K5E3 = K4E3 > K3E3

E4>E5>E3

Lipid mixing efficiency with reference to peptide K:

K5E4 > K4E4 > K4E5 > K5E5 = K3E4 = K3E5 > K5E3 = K4E3 > K3E3

K5>K4>K3

B) Content mixing:

Content mixing efficiency with reference to peptide E :

K5E4 > K4E4 > K3E4 > K5E3 = K4E3 = K5E5 > K4E5 = K3E3 = K3E5

E4>E3>E5

Content mixing efficiency with reference to peptide K :

K5E4 > K4E4 > K3E4 > K5E3 = K4E3 = K5E5 > K4E5 = K3E3 = K3E5

K5>K4>K3

Figure S4. Comparison of liposome membrane fusion efficiency for different length E and K peptides.

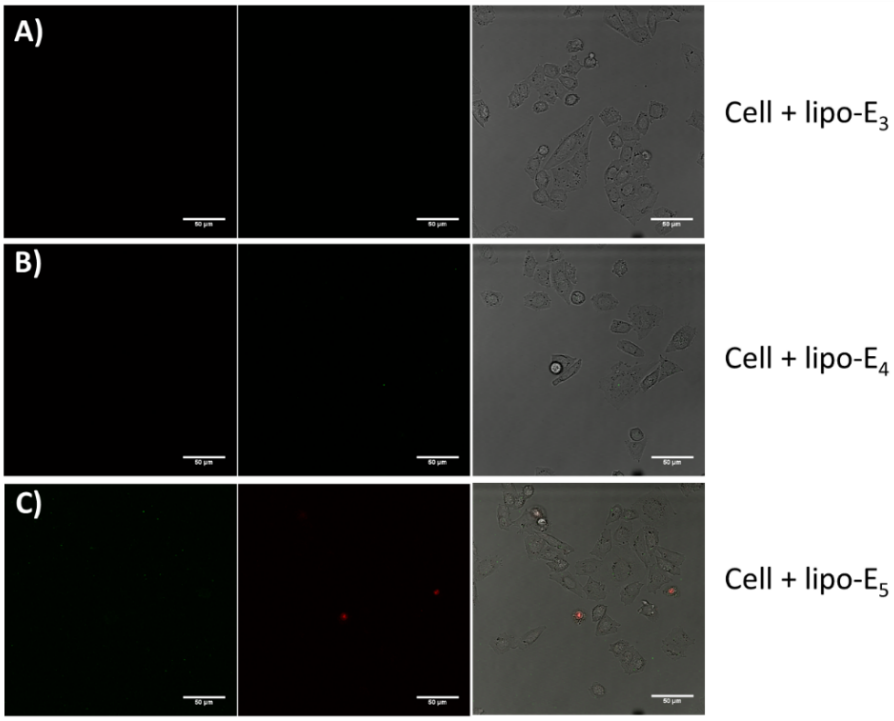

Figure S5. Non-CPK decorated cells incubated with CPE-modified liposomes containing PI and NBD-PE. Scale bar: 50 μm.

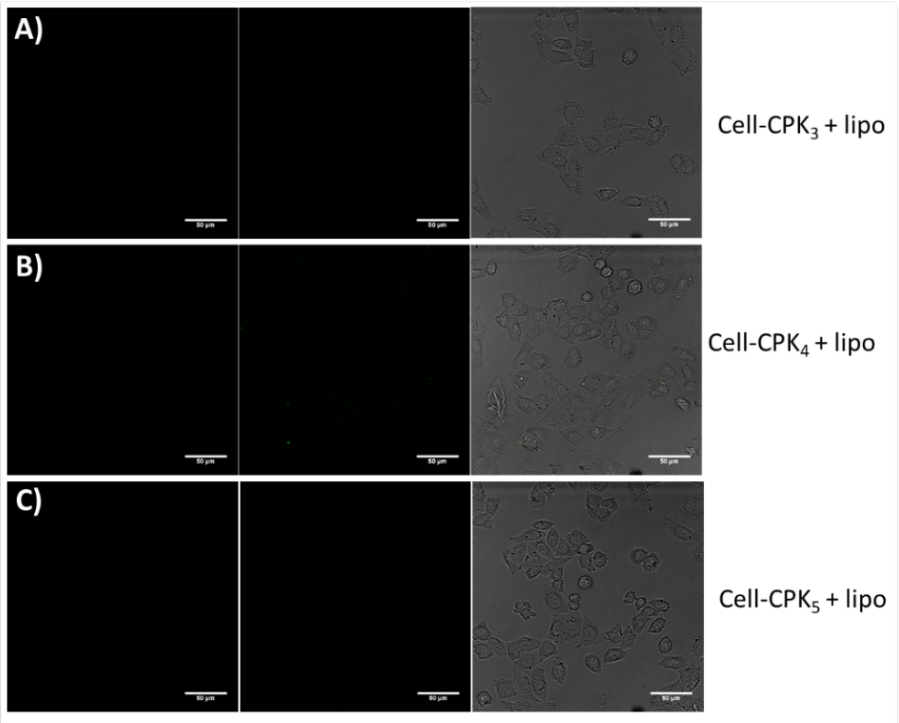

Figure S6. CPK-decorated cells incubated with non-CPE modified liposomes containing PI and NBD-PE. Scale bar: 50 µm.

Table S1. Calculated mass and recorded mass by LC-MS for all peptides and lipopeptides.

peptide	Mass (calcd.) / Da	Mass (found) / Da
K_3	$[M + 2H^+]^{2+}$ 1282.8	1281.5
E_3	$[M + H^+]^{+}$ 1284.2	1283.0
K_4	$[M + 2H^+]^{2+}$ 1659.5	1658.5
	$[M + 3H^+]^{3+}$ 1106.6	1105.5
E_4	$[M + 2H^+]^{2+}$ 1161.4	1660.5
	$[M + 3H^+]^{3+}$ 1107.9	1106.7
K_5	$[M + 3H^+]^{3+}$ 1359.0	1357.0
E_5	$[M + 3H^+]^{3+}$ 1360.6	1358.4
CPK_4	$[M + 2H^+]^{2+}$ 1869.4	1866.4
	$[M + 3H^+]^{3+}$ 1246.6	1244.3
CPE_4	$[M + 2H^+]^{2+}$ 1871.2	1868.8
	$[M + 3H^+]^{3+}$ 1247.8	1245.4
CPK_5	$[M + 2H^+]^{2+}$ 2245.5	2244.6
	$[M + 3H^+]^{3+}$ 1497.3	1495.5
	$[M + 4H^+]^{4+}$ 1123.2	1121.5
CPE_5	$[M + 2H^+]^{2+}$ 2246.3	2247.0
	$[M + 3H^+]^{3+}$ 1497.9	1497.3
Fluo-K_4	$[M + 2H^+]^{2+}$ 1876.5	1874.0
	$[M + 3H^+]^{3+}$ 1251.3	1249.3
Fluo-E_4	$[M + 2H^+]^{2+}$ 1878.5	1876.0
	$[M + 3H^+]^{3+}$ 1252.7	1250.6

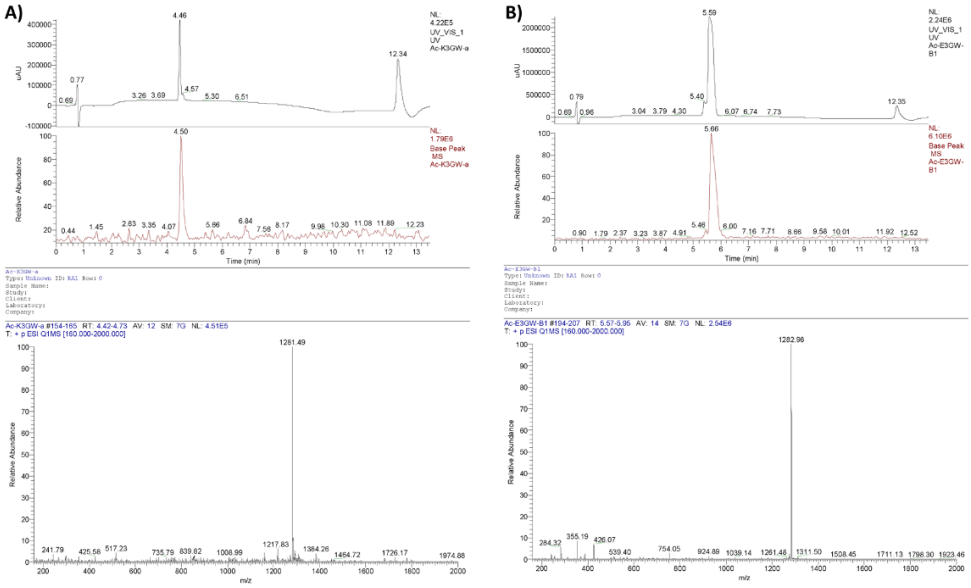

Figure S7. LC-MS of: A) K_3 and B) E_3.

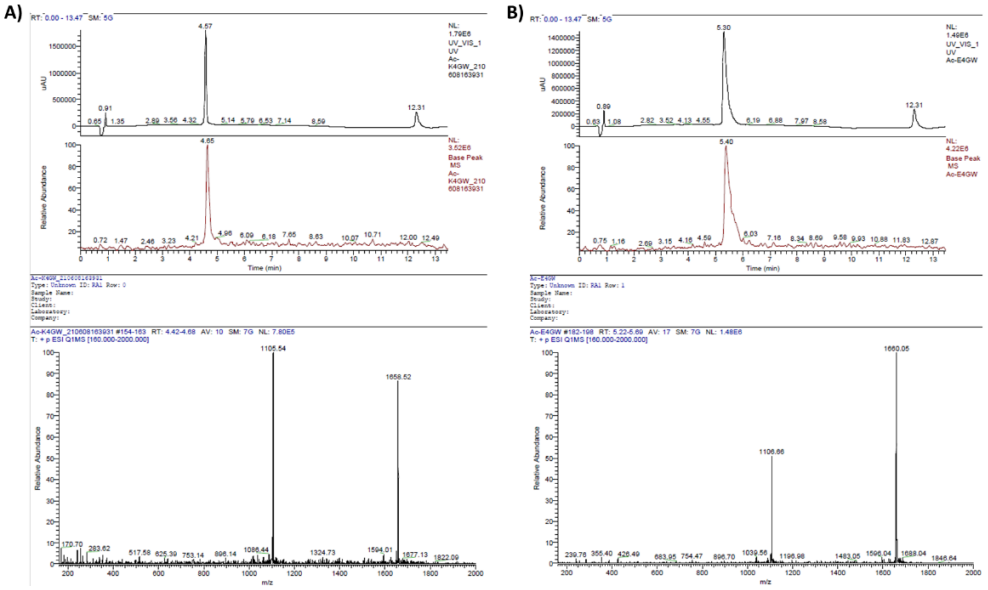

Figure S8. LC-MS of: A) K_4 and B) E_4.

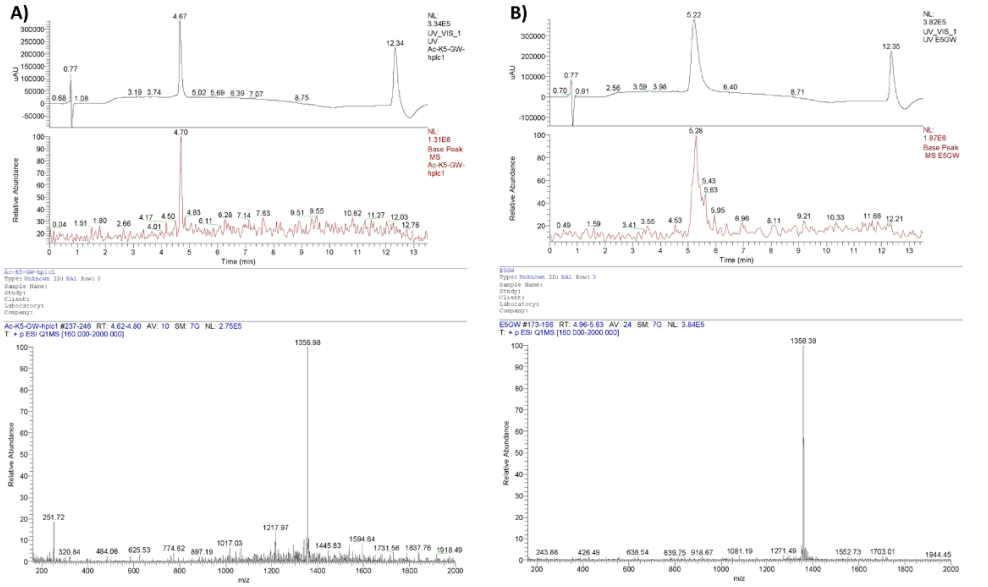

Figure S9. LC-MS of: A) K_5 and B) E_5.

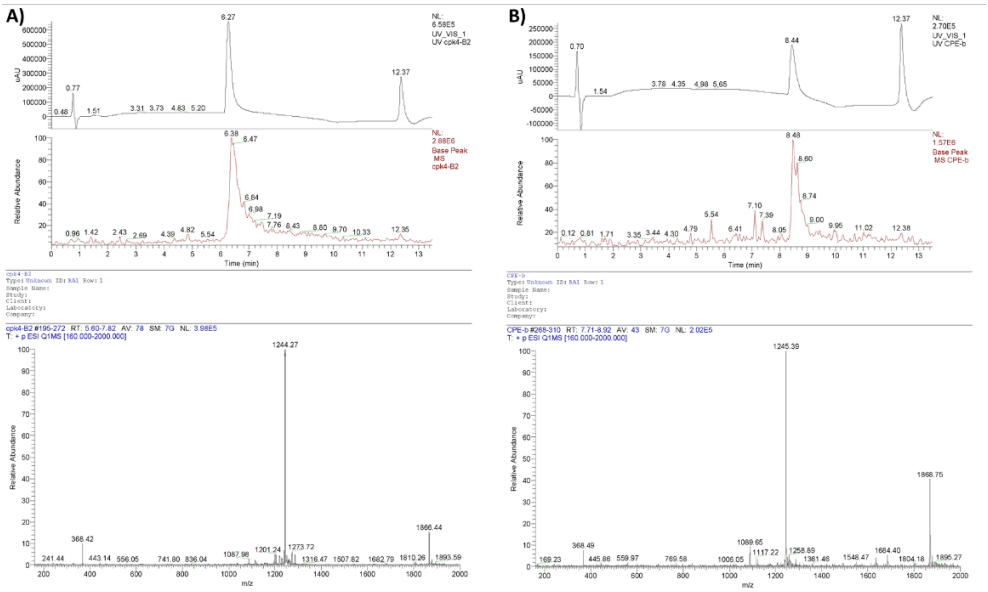

Figure S10. LC-MS of: A) CPK_4 and B) CPE_4.

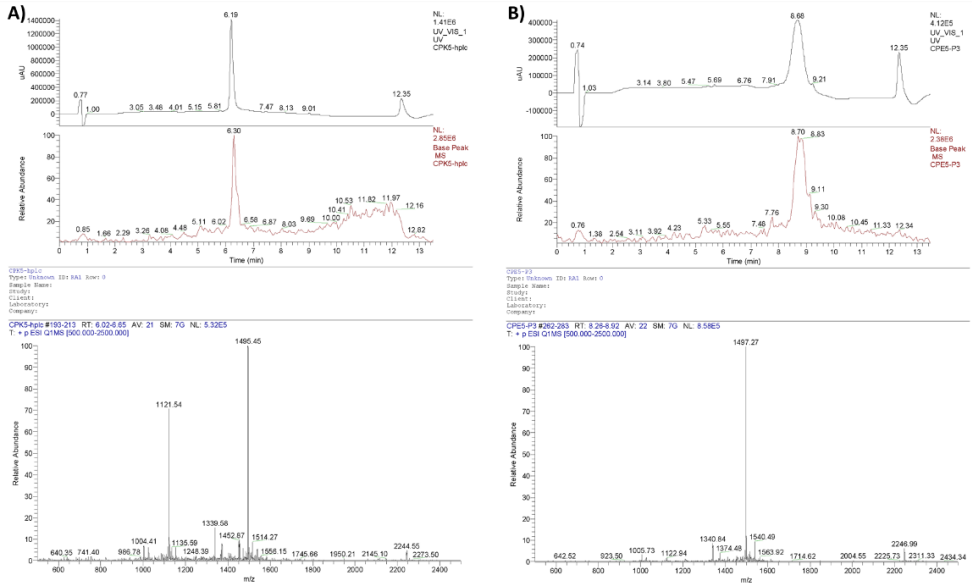

Figure S11. LC-MS of: A) CPK_5 and B) CPE_5.

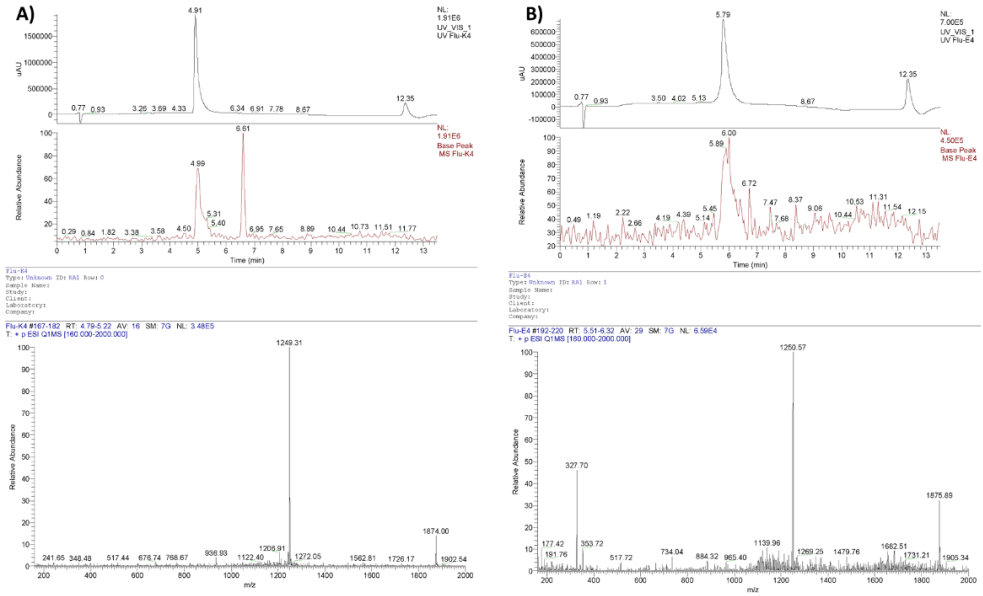

Figure S12. LC-MS of: A) fluo-K_4 and B) fluo-E_4.

Chapter 4

Coiled-coil Forming Peptide Dimers: Structure, Self-Assembly and Fusogenicity

ABSTRACT

Efficient delivery of extracellular molecules into mammalian cells is essential yet challenging for cell therapeutics. Current drug delivery strategies adopt vesicles or nanoparticles as drug carriers capable of transporting drugs into cells via endocytosis to enhance drug delivery efficiency with minimal toxicity. However, this drug delivery strategy suffers from low drug release due to poor endo-lysosomal escape. Thus the majority of the drug is eliminated from the cell before it reaches the cytoplasm. Here, we developed a drug delivery system using a membrane fusion strategy, triggered by heterodimeric coiled-coil formation between peptides K_4 and E_4. This drug delivery system is independent of endo-lysosomal escape pathways thereby enhancing cytosolic drug delivery. In this chapter, we investigate how the secondary structure, self-assembly and lipid membrane affinity of three novel K_4 dimers affects fusion and concomitant drug delivery. Previous studies revealed that K_4 has a dual role in membrane fusion: coiled-coil formation with peptide E bringing opposing membranes into close proximity, but also interacting with the membrane which facilitates membrane fusion. Therefore we hypothesized that dimeric K_4 variants should be more efficient at promoting fusion as they can fulfil both these roles simultaneously. Three K_4 dimers were designed by linking K_4 monomer at either their N- or their C-terminus, to form linear dimers (NLK_4 or CLK_4), or in the center of the peptide to form a parallel dimer (PK_4). Self-assembly studies revealed that linear K_4 dimers tend to dimerize to a possible tetramer-like homodimer, while PK_4 tends to form temperature-dependent aggregates. Fusion assays revealed that PK_4 has the highest capacity to trigger both liposome-liposome fusion and cell-liposome fusion using peptide modified liposomes. This study, therefore, describes a novel fusogenic drug delivery system but also yields insights as to the influence of conformation, charge, and steric effects of the K/E coiled-coil peptides in triggering efficient membrane fusion.

INTRODUCTION

Efficient intracellular delivery of drugs is pivotal to treating diseases efficiently.[1-3] However, many drugs are unable to enter cells due to their charge, size, or solubility and are therefore unable to cross the plasma membrane.[4-6] Furthermore, drugs that have a therapeutic effect in one organ/tissue may be toxic in other tissues.[7-8] Although significantly advanced drug discoveries have been made,[9-11] target specificity and control over drug delivery into cells remain challenging.

Liposome-assisted drug delivery systems have progressed rapidly in many biological areas because of their advantages in stabilizing therapeutic compounds, overcoming the barrier for cellular and tissue uptake, and reducing cytotoxicity.[12-14] Liposomes can be used to deliver not only traditional lipophilic and hydrophilic drugs into cells, but also biomacromolecular proteins and nucleic acids.[15-17] However, a major challenge for many applications of liposome-assisted drug delivery systems remains the inefficiency of cytosolic drug release due to inefficient endo-lysosomal escape, resulting in drug degradation or exocytosis.[18-21]

Membrane fusion is a fundamental process in life, which occurs between separate lipid bilayers that merge into one membrane resulting ultimately in content transport.[22-24] Studies show that the SNARE (soluble N-ethylmaleimide-sensitive factor attachment protein receptors) family of proteins play a key role in non-viral membrane fusion during various intracellular exocytosis processes, such as autophagy and neuronal endocytosis.[25-27] Inspired by this biological process, artificial membrane fusion models systems have been constructed and these systems are able to induce liposome-liposome fusion resulting in lipid mixing and content mixing.[28-31] Unfortunately, only a few of these systems are able to induce liposome-cell fusion, limiting their utility in drug delivery applications.

In previous studies, a minimal membrane fusion model was designed based on the complementary coiled-coil forming peptides "K" $(KIAALKE)_3$ and "E" $(EIAALEK)_3$.[32-33] Conjugating these peptides via short poly(ethene glycol) (PEG) linker to cholesterol resulted in the lipopeptides CPK_3 and CPE_3. These molecules readily insert into lipid bilayers and have the ability to induce liposome-liposome membrane fusion. Mechanistic studies showed that peptide K plays an essential role in membrane fusion.[34-36] Not only does it form a coiled-coil with the complimentary peptide E, but it also has a high affinity to phospholipid membranes because of its structural specificity and positive charge.[34-36] Peptide K membrane

interactions induce positive membrane curvature and destabilize the membrane, facilitating membrane fusion. Extension of the peptides from 3 to 4 heptads (*i.e.* CPK_4 and CPE_4) increases membrane interactions, enabling cell-liposome fusion while only liposome docking onto the membrane of cells was observed for CPK_3/CPE_3.[37-38] A study investigating the effect of the PEG spacer shows that the distance between peptide and membrane is another key factor which influences membrane fusion efficiency.[39-40] A short spacer prevents efficient coiled-coil formation due to steric effects, while too long a spacer decreases membrane fusion efficiency.

Considering that the membrane affinity of peptide K and coiled-coil formation influences membrane fusion, three dimeric K_4 peptides with different structures were designed (Scheme 1A). Ideally, K_4 dimers are able to form coiled coils with two complimentary E_4 peptides attached to two lipid membranes, thus connecting two opposing membranes and inducing efficient membrane fusion. Furthermore, a K_4 dimer is able to interact with two lipid membranes, which also enhances membrane fusion efficiency. These K_4 dimers may have different fusion efficiencies due to different membrane affinities and different interaction manners when forming a coiled-coil with peptide E_4 (Scheme 1B). In this chapter, we characterized the peptide folding, self-assembly and fusogenicity of these dimeric K_4 peptides. The secondary structure and thermal stability of the K_4 dimers and their coiled-coil formation were studied by circular dichroism (CD) spectroscopy. Homodimer formation of linear K_4 dimers was evaluated employing a CD titration assay. Using dynamic light scattering (DLS), particle formation of K_4 dimers was studied. Next, we determined the affinity of the K_4 dimers for lipid membranes using a tryptophan fluorescence assay. The ability to induce fusion was evaluated by performing lipid-mixing and content-mixing assays. Cell studies show the potential application of K_4 dimers to deliver liposomes as a potential drug delivery tool. Moreover, this research could help to better understand the influence of peptide conformation, charge, and steric effects on the E/K coiled-coil induced membrane fusion.

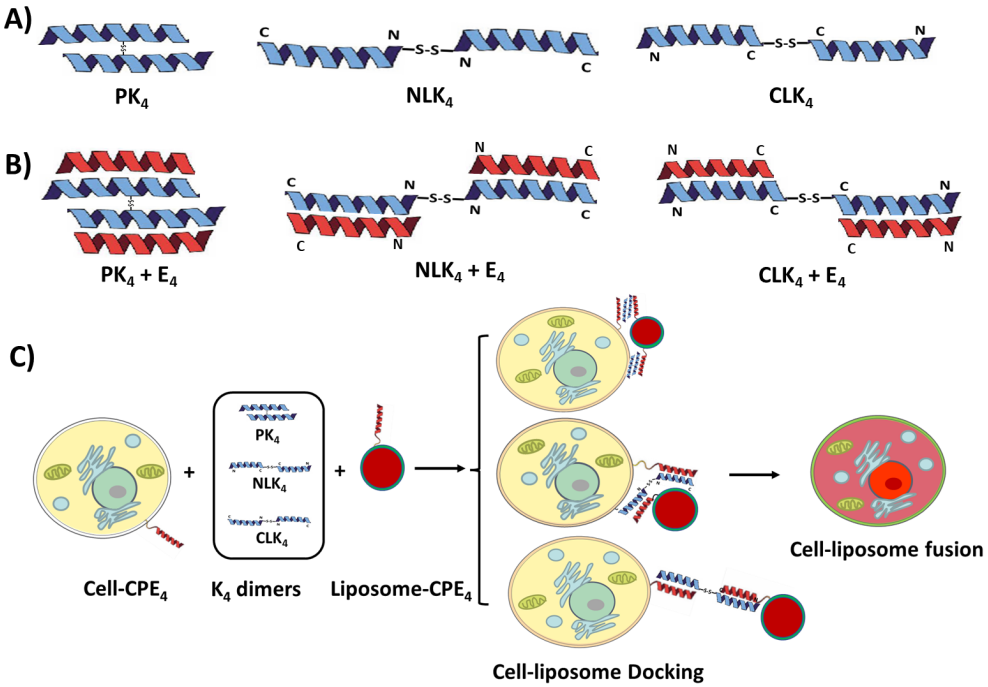

Scheme 1. Schematic representation of (A) three K_4 dimers, (B) the coiled-coil structure of three K_4 dimers and peptide E_4, (C) cell-liposome fusion induced by different coiled-coils.

RESULTS AND DISCUSSION

1. Dimeric K_4 peptide design and synthesis

To synthesize K_4 dimers, a cysteine was introduced into the original amino acid sequence either at the terminus or at the *f*-position in the second heptad of peptide K. Through disulfide bond formation, the various K_4 dimers were obtained (Figure S1). Parallel PK_4 was obtained by conjugating two K_4 peptides with glutamic acid at the *f*-position in the second heptad mutated to cysteine (Scheme 1A). One peptide was extended with a glycine-tryptophan (-GW) for peptide concentration determination and tryptophan fluorescence measurements. Two linear K_4 dimers were also synthesized. A cysteine was added either to the N-terminus or the C-terminus of K_4. Disulfide bond formation between two K_4 monomers at the N-terminus resulted in a linear dimeric structure, denoted NLK_4. In CLK_4, a disulfide bond between cysteines at the C-terminus of the K_4 monomer peptides was formed.

The positive charge of the lysine side chains, and the hydrophobic face of the helix, are two factors influencing the membrane affinity of peptide K_4.[36] The synthesized

K_4 dimers have double the amount of positive charge and a well-defined hydrophobic interface, which is expected to result in a higher membrane affinity and destabilization. Since the two K_4 monomers are close to each other in PK_4, this dimer will have a high charge density in solution. However, the positive charge may be distributed more evenly on linear K_4 dimers, therefore the charge density on NLK_4 and CLK_4 is likely to be lower than for PK_4. Such a charge density difference may influence the affinity of the different K_4 dimers for the membrane.

Apart from charge density, the three-dimensional structure was another factor we considered for K_4 dimer design. Peptides K and E form a parallel heterodimeric coiled-coil structure,[41] so one K_4 dimer is expected to interact with two E_4 peptides. Scheme 1B shows the possible binding modes of each K_4 dimer with free peptide E_4 in solution and CPE_4 incorporated into the cell membrane. For PK_4, one K_4 dimer interacts with two E_4 peptides to form a 'sandwich' double dimeric coiled-coil structure. On a cell membrane, such a 'sandwich' structure can be also formed between one K_4 dimer and two CPE_4 modified membranes (Scheme 1C). In the case of the linear K_4 dimers, one K_4 dimer can also bind to two E_4 peptides to form a linear coiled-coil structure. Due to the parallel coiled-coil interaction between peptide K and peptide E, NLK_4 and CLK_4 have different orientations of coiled-coil formation (Scheme 1B). CPE_4 modified cell membranes and liposomes binding by NLK_4 will be very close to each other while liposomes tend to be further away from the cell membrane when using CLK_4 (Scheme 1C). These differences between the three K_4 dimers can yield a better understanding of how charge properties and steric effects in K peptide dimers influence membrane fusion.

2. Secondary Structure Analysis

The secondary structure of the K_4 dimers in solution was studied using circular dichroism (CD) spectroscopy (Figure 1A). Both CLK_4 and NLK_4 adopted a highly helical conformation which was comparable to monomeric K_4 (Table 1). Previous studies have shown that both K_4 and E_4 tend to form homodimers.[34, 42] We suspect that linear K_4 dimers may form a 'tetramer-like' dimeric structure or a hairpin structure, stabilizing the α-helix structure. Surprisingly, PK_4 shows a highly distorted non-α-helix signal. This might be because the high charge density of PK_4 hinders α-helix formation. Alternatively, due to the specific structure, PK_4 may not be able to dimerize, but rather interacts with other peptides resulting in aggregation.

Table 1. Normalized mean residue molar ellipticity and percentage helicity of peptides

Peptide	[θ] / deg cm^2 dmol^{-1}	Helicity (%) [a]
K_4	-29894.2	89
E_4	-25063.8	80
PK_4	-8550.3	25
NLK_4	-34322.4	92
CLK_4	-39613.2	105
PK_4-E_4	-34330.3	90
NLK_4-E_4	-31438.4	83
CLK_4-E_4	-35300.8	92

[a]The percentage of α-helicity was calculated using Equation 2 (see experimental section).

Next, the interaction of the K_4 dimers with peptide E_4 was investigated. Equimolar mixing of PK_4 and E_4 resulted in a strong increase of the CD signal with minima at 208 and 222 nm, indicative of coiled-coil formation (Figure 1B). In contrast, peptide E_4 and CLK_4 didn't interact as the resulting CD spectrum was the average of the two individual spectra (Figure 1C). This suggests that the 'tetramer-like' homodimer or helical hairpin of CLK_4 is too stable, preventing interaction with E_4. NLK_4 did interact with E_4 as an increase in CD intensity was obtained (Figure 1D). This result suggests that NLK_4 may also form a tetramer-like homodimer or a hairpin, albeit with a lower stability such that it still interacts with peptide E_4 to form heteromeric coiled coils.

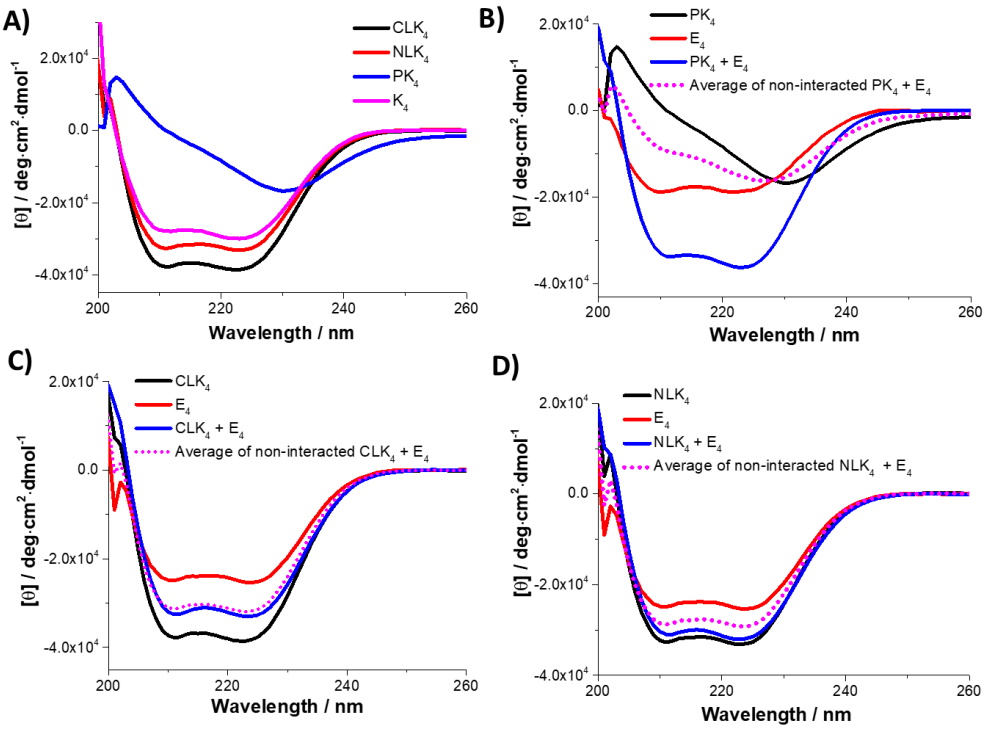

Figure 1. CD specta of (A) K_4 dimers and monomer. (B) $PK_4 \pm E_4$, (C) $CLK_4 \pm E_4$, D) $NLK_4 \pm E_4$. The blue line is the measured spectrum, the dotted line is the calculated average spectrum from the K_4 dimer and peptide E_4. Spectra were recorded in PBS (pH 7.2) at 20 ℃. [K_4 dimer] = 5 μM, [K_4 monomer] = 10 μM and [E_4] = 10 μM.

Temperature-dependent CD spectroscopy was applied to determine the thermo-stability of the peptides. The K_4 monomer shows a typical "S" shaped melting curve with the melting temperature (T_m) at 50 ℃. In contrast, the linear K_4 dimers CLK_4 and NLK_4 remained highly helical over the entire temperature range. Even at 95 ℃, a decrease of only 44% and 46% in ellipticity was observed (Figure 2A), revealing the very high thermal stability of these two K_4 dimers. PK_4 formed a non-α-helical secondary structure (Figure 1A), and the temperature-dependent CD measurement was also unusual, showing a "V" shape melting curve with the highest ellipticity at ~ 60 ℃. To better understand this unusual behaviour, full CD spectra were obtained at different temperatures (Figure 2B). A signature α-helical CD signal was gradually obtained when the temperature was raised from 5 ℃ to 60 ℃. Upon further heating to 90 ℃, the helical secondary structure disappeared again. Thus, PK_4 changes from a distorted non-α-helical state to an α-helix and then eventually to a different non-helical state, revealing the temperature-

dependent nature of PK_4.

Next, the thermal stability of the helical peptides was determined in the presence of peptide E_4 (Figure 2C). The high thermal stability of NLK_4 and CLK_4 was further enhanced in the presence of E_4, with only a 30% and 32% decrease in ellipticity upon heating to 90 °C. This suggests that both linear dimers indeed interact with E_4. It is also possible that the homodimeric CLK_4 and NLK_4 species gradually dissociate to monomeric species and thus form more stable CLK_4/E_4 heterodimers when the temperature is increased. In contrast, the coiled coil formed by PK_4 and E_4 shows poor thermal stability as an 89% ellipticity decline was observed. Indeed, a typical sigmoidal melting curve was obtained with a T_m of 55 °C. The overall thermo-stability study shows that the linear K_4 dimers have high thermo-stability, which increases further upon the addition of E_4. In summary, PK_4 shows complex (self) assembly behaviour at different temperatures and the interaction with peptide E_4 is rather weak.

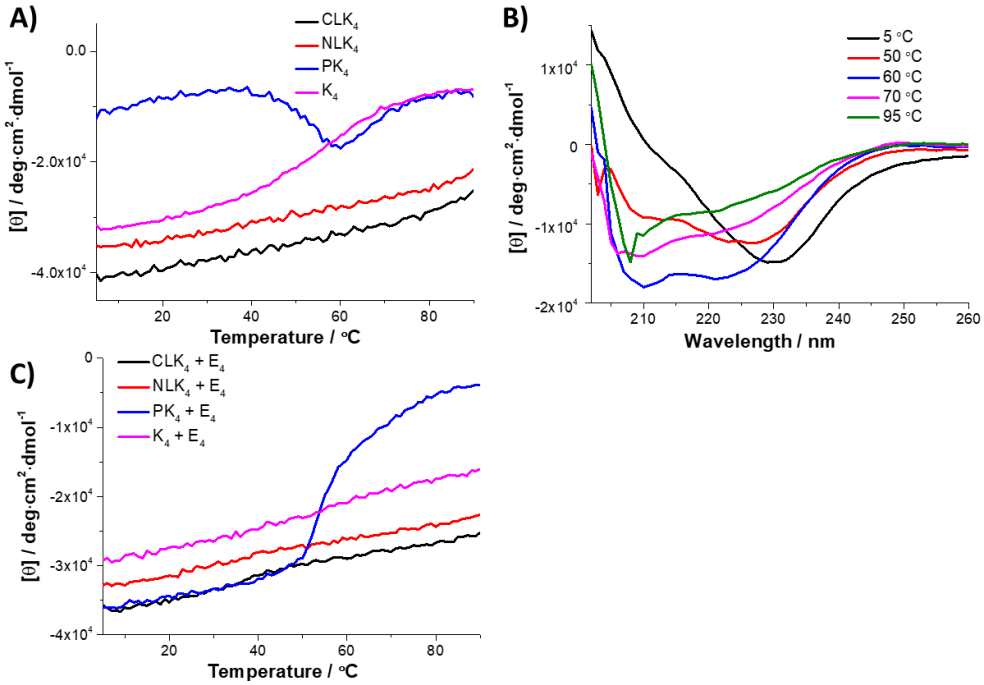

Figure 2. (A) Melting curves of K_4 dimers and monomer. (B) CD spectra of PK_4 at different temperatures. (C) Melting curves of PK_4 + E_4, NLK_4 + E_4, CLK_4 + E_4 and K_4 + E_4. Spectra were recorded in PBS (pH 7.2). [K_4 dimers] = 5 μM, [K_4] =10 μM, [E_4] = 10 μM.

3. Homodimer formation of linear K_4 dimers

The CD study revealed that a higher-order structure may exist for the linear K_4 dimers as evidenced by the increased helicity and T_m. Based on the structure of the linear K_4 dimeric peptides, we suspect that either a hairpin structure or a 'tetramer-like' homodimer structure may form, resulting in homomeric coiled-coil formation. If intramolecular-homodimerization occurs, its (dis)-assembly should be concentration-independent. However, if intermolecular dimerization occurs, the CD spectrum is expected to be concentration-dependent. Therefore, a concentration-dependent CD titration assay was performed (Figure 3).[43] A significant change in CD signal as a function of linear K_4 dimer concentration was observed, suggesting that these linear K_4 dimers tend to form tetramer-like homodimeric structures instead of hairpin structures. The dimerization affinity constant, K_a was determined for NLK_4 and CLK_4 (Table 2). CLK_4 has a higher K_a, which is consistent with the slightly increased stability of CLK_4 in comparison to NLK_4 as observed in the previous CD experiments. Figure 4 shows a representation of the possible tetramer-like homodimers of NLK_4 and CLK_4. Homodimer formation may influence membrane fusion induced by these peptides as homodimerization blocks the hydrophobic face of the helical peptide, hindering the coiled-coil interaction with E_4.

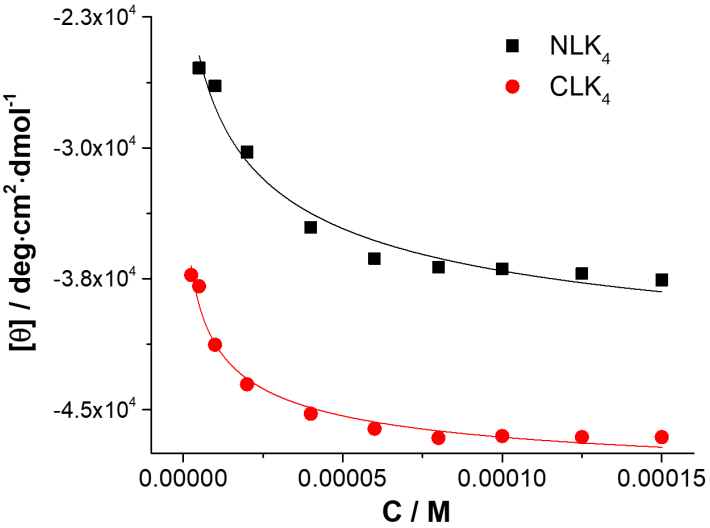

Figure 3. CD titration to determine homodimer formation of linear K_4 dimers and nonlinear fitting obtained based on equation 3 (see experimental section). The mean residue molar ellipticity at 222 nm was plotted against the concentration. Data were recorded in PBS (pH 7.2) at 20 °C.

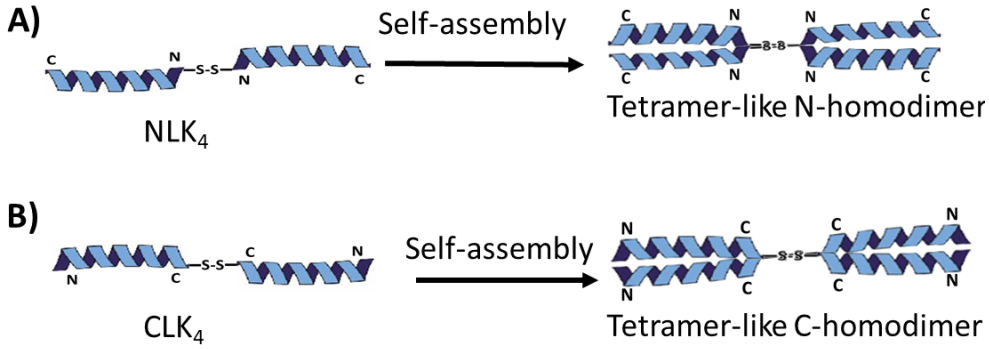

Figure 4. Proposed tetramer-like homodimer formation of linear K_4 dimers, A) NLK_4 and B) CLK_4.

Table 2. Non-linear fitting results from CD titration using equation 3 (see experimental section).

K_4 dimer	$[\Theta]_m$ [a] deg cm^2 dmol^{-1}	$[\Theta]_d$ [b] deg cm^2 dmol^{-1}	K_a (10^4) [c]	R^2 [d]
NLK_4	-18241.3	-44648.1	4.30	0.965
CLK_4	-30822.1	-49993.5	13.0	0.974

Determined using equation 3, [a] $[\Theta]_m$ and [b] $[\Theta]_d$ are the fitted constant which represents the normalized mean residue molar ellipticity when the K_4 dimer forms no tetramer-like homodimer or a fully tetramer-like homodimer respectively. [c] K_a is the fitted peptide affinity constant of homodimer tetramer-like formation. [d] R-squared represents the coefficient of determination, which has been used to determine the "goodness of fit".

4. Self-assembly of K_4 dimers

PK_4 consists of two K_4 monomers connected by a disulfide bond between cysteines at *f* positions.[44] Since K_4 tends to form a helical structure in solution, PK_4 may have two hydrophobic faces exposed to the solution, which makes the structure susceptible to high order self-assembly in order to shield the hydrophobic face. Indeed, PK_4 shows a completely different CD spectrum compared to the other peptides (Figure 1A), indicative of self-assembly. In contrast, the linear K_4 dimer variants form an intermolecular homodimer and this discrete assembly not only enhances the helicity but also shields the hydrophobic face. To study the self-assembly behaviour of all dimeric K_4 peptides, dynamic light scattering (DLS) studies were performed. We used the derived count rate (DCR) as an indicator of

particle formation, as it is dependent on particle concentration and size. The solution behavior of all K_4 dimers and K_4 monomer were studied in H_2O and PBS. In H_2O, no particles formed as evidenced by the low DCR (Figure 5A). In PBS, a high DCR was obtained for PK_4 while the other peptides show a very low DCR, revealing the tendency of PK_4 to aggregate while the other peptides were fully soluble (Figure 5A). This finding is in line with the CD data of PK_4, which can also be explained by aggregation induced distortion of the spectrum (figure 1A). Thus, PK_4 forms large aggregates to shield the exposed hydrophobic faces of the helical peptides from the solvent.

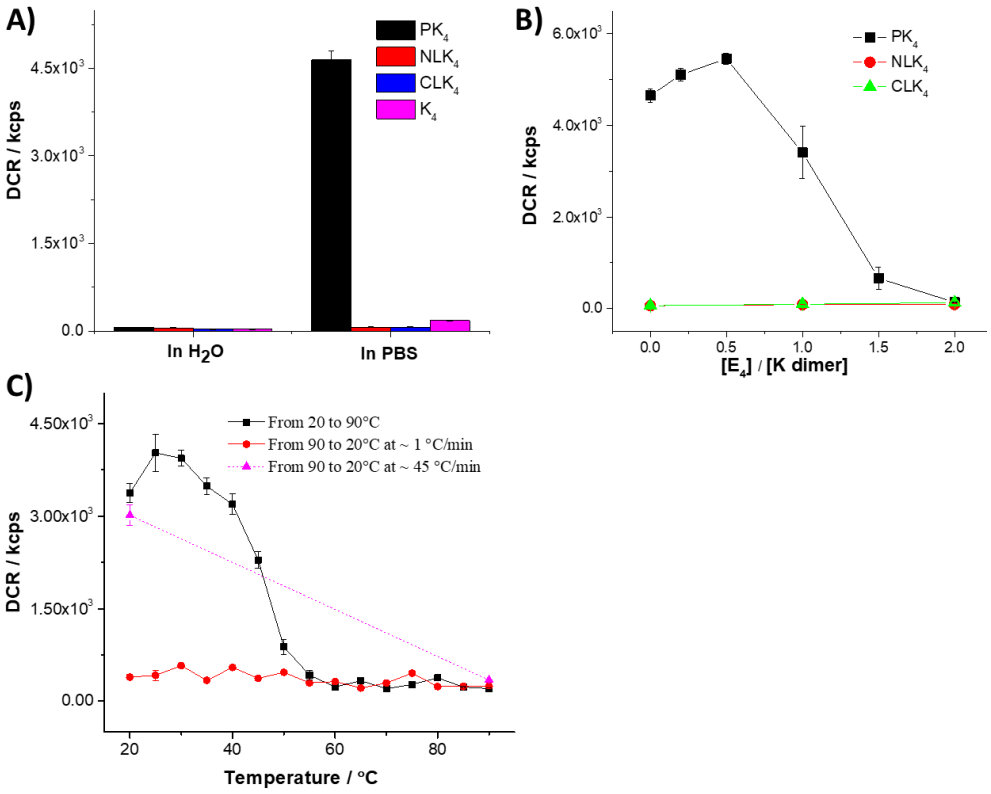

Figure 5. (A) DCR of K_4 dimers (10 μM) and K_4 monomer (20 μM) in H_2O or PBS (pH 7.2) at 20 °C. (B) DLS titration assay: peptide E_4 was titrated into the K_4 dimers (10 μM) in PBS (pH 7.2). (C) Temperature-dependent DCR for PK_4 in PBS (pH 7.2), [PK_4] =10 μM.

To verify this hypothesis, a DLS titration assay was performed (Figure 5B), where peptide E_4 was titrated into a solution of PK_4. Coiled-coil formation between peptide E/K is stronger than homodimerization.[34] Thus the addition of peptide E_4 should result in the disappearance of large assemblies. At a low E/K ratio, the DCR

gradually increased. This might be because E_4 initially interacts with PK_4 exposed on the surface of the assembled particles, resulting in the size increase. With additional amounts of E_4, the DCR decreased dramatically. Quite low DCR was obtained when two equivalents of E_4 was added, which indicates that large assemblies were no longer present (Figure 5B). Thus, the DLS titration assay revealed that PK_4 forms coiled coils with peptide E_4 at a 1:2 stoichiometric ratio, as anticipated. The scheme illustrating the process of particle formation of PK_4 as determined by the DLS titration assay is shown in Figure 6.

The CD study reveals that the secondary structure of PK_4 depends on temperature. Therefore, a temperature-dependent DLS assay was performed (Figure 5C). The highest DCR was observed at 25 °C, suggesting the presence of many large particles. Increasing the temperature further resulted in a decrease of the DCR, revealing that the PK_4 assemblies gradually dissociate at higher temperatures, confirming the temperature-dependent CD spectra of PK_4. Upon heating, the particles gradually dissociate to fully dissociated isolated dimers or small assemblies resulting in a CD spectrum typical for α-helices (Figure 2B). Further heating resulted in unfolding of the peptide (Figure 2B, figure 6D & 6E).

Surprisingly, no particles were reformed upon slowly cooling from 90 °C to 20 °C as the DCR remained low (Figure 5C). This suggests that upon cooling, the PK_4 monomers form more thermodynamically stable, aligned, homomeric coiled coils which further self-assemble into more homogeneous small particles, Figure 6F. This process seems similar to DNA annealing, in which slow cooling of two single-stranded oligonucleotides with complementary sequences results in perfectly matched double-stranded DNA. To study whether the speed of cooling influences PK_4 self-assembly, the experiment was repeated with fast cooling to 20 °C from 90 °C within 2 min. A high DCR close to the initial value was obtained, revealing that large particles were re-formed after fast cooling (Figure 5C & Figure 6G). This shows that these large particles are kinetically-trapped assemblies while the smaller particles are the more stable thermodynamically favoured state.

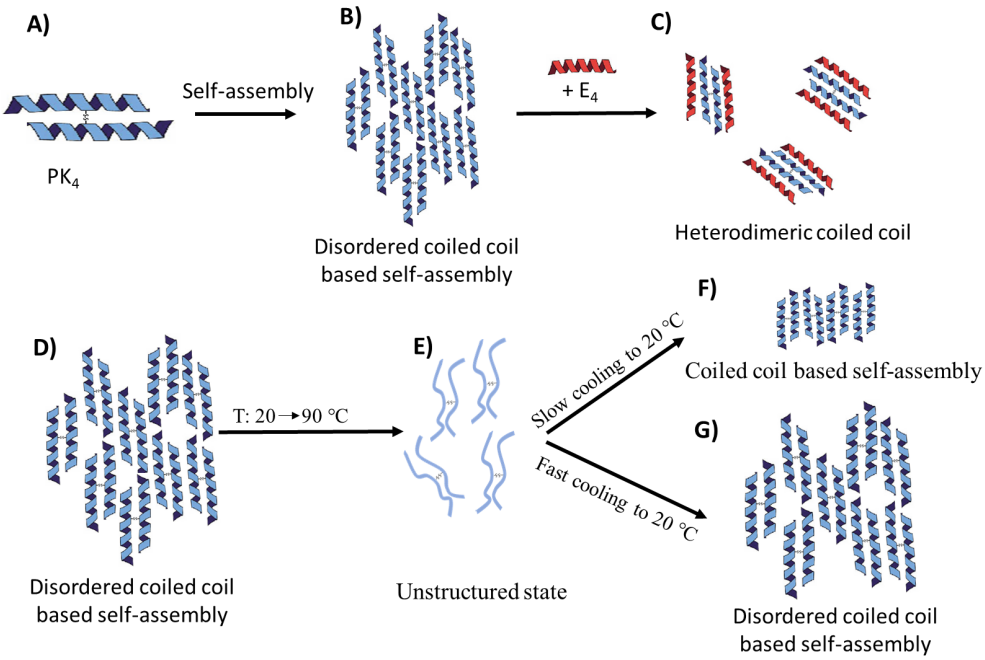

Figure 6. PK_4 (dis) assembly (A-C) in the presence of peptide E_4 and as a function of temperature (D-G).

Transmission Electron Microscopy (TEM) imaging was applied to visualize the PK_4 assemblies. Unstructured aggregates were observed for PK_4 in PBS (Figure 7A). In the presence of two equivalents of peptide E_4, the aggregates were no longer observed (Figure 7B), consistent with the DLS study. This further supports the hypothesis that the addition of peptide E_4 results in the formation of soluble PK_4/E_4 coiled-coil complexes. The temperature-dependent DLS study showed that the DCR change depends on the rate of cooling of the PK_4 solution. As expected, TEM imaging reveals quite different structures of PK_4. In the fast cooled sample (~45 °C/min), large aggregates were observed; which is similar to the PK_4 aggregates obtained without heating and cooling (Figure 7C). In contrast, only small particles were observed upon slow cooling samples (~1 °C/min, see Figure 7D). In summary, these results reveal that PK_4 aggregates in PBS are able to interact with E_4 to form more stable and soluble coiled-coil complexes. Furthermore, PK_4 self-assembly is a kinetic process and the size of the self-assembled PK_4 aggregates depends on the rate of cooling.

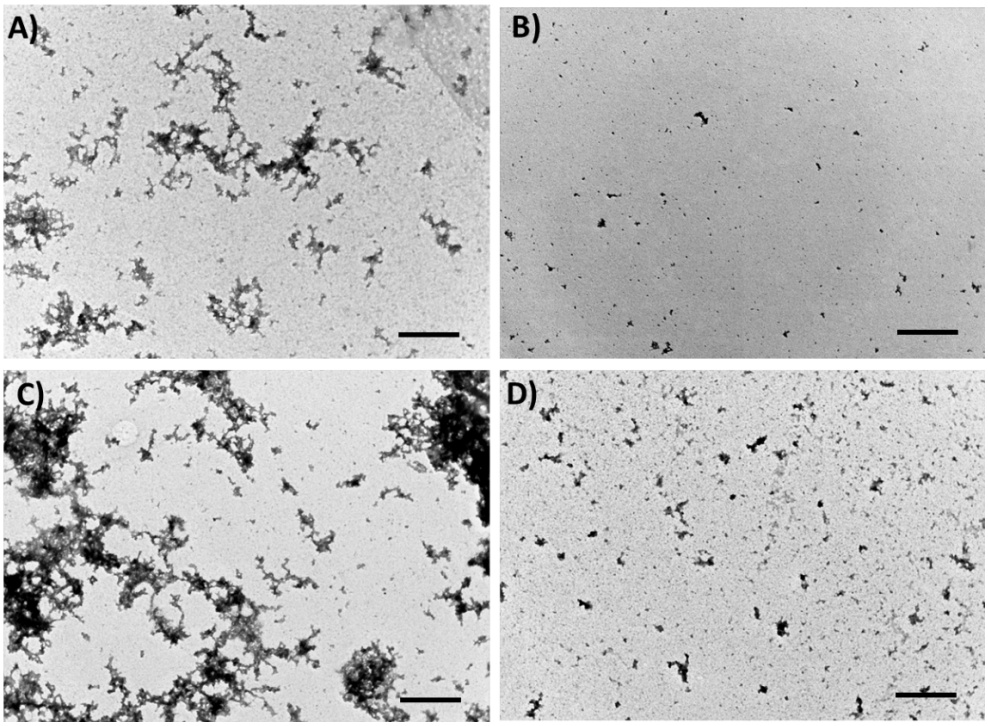

Figure 7. TEM images of PK_4 based structures. A) PK_4 peptide aggregates, B) PK_4 + E_4, C) PK_4 subjected to a fast cooling process and D) PK_4 after a slow cooling process. [PK_4] = 10 μM, [E_4] = 20 μM, all samples were prepared in PBS (pH 7.2) at 20 ℃. Scale bar: 500 μm.

5. Membrane affinity of K_4 dimers

As described previously, peptide K_4 plays an essential role in the E/K coiled-coil membrane fusion system because it induces membrane curvature, and destabilizes the lipid membrane facilitating membrane fusion.[36] The lysine snorkelling mechanism was proposed to explain the interaction between the lysine-rich K peptides and the lipid membrane,[45] which suggests that structural specificity plays a crucial role in peptide-membrane affinity. Peptide K_4 adopts a helical structure in which the hydrophobic amino acids (at the "*a*" and "*d*" positions) form one face of the peptide while the lysines (at "*e*" and "*g*" positions) lie on both sides of this hydrophobic face. When interacting with a lipid membrane, the hydrophobic face of the peptide inserts into the hydrophobic centre of the membrane and the positive amines on the side chain of lysine interacts with the negative phosphate groups of the lipids through electrostatic interactions. Therefore, the K_4 dimers in the current

study are expected to have a high affinity for lipid bilayers.

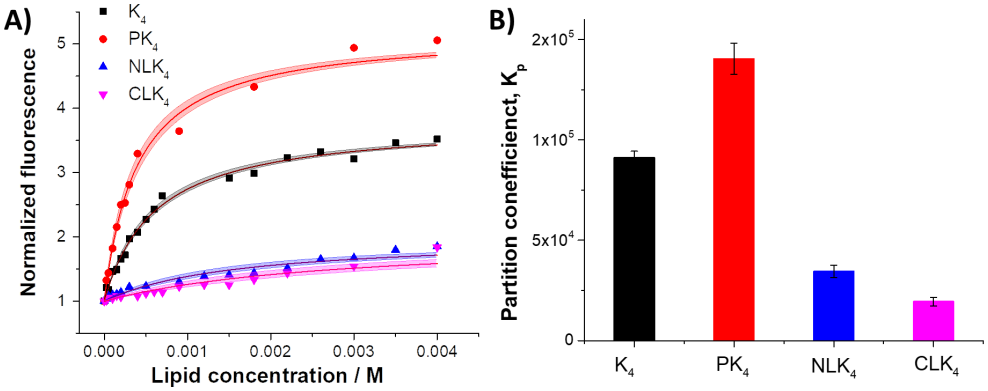

Figure 8. (A) Tryptophan fluorescence titration assay and nonlinear fitting based on equation 4 (see experimental section). The shadow following each fitting curve represents the 95% confidence interval of the fit. (B) The membrane partition coefficient (K_p) of three K_4 dimers and K_4 monomer was calculated during fitting.

Tryptophan is intrinsically fluorescent and its fluorescence is sensitive to its environment; insertion into a hydrophobic membrane leads to a fluorescence increase. To compare the membrane partition coefficient (K_p) of the K_4 peptide variants, a tryptophan fluorescence titration assay was performed (Figure 8 and Table 3). The tryptophan fluorescence of PK_4 increased nearly fivefold in the presence of a lipid membrane. In contrast, the fluorescence of the linear K_4 dimers hardly increased, revealing an inability to interact with a lipid membrane. The K_p of each peptide was determined by a non-linear fitting procedure (Figure 8B). The highest partition coefficient was calculated for PK_4, revealing that this dimer has the highest lipid membrane affinity, confirming our hypothesis that as PK_4 has a higher charge density it interacts more strongly with lipid membranes. Although the linear K_4 dimers are identical in composition but differ in structure, they show a low affinity for lipid membranes. This result can be explained by the fact that linear K_4 dimers tend to form a 'tetramer-like' dimeric structure thereby shielding the hydrophobic face of the peptides. As a result, these linear dimers are unable to interact with a membrane.

Table 3. Lipid membrane affinity determined by tryptophan fluorescence titrations.

peptide	K_p [a] (10^3)	R^2 [b]
K_4	91.1	0.99
PK_4	140.4	0.99
NLK_4	34.5	0.94
CLK_4	19.4	0.88

[a] The membrane partition coefficient (K_p) was obtained by a nonlinear fitting curve (Figure 8) based on equation 4 (see experimental section). [b] The R-squared represent the coefficient of determination.

6. Liposome fusion

The fusogenic properties of the different coiled-coil peptides were studied using lipid-mixing and content-mixing assays. Previous studies have shown that the fusogenic properties of coiled-coil peptides are correlated to the stability of the peptides and the affinity of the K peptide for the lipid membrane.[32, 35] PK_4 forms a strong coiled-coil with peptide E_4 and has a high affinity for lipid membranes, suggesting that the PK_4-E_4 coiled-coil combination may be highly fusogenic.

The lipid mixing assay was based on the Förster resonance energy transfer (FRET) pair nitrobenzoxadiazole (NBD, donor fluorophore) and lissamine rhodamine (LR, acceptor fluorophore).[33, 43] These dyes were attached to lipids and incorporated into the same lipid membrane. When membrane fusion occurs between fluorescent lipid-modified liposomes and non-fluorescent liposomes, the average distance between the NBD and LR fluorophores increases resulting in enhanced NBD emission. In this assay, both sets of liposomes contained 1% CPE_4 and liposome fusion was initiated by K_4 dimer addition. For comparison, lipid mixing facilitated by CPK_4 and CPE_4 was studied as well. PK_4 addition triggered efficient lipid mixing in contrast to the other two linear K_4 dimers (Figure 9A). The final lipid mixing efficiency of PK_4/CPE_4 is even higher than measured for CPK_4/CPE_4. The linear K_4 dimers cannot trigger membrane docking between CPE_4 modified liposomes due to their low lipid membrane affinity as a result of their tendency to form homodimers. In control experiments (Figure S2), a low fluorescence increase was observed when PK_4 was added to plain liposomes (*i.e.* liposomes without CPE_4).

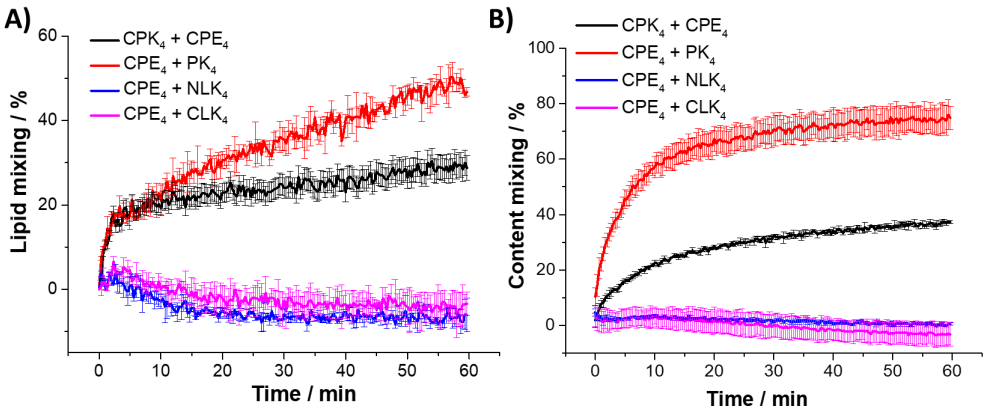

Figure 9. Lipid mixing (A) and content mixing (B) assays. The y-axis represents the percentage fluorescence increase due to liposome docking or membrane fusion.

Next, a content mixing assay was performed. Liposomes were either loaded with sulphorhodamine-B (SRb) at a self-quenching concentration or contained only buffer. Both liposomes were modified with 1% CPE_4. Upon membrane fusion, content mixing results in SRb dilution and fluorescence dequenching. Efficient content mixing was obtained using PK_4 while no fluorescence increase was observed for NLK_4 and CLK_4 (Figure 9B). Surprisingly, content mixing was significantly higher for PK_4/CPE_4 compared to CPK_4/CPE_4. As a control experiment (Figure S2), a leakage test was performed by mixing SRb liposomes with the different K_4 dimers. PK_4 induced liposome leakage but at a low level compared to the PK_4/CPE_4 induced content mixing. This is not surprising because PK_4 has a very high affinity for lipid membranes. When PK_4 was added to a liposome mixture containing both non-CPE_4 modified liposomes (no dye) and SRb liposomes, the content mixing curve was slightly higher than the leakage control, revealing that even in the absence of CPE_4, PK_4 weakly induces liposome fusion, along with leakage. In contrast, no linear K_4 dimer was able to induce non-CPE_4 modified liposome fusion or leakage which might be due to the low membrane affinity or homodimer formation. This high membrane affinity of fusogenic PK_4 makes the PK_4/CPE_4 pair suitable for liposome-cell fusion.

7. Cell membrane labelling

Decorating cell membranes with lipopeptides was demonstrated in previous studies.[37-38, 46] In order to confirm coiled-coil formation between K_4 dimers and lipopeptide-E_4, and also to determine whether K_4 dimers interact with another E_4 peptide after combining with lipopeptide CPE_4, a cell membrane labelling assay

was performed (Figure 10A). K_4 dimers were added to CPE_4 modified Hela cells resulting in coiled-coil formation. Next, carboxyfluorescein labeled peptide E_4 (fluo-E_4) was added to probe binding to the K4 dimer at the cell surface.

In a control experiment, CPE_4 decorated cells were incubated with fluo-E_4 and no fluorescence was detected at the cell membrane (Figure S3A). Fluorescence was observed when the membrane labelling assay was performed using CPK_4 decorated cells + fluo-E_4 (Figure 10B), which is in line with the previous study.[38] The cell membrane with the highest amount of fluorescence was observed by performing the cell membrane labeling assay using PK_4 (Figure 10C), indicative of efficient coiled-coil interaction between PK_4 and E_4 on the membrane. Figure S3B shows that even for cells without CPE_4 decoration, the addition of PK_4 and fluo-E_4 resulted in some fluorescence at the cell membrane. However, the fluorescence intensity is significantly lower and the distribution is less homogeneous. The PK_4 peptides likely form particles in DMEM (Figure S4) which interact with the negatively charged cell membrane through electrostatic interactions. These particles also mediate the interaction between the CPE_4 labelled cell membrane and the fluorescent E_4 peptides, as in these images there also appears to be 'clusters' of fluorescence. In contrast, cell membrane labelling with NLK_4 resulted in only treated cells with very weak fluorescently labelled membranes (Figure 10D) while CLK_4 showed almost no fluorescent labeling (Figure 10E). In the control experiment, no cell membrane labelling was observed when the cell was not decorated with CPE_4 (Figure S3C & S3D). These results suggest that the linear dimeric K_4 peptides are unable to interact with CPE_4 at the cell membrane or fluo-E_4. The tetramer-like homodimer formation of the linear K_4 dimers could be responsible for the low membrane labelling. The hydrophobic face of the linear dimeric K_4 peptides is buried, which makes the interaction with peptide E_4 less favourable. Because CLK_4 forms more stable homodimers than NLK_4, the cell membrane labelling efficiency with CLK_4 was very low.

The cell membrane labelling assay reveals that PK_4 efficiently forms coiled coils with CPE_4 and free fluo-E_4 on the cell membrane. Due to homodimer formation, the linear K_4 dimer variants show very low cell membrane labelling affinity. Combined this study suggests that PK_4 is the best choice for future drug delivery applications.

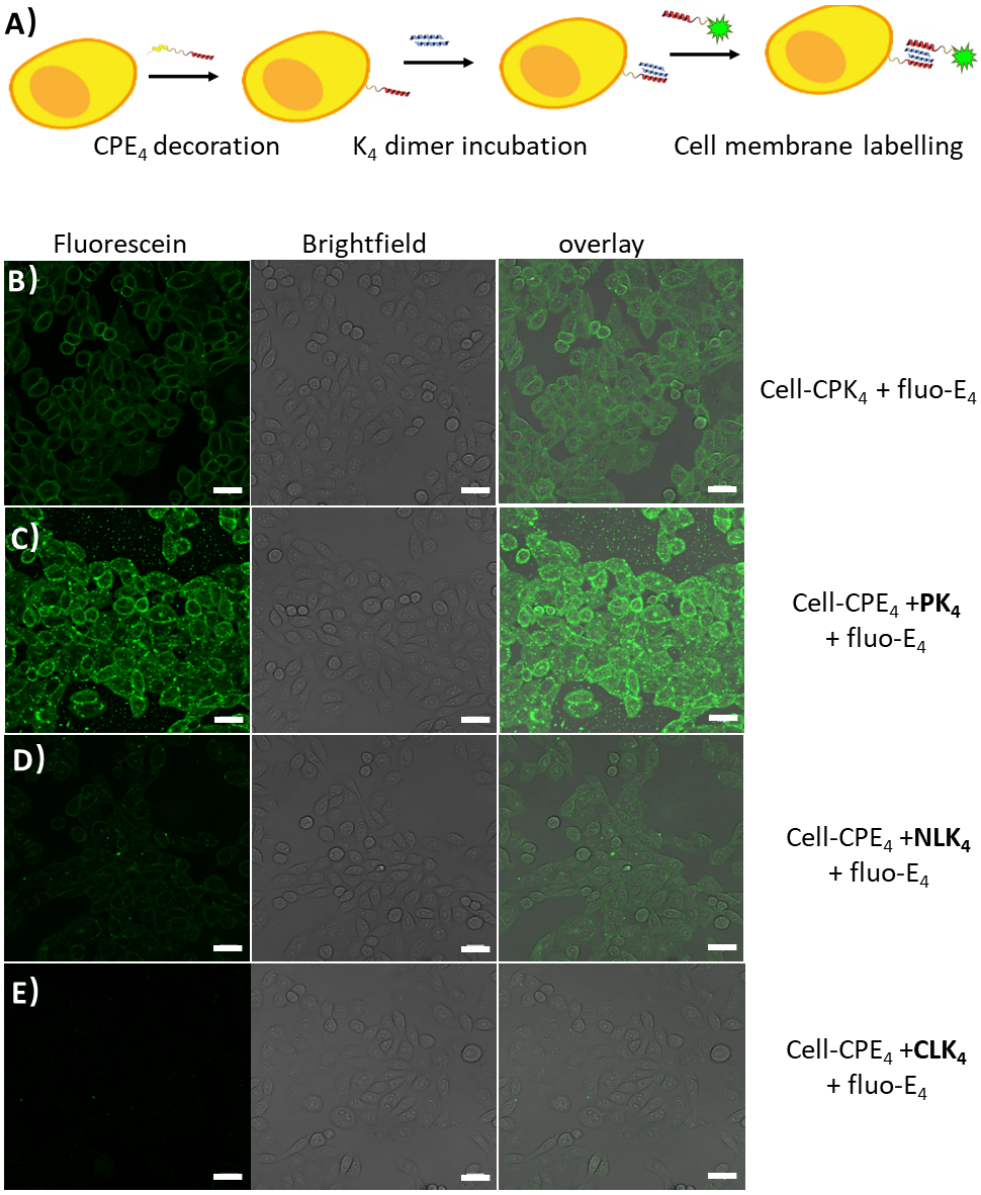

Figure 10. (A) Scheme of cell membrane labelling using PK_4 as an example. (B) CPK_4 decorated Hela cell membrane labelling by adding fluo-E_4. CPE_4 decorated Hela cell incubated with PK_4 (C), NLK_4 (D) or CLK_4 (E), then fluorescent membrane labelling is obtained by adding fluo-E_4. Green channel: fluorescein. Scale bar: 30 µm.

8. Cell-liposome fusion - NBD/propidium iodide (PI) delivery

To investigate whether it is possible to use K_4 dimers to induce efficient cell-liposome membrane fusion, a membrane fusion assay was performed (Figure 11A). Cells were decorated with CPE_4 and the K_4 dimers were added. Next, CPE_4 modified liposomes containing PI and labelled with NBD were added to induce cell-liposome membrane fusion. PI is a membrane-impermeable fluorescent dye, therefore delivery of liposomal propidium iodide (PI) into cells is a convincing indicator for the membrane fusion pathway.

Confocal imaging was applied to visualize cell-liposome fusion induced by the different coiled-coil peptides. Figure 11A shows the result of cell-liposome membrane fusion between CPK_4 decorated cells and CPE_4 modified liposomes. NBD fluorescence was observed at the membranes while PI stained the cytoplasm red (Figure 11B), which is consistent with previous results.[37] In this study, the highest PI delivery efficiency was obtained when CPE_4 decorated cells were fused with CPE_4 modified liposomes induced by coiled-coil formation with the addition of peptide PK_4 (Figure 11C). In contrast, cell-liposome fusion using the linear K_4 dimers resulted in very low efficiency. With the NLK_4 peptide, only weak fluorescence was obtained both on the cell membrane and in the cytoplasm (Figure 11D), suggesting a low efficiency of cell-liposome fusion. Almost no membrane- and cytoplasm-fluorescence was observed when using CLK_4 (Figure 11E). These results are consistent with the cell membrane labeling results which are because CLK_4 forms homodimers more readily and has a lower affinity for lipid membranes than NLK_4. In contrast, the PK_4 dimer forms coiled coils with the E_4 peptide efficiently and it has a high affinity for the cell membrane, resulting in highly efficient cell-liposome membrane fusion.

In control experiments, no fluorescence was observed in cells when plain liposomes (liposome contains no CPE_4) were used (Figure S5), revealing that coiled-coil formation plays an essential role in membrane fusion. In the absence of a K_4 dimer, fusion between cells and CPE_4 modified liposomes was not achieved (Figure S6A). However, fluorescent cells were observed when PK_4 was used in combination with CPE_4 modified liposomes, (Figure S6B), even without CPE_4 on the cell membrane. This can be explained by the fact that PK_4 assembles into positively charged particles (Figure S4) and is capable of interacting with negatively charged cell membranes. This makes it possible for CPE_4 modified liposomes to interact with PK_4 clusters through coiled-coil formation, resulting in

liposome uptake. There is also weak NBD staining on the cell membrane with high PI staining inside the cells, (Figure S6B). We suspect that, in this case, most liposomes enter the cells via endocytosis, thus NBD does stain the cell membrane homogeneously or strongly, but PI is released into the cytoplasm. Due to the low affinity of linear K_4 dimers for the lipid membrane, membrane fusion between non-CPE_4 decorated cells and CPE_4 modified liposomes was not observed (Figure S6C & 6D).

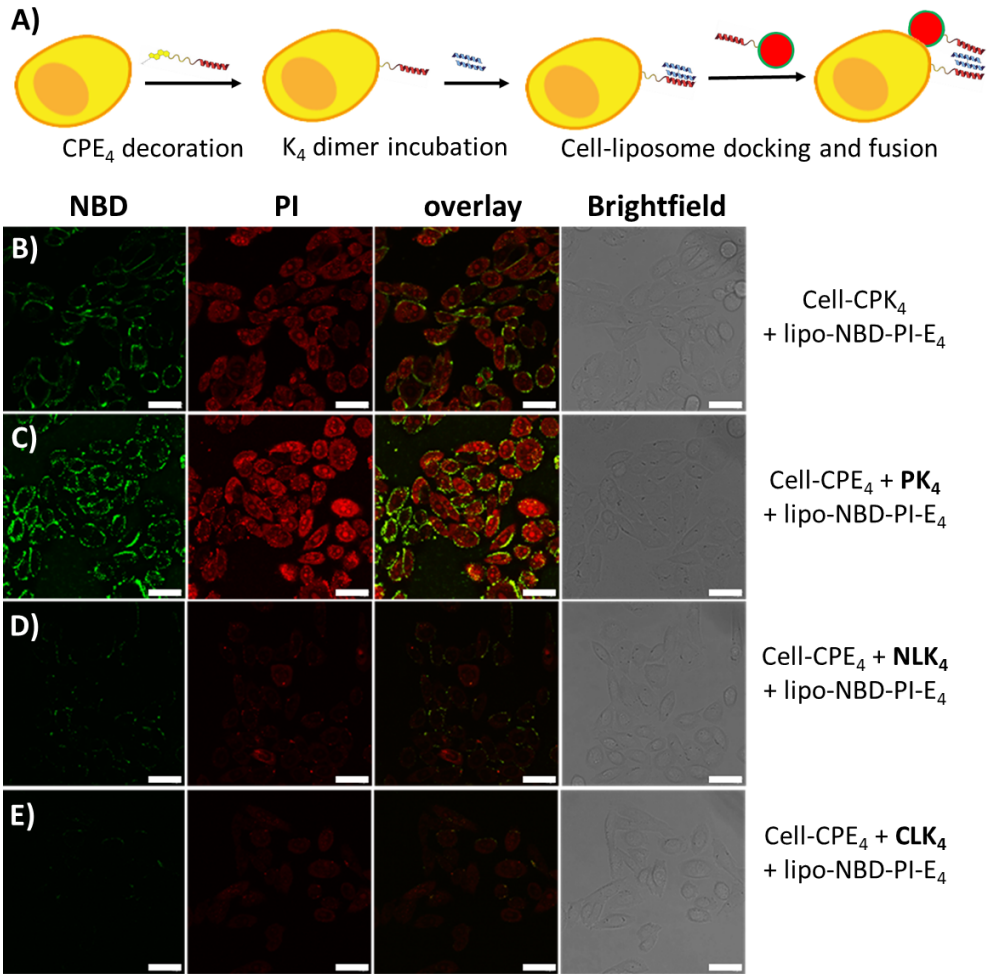

Figure 11. (A) Scheme of the cell-liposome fusion assay. (B) Cell-liposome fusion between CPK_4 decorated Hela cells and CPE_4 modified liposomes containing NBD and PI. Cell-liposome fusion between CPE_4 decorated Hela cells and CPE_4 modified liposomes triggered by different K_4 dimers, (C) PK_4, (D) NLK_4 and (E) NLK_4. Green channel: NBD, red channel: PI. Scale bar: 30 μm.

CONCLUSION

In this study, three different K_4 dimers were designed, synthesized and characterized. CD measurements show that these K_4 dimers adopt different secondary structures in buffered solutions. The CD spectrum of PK4 suggests aggregation of the peptides while the linear K_4 dimers appeared to fold into typical helical structures. The three K_4 dimers show different affinities for the complementary peptide E_4 resulting in coiled coils with different thermostabilities. The DLS study revealed that PK_4 indeed forms particles in solution, confirming the non-helical CD spectra. In the DLS titration assay, peptide E_4 induces the PK_4 particles to dissociate by forming soluble heterodimeric coiled coils evidenced by the strong α-helical signal observed by CD spectroscopy. The linear K_4 dimers were found to self-associate by CD titration assays and this self-assembly behaviour influences heterodimeric coiled-coil formation with peptide E_4. Furthermore, these linear K_4 dimers have a low affinity for the lipid membrane and are also incapable of triggering efficient membrane fusion. Temperature-dependent CD studies reveal that the secondary structure of PK_4 changes with temperature and it adopts maximum helicity at 60 °C. The membrane affinity study of the K_4 dimers reveals that PK_4 has the highest lipid membrane affinity while linear K_4 dimers hardly interact with a lipid membrane, most likely due to homodimer formation. These results are consistent with the liposome membrane fusion results that show that the PK_4-E_4 coiled-coil results in the highest efficiency in both lipid and content mixing, while almost no liposome membrane fusion was obtained using linear K_4 dimers. Because of the high affinity of PK_4 to lipid membranes, PK_4 induces some membrane fusion by itself, along with liposome leakage. These results confirm our hypothesis that the affinity properties of peptide K for cell membranes, which resulting in destabilization of the lipid membrane is pivotal for inducing efficient membrane fusion.

In cell assays, cell membrane labelling and cell-liposome fusion were achieved using the K_4-dimer/E_4 system. The highest level of NBD and PI delivery was obtained using the PK_4/CPE_4 combination, consistent with the liposome fusion assays. In contrast, weak membrane labelling and NBD-PI delivery were obtained using the NLK_4/E_4 coiled-coil pair, while no membrane labelling and NBD-PI delivery were achieved with CLK_4/E_4 coiled-coil. This can be explained by the peptide study showing that NLK_4 has a lower tendency to dimerize and a higher affinity for the lipid membrane than CLK_4. In summary, this study of K_4 dimer

based self-assembly and coiled-coil formation, together with their properties for triggering membrane fusion could not only contribute to the design and development of coiled-coil peptide-based membrane fusion systems but also provides a more efficient system for potential drug delivery applications.

EXPERIMENTAL SECTION

Chemicals and materials

All chemicals were purchased from Sigma and used directly without further purification unless otherwise stated. All amino acids and HCTU were obtained from Novabiochem. All solvents, in addition to piperidine, trifluoroacetic acid (TFA) and acetic anhydride were purchased from Biosolve. Tentagel HL RAM resin was purchased from Iris Biotech GmbH. Oxyma pure was obtained from Carl Roth GmbH. All lipids were purchased from Avanti Polar Lipids. µ-Slide 8 Well confocal chambered coverslips were purchased from Ibidi. All cell culture supplies were purchased from Starstedt. Ultrapure water was obtained from Milli-Q^{TM} purification system from Millipore (Amsterdam, The Netherlands).

Peptides synthesis

All peptides were synthesized using Fmoc chemistry on a CEM Liberty Blue microwave-assisted peptide synthesizer. A Tentagel HL RAM resin (0.22 mmol/g) was used as the solid phase for peptide synthesis. The Fmoc group was removed with 20% piperidine in DMF by heating to 90 ℃ for 1 min. In the reaction, 5 eqv. of DIC and 5 eqv. Oxyma and 5 eqv. of amino acid were added to the reaction vessel and heated to 90 ℃ for 4 minutes. DMF was used as the solvent. All the peptides sequences are listed in Table S1. Except for the ones for synthesising lipidated and fluorescent peptides, all peptides were acetylated at N-terminus.

Synthesis of PK$_4$: K$_4$GW-Cys14 and K$_4$-Cys14 were synthesized and purified by HPLC (see below). K$_4$GW-Cys14 (66 mg, 20 µmol) was dissolved in 15 mL of water and activated with 2,2′-Dithiobis(5-nitropyridine) (62 mg, 200 µmol) dissolved in 5 mL of acetone. For this, the K$_4$GW-Cys14 solution was added to the flask containing 2,2′-Dithiobis(5-nitropyridine) dropwise while stirring. The reaction was stirred overnight and turned yellow gradually. After filtration, the reaction mixture was dried under a N_2 flow. The crude peptide was dissolved in 20 mL water and purified by HPLC (see below) and lyophilized yielding a white K$_4$GW-Cys14-S-nitropyridine solid powder (50 mg, 14.5 µmol, yield: 72.5%).

Peptide K_4GW-Cys14-S-nitropyridine (20 mg, 5.8 μmol) was mixed with peptide K_4-Cys14 (20 mg, 6.6 μmol) and dissolved in 10 mL HEPES buffer (pH 8.1). The solution turned yellow gradually and after 30 minutes, the peptide was purified by direct injecting of the reaction mixture in HEPES into the HPLC (see below) and lyophilized to yield a white powder (22mg, 3.5 μmol, yield: 59.8%).

Synthesis of NLK_4: CG-K_4GW and CG-K_4 were synthesized and purified. CG-K_4GW (70 mg, 20 μmol) was dissolved in 15 mL of water in a flask and 5 mL 2,2′-Dithiobis(5-nitropyridine) (62mg, 200 μmol) solution in acetone was added dropwise while stirring. After filtration, the reaction mixture was dried under an N_2 flow. The crude peptide was dissolved in 20 mL water and purified by HPLC (see below) and lyophilized yielding a white CG-K_4GW-S-nitropyridine solid powder (60 mg, 16.5 μmol, yield: 82%). Peptide CG-K_4GW-S-nitropyridine (20 mg, 5.5 μmol) was mixed with peptide CG-K_4 (20 mg, 6.2 μmol) and dissolved in 10 mL HEPES buffer (pH 8.1). The solution turned yellow gradually and after 30 minutes, the peptide was purified by directly injecting the reaction mixture into the HPLC (see below), followed by lyophilization to yield a white powder (20 mg, 3 μmol, yield: 54.2%).

Synthesis of CLK_4: K_4GW-GC and K_4-GC were synthesized and purified. CG-K_4GW (70 mg, 20 μmol) was dissolved in 15 mL of water in a flask and 5 mL 2,2′-Dithiobis(5-nitropyridine) (62 mg, 200 μmol) solution in acetone was added dropwise while stirring. After filtration, the reaction mixture was dried under an N_2 flow. The crude peptide was dissolved in 20 mL water and purified by HPLC (see below) and lyophilized yielding a white CG-K_4GW-S-nitropyridine solid powder (55 mg, 15,7 μmol, yield: 78%). Peptide CG-K_4GW-S-nitropyridine (20 mg, 5.5 μmol) was mixed with peptide CG-K_4 (20 mg, 6.2 μmol) and dissolved in 10 mL HEPES buffer (pH 8.1). The solution turned yellow gradually and after 30 minutes, the peptide was purified by directly injecting the reaction mixture into the HPLC (see below) and lyophilized to yield a white powder (18 mg, 2.7 μmol, yield: 48.8%).

Lipopeptide Synthesis

The synthesis of the lipopeptides (CPK_4 and CPE_4) is described in **Chapter 3**.

Fluo-K_4/Fluo-E_4 Synthesis

The synthesis of the fluorescent peptides (fluo-K_4 and fluo-E4) is described in

Chapter 3.

Peptide purification

All peptides were purified with reversed-phase HPLC on a Shimadzu system with two LC-8A pumps and an SPD-20A or MPD-20A UV-Vis detector. A Vydac C4 column (22 mm diameter, 250 mm length, 10 μm particle size) was used for lipopeptides CPK_4 and CPE_4. A linear gradient from 20% to 80% acetonitrile (with 0.1% TFA) in water (with 0.1% TFA) was performed at a 12 mL/min flow rate over 36 mins.
All other peptides were purified using a Phenomenex Kinetix Evo C18 column (21.2 mm diameter, 150 mm length, 5 μm particle size). The 'K' peptides, which include K_4, K_4-Cys14, K_4GW-Cys14, CG-K_4, CG-K_4-GW, K_4-GC, WG-K_4-GC, fluo-K_4 and all the three K_4 dimers were purified using a linear gradient from 20% to 45% acetonitrile (with 0.1% TFA) in water (with 0.1% TFA) with a 12 mL/min flow rate over 28 mins. The E4 and fluo-E_4 peptides were purified using a linear method gradient from 20% to 55% acetonitrile (with 0.1% TFA) in water (with 0.1% TFA) with a 12 mL/min flow rate over 28 mins. All peptides were characterized by LC-MS, see Figure S9-11 and Table S2.

CD Spectroscopy

CD measurements were performed on a JASCO J-815 CD spectrometer equipped with a Peltier temperature controller. All room temperature CD was carried out at 20 ℃ with a 2 mm path length quartz cuvette. Data points were recorded every 1 nm from 190 nm to 260 nm, with a 1 second response time, 2 nm bandwidth and 5 sequentially recorded spectra averaged at a scanning speed of 200 nm/min.

After the data were collected, the mean residue molar ellipticity was calculated using equation 1:

$$[\theta] = (1000 \times [\theta]_{obs})/(cnl) \quad (1)$$

Where [θ] is the mean residue molar ellipticity in $deg \cdot cm^2 \cdot dmol^{-1}$, $[\theta]_{obs}$ represents the observed ellipticity in mdeg, c is the concentration of peptide in mM, n represents the number of amino acids in the peptide and l is the path length of the cuvette in mm.

The percentage of helicity of the peptides (F_{helix}) can be calculated by equation 2:

$$F_{helix} = 100\% ([\theta]_{222} - [\theta]_0) / ([\theta]_{max} - [\theta]_0) \quad (2)$$

In equation 2, $[\theta]_{222}$ represents the mean residue molar ellipticity of peptide at 222 nm, $[\theta]_0$ is the mean residue ellipticity of the peptide when the peptide is in an entirely random coil conformation, $[\theta]_{max}$ is the maximum theoretical mean residue ellipticity. The details for calculating $[\theta]_0$ and $[\theta]_{max}$ can be found in chapter 3.

Temperature-dependent CD measurements were performed with the same instrument, using the same cuvette. The melting curves of all peptides were obtained by recording the ellipticity at 222 nm from 5 ℃ to 95 ℃ with a 1 ℃ data pitch and with a 60 ℃/h temperature ramp. The delay time for each data point was 2 seconds.

CD titration and nonlinear fitting for homodimer formation

The CD titration study was performed on the same JASCO J-815 CD spectrometer. The measurements were carried out at 20 ℃ with a 1 mm path length quartz cuvette. All the parameters are the same as described above except the low sensitivity detection mode was used in this study. The concentration of each linear K_4 dimer varied from 2.5 μM to 150 μM. The normalized mean residue molar ellipticity was calculated based on equation 1.

The non-linear fitting curve for the concentration-dependent CD titration used to determine homodimer formation was based on equation 3:

$$[\theta] = \frac{K_d\left(-1+\sqrt{1+\frac{8[P_t]}{K_d}}\right)\{2[\theta_m]+\left(-1+\sqrt{1+\frac{8[P_t]}{K_d}}\right)[\theta_d]\}}{8[P_t]} \quad (3)$$

where $[\theta]$ represents the mean residue ellipticity in deg·cm^2·dmol^{-1}, $[\theta_m]$ and $[\theta_d]$ represents the normalized mean residue molar ellipticity contributed by the peptide monomer or homodimer, K_d represents the dissociation constant and $[p_t]$ represents the total concentration of peptide. The K_a (K_a = 1 / K_d) of each K_4 dimer was calculated and summarized in Table 2.

Dynamic light scattering (DLS)

DLS measurements were performed on a Zetasizer Nano S (Malvern Instruments, Malvern, UK) equipped with a green laser (532 nm). All the derived count rate (DCR) measurements were performed in a low volume cuvette (Brand, Wertheim, Germany) by non-invasive backscatter mode (automatic mode), detecting the

scattered light at 175°. Except for the temperature-dependent DLS assay, data was collected in triplicate at 20 ℃. All K_4 dimers were measured at a concentration of 10 μM and K_4 at 20 μM.

DLS titration

For the DLS titration assay (PK_4 as the example), a guest solution that contained 200 μM of E_4 and 10 μM of PK_4 was gradually added into the host solution containing 10 μM of PK_4. During the titration assay, the concentration of PK_4 was kept at 10 μM while the concentration of E_4 was varied from 0 to 20 μM. In every titration, the DCR was measured after 3 minutes of incubation to stabilize the particles. The process for all the other titration assays is similar.

Temperature-dependent DLS

For temperature-dependent DLS measurements, data were collected in duplicate every 5 ℃ from 20 ℃ to 90 ℃ and then the temperature was decreased from 90 ℃ to 20 ℃ at a speed of 1 ℃/min. In the fast temperature drop temperature-dependent DLS assay, the sample was slowly heated up from 20 ℃ to 90 ℃ (1 ℃/min), then a DLS measurement was performed at 90 ℃. Next, the sample was cooled from 90 ℃ to 20 ℃ over 2 min (~ 45 ℃/min), the DCR was measured after 3 min of incubation.

Tryptophan fluorescence titration assay

Tryptophan fluorescence titration assays were performed in 96-well plates using a TECAN Infinite M1000 Pro microplate reader. Details of liposome preparation are described in the next section. For each titration assay, 2.5 μM of the peptide was mixed with liposomes with a series of lipid concentrations ranging from 25 μM to 4500 μM. After mixing, the 96-well plate was incubated at room temperature for 60 min before fluorescence measurements were recorded. The fluorescence spectrum was obtained by recording the emission from 450 to 310 nm using an excitation wavelength of 275 nm.

The fluorescence of each measurement was normalized to the free peptide fluorescence intensity, *i.e.* in the absence of liposomes. Maximum tryptophan fluorescence was observed around 340 nm and used to obtain the titration curve. The nonlinear fitting and partition constant were based on equation 4:[43]

$$F = 1 + (F_{max} - 1)(K_pX)/(55.3 + K_pX) \qquad (4)$$

F is the normalized fluorescence and F_{max} is the maximum fluorescence when all peptide interacts with the lipid membrane. K_p is the molar partition coefficient. X represents the concentration of peptide in M and 55.3M is the assumed constant of water concentration at room temperature. The partition coefficient and the standard error of fitting was achieved using the least-squares method by fitting the experimental result to equation 4.

Lipopeptide Micelles and Liposome Preparation

Lipopeptide (CPK_4 or CPE_4) was dissolved in chloroform/methanol (1:1) at a concentration of 200 μM. 50 μL CPK_4 or CPE_4 stock solution was dried to a film in a 20 ml glass vial under N_2 flow. DMEM (1 mL) was added to the glass vials to rehydrate the lipopeptide film. The vials were sonicated in a sonication bath for 5 min at 55 ℃ to obtain lipopeptide micelle solutions (10μM).

The liposomes used for tryptophan fluorescence titration studies were prepared by the extrusion method. DOPC/DOPE/cholesterol (50/25/25%) was dissolved in chloroform/methanol (1:1) at a total concentration of 10 mM. 1 mL of this solution was dried to form a lipid film in a 20 ml glass vial under N_2 flow for 2 h, followed by incubation in a vacuum desiccator for 30 min. Lipid film rehydration in 1 mL of PBS was followed by vortexing at maximum speed for 30 s. Liposomes were obtained by extrusion using an Avanti mini extruder with 100 nm polycarbonate membranes at 55 ℃. The liposomes were characterized by DLS and the average size was found to be 100 nm with a polydispersity index (PDI) below 0.2.

All liposomes used in liposome membrane fusion and cell-liposome fusion studies were prepared similarly. The list of liposomes and their lipid composition is shown in Table S3. The preparation of lipo-NBD-PI-E_4 liposomes is shown as an example. The lipid mixture containing DOPC/DOPE/cholesterol/DOPE-NBD (49.5/24.75/24.75/1%) was dissolved in chloroform/methanol (1:1) at a total lipid concentration of 10 mM. The lipid film was prepared in 20 mL glass vials by drying 100 μL of lipid stock solution mixed with 100 μL lipopeptide solution (1% mole ratio of total lipid) under N_2 flow for 2h. The glass vials were transferred to a vacuum desiccator for 30 min to remove the remaining solvent. A propidium iodide (PI) solution was prepared by dissolving 10 mg of PI in 1 mL hot PBS (60 ℃). The lipid film was rehydrated by adding 1 mL of PI solution and vortexing at high speed for 30s. Liposomes were prepared using the sonication method by sonicating the lipid solution using a Branson 2510 bath sonicator for 3 min at 55 ℃.

G25 size-exclusion PD-10 Columns (GE-Healthcare, USA) were used to separate liposomes from the non-encapsulated PI. The quality of the liposome was determined by DLS and the average size was found to be around 100 nm with a PDI below 0.25. A 500 μM liposome solution contains 1% DOPE-NBD, 1% CPE_4 and 10 mg/mL of encapsulated PI. The PI loaded and sulphorhodamine-B (SRb) loaded liposomes were purified using a G25 size-exclusion PD-10 column, all other liposomes were used without additional purification.

Liposome membrane fusion—lipid mixing and content mixing

For the lipid mixing assays, lipo-NBD/LR-E_4 and lipo-E_4 were mixed (1:1) at a total lipid concentration of 200 μM. For each experiment, 200 μL of the liposome mixture was transferred to a black 96 well-plate followed by the addition of K_4 dimer (50 μl, 8 μM). For the non-CPE_4 modified liposome control, lipo-NBD/LR and lipo-free were mixed (1:1) at a total lipid concentration of 200 μM. 200 μL of this liposome mixture was used and K_4 dimer (50 μl, 8 μM) was added before the measurement. For the positive control, 200 μL of 200 μM lipo-NBD/LR-positive was mixed with 50 μL of PBS. For the negative control, 100 μL of 200 μM lipo-NBD/LR-E_4 was mixed with 150 μL PBS. For the CPK_4-CPE_4 control, 100 μL of 200 μM lipo-NBD/LR-E_4 mixed 50 μL of PBS, following by adding 100 μL of 200 μM Lipo-K_4. The NBD emission at 530 nm was measured every 20 s and followed over 1 h. The standard deviation was calculated by two independent samples, and the experiment was repeated two times.

For content mixing assays, the process and concentrations of all components were identical to the lipid mixing assays except that the membrane dye (NBD/LR) was replaced by the soluble dye (SRb). An additional liposome leakage control was performed, which 100 μL of lipo-SRb was mixed with 100 μL PBS followed by the addition of 50 μL of 8 μM K_4 dimers. SRb emission at 585 nm was measured every 20 s for 1 h. The standard deviation was calculated from two independent samples, and the experiment was repeated twice.

All fluorescence measurements were performed using a TECAN Infinite M1000 Pro microplate reader. The fusion efficiency of both lipid mixing and content mixing was calculated based on equation 5:

$$\%F_t = 100\% \times (F_t - F_0)/(F_{max} - F_0) \qquad (5)$$

Where $\%F_t$ is the percentage of fluorescence increase, F_t is the fluorescence

intensity at a specific time t, F_{max} is the fluorescence intensity from the positive control at the same time t and F_0 is the fluorescence intensity from negative control at the same time.

Cell labelling

5×10^4 Hela cells were seeded in ibidi µ-Slide 8 well plates with 200 µL of DMEM for 24h at 37 °C in a 7% CO_2 atmosphere. DMEM was removed from the cell culture and then 200 µL of CPK_4 or CPE_4 (10 µM) solution was added to each well containing cells and incubated for 1.5 h. After the lipopeptide was washed away, 200 µL of different K_4 dimers (10 µM in DMEM) was added and incubated for 10 min. The K_4 dimers solution was removed and the cells were washed three times with DMEM. Then fluo-E_4 (200 µL, 20 µM in DMEM) was added to the wells. After 15 min incubation, all wells were thoroughly washed using DMEM before imaging using confocal microscopy.

Cell-liposome fusion assay—PI delivery

5×10^4 Hela cells were seeded in ibidi µ-Slide 8 well plates with 200 µL of DMEM at 37 °C in a 7 % CO_2 atmosphere. After 24h, the medium was removed and cells were washed with fresh DMEM, following by the addition of 200 µL CPK_4 (10 µM) or CPE_4 (10 µM) and incubated for 1.5 min. After excess lipopeptide was washed away, 200 µL of the K_4 dimer (10 µM in DMEM) was added and incubated for 10 min. Liposomes in PBS were diluted with DMEM to reduce the toxicity of cells by buffer (PBS < 50 %). After the cells were washed three times with DMEM, CPE_4-decorated liposomes (200 µL, [lipid] = 250 µM) containing PI and labelled with NBD were added and incubated for 15 minutes at 37 °C. Next, the liposomes were removed and the cells were washed three times with DMEM. Confocal microscopy imaging was performed after the cells were incubated for another 30 min.

Confocal Microscopy

Confocal imaging was performed using a Leica TCS SP8 confocal laser scanning microscope with the Leica application suite advanced fluorescence software (LAS AF, Leica Microsystems B.V., Rijswijk, The Netherlands). The fluo-K_4, fluo-E_4 and NBD fluorescence was excited by a laser at 488 nm and the emission was detected from 495 nm to 550 nm. The PI fluorescence was excited by a laser at 535 nm and the emission was detected from 600 nm to 700 nm. For each set of experiments, all settings were kept the same.

REFERENCES

(1) Aminu, N.; Bello, I.; Umar, N. M.; Tanko, N.; Aminu, A.; Audu, M. M. The influence of nanoparticulate drug delivery systems in drug therapy. *Journal of Drug Delivery Science and Technology* **2020,** *60*, 101961.

(2) Fenton, O. S.; Olafson, K. N.; Pillai, P. S.; Mitchell, M. J.; Langer, R. Advances in biomaterials for drug delivery. *Advanced Materials* **2018,** *30*, 1705328.

(3) Paolino, D.; Sinha, P.; Fresta, M.; Ferrari, M. Drug delivery systems. *Encyclopedia of medical devices and instrumentation* **2006**.

(4) Savjani, K. T.; Gajjar, A. K.; Savjani, J. K. Drug solubility: importance and enhancement techniques. *ISRN Pharm* **2012,** *2012*, 195727.

(5) Yue, Z. G.; Wei, W.; Lv, P. P.; Yue, H.; Wang, L. Y.; Su, Z. G.; Ma, G. H. Surface charge affects cellular uptake and intracellular trafficking of chitosan-based nanoparticles. *Biomacromolecules* **2011,** *12*, 2440.

(6) Mosquera, J.; Garcia, I.; Liz-Marzan, L. M. Cellular Uptake of Nanoparticles versus Small Molecules: A Matter of Size. *Acc Chem Res* **2018,** *51*, 2305.

(7) Lee, J. H.; Yeo, Y. Controlled Drug Release from Pharmaceutical Nanocarriers. *Chem Eng Sci* **2015,** *125*, 75.

(8) Sethi, M.; Sukumar, R.; Karve, S.; Werner, M. E.; Wang, E. C.; Moore, D. T.; Kowalczyk, S. R.; Zhang, L.; Wang, A. Z. Effect of drug release kinetics on nanoparticle therapeutic efficacy and toxicity. *Nanoscale* **2014,** *6*, 2321.

(9) AlQahtani, A. D.; O'Connor, D.; Domling, A.; Goda, S. K. Strategies for the production of long-acting therapeutics and efficient drug delivery for cancer treatment. *Biomed Pharmacother* **2019,** *113*, 108750.

(10) Khodabakhsh, F.; Salimian, M.; Hedayati, M. H.; Ahangari Cohan, R.; Norouzian, D. Challenges and advancements in the pharmacokinetic enhancement of therapeutic proteins. *Preparative Biochemistry & Biotechnology* **2021,** *51*, 519.

(11) Verbeke, R.; Lentacker, I.; De Smedt, S. C.; Dewitte, H. Three decades of messenger RNA vaccine development. *Nano Today* **2019,** *28*, 100766.

(12) Allen, T. M.; Cullis, P. R. Liposomal drug delivery systems: from concept to clinical applications. *Adv Drug Deliv Rev* **2013,** *65*, 36.

(13) Sercombe, L.; Veerati, T.; Moheimani, F.; Wu, S. Y.; Sood, A. K.; Hua, S. Advances and Challenges of Liposome Assisted Drug Delivery. *Front Pharmacol* **2015,** *6*, 286.

(14) Lian, T.; Ho, R. J. Trends and developments in liposome drug delivery systems. *J Pharm Sci* **2001,** *90*, 667.

(15) Vaughan, H. J.; Green, J. J.; Tzeng, S. Y. Cancer-Targeting Nanoparticles for Combinatorial Nucleic Acid Delivery. *Adv Mater* **2020,** *32*, e1901081.

(16) Swaminathan, J.; Ehrhardt, C. Liposomal delivery of proteins and peptides. *Expert Opin Drug Deliv* **2012,** *9*, 1489.

(17) Kube, S.; Hersch, N.; Naumovska, E.; Gensch, T.; Hendriks, J.; Franzen, A.; Landvogt, L.; Siebrasse, J. P.; Kubitscheck, U.; Hoffmann, B.; Merkel, R.; Csiszar, A. Fusogenic Liposomes as Nanocarriers for the Delivery of Intracellular Proteins. *Langmuir* **2017,** *33*, 1051.

(18) Rayamajhi, S.; Marchitto, J.; Nguyen, T. D. T.; Marasini, R.; Celia, C.; Aryal, S. pH-responsive cationic liposome for endosomal escape mediated drug delivery. *Colloids Surf B Biointerfaces* **2020,** *188*, 110804.

(19) Lechanteur, A.; Sanna, V.; Duchemin, A.; Evrard, B.; Mottet, D.; Piel, G. Cationic liposomes carrying siRNA: impact of lipid composition on physicochemical properties, cytotoxicity and endosomal escape. *Nanomaterials* **2018,** *8*, 270.

(20) Smith, S. A.; Selby, L. I.; Johnston, A. P. R.; Such, G. K. The Endosomal Escape of Nanoparticles: Toward More Efficient Cellular Delivery. *Bioconjug Chem* **2019,** *30*, 263.

(21) Brock, D. J.; Kondow-McConaghy, H. M.; Hager, E. C.; Pellois, J. P. Endosomal Escape and Cytosolic Penetration of Macromolecules Mediated by Synthetic Delivery Agents. *Bioconjug Chem* **2019,** *30*, 293.

(22) Jahn, R.; Lang, T.; Südhof, T. C. Membrane fusion. *Cell* **2003,** *112*, 519.

(23) Wickner, W.; Schekman, R. Membrane fusion. *Nat Struct Mol Biol* **2008,** *15*, 658.

(24) Chernomordik, L. V.; Kozlov, M. M. Mechanics of membrane fusion. *Nat Struct Mol Biol* **2008,** *15*, 675.

(25) Chen, Y. A.; Scheller, R. H. SNARE-mediated membrane fusion. *Nature reviews Molecular cell biology* **2001,** *2*, 98.

(26) Jahn, R.; Scheller, R. H. SNAREs--engines for membrane fusion. *Nat Rev Mol Cell Biol* **2006,** *7*, 631.

(27) Wang, Y.; Li, L.; Hou, C.; Lai, Y.; Long, J.; Liu, J.; Zhong, Q.; Diao, J. SNARE-mediated membrane fusion in autophagy. *Semin Cell Dev Biol* **2016,** *60*, 97.

(28) Mazur, F.; Chandrawati, R. Peptide-Mediated Liposome Fusion as a Tool for the Detection of Matrix Metalloproteinases. *Adv Biosyst* **2019,** *3*, e1800330.

(29) Schmid, Y. R. F.; Scheller, L.; Buchmann, S.; Dittrich, P. S. Calcium-Mediated Liposome Fusion to Engineer Giant Lipid Vesicles with Cytosolic Proteins and Reconstituted Mammalian Proteins. *Adv Biosyst* **2020,** *4*, e2000153.

(30) Löffler, P. M.; Ries, O.; Rabe, A.; Okholm, A. H.; Thomsen, R. P.; Kjems, J.; Vogel, S. A DNA-Programmed Liposome Fusion Cascade. *Angewandte Chemie International Edition* **2017,** *56*, 13228.

(31) Meng, Z.; Yang, J.; Liu, Q.; de Vries, J. W.; Gruszka, A.; Rodríguez-Pulido, A.; Crielaard, B. J.; Kros, A.; Herrmann, A. Efficient Fusion of Liposomes by Nucleobase Quadruple-Anchored DNA. *Chemistry–A European Journal* **2017,** *23*, 9391.

(32) Zheng, T.; Voskuhl, J.; Versluis, F.; Zope, H. R.; Tomatsu, I.; Marsden, H. R.; Kros, A. Controlling the rate of coiled coil driven membrane fusion. *Chem Commun (Camb)* **2013,** *49*, 3649.

(33) Versluis, F.; Voskuhl, J.; van Kolck, B.; Zope, H.; Bremmer, M.; Albregtse, T.; Kros, A. In situ modification of plain liposomes with lipidated coiled coil forming peptides induces membrane fusion.

J Am Chem Soc **2013,** *135*, 8057.

(34) Rabe, M.; Zope, H. R.; Kros, A. Interplay between Lipid Interaction and Homo-coiling of Membrane-Tethered Coiled-Coil Peptides. *Langmuir* **2015,** *31*, 9953.

(35) Rabe, M.; Schwieger, C.; Zope, H. R.; Versluis, F.; Kros, A. Membrane interactions of fusogenic coiled-coil peptides: implications for lipopeptide mediated vesicle fusion. *Langmuir* **2014,** *30*, 7724.

(36) Rabe, M.; Aisenbrey, C.; Pluhackova, K.; de Wert, V.; Boyle, A. L.; Bruggeman, D. F.; Kirsch, S. A.; Bockmann, R. A.; Kros, A.; Raap, J.; Bechinger, B. A Coiled-Coil Peptide Shaping Lipid Bilayers upon Fusion. *Biophys J* **2016,** *111*, 2162.

(37) Yang, J.; Bahreman, A.; Daudey, G.; Bussmann, J.; Olsthoorn, R. C.; Kros, A. Drug Delivery via Cell Membrane Fusion Using Lipopeptide Modified Liposomes. *ACS Cent Sci* **2016,** *2*, 621.

(38) Zope, H. R.; Versluis, F.; Ordas, A.; Voskuhl, J.; Spaink, H. P.; Kros, A. In vitro and in vivo supramolecular modification of biomembranes using a lipidated coiled-coil motif. *Angew Chem Int Ed Engl* **2013,** *52*, 14247.

(39) Daudey, G. A.; Zope, H. R.; Voskuhl, J.; Kros, A.; Boyle, A. L. Membrane-Fusogen Distance Is Critical for Efficient Coiled-Coil-Peptide-Mediated Liposome Fusion. *Langmuir* **2017,** *33*, 12443.

(40) Daudey, G. A.; Schwieger, C.; Rabe, M.; Kros, A. Influence of Membrane-Fusogen Distance on the Secondary Structure of Fusogenic Coiled Coil Peptides. *Langmuir* **2019,** *35*, 5501.

(41) Lindhout, D. A.; Litowski, J. R.; Mercier, P.; Hodges, R. S.; Sykes, B. D. NMR solution structure of a highly stable de novo heterodimeric coiled-coil. *Biopolymers* **2004,** *75*, 367.

(42) Rabe, M.; Boyle, A.; Zope, H. R.; Versluis, F.; Kros, A. Determination of oligomeric states of peptide complexes using thermal unfolding curves. *Biopolymers* **2015,** *104*, 65.

(43) Crone, N. S. A.; Kros, A.; Boyle, A. L. Modulation of Coiled-Coil Binding Strength and Fusogenicity through Peptide Stapling. *Bioconjug Chem* **2020,** *31*, 834.

(44) Mason, J. M.; Arndt, K. M. Coiled coil domains: stability, specificity, and biological implications. *Chembiochem* **2004,** *5*, 170.

(45) Pluhackova, K.; Wassenaar, T. A.; Kirsch, S.; Bockmann, R. A. Spontaneous adsorption of coiled-coil model peptides K and E to a mixed lipid bilayer. *J Phys Chem B* **2015,** *119*, 4396.

(46) Kong, L.; Askes, S. H.; Bonnet, S.; Kros, A.; Campbell, F. Temporal control of membrane fusion through photolabile PEGylation of liposome membranes. *Angewandte Chemie* **2016,** *128*, 1418.

APPENDIX 4

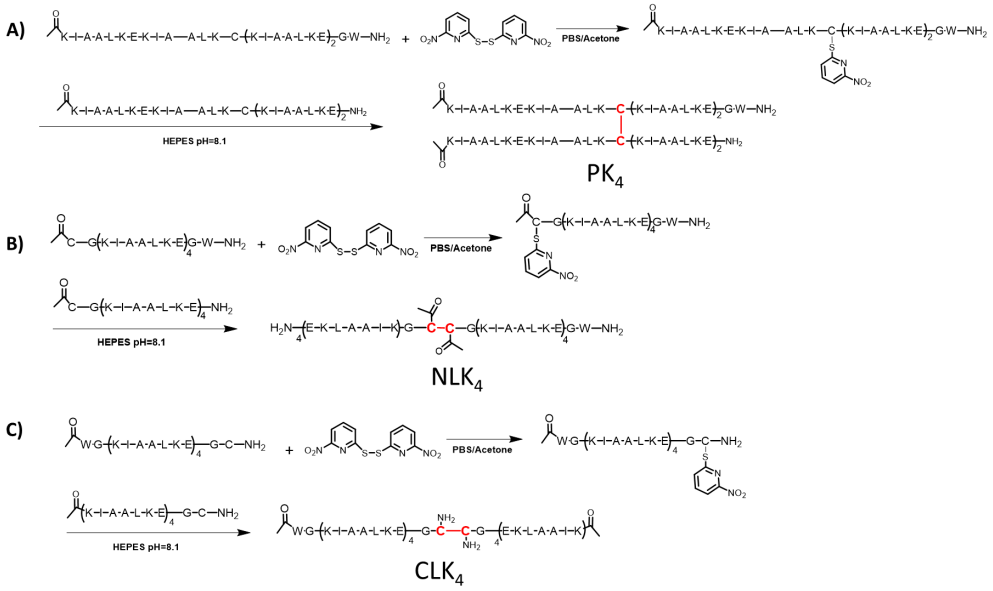

Figure S1. Synthetic route of K_4 dimers, (A) PK_4, (B) NLK_4 and (C) CLK_4.

Table S1. Sequences of monomer peptides used in this work

Peptides[a]	**Sequence**					
	ef	*gabcdef*	*gabcdef*	*gabcdef*	*gabcdef*	*ga*
K_4		KIAALKE	KIAALKE	KIAALKE	KIAALKE	GW-NH_2
E_4		EIAALEK	EIAALEK	EIAALEK	EIAALEK	GW-NH_2
K_4-Cys14		KIAALKE	KIAALKC	KIAALKE	KIAALKE	-NH_2
K_4GW-Cys14		KIAALKE	KIAALKC	KIAALKE	KIAALKE	GW-NH_2
CG-K_4	CG	KIAALKE	KIAALKE	KIAALKE	KIAALKE	-NH_2
CG-K_4GW	CG	KIAALKE	KIAALKE	KIAALKE	KIAALKE	GW-NH_2
K_4-GC		KIAALKE	KIAALKE	KIAALKE	KIAALKE	GC-NH_2
WG-K_4GC	WG	KIAALKE	KIAALKE	KIAALKE	KIAALKE	GC-NH_2
Fluo-E4	Fluo-GG	KIAALKE	KIAALKE	KIAALKE	KIAALKE	GW-NH_2

[a]All peptides except the ones for synthesising lipodated and fluorescent peptides were acetylated at N-terminus.

Table S2. Calculated mass and found mass via LC-MS of all K_4 dimers.

Peptide	Mass (calcd.) / Da	Mass (found) / Da
PK_4	$[M + 5H]^{5+}$ 1268.2	1267.5
	$[M + 4H]^{4+}$ 1585.0	1584.3
	$[M + 3H]^{3+}$ 2113.0	2113.0
NLK_4	$[M + 5H]^{5+}$ 1342.4	1341.8
	$[M + 4H]^{4+}$ 1677.8	1677.2
	$[M + 3H]^{3+}$ 2236.7	2237.5
CLK_4	$[M + 5H]^{5+}$ 1342.4	1341.8
	$[M + 4H]^{4+}$ 1677.8	1677.9
	$[M + 3H]^{3+}$ 2236.7	2237.5

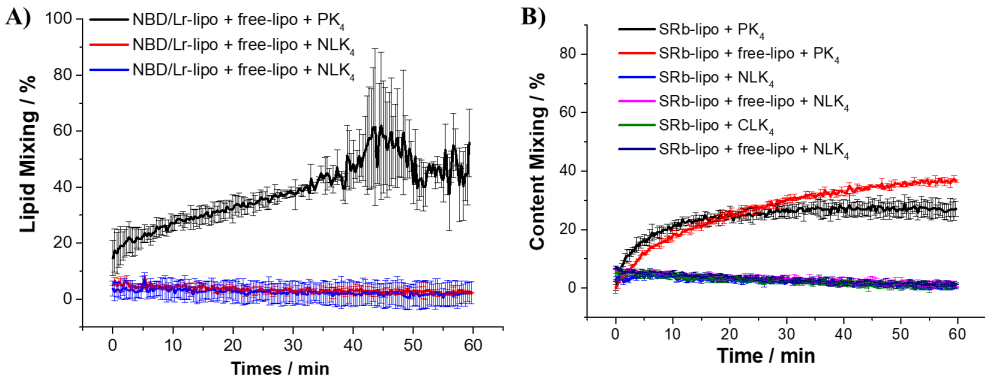

Figure S2. Control experiments from lipid mixing (A) and content mixing (B) assays.

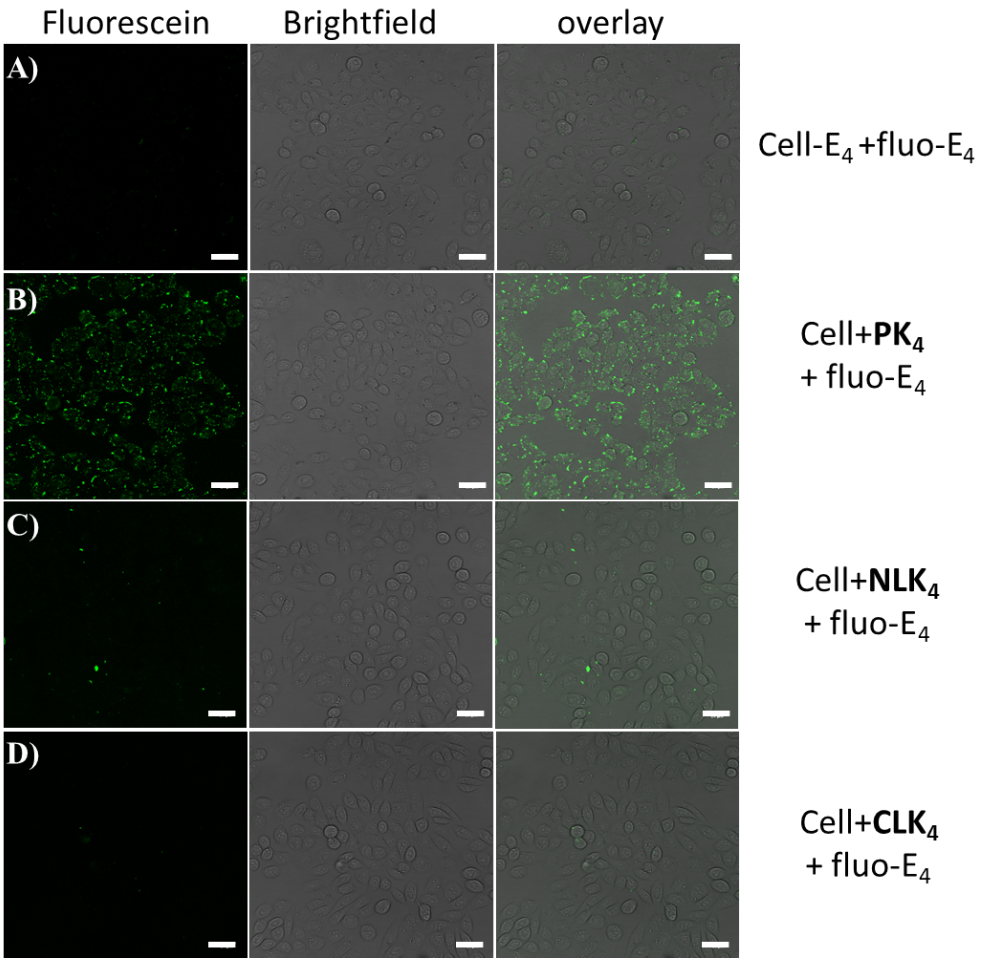

Figure S3. Control experiments from cell membrane labeling. Scale bar: 30 μM.

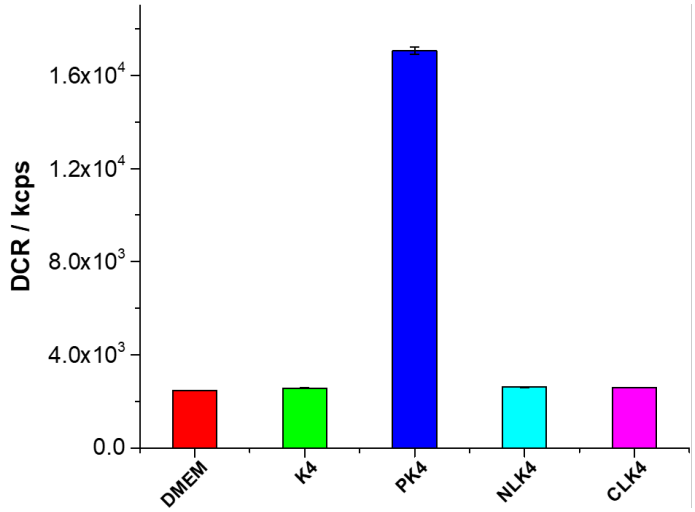

Figure S4. DCR results of K_4 monomer and K_4 dimers in DMEM.

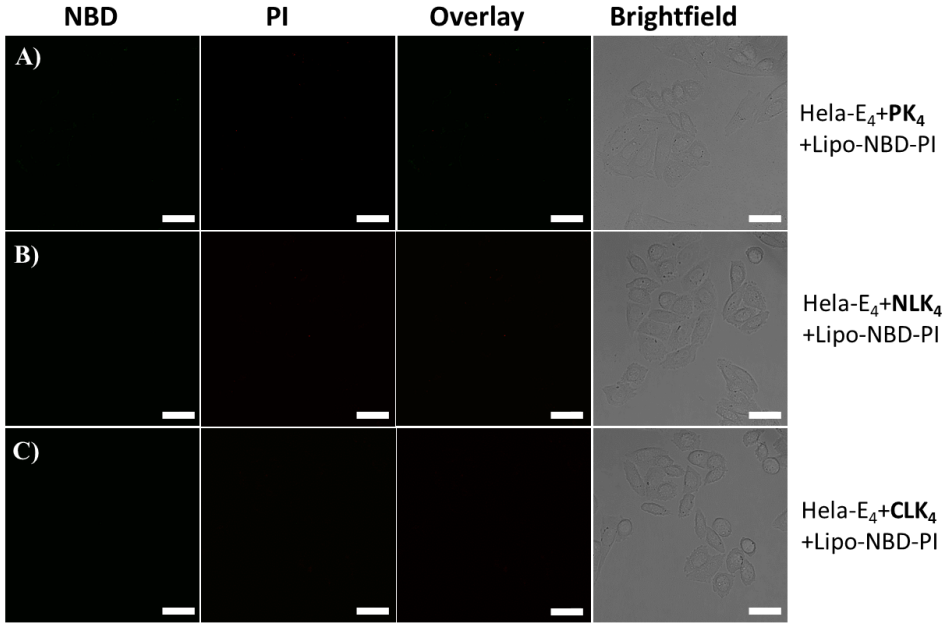

Figure S5. Control experiments from cell-liposome fusion. CPE_4 decorated cells with non-CPE_4 liposomes. Scale bar: 30 μM.

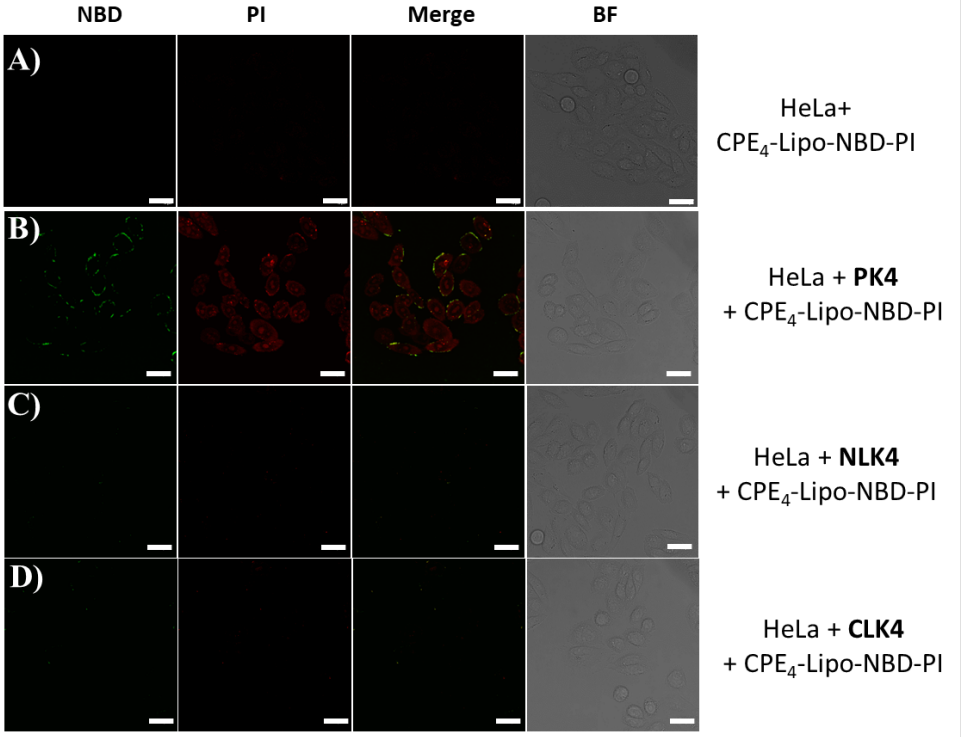

Figure S6. Control experiments from cell-liposome fusion. Cells were not decorated with CPE_4 and liposomes were modified with CPE_4. Scale bar: 30 μM.

Table S3. Liposomes used for liposome membrane fusion and cell-liposome membrane fusion.

Studies	liposome	Lipid composition	Content	Purification
Lipid mixing	lipo-NBD/LR-positive	DOPC/DOPE/cholesterol/NBD/LR (49.75/24.87/24.87/0.25/0.25%)	-	No purification
	Lipo-NBD/LR-E_4	DOPC/DOPE/cholesterol/NBD/LR/CPE_4 (49/24.5/24.5/0.5/0.5/1%)	-	No purification
	Lipo-NBD/LR	DOPC/DOPE/cholesterol /NBD/LR (49.5/24.75/24.75/0.5/0.5%)	-	No purification
	Lipo-E_4	DOPC/DOPE/cholesterol/CPE_4 (49.5/24.75/24.75/1%)	-	No purification
	Lipo-K_4	DOPC/DOPE/cholesterol/CPK_4 (49.5/24.75/24.75/1%)	-	No purification
	Lipo-free	DOPC/DOPE/cholesterol (50/25/25%)	-	No purification
Content mixing	Lipo-SRb-positive	DOPC/DOPE/cholesterol (50/25/25%)	10mM SRb	G25 size-exclusion
	Lipo-SRb-E_4	DOPC/DOPE/cholesterol/CPE_4 (49.5/24.75/24.75/1%)	20mM SRb	G25 size-exclusion
	Lipo-SRb	DOPC/DOPE/cholesterol (50/25/25%)	20mM SRb	G25 size-exclusion
	Lipo-E_4	DOPC/DOPE/cholesterol/CPE_4 (49.5/24.75/24.75/1%)	-	No purification
	Lipo-K_4	DOPC/DOPE/cholesterol/CPK_4 (49.5/24.75/24.75/1%)	-	No purification
	Lipo-free	DOPC/DOPE/cholesterol/CPE_4 (49.5/24.75/24.75/1%)	-	No purification
Cell-liposome fusion assay	Lipo-NBD-PI-E_4	DOPC/DOPE/cholesterol/CPE_4 (49.5/24.75/24.75/1%)	10 mg/mL PI	G25 size-exclusion
	Lipo-NBD-PI	DOPC/DOPE/cholesterol/CPE_4 (49.5/24.75/24.75/1%)	10 mg/mL PI	G25 size-exclusion

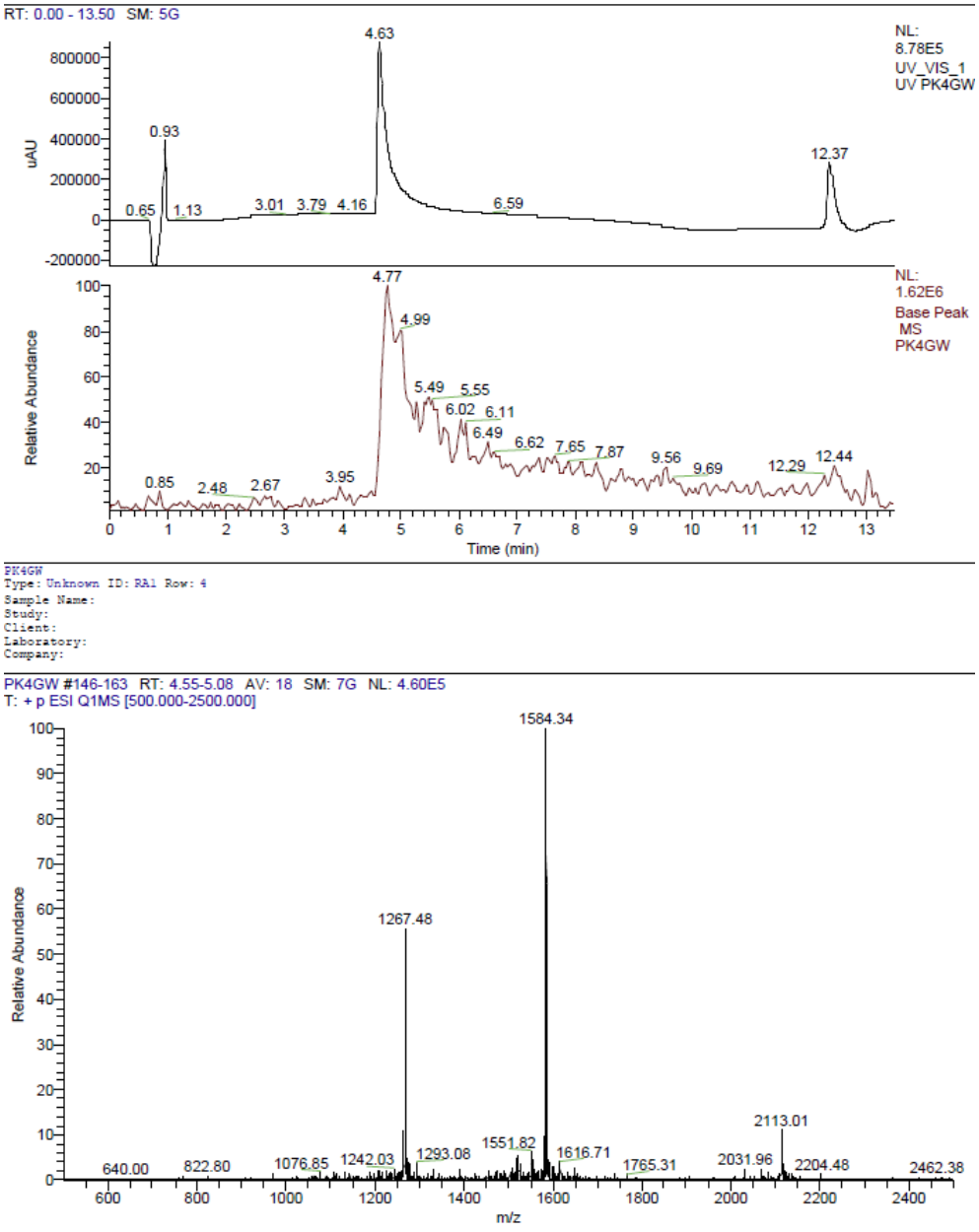

Figure S9. LC-MS spectrum of PK_4.

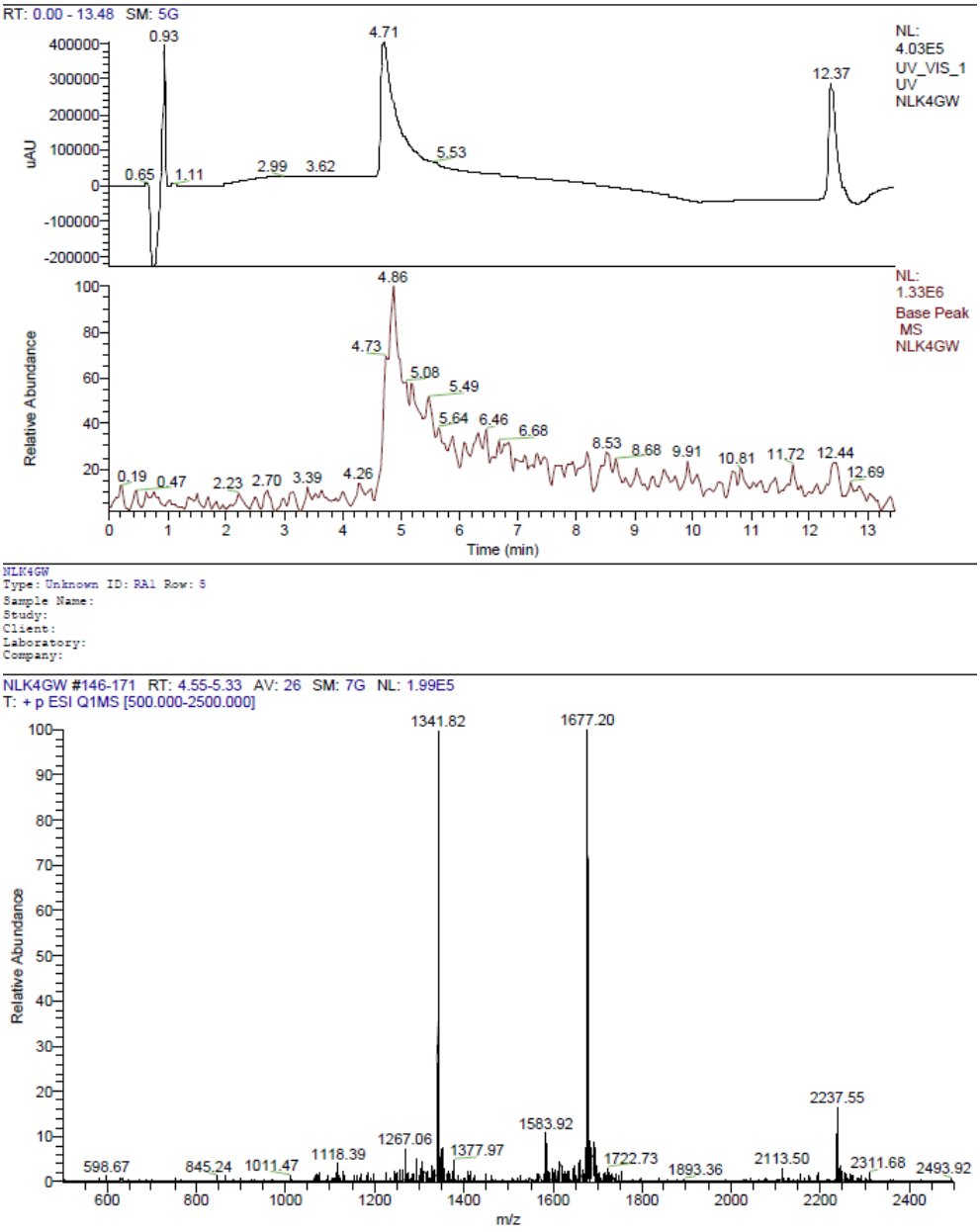

Figure S10. LC-MS spectrum of NLK_4.

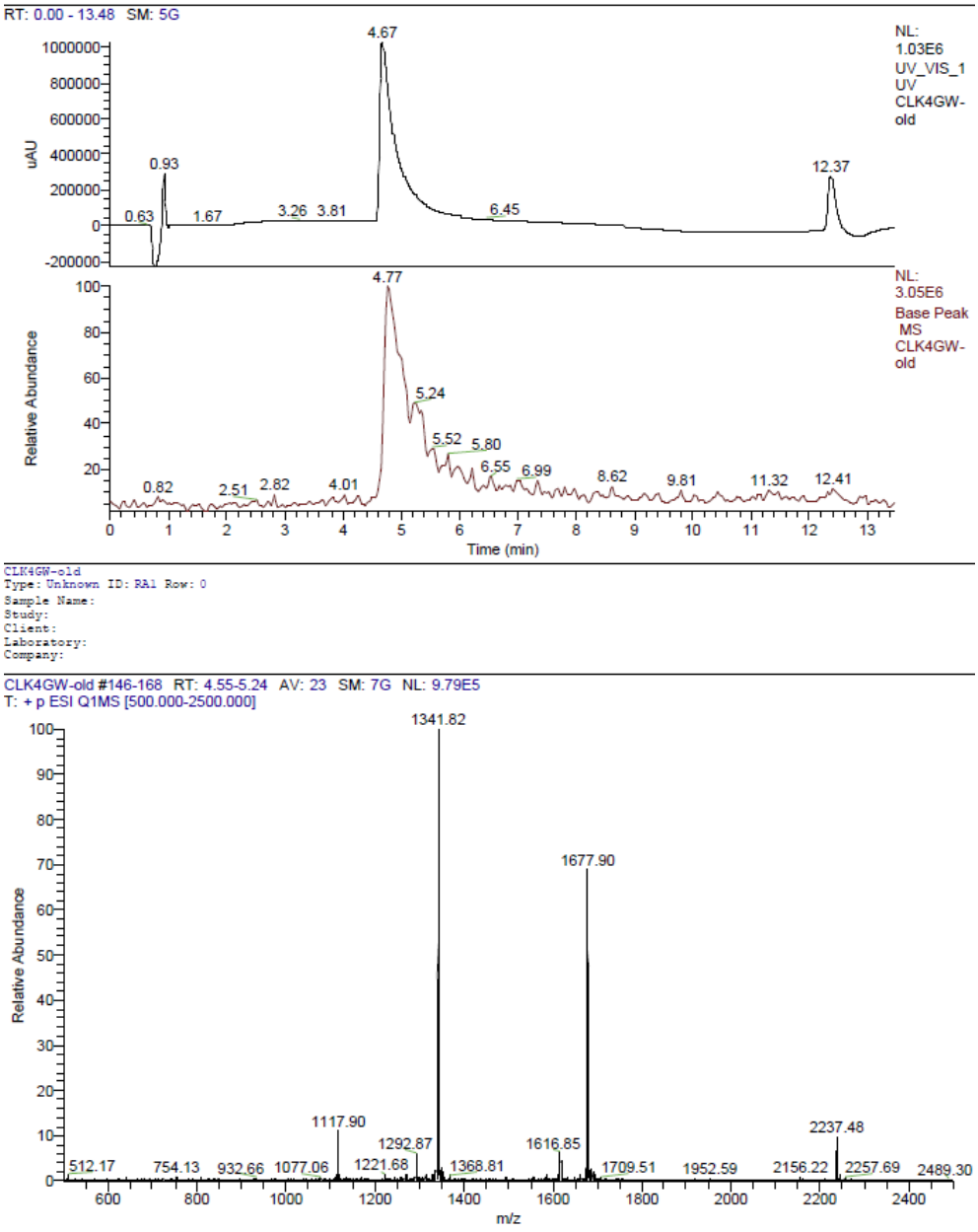

Figure S11. LC-MS spectrum of CLK_4.

Chapter 5

L-forms Fusion Triggered by Coiled-coil Peptides

ABSTRACT

Genetic recombination plays an essential role in biological evolution. It not only increases biodiversity in nature but also helps species to survive in changing environments. Recombination by cell transfection or bacterial transformation is widely used in laboratory settings. However, gene recombination on a large scale remains challenging. Herein, we report fusion between cell wall deficient bacteria (*i.e.* L-forms) triggered by coiled-coil peptides, resulting in chromosome recombination. Two L-form strains with different antibiotic resistance and fluorescence markers were designed for this study. L-form cell-cell membrane fusion was obtained using the PK_4/CPE_4 coiled-coil peptide pair and the fused L-forms were enriched by double antibiotic selection in the liquid phase. The resulting L-forms were found to contain both antibiotic resistance and fluorescence markers. In addition, we studied the viability and cell division of enriched L-forms and chromosome segregation during the fused L-form division process on solid phase medium.

INTRODUCTION

The bacterial cell is a complex structure consisting of many components that each provide a function and purpose. A major component is the cell wall which provides shape, protection and resistance.[1-2] It is however possible for a cell to survive without this cell wall, as seen for naturally wall-deficient cells of the Mycoplasma species and also in the case of stress-induced wall deficient L-forms.[3] The application of stressors like osmotic stress, heat, pH, antibiotics and cell wall targeting enzymes can result in the formation of wall-deficient forms (S cells, L-forms, protoplasts), which ultimately reverse back to bacteria with a cell wall.[4] These cells are often spherical in shape and either reproduce indefinitely in a wall less state (L-forms) or they are simply a transition phase (S cells or protoplasts).[5] L-forms have been found to play a role in intracellular pathogenesis (Listeria monocytogenes, Mycobacterium tuberculosis),[6-7] persisting infections (Escherichia coli),[8] and food infections (L. monocytogenes) indicating the importance of studying their growth and function from an ecological perspective. Furthermore, the recent discovery of L forms derived from Streptomyces has triggered interest in their growth, antibiotic production and application.[9]

Streptomyces are a well-known resource of bioactive molecules, many of which are of commercial importance.[10-11] Apart from naturally produced antibiotics, the process of protoplast fusion has been applied to these species for genome shuffling to obtain innovative antimicrobials. The process involves generating protoplasts of the same or different species followed by fusion.[12] Indeed, this approach has yielded highly productive strains and novel antibiotics. However, a disadvantage is that the fused protoplasts revert back to the walled state, thus the recombined chromosomes would separate from each other. It was recently hypothesized that the use of L-forms, instead of protoplasts, for fusion could overcome this disadvantage and provide a framework for novel compound production.[9] As a first step towards testing this hypothesis, we present in this chapter the first example of fusion between L-forms of the species *Kitasatospora viridifaciens*. This species is a tetracycline producer, [13] therefore the fusion of such L-forms can be used to test the production of this antibiotic in future.

Coiled coils are fundamental folding motifs common in proteins and play an essential role in various processes of life.[14-16] A well-known example of a functional coiled coil is the SNARE protein complex, which mediates membrane fusion.[17-18] In our group, a synthetic membrane fusion model system based on

designed coiled-coil peptides was developed.[19-22] This system is able to induce liposome-liposome and cell-liposome membrane fusion. In **Chapter 4** we presented a membrane fusion system based on the novel dimeric peptide PK_4 and its complementary lipopeptide partner CPE_4. This system is more fusogenic than our previously employed CPK_4/CPE_4 coiled-coil pair. In this chapter, we studied L-form membrane fusion initiated by the coiled-coil interaction between PK_4 and E_4 (Scheme 1). For the first time, we have achieved fusion of wall deficient L-forms of *Kitasatospora viridifaciens*. Combining fusion with antibiotic enrichment resulted in a cell culture containing more than 97% of the fused L-forms. We also investigated how and if chromosome segregation takes place after fusion. Through this work, we developed a feasible method to achieve L-form membrane fusion, which may have potential applications in studying genome shuffling and the development of new hybrid bacterial species.

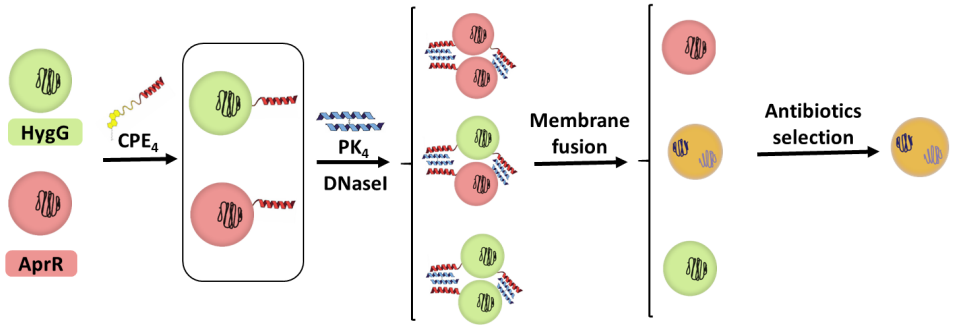

Scheme 1. Coiled-coil peptides associate with L-form membranes and induce cell-cell fusion.

RESULTS AND DISCUSSION

1. L-form phenotype

In this study, permanent wall-deficient cells (L-forms) of *Kitasatospora viridifaciens* were prepared by exposure to lysozyme and penicillin G (a cell wall targeting antibiotic).[5] In order to detect L-form fusion and select for the fused L-forms, two kinds of markers were introduced. A fluorescence marker (GFP or mCherry) was introduced for visualizing and tracking the cells during fusion with confocal microscopy and for quantification with flow cytometry. The introduction of antibiotic resistance markers (apramycin or hygromycin) enables selection and enrichment of fused cells. Two genetically modified L-form strains were obtained by transforming the wild type with the appropriate plasmids. The resulting HygG

strain expresses eGFP and is resistant to hygromycin B while the AprR strain expresses mCherry and has resistance to apramycin.

We first confirmed antibiotic resistance by determining the minimum inhibitory concentration (MIC) of each strain to both antibiotics (Figure 1A). The colony forming units (CFU) were used to quantify the minimum concentration of antibiotics required for killing each strain. The strain expressing resistance to apramycin (AprR) grew on all concentrations of apramycin while showing a MIC of 2 µg/mL for hygromycin B. The strain expressing hygromycin resistance (HygG) grew on all concentrations of hygromycin B while showing a MIC of 20 µg/mL for apramycin. These findings reaffirmed that the inserted resistance genes do not provide cross-resistance to the antibiotics used. Confirmation of the fluorescence reporters was obtained using microscopy with cytoplasmic mCherry detected in the AprR strain and GFP detected in the HygG strain (Figure 1B), no bleed-through was observed in the two channels.

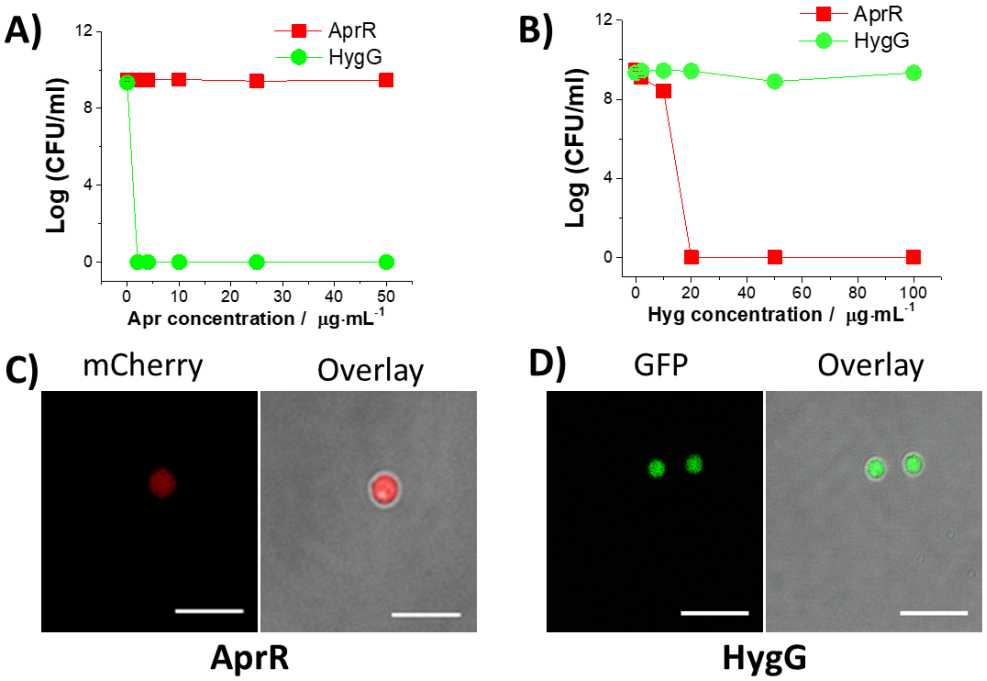

Figure 1. Antibiotic susceptibility testing: AprR and HygG strains grow in the presence of apramycin, A) or hygromycin, B). Fluorescence marker testing by fluorescence microscopy indicates a positive signal in the red channel for AprR, C) and in the green channel for HygG, D) Scale bar: 10 µm.

2. L-form membrane fluorescence labelling using coiled-coils

In order to apply the PK_4/CPE_4 coiled-coil membrane fusion system to trigger L-form fusion, it was necessary to first confirm that lipopeptide CPE_4 can be incorporated into L-form membranes. In previous studies, it was shown that the lipopeptide CPE_4 spontaneously incorporates into mammalian cell membranes.[23-24] However the lipid composition of L-forms differs from mammalian cells, which could influence the efficiency of membrane modification. To investigate CPE_4 incorporation into L-form membranes, a fluorescence labelling assay was performed (Figure 2A). Wild type L-forms devoid of any fluorescence were used in this assay. As expected, in the absence of CPE_4, fluorescein-labelled peptide K_4 (fluo-K_4) did not bind to the L-form membrane (Figure 2B). With CPE_4 present in the membrane, fluo-K_4 did bind to the lipopeptides resulting in homogenous labelling (Figure 2C). These results confirm that the cholesterol anchor inserts into the L-form lipid membrane and thus modification of the membrane with CPE_4 is possible. In addition, it can still form coiled coils with the complementary peptide K_4.

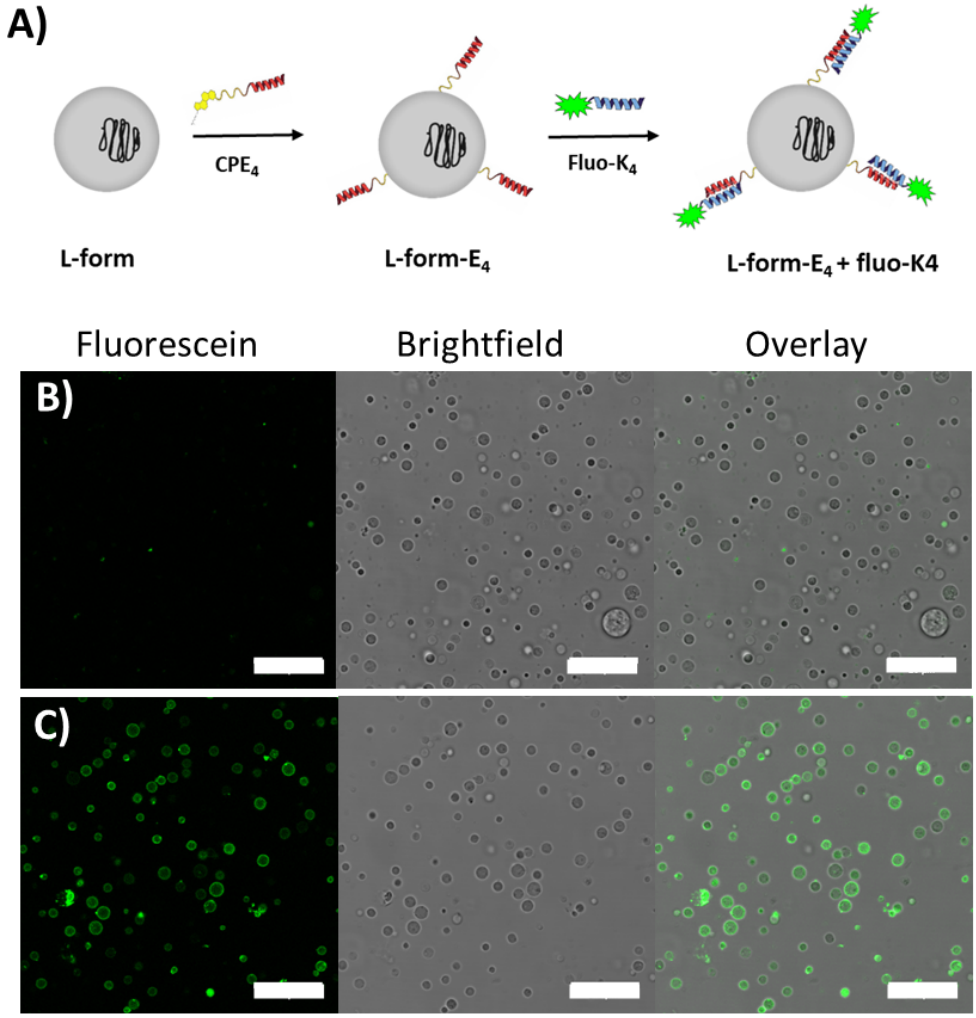

Figure 2. L-form membrane labelling assay. A) Scheme to illustrate the L-form membrane labelling process, B) L-form + fluo-K_4, C) L-form-E_4 + fluo-K_4. Scale bar: 20 µm.

3. Coiled-coil peptide triggered L-form cell-cell membrane fusion

Next, the possibility of using the PK_4/CPE_4 coiled-coil pair to trigger L-form cell-cell membrane fusion was investigated. If HygG and AprR phenotypes fuse and resulting in content mixing, the fused L-forms should contain both GFP and mCherry. Additionally, these L-forms should be resistant to both antibiotics.

To induce fusion, HygG and AprR were both decorated with CPE_4 (Scheme 1). Peptide PK_4 was subsequently added to a mixture containing an equal number of

HygG and AprR cells. Due to coiled-coil formation between peptide PK_4 and the CPE_4 bound to the L-forms, this mixture should ultimately result in fusion. Since bacteria can take up free DNA from the surroundings, DNase was added to the medium in order to degrade DNA released from lysed L-forms to prevent it from being taken up by other cells, resulting in a false positive strain that is resistant to both antibiotics. This precautionary measure was taken as PK_4 has a high membrane affinity and can destabilize membranes facilitating membrane fusion (see Chapter 4 of this thesis), but also potentially induces lysis. Successful membrane fusion events were imaged using confocal microscopy to search for fused, doubly-fluorescent cells. Indeed, orange cells were obtained in the L-form mixture, suggesting that membrane fusion was achieved (Figure 3A). Due to the fact that HygG and AprR were both decorated with CPE_4, the addition of PK_4 not only induces fusion between L-forms with different markers but also between L-forms with the same markers, resulting in a low ratio of fused cells containing resistance to both antibiotics.

To confirm the viability of the fused L-forms and to calculate the efficiency of cell-cell fusion, the L-forms were transferred to an agar plate containing both antibiotics (apramycin and hygromycin). Fusion efficiency was calculated by counting the number of colonies on the double antibiotic selection plates divided by the number of AprR or HygG colonies obtained on single antibiotic selection plates. As a control, AprR and HygG were mixed in a 1:1 ratio and directly plated on double selection media. After four days' culture, colonies were found on the plates of the experimental group while no colonies were found on the plates of the control group. Analysis of the colonies showed that approximately 1 in 100,000 cells is fused. A range of PK_4 concentrations were subsequently tested and the results show that, with a higher concentration of PK_4, a higher fusion efficiency was achieved, (Figure 3B). Control experiments showed that even higher concentrations of PK_4 led to more L-form lysis (Figure 3C,3D & 3E), and therefore we decided not to use concentrations > 50 µM.

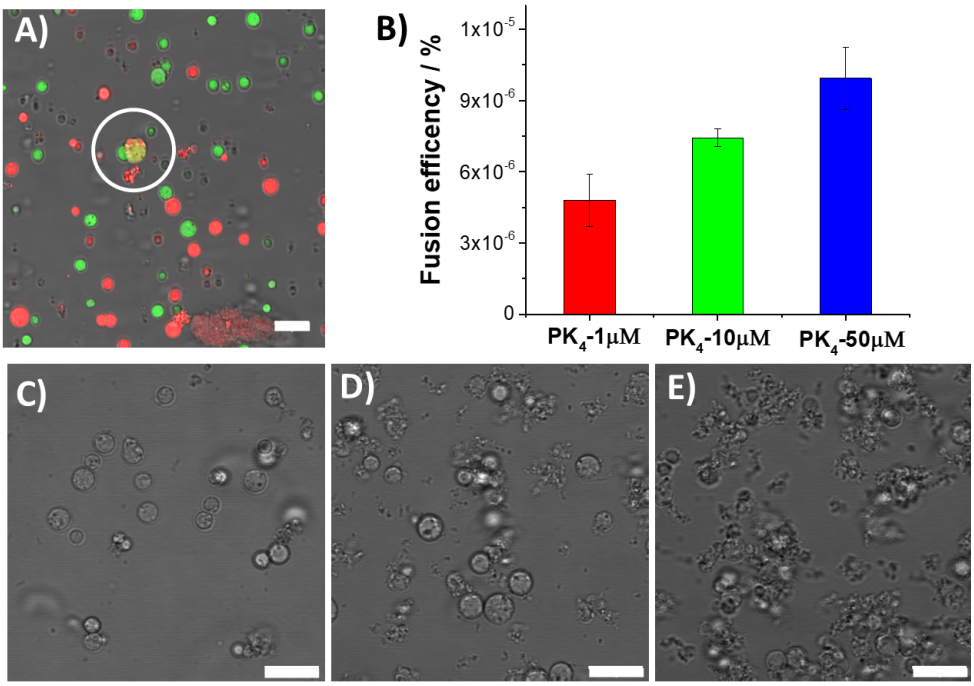

Figure 3. A) L-form mixture after cell-cell fusion, Green: GFP, Red: mCherry. B) L-form fusion efficiency is dependent on PK_4 concentration. L-forms with different concentrations of PK_4: C) 1 μM, D) 10 μM and E) 50 μM. Scale bar: 10 μm.

Next, we selected a colony from the double antibiotic-containing agar plate with a diameter of around 1.5 mm. The colony contained both green and red L-forms, as observed with confocal microscopy (Figure 4A). More red L-forms were found close to the centre and green L-forms were distributed at the edges of the colony. The shape of the colony is approximately round, which suggests that all daughter cells in the colony come from one mother cell. This mother cell must contain two sets of antibiotic resistance genes so that it survives on the double-antibiotic plate, and the daughter cells must also contain both genes as they survived. Additionally, the mother cell should contain both GFP and mCherry genes as both green and red L-forms were found in the colony. Unfortunately, no significant regions of orange were observed, as we expected after fusion. Interestingly, a few orange L-forms were observed on one edge of the colony (Figure 4B). L-forms typically contain multiple chromosomes due to the absence of a cell wall, which regulates chromosome segregation during division. After cell-cell fusion, the fused L-forms contain both sets of chromosomes which allow the L-form to exhibit orange fluorescence and to survive on the double antibiotic plates. After cell division, it

appears that two kinds of chromosomes contain different fluorescent protein genes but that the antibiotic resistance genes can go to the same, or different, daughter cells. Thus the daughter cells that survive on the plate show either single fluorescence or are doubly fluorescent and thus appear orange. Multiple mechanisms can explain the coexistence of these only green and red regions in the colony. First is the possibility of recombination of the resistance genes resulting in one chromosome containing both resistance markers but only one fluorescence marker. A second reason could be due to the atypical division process wherein the daughter cell remains connected to the mother cell during growth. This could result in unequal distribution of cytoplasmic material. Thirdly, differential expression of the fluorescence genes in the cell could occur due to competition between transcription factors and regulatory elements. The same reasoning can be provided for an unequal distribution of the chromosomes within a given cell resulting in the dominant chromosome providing the phenotype green or red. This aspect requires time-lapse imaging of a single colony to follow gene expression over time. Lastly, the cells could be exchanging cytoplasmic contents over short ranges to create an alternating green and red pattern. Some of these mechanisms are dependent on the environment (*i.e.* solid media) they are grown in and can be tested by changing to a more homogeneous environment with agitation (*i.e.* liquid media).

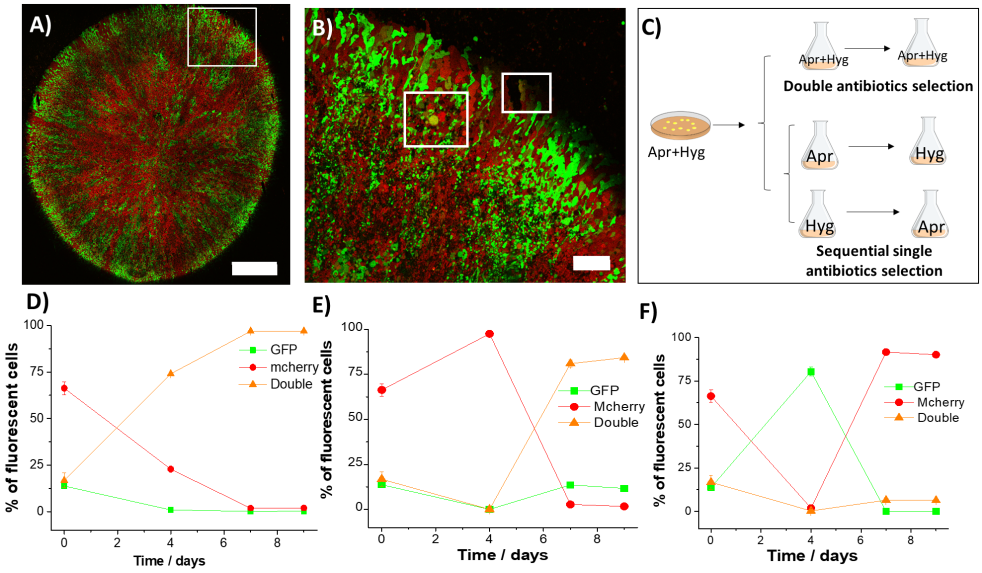

Figure 4. Image of a colony on a double antibiotic agar plate: (A) the whole colony, scale bar 300 μm; (B) zoom in on the edge of the colony, scale bar 50 μm. (C) The scheme illustrates fused L-form enrichment. FACS of L-form populations during fused L-form enrichment with double antibiotics (D), or sequential single antibiotics selection: (E) Apr + Hyg, (F) Hyg + Apr.

4. Fused L-form enrichment by antibiotic selection in liquid media

This study shows that solid-state antibiotic selection is not good enough to obtain a high ratio of doubly fluorescent L-forms as predominantly green and red L-forms were found in the colony. As described above, L-forms growing close to each other on solid media could provide protection (by exchanging some cytoplasmic material) and create daughter cells, which survive in the presence of both antibiotics. To verify this hypothesis, we picked colonies from the agar plate and resuspended them in liquid medium. Two antibiotic selection strategies were then applied (Figure 4C). For the first selection strategy, an L-form suspension was cultured in media with double the concentration (apramycin: 100 μg/mL, hygromycin B: 200 μg/mL) of both antibiotics. FACS analysis and cell imaging were performed at different time points (0, 4, 7 and 9 days) after inoculation. More red than green L-forms were found from the picked colonies (Figure 4D & 5A). After 4 days of selection, the ratio of both red and green L-forms showed a large decline and 74% of doubly fluorescent L-forms were observed (Figure 4D & 5B). On day 7, the ratio of doubly fluorescent cells increased to 97% with less than 2% of red cells

and 1% of green cells (Figure 4D & 5C). These L-forms continued to grow in media containing both antibiotics for another two days and no obvious change in the ratios was found (Figure 5D).

The other strategy employed was sequential antibiotic selection, wherein the inoculated L-forms were cultured in one antibiotic at a double concentration for 4 days, followed by changing to the other antibiotic at a double concentration and continuing culturing for several days. Flow cytometry was used to quantify L-forms expressing different fluorescent proteins at different time points. Two different results were obtained in the sequential antibiotic selection approach. Double fluorescent L-form enrichment was achieved by first culturing the L-forms in apramycin (100 μg/ml) for four days then switching to hygromycin B (200 μg/ml). After enrichment, the doubly fluorescent L-forms reach 84% (Figure 4E). Conversely, when L-forms were first cultured in the presence of hygromycin B and then apramycin, only 6% of doubly fluorescent L-forms were found and more than 90% of the L-forms show only red fluorescence (Figure 4F). These results show that the double antibiotic selection strategy is better than sequential antibiotic selection to obtain fused L-forms enrichment. The enriched cells not only show double antibiotic resistance but also contain both fluorescent proteins. This selection experiment in liquid medium also confirms that cell-cell fusion was obtained rather than recombination of the antibiotic resistance genes.

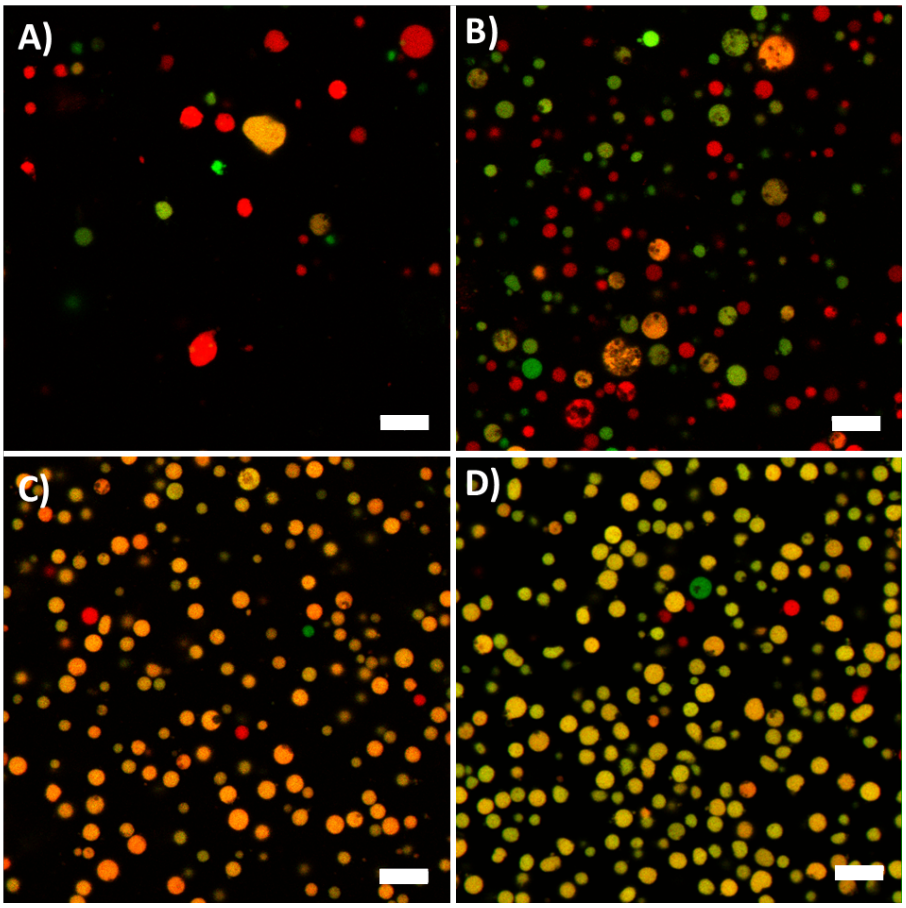

Figure 5. Fused L-form enrichment by double antibiotic selection at a double concentration at differing time intervals: (A) 0 days, (B) 3 days, (C) 7 days and (D) 9 days. Scale bar: 10 μm.

5. Tracking cell division of fused L-forms by time-lapse confocal microscopy and colony imaging

Cell-cell fusion results in the mixing of cytoplasmic and genomic contents. After several generations of double antibiotic selection, dual-labelled, and double antibiotic resistant L-forms with >97% purity were obtained. To study the viability growth and division of these fused L-forms, time-lapse confocal microscopy was employed. For this experiment, the L-forms were grown in media with double antibiotics. Figure 6 shows the process of L-form division for 12.5 hours. Round shaped L-forms were present at the start of the time-lapse experiment. After 100 min of incubation at 30°C, characteristic membrane deformation and blebbing were

observed. Gradually, daughter cells formed, still attached to the mother cells. Due to the production of daughter cells, the mother L-forms became smaller over time. Ultimately, the mother cells disappeared and divided into several daughter L-forms. Given the non-binary nature of cell division in wall-deficient cells, it was difficult to track the exact number of daughter cells originating from one mother cell. The newly formed daughter cells were typically producing more GFP than mCherry, suggesting that GFP is expressed more easily. Furthermore, after prolonged imaging, the fluorescence faded due to photobleaching. Because culturing L-forms in the confocal well plate (no shaking, less media) is not possible, we did not manage to obtain the nuances of cell division using the current set up.

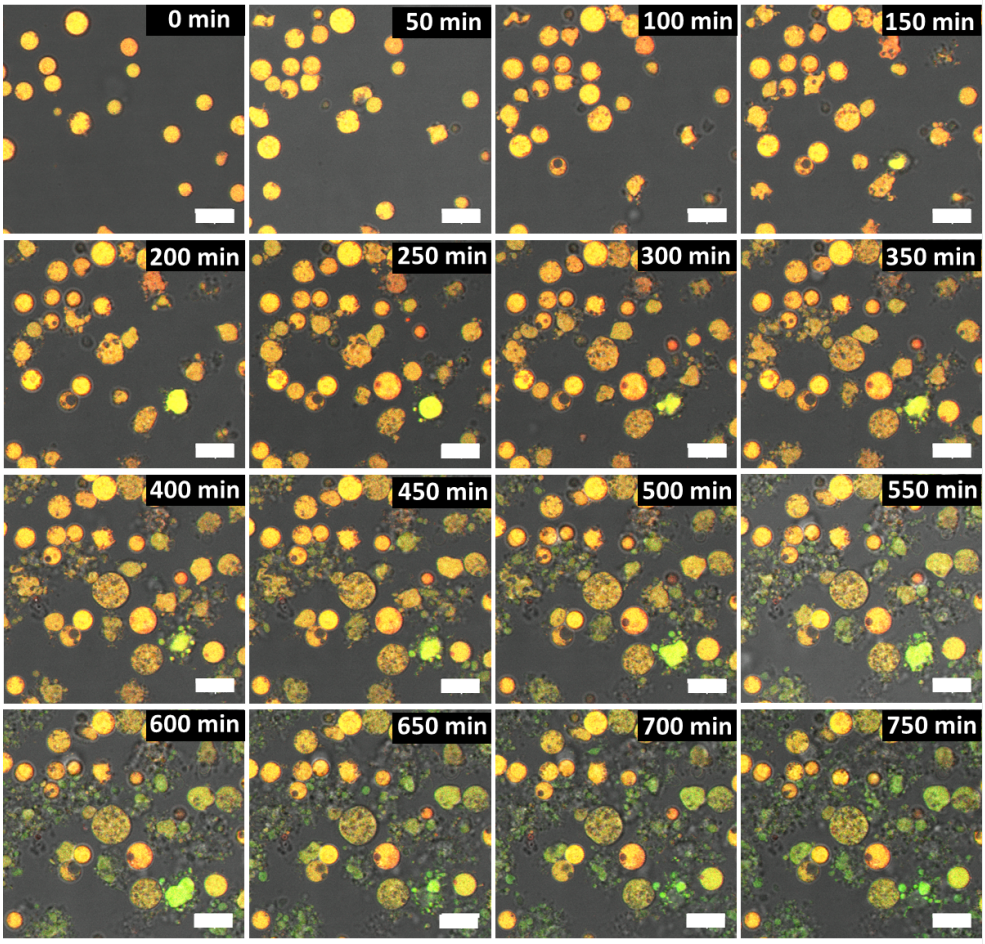

Figure 6. Time-lapse study of fused L-form division. Scale bar: 10 µm.

The fused L-forms contain two sets of chromosomes with a different number of

copies. One set of chromosomes contains GFP and Hyg resistance genes while the other set of chromosomes contains mCherry and Apr resistance genes. With both antibiotics present during L-form culturing, only cells that contain both sets of chromosomes survive and produce daughter cells. Without antibiotics, there is a chance that the daughter cells only contain one set of chromosomes due to the unregulated chromosome segregation during cell division. To find evidence of chromosome segregation, the enriched L-forms were seeded on a solid agar plate without antibiotics. Chromosome segregation in this scenario will result in regions of the colony expressing either only green or only red fluorescence. To our surprise, a perfect orange colony was obtained (Figure 7A). The color of the whole colony is not homogenous. On the edge of the colony, some L-forms with only green or red fluorescence was observed, (Figure 7B), but the percentage of these is low compared to the orange cells. This suggests that fused L-forms are very stable after double antibiotic enrichment and chromosome segregation is difficult to achieve in short culturing regimes in the solid-state even when no antibiotics are present. In addition, a yellow-green ring was found on the outermost part of the colony. This result is consistent with the data in the time-lapse study of L-form culturing that shows yellow-green cells were formed after cell division. This suggests that GFP may be expressed before mCherry in newly formed L-forms. Another reason for slow segregation in the absence of selection is that there might be too many copies of each set of chromosomes in the fused L-forms after enrichment. A higher number of chromosomes would then require a longer time for segregational loss.

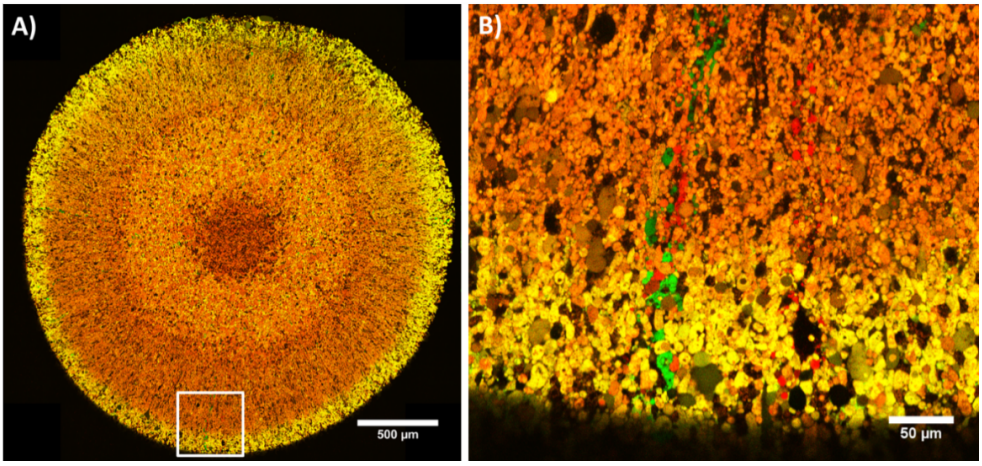

Figure 7. Imaging of fused L-form cultures on an antibiotic-free agar plate. A) The whole colony (scale bar: 500 µM) and B) the edge of the colony (scale bar: 50 µM).

CONCLUSION

In this work, we achieved fusion between L-forms using coiled-coil peptides for the first time. For this study, fluorescent protein markers and antibiotic markers were introduced into L-forms of Kitasatospora viridifaciens and two different strains (AprR and HygG) were produced. By performing an L-form membrane-labelling assay, we verified that CPE_4 incorporates spontaneously into L-form membranes and is able to form coiled coils with the complementary peptide K_4. The addition of the parallel dimeric peptide PK_4 to CPE_4 decorated L-forms resulted in fusion. Imaging of colonies after fusion revealed the presence of green, red, and orange L-forms, suggesting that gene-expressing in fused L-forms is unstable. L-form enrichment was achieved by culturing L-forms from colonies on double antibiotic selection media. After cell enrichment, 97% of the L-forms obtained contained double fluorescent protein markers as well as double antibiotic resistance markers. Division of fused L-form was studied by time-lapse imaging. Cell division was observed and occurred mainly by blebbing, showing the viability of the fused L-forms. We also studied chromosome segregation of the fused L-forms by culturing on an agar plate without antibiotics. After enrichment, the fused L-forms were found to be very stable and chromosome segregation was slow. In future experiments, we will test the biosynthetic capabilities of the fused cells compared to their parental strains. This study may open up a new field of genetic recombination by cell-cell fusion, which will have potential applications in biotechnological applications (*e.g.* novel antibiotics) as well as a model for the evolution of early cells (*i.g.* origin of life study).

EXPERIMENTAL SECTION

Media and L-form strains

L-phase broth (LPB) was used to culture L-forms in the liquid state. LPB contains 0.15% yeast extract, 0.25% bacto-peptone, 0.15% oxoid malt extract, 0.5% glucose, 0.64M sucrose, 1.5% oxoid tryptic soy broth powder (all w/v) and 25mM $MgCl_2$. The L-form culture was grown in a 50 mL flask containing 10 mL LPB and incubated at 30 ℃ with 100 rpm shaking.

L-Phase Medium (LPMA) was used to support the L-form growth in the solid state. It contains 0.5% glucose, 0.5% yeast extract, 0.5% peptone, 20% sucrose, 0.01% MgSO4·7H2O and 0.75% Iberian agar (all w/v). After autoclaving, the medium was supplemented with $MgCl_2$ to 25 mM and horse serum to 5% (v/v).

The P-buffer contains sucrose 10.3%, K_2SO_4 0.025%, $MgCl_2 \cdot 6\ H_2O$ 0.2%, , KH_2PO_4 (0.005%), $CaCl_2 \cdot 2\ H_2O$ (0.368%) ,TES buffer (0.573%). TES buffer contains $ZnCl_2$ 36µM, $FeCl_3 \cdot 6H_2O$ 74µM, $CuCl_2 \cdot 2H_2O$ 5.8µM, $MnCl_2 \cdot 4H_2O$ 5µM, $Na_2B_4O_7 \cdot 10H_2O$ 2.6µM and $(NH_4)_6Mo_7O_{24} \cdot 4H_2O$ 0.8µM. The P-buffer was used in cell membrane labelling assays, cell-cell membrane fusion assays and in FACS studies.

All L-form strains used in this study were obtained from the lab of Molecular Biotechnology, Institute of Biology, Leiden University. The *Kitasatospora viridifaciens* L-forms were made as previously reported.[5] The GFP expressing phenotype HygG was made by introducing insertion plasmid pIJ82-eGFP which contains the gene *hph* (confers resistance to hygromycin B) into the wild type L-form. The mCherry expressing phenotype AprR was made by transforming the pSet152-mCherry plasmid which contains the gene *aac(3)IV* (confers resistance to apramycin). All genes are under constitutive expression and inserted in the same site (*attB*) on the chromosome. The plasmids were introduced into L-forms via PEG-assisted transformation.[25] L-form cultures were grown for 4 days. Cultures were centrifuged to remove the spent media and the pellet was resuspended in 1/4th volume P-buffer. Approximately 500 ng plasmid was added to the resuspended pellet and mixed thoroughly. PEG1000 was added to this mix at a final concentration of 25 w% and mixed gently. After a brief incubation of 5 minutes on the bench, the tube was centrifuged. The supernatant was discarded and the pellet was resuspended in LPB medium and incubated for 2 hours. The culture was then centrifuged again and the pellet resuspended in 100 µL LPB for plating on LPMA media containing selective antibiotics apramycin or hygromycin. After 4 days of incubation single colonies were picked and restreaked on LPMA with antibiotics for confirmation along with fluorescence microscopy.

Minimum inhibitory concentration (MIC) determination

LPMA plates containing different concentrations of antibiotics were prepared. The concentrations of apramycin used were 0, 2, 4, 10, 25 and 50 µg/ml whereas hygromycin was used at 0, 2, 10, 20, 50 and 100 µg/ml. A 3-day old L-form culture was serially diluted and the dilutions were used for spotting 10 µl onto each plate. The serial dilution was done to determine the MIC. The plates were incubated at 30°C for five days before colony counting was performed to determine the CFU/ml.

Peptides synthesis and stock solution preparation

The synthesis and purification of all peptides used in this chapter are described elsewhere in this thesis (**Chapter 3** and **Chapter 4**). Stock solutions of CPE_4 and PK_4 were prepared in DMSO at a concentration of 10 mM and 1 mM respectively. Fluo-K_4 was dissolved in H_2O at a concentration of 200 μM.

L-form membrane labelling

Wild type L-forms (3×10^8) were suspended in 1 ml of P-buffer (OD_{600} = 0.4). 10 μL of CPE_4 stock solution was added to the L-form suspension to obtain a final concentration of 100 μM. After 30 min of incubation at 30 °C with shaking at 100 rpm, the L-forms were washed two times, by centrifugation, using P-buffer. The L-forms were then suspended in 900 μL P buffer and 100 μL of fluo-K_4 was added to a final concentration of 20 μM. After 5 min of incubation, the L-forms were washed three times using P-buffer to remove free fluo-K_4. L-form imaging was performed on a Leica SP8 confocal microscopy. Excitation: 488 nm, emission: 500-550 nm.

L-form cell-cell membrane fusion

L-form fusion was performed in P-buffer containing DNase (1 mg/mL) to ensure that all extracellular DNA present in the culture (due to cell lysis) is degraded and the resistance genes are unavailable for cellular uptake. 3×10^8 of AprR and HygG (1:1) cells in 1 ml of P-buffer (OD_{600} = 0.4) were incubated with CPE_4 at 100 μM for 30 min at 30 °C. The L-forms were washed with P-buffer twice after incubation by centrifugation at 1000 g and resuspended in 1 mL of fresh P-buffer. PK_4 was added to the L-form suspension to a concentration of 1, 10 or 50 μM. After 10 min of incubation, the L-forms were centrifuged (1000 g) and washed once before seeding on agar plates containing both antibiotics. The assay was performed in quadruplicate. After cell-cell membrane fusion, cell imaging was performed on a Leica SP8 confocal microscopy. Channels: GFP excitation: 488 nm, emission: 500-550 nm; mCherry excitation: 535 nm, emission: 550-600 nm.

Cell-cell membrane fusion efficiency calculation and colony imaging

Cell-cell fusion efficiency was calculated by counting CFU of colonies on double antibiotic selection (fused cells) and single antibiotic selection (parent cells) plates. The efficiency of fusion was calculated by counting the number of colonies on double antibiotic selection plates divided by the number of AprR or HygG colonies

obtained on single antibiotic selection plates. As a control, AprR and HygG were mixed in a 1:1 ratio and directly plated on double selection media.

A colony of ~1.5 mm diameter was picked up by cutting the gel and placing it upside down on the ibidi µ-Slide 8-well plate. The colony was plastered to the bottom surface of the slide. Colony imaging was performed on a Leica SP8 confocal microscope. In order to image the whole colony, the tile scan function was used. For each tile, five layers were recorded. The overall colony image was obtained by merging all the tiles. Channels: GFP excitation: 488 nm, emission: 500-550 nm; mCherry excitation: 535 nm, emission: 550-600 nm.

Time-lapse confocal imaging

Time-lapse confocal imaging was performed also using a Leica SP8 confocal microscope equipped with a temperature controllable incubator set at 30 ℃. 3×10^5 L-forms were seeded in ibidi µ-Slide 8 Well plates with 300 µL LPB. The samples were placed on the stage for 30 min in order to make the flowing L-forms sediment to the bottom of the plate before imaging. A low laser power (0.5% for 488 nm and 0.2% for 535 nm) and high gain (750 for both channels) was used in order to obtain high-quality images as well as to prevent fluorescent protein bleaching. L-form were imaged every 5 min for 13 hours using a 63× oil immersion objective.

L-form Enrichment

Approximately 30 colonies from the double antibiotic selection plate were picked and resuspended in 1.5 mL LPB. The fused L-form enrichment was performed in 50 ml flasks with 10 mL of LPB. For double antibiotic selection, the medium contained 100 µg/mL Apr and 200 µg/mL Hyg. L-forms were grown in an incubator with 100 rpm shaking at 30℃. L-form subculture was performed after 4 days and 7 days by transferring 200 µL L-form suspension to a new flask containing the same amount of LPB and antibiotics. For sequential single antibiotic selection, L-forms were inoculated in a flask containing either 100 µg/mL Apr and 200 µg/mL Hyg. After 4 days culturing, the L-forms were subcultured by transfer to a new flask containing different antibiotics to the inoculated flask. After 3 days, the L-forms were subcultured again in a new flask with the same antibiotics. Fluorescence assisted cell sorting (FACS) was used to quantify the L-form population.

FACS

L-form cultures from different time points were first washed twice by centrifugation and resuspended in P-buffer (~1×10^5 cell/ml) to remove the background arising from the LPB (yellow-coloured medium) and green pigment produced by the L-forms. Next, 100 to 200 µL of culture was analyzed by FACS. The S3e Cell sorter (Bio-Rad) works by generating droplets of the culture such that each droplet consists of roughly 1 cell or particle. This droplet passes through a laser to excite the fluorescent proteins inside the cell. Using a combination of lasers (488 and 561 nm) and emission filters (FL1: 525/30nm and FL2: 586/25) the presence of multiple fluorescent proteins inside a single cell was detected. For all cultures, approximately 20,000 events were tested with 2 technical replicates. The readout obtained was a signal for either GFP or mCherry that was displayed as a scatter plot with the green and red channels as axes. The graph was then divided into 4 quadrants namely green, red, double label and no label. Percentages of cells within the population that fall into each category was obtained using the ProSort™ software version 1.6.

REFERENCES

(1) Dmitriev, B.; Toukach, F.; Ehlers, S. Towards a comprehensive view of the bacterial cell wall. *Trends Microbiol* **2005,** *13*, 569.

(2) Egan, A. J.; Cleverley, R. M.; Peters, K.; Lewis, R. J.; Vollmer, W. Regulation of bacterial cell wall growth. *FEBS J* **2017,** *284*, 851.

(3) Razin, S.; Hayflick, L. Highlights of mycoplasma research--an historical perspective. *Biologicals* **2010,** *38*, 183.

(4) Ultee, E.; Ramijan, K.; Dame, R. T.; Briegel, A.; Claessen, D. Stress-induced adaptive morphogenesis in bacteria. *Adv Microb Physiol* **2019,** *74*, 97.

(5) Ramijan, K.; Ultee, E.; Willemse, J.; Zhang, Z.; Wondergem, J. A. J.; van der Meij, A.; Heinrich, D.; Briegel, A.; van Wezel, G. P.; Claessen, D. Stress-induced formation of cell wall-deficient cells in filamentous actinomycetes. *Nat Commun* **2018,** *9*, 5164.

(6) Slavchev, G.; Michailova, L.; Markova, N. Stress-induced L-forms of Mycobacterium bovis: a challenge to survivability. *New Microbiol* **2013,** *36*, e66.

(7) Studer, P.; Staubli, T.; Wieser, N.; Wolf, P.; Schuppler, M.; Loessner, M. J. Proliferation of Listeria monocytogenes L-form cells by formation of internal and external vesicles. *Nat Commun* **2016,** *7*, 13631.

(8) Glover, W. A.; Yang, Y.; Zhang, Y. Insights into the molecular basis of L-form formation and survival in Escherichia coli. *PLoS One* **2009,** *4*, e7316.

(9) Shitut, S.; Bergman, G. Ö.; Kros, A.; Rozen, D. E.; Claessen, D. Use of Permanent Wall-Deficient Cells as a System for the Discovery of New-to-Nature Metabolites. *Microorganisms* **2020,** *8*, 1897.

(10) Běhal, V. Bioactive products from Streptomyces. *Adv Appl Microbiol* **2000,** *47*, 113.

(11) Procopio, R. E.; Silva, I. R.; Martins, M. K.; Azevedo, J. L.; Araujo, J. M. Antibiotics produced by Streptomyces. *Braz J Infect Dis* **2012,** *16*, 466.

(12) Gokhale, D.; Puntambekar, U.; Deobagkar, D. Protoplast fusion: a tool for intergeneric gene transfer in bacteria. *Biotechnology advances* **1993,** *11*, 199.

(13) Ramijan, K.; van Wezel, G. P.; Claessen, D. Genome sequence of the filamentous actinomycete Kitasatospora viridifaciens. *Genome announcements* **2017,** *5*, e01560.

(14) Apostolovic, B.; Danial, M.; Klok, H. A. Coiled coils: attractive protein folding motifs for the fabrication of self-assembled, responsive and bioactive materials. *Chem Soc Rev* **2010,** *39*, 3541.

(15) Crick, F. The packing of α-helices: simple coiled-coils. *Acta crystallographica* **1953,** *6*, 689.

(16) Mason, J. M.; Arndt, K. M. Coiled coil domains: stability, specificity, and biological implications. *Chembiochem* **2004,** *5*, 170.

(17) Harbury, P. A. Springs and zippers: coiled coils in SNARE-mediated membrane fusion. *Structure* **1998,** *6*, 1487.

(18) Skehel, J. J.; Wiley, D. C. Coiled coils in both intracellular vesicle and viral membrane fusion. *Cell* **1998,** *95*, 871.

(19) Versluis, F.; Voskuhl, J.; van Kolck, B.; Zope, H.; Bremmer, M.; Albregtse, T.; Kros, A. In situ modification of plain liposomes with lipidated coiled coil forming peptides induces membrane fusion. *J Am Chem Soc* **2013,** *135*, 8057.

(20) Yang, J.; Bahreman, A.; Daudey, G.; Bussmann, J.; Olsthoorn, R. C.; Kros, A. Drug Delivery via Cell Membrane Fusion Using Lipopeptide Modified Liposomes. *ACS Cent Sci* **2016,** *2*, 621.

(21) Yang, J.; Shimada, Y.; Olsthoorn, R. C.; Snaar-Jagalska, B. E.; Spaink, H. P.; Kros, A. Application of Coiled Coil Peptides in Liposomal Anticancer Drug Delivery Using a Zebrafish Xenograft Model. *ACS Nano* **2016,** *10*, 7428.

(22) Zheng, T.; Voskuhl, J.; Versluis, F.; Zope, H. R.; Tomatsu, I.; Marsden, H. R.; Kros, A. Controlling the rate of coiled coil driven membrane fusion. *Chem Commun (Camb)* **2013,** *49*, 3649.

(23) Zope, H. R.; Versluis, F.; Ordas, A.; Voskuhl, J.; Spaink, H. P.; Kros, A. In vitro and in vivo supramolecular modification of biomembranes using a lipidated coiled-coil motif. *Angew Chem Int Ed Engl* **2013,** *52*, 14247.

(24) Oude Blenke, E. E.; van den Dikkenberg, J.; van Kolck, B.; Kros, A.; Mastrobattista, E. Coiled coil interactions for the targeting of liposomes for nucleic acid delivery. *Nanoscale* **2016,** *8*, 8955.

(25) Kieser, T.; Bibb, M. J.; Buttner, M. J.; Chater, K. F.; Hopwood, D. A. *Practical streptomyces genetics*, John Innes Foundation Norwich: 2000; Vol. 291.

Chapter 6

Summary and Perspectives

Coiled coils are an important structural motif in proteins, playing an essential role in a multitude of biological processes. Moreover, the programmable assembly properties of coiled coils makes it an ideal building block for designing responsive bioactive materials. In this thesis, the heterodimeric coiled-coil pair "E/K" was used for the development of a novel cell sorting protocol and controlling membrane fusion between liposomes and complex biological membranes.

In **chapter 2**, we designed a magnetic-activated cell sorting (MACS) method based on the short coiled-coil-forming peptide pair K_3 and E_3. Divinyl sulfone modified dextran (Dextran-DVS) was synthesized and used as a coating for magnetic iron oxide particles (IOPs). This coating strategy not only makes IOP functionalization trivial but also permits the number of functional groups on the IOPs to be controlled by changing the degree of substitution (DS) of dextran-DVS. Introduction of a cysteine into peptides E_3 and K_3 enabled the facile synthesis of coiled-coil peptide-modified magnetic particles IOPs-E_3 and IOPs-K_3. Successful functionalization of the magnetic particles was demonstrated by tryptophan fluorescence measurements and an IOP surface fluorescence-labelling assay. A MACS assay was performed using both IOPs-E_3 and IOPs-K_3 and cells functionalized with the complementary lipopeptide (denoted CPE_3 and CPK_3). Using IOPs-E_3, a mixture of CPK_3-decorated cells and non-decorated cells were efficiently separated after applying an external magnetic field. The novel MACS protocol was tested on three different cell lines (Hela, CHO and NIH3T3) and high levels of selection were obtained. Another advantage of this system is that the IOPs can be easily dissociated from the cells via trypsinization resulting in separated cells with high viability. When MACS was performed using IOPs-K_3, poor cell separation was observed, likely due to electrostatic interactions between the positively-charged K_3 and the negatively-charged cell membrane. It is believed that these electrostatic interactions interfere with the cell separation process. Finally, for future experiments peptide K_3 was expressed at the cell membrane of three cell lines and IOPs-E_3 was used for separation and enrichment. Using MACS, the population of K_3 expressing cells was enriched. This study shows the advantages of using coiled coils as a novel noncovalent conjugation material for cell sorting. We believe this MACS system has potential applications in a wide range of biomedical areas, such as cell selection after genetic modification.

In **chapter 3**, we studied the fusogenicity of coiled-coil pairs as a function of peptide length. For this study, three-, four- and five-heptad variants of K and E peptides were synthesized. The secondary structure of these peptides shows that the

four and five heptad peptides tend to form homodimers, with peptide K being more prone to homodimerization than peptide E. K_n peptides were also found to have higher thermal stabilities when compared to E_n peptides of the same length, and longer peptides had higher thermal stabilities than shorter peptides. For the thermostability of the E_n/K_n coiled coils, the same trend was observed. Chemical denaturation experiments using GdnHCl showed that higher-order self-assemblies may exist for peptides K_5 and E_5. Lipopeptide variants (*i.e.* CPK_n and CPE_n) were synthesized with different peptide lengths and fusogenicity was investigated by performing lipid and content-mixing assays. The K_5-E_4 coiled-coil pair had the best fusogenicity in these liposome fusion assays. Subsequently, cell membrane labelling assays were performed, showing that all CPK_n are able to decorate cell membranes and form coiled coils with the complementary peptide E_n. Liposome-cell membrane docking assays using CPK_n-modified cells and CPE_n-modified liposomes revealed that the coiled-coil pairs with four- and five-heptads induced the highest amount of cell-liposome docking. Selected coiled-coil pairs were further investigated for their capacity to trigger cell-liposome fusion. The CPK_4/CPE_4 coiled-coil pair was optimal for efficient cell-liposome membrane fusion, while CPK_5/CPE_4 induced liposome-liposome fusion most effectively. The results show that coiled-coil pairs containing peptide K_5 induce high levels of cell-liposome docking, but this does not translate into efficient drug delivery into cells. This is probably because peptide K_5 forms homodimers which weakens its interaction with lipid membranes, possibly resulting in less efficient fusion pore formation. In this study, we obtained new insights and information regarding the structure, self-assembly, thermostability, and fusogenicity of different lengths of coiled-coil peptides. These results illustrate that fusogenicity is not only related to coiled-coil stability but is also influenced by competing peptide-peptide and peptide-membrane interactions. This study will aid the design of better fusogens with potential applications in membrane fusion mediated drug delivery over complex biological membranes.

In the E/K coiled-coil peptide-mediated membrane fusion system, peptide K not only forms coiled coils with peptide E in order to bring two lipid membranes together but also interacts with the lipid membrane, facilitating efficient membrane fusion. In **chapter 4**, three K_4 dimers were designed, synthesized and characterized to enhance fusion as coiled-coil formation and membrane interaction can occur simultaneously. The parallel K_4 dimer (denoted PK_4) formed peptide aggregates in

a buffered solution, which dissolved upon the addition of the complementary peptide E_4GW, resulting in heterodimeric coiled-coil formation. The linear K_4 dimers (denoted NLK_4 and CLK_4) assembled into 'tetramer-like' homodimers. These highly stable structures did not form heterodimeric coiled coils with peptide E_4, which is likely to be detrimental for efficient membrane fusion. The highest membrane affinity was obtained for PK_4 in comparison to the K_4 monomer and linear K_4 dimers. The fusogenicity of all K_4-dimer based coiled-coils was evaluated by performing lipid and content-mixing assays. As expected, the PK_4/CPE_4 coiled-coil pair showed the best capacity for triggering both lipid mixing and content mixing, while the linear K_4-dimer based coiled-coils induced only a low level of fusion. This is consistent with the hypothesis that the membrane affinity of peptide K is related to the fusogenicity of the resulting heterodimeric coiled-coil. Fusion of liposomes with cells was achieved with PK_4/CPE_4 resulting in highly efficient propidium iodide (PI) delivery. This study will therefore help us understand the relationship between peptide self-assembly, membrane affinity, and fusogenicity of coiled-coil peptides, which may aid in the development of membrane fusion based drug delivery systems.

Since PK_4/CPE_4 proved to be more fusogenic than CPK_4/CPE_4, PK_4/CPE_4 was used to induce fusion between cell wall deficient bacteria (*i.e.* L-forms) in **chapter 5**. Two L-form strains containing double identifying markers were designed. For this study, one strain expresses eGFP and is resistant to hygromycin, while the other strain expresses mCherry and is resistant to apramycin. A L-form membrane fluorescence labelling assay showed that CPE_4 can be used to modify L-form membranes with coiled coils. A fusion assay between the two L-form strains was performed using the PK_4/CPE_4 pair. Fused L-forms were obtained and enriched in a liquid medium containing both antibiotics. After several generations of selection, the purity of the doubly fluorescent cells was > 97%. The process of cell division was tracked by time-lapse confocal microscopy showing the viability of the fusant. We also found that the fused L-forms stably express genes from the two sets of chromosomes and chromosome segregation was found to be slow. The work in this chapter presents a new method for making genomic combined hybrid species by cell-cell membrane fusion, which is important for understanding the evolution of protocells and designing synthetic cells.

The studies described in this thesis also leave some questions open. We discovered a new fusogenic peptide, PK_4 and showed that the PK_4/CPE_4 coiled-coil pair shows

the highest fusogenicity of all tested coiled coils to date. However, the introduction of this peptide makes the membrane fusion system more complex, as it now contains three components. In future studies, we could therefore conjugate a cholesterol anchor to the PK_4 peptide, which may simplify the current system and more easily facilitate drug delivery applications. Another issue in the L-form membrane fusion study was that chromosome segregation was difficult in fused L-forms after double antibiotic enrichment. Future studies on this issue can focus on investigating the genomic sequences of fused and enriched L-forms.

In this thesis, we built coiled-coil peptide-based biomaterials for a range of applications. By knowledge-guided design and modification, coiled coil induced membrane fusion systems are expected to achieve drug delivery *in vivo*. Finally, L-forms obtained by coiled-coil induced fusion of different strains are expected to be an ideal model for studying questions related to the origin of life and the discovery of novel antibiotics.

Chapter 7

Nederlandse Samenvatting en Perspectieven

Coiled coils zijn een belangrijk structuurmotief in eiwitten, en zijin essentiele voor het verloop van diverse biologische processen. De mogelijkheid om coiled-coil structuren te ontwerpen met geprogrammeerde oligomerisatie en oriëntatie maakt ze een ideaal motief voor de ontwikkeling van responsieve en bioactieve materialen. In dit proefschrift wordt de heterodimerische coiled coil “E/K” gebruikt voor de ontwikkeling van een nieuwe protocollen om cellen te scheiden en om membraanfusie tussen liposomen en biologische membranen te stimuleren.

In **hoofdstuk 2** is een nieuwe methode voor de scheiding van cellen deeltjes met behulp van magnetische (magnetic-activated cell sorting, MACS) ontwikkeld, gebaseerd op de coiled coil interactie tussen de peptiden K_3 en E_3. Divinylsulfon gemodificeerd dextraan (Dextran-DVS) is gesynthetiseerd en toegepast als coating voor magnetische ijzeroxide deeltjes (IOPs). Deze coating strategie maakt het niet alleen mogelijk om IOPs te functionaliseren, maar geeft ook de mogelijkheid om de hoeveelheid functionele groepen op de IOPs te controleren door de substitutiegraad (DS) van Dextrans-DVS aan te passen. Introductie van cysteïne in peptide E_3 en K_3 resulteert in de synthese preparatie van magnetische deeltjes gemodificeerd met coiled-coil peptiden; IOPs-E_3 en IOPs-K_3. Succesvolle functionalisatie van de magnetische deeltjes wordt aangetoond door tryptofaan-fluorescentie van de peptiden, alsmede door de binding van de complementaire coiled-coil peptide voorzien van een fluorescent label. Een MACS experiment was uitgevoerd met zowel IOPs-E_3 als IOPS-K_3 en cellen gefunctionaliseerd met de complementaire lipopeptiden (respectievelijk CPK_3 of CPE_3). Het gebruik van IOPS-E_3 resulteerde in een efficiënte scheiding van cellen met CPK_3 op het oppervlakte en cellen zonder deze peptide na toepassing van een extern magnetisch veld. Dit nieuwe MACS protocol is getest op drie verschillende cellijnen (Hela, CHO en NIH3T3), met een hoge selectiviteit voor gelabelde cellen in alle gevallen. Een extra voordeel van dit systeem is de eenvoudige dissociatie van cellen gebonden aan IOPs door gebruik van trypsine, wat resulteerde in een hoge levensvatbaarheid van de gescheiden cellen. Uitvoering van het MACS protocol met IOPs-K_3 resulteerde in slechte scheiding tussen cellen, waarschijnlijk door elektrostatische interacties tussen de positief geladen K_3 peptiden en het negatief geladen celmembraan. Deze elektrostatische interacties beinvloeden de dissociatie van cellen van de IOPs negatief. Als laatste stap zijn de drie cellijnen gemodificeerd zodat K_3 gepresenteerd wordt op het celmembraan, en IOPs-E_3 is gebruikt voor hun scheiding. Met behulp van MACS kon de concentratie van K_3-producerende cellen verrijkt worden. Deze studie laat de voordelen zien van coiled

coils als een nieuwe, niet-covalente conjugatiemethode voor het scheiden van cellen. Het beschreven MACS protocol kan worden gebruikt in verschillende biomedische toepassingen, zoals celscheiding na genetische modificatie.

In **hoofdstuk 3** is de fusogeniciteit van coiled-coil peptiden als functie van de peptidelengte onderzocht. Voor dit onderzoek zijn varianten van peptiden K en E gesynthetiseerd met een sequentie die bestond uit drie-, vier- of vijf- keer dezelfde 'heptad repeat'. De secundaire structuur van de vier en vijf heptad-peptiden induceert homodimerisatie, waarbij peptide K meer homodimerisatie vertoond dan peptide E. K_n-peptiden demonstreerden ook een hogere thermische stabiliteiten in vergelijking met E_n-peptiden van dezelfde lengte, waarbij langere peptiden in het algemeen een hogere thermische stabiliteit vertoonden. De stabiliteit van E_n/K_n coiled coils vertoonde dezelfde trends als voor de peptiden op zichzelf. Denaturatie experimenten met guanidine hydrochloride (GdnHCl) suggereerden zelfassemblage voor peptiden K_5 en E_5. Gelipideerde varianten van peptiden met verschillende lengtes (CPK_n en CPE_n) werden gesynthetiseerd en de fusogeniciteit van deze peptiden is getest in experimenten die de menging van lipiden-membranen en de inhoud van liposomen kan aantonen. De K_5-E_4 coiled coil vertoonde de hooggte fusogeniciteit in deze fusie-experimenten. Vervolgens zijn de peptiden ook getest in cel-labeling experimenten, met als resultaat dat alle CPK_n varianten in staat zijn om aan de buitenkant van cellen te binden en coiled coils te vormen met complementaire E_n peptiden. Bindingsstudies tussen liposomen met CPE_n en celmembranen gemodificeerd met CPK_n laten zien dat de grootste hoeveelheid liposoom binding verkregen wordt door de peptiden met 4 of 5 heptad repeats. Geselecteerde coiled coils zijn verder onderzocht voor hun capaciteit om membraanfusie te faciliteren. CPK_4/CPE_4 leverde de beste resultaten op in cell-liposoom fusie, terwijl de CPK_5/CPE_4 de hoogste efficiëntie vertoonde in fusiestudies met liposomen. Deze resultaten laten zien dat liposoom-binding door coiled-coils met K_5 niet direct transleert in efficiënte aflevering van de inhoud van liposomen in cellen. Dit is waarschijnlijk omdat peptide K_5 een homodimeer kan vormen wat deinteractie met het membraan verzwakt, mogelijk resulterend in minder efficiënte formatie van fusieporiën. In deze studie hebben we nieuwe informatie verkregen over de structuur, zelfassemblage, thermische stabiliteit en fusogeniciteit van coiled-coil peptiden met verschillende lengtes. Deze resultaten laten zijn dat fusogeniciteit niet alleen afhankelijk is van de stabiliteit van de coiled coil, maar ook beïnvloed wordt door competitieve interacties tussen peptiden

ondercing en met lipidenmembranen. Deze studie helpt de ontwikkeling van nieuwe fusogene moleculen met potentiële applicaties in medicijn afgifte doormiddel van liposoom fusie met complexe biologische membranen.

In het E/K membraanfusiesysteem wordt er een coiled-coil gevormd tussen peptide E en K om twee lipidenmembranen samen te brengen, maar van peptide K is ook bekend dat deze interacties heeft met het lipidenmembraan zelf, wat efficiëntere fusie van membranen faciliteert. In **hoofdstuk 4** zijn drie verschillende dimeren van peptide K ontworpen, geprepareerd en gekarakteriseerd, gebaseerd op de aanname dat dimeren van peptide K tegelijkertijd coiled coil en membraaninteracties kunnen vormen en daardoor de efficiëntie van membraanfusie verhoogd wordt. De parallelle K_4 dimeer (PK_4) vormde peptiden-aggregaten in oplossing, welke verdwenen na toevoeging van zijn coiled coil bindingspartner E_4, resultereny in de vorming van heterodimerische coiled coils. De lineaire dimeren van K_4 (NLK_4 of CLK_4) zelf-assembleerden als ‘tetrameer-achtige’ homdimeren. Deze zeer stabiele structuren waren niet in staat om een heterodimerische coiled coil te vormen met peptide E_4, wat waarschijnlijk efficiënte membraan fusie inhibeert. De hoogste affiniteit voor lipidenmembranen is gemeten voor PK_4 in vergelijking met K_4 en de twee lineaire K_4-dimeren. De fusogeniciteit van alle K_4 varianten werd bepaald door middel van lipide en inhouds-menging experimenten. Zoals verwacht resulteerde het coiled-coil paar PK_4/CPE_4 in de meest efficiënte fusie in beide experimenten, waarbij de lineaire dimeren van K_4 alleen lage levels van membraanfusie induceerde. Dit is consistent met de hypothese dat de membraanaffiniteit van peptide K gerelateerd is aan de fusogeniciteit van de heterodimerische coiled-coil. Fusie van liposomen met celmembranen was succesvol met PK_4/CPE_4 en resulteerde in efficiënte aflevering van propidium iodide (PI) in de cellen. Deze studie help ons met het begrijpen van de zelfassemblage van peptiden, de membraanaffiniteit en de fusogeniciteit van coiled coils, wat kan helpen in de ontwikkeling van systemen voor de aflevering van medicijnen gebaseerd op membraanfusie.

Omdat PK_4/CPE_4 een hogere efficiëntie van membraanfusie vertoonde in vergelijking met CPK_4/CPE_4, is deze in **hoofdstuk 5** gebruikt om fusie tussen bacteriën zonder celwand (L-Forms) te induceren. Twee verschillende soorten L-forms zijn hiervoor gebruikt, beide met twee unieke eigenschappen voor identificatie. Voor deze experimenten produceerde één van de L-forms het eiwit eGFP met resistentie voor het antibioticum hygromycin, en de andere soort bevat

het eiwit mCherry produceerde resistentie voor het antibioticum apramycin. Experimenten met het fluorescente labelen van de membranen lieten zien dat CPE_4 gebruikt kan worden voor het modificeren van L-form membranen met coiled-coil peptiden. Een fusiestudie tussen de twee L-form soorten is uitgevoerd met het coiled-coil paar PK_4/CPE_4. Gefuseerde L-forms werden verkregen, en verrijkt in medium dat beide eerder genoemde antibiotica bevat. Na meerdere generaties van selectie was de zuiverheid van de dubbel gelabelde fluorescente cellen >97%. Het proces van celdeling werd gevolgd door time-lapse microscopie waarbij de gezondheid van de gefuseerde cellen is aangetoond. We hebben ook geobserveerd dat de gefuseerd L-forms stabiele genexpressie vertoonden van beide originele cellijnen, en dat scheiding van de chromosomen een langzaam proces is. Het werk in dit hoofdstuk presenteert een nieuwe methode, gebaseerd op membraanfusie tussen cellen, voor het genereren van hybride organismen waarbij meerdere genomen gecombineerd zijn. Dit is een belangrijke stap is in het begrijpen van de evolutie van protocellen en het ontwerp van synthetische cellen.

De onderzoeken beschreven in deze thesis laten ook enkele vragen onbeantwoord. Een nieuwe fusogene peptide, PK_4 is ontdekt en er is aangetoond dat de combinatie PK_4/CPE_4 één van de meest fusogene coiled coil combinaties tot op heden. De introductie van deze nieuwe variant maakt het achterliggende fusiemechanisme wel complexer, omdat het daarmee 3 componenten bevat. In toekomstige onderzoeken zou het interessant zijn om cholesterol te conjugeren aan PK_4, ter simplificatie van het modelsysteem en om medicijn aflevering makkelijker te maken. Een ander probleem in het onderzoek naar gefuseerde L-forms is de lastige scheiding van chromosomen na verrijking van gefuseerde cellen door antibiotica-selectie. Het karakteriseren van de genoomsequentie van gefuseerd L-forms is een belangrijke stap in het voortzetten van dit onderzoek.

In deze thesis hebben we meerdere biomaterialen met verschillende applicaties ontwikkeld, gebaseerd op coiled-coil peptiden. Het verder ontwikkelen en aanpassen van dit coiled-coil membraanfusie systeem, met de hier vergaarde kennis over de werking van dit systeem, brengt *in vivo* toepassing van membraanfusie voor het afleveren van medicijnen dichterbij. Ten slotte, hybride L-forms verkregen door de coiled-coil fusie van verschillende soorten L-forms zijn een ideaal platform voor onderzoek naar de oorsprong van het leven en de ontwikkeling van nieuwe soorten antibiotica.

ABBREVIATIONS

CHO	Chinese Hamster Ovary cell
CD20	Cluster of Differentiation 20
CY5	Cyanines 5
Cys	Cysteine
CD	circular dichroism
CFU	colony forming units
DLS	Dynamic light scattering
DIC	N,N’-Diisopropylcarbodiimide
DIPEA	N,N-Diisopropylethylamine
DMF	Dimethyl Formamide
DCM	Dichloromethane
DS	Degree of subtitution
DMEM	Dulbecco's Modified Eagle Medium
DCR	Derived Count Rate
DVS	Divinyl Sulfone
DMSO	Dimethyl Sulfoxide
DOPE	1,2-dioleoyl-sn-glycero-3-phosphoethanolamine
DOPC	1,2-dioleoyl-sn-glycero-3-phosphocholine
EDTA	Ethylenediaminetetraacetic acid
FACS	Fluorescence-activated Cell Sorting
FSC	forward scatter
FRET	Förster resonance energy transfer
FCS	Fetal Calf Serum
GFP	Green Fluorescence Protein
GdnHCl	Guanidinium chloride
HPMA	2-Hydroxypropyl Methacrylate
HCTU	2-(6-Chloro-1-H-benzotriazole-1-yl)-1,1,3,3-tetramethylaminium

	hexafluorophosphate
HPLC	High Performance Liquid Chromatography
IOPs	Iron Oxide Particles
LrB	LrB: Lissamine rhodamine B
LC-MS	Liquid chromatography–mass spectrometry
LPMA	L-Phase Medium
LPB	L-phase broth
MACS	Magnetic-activated Cell Sorting
MWCO	Molecular weight cut-off
MeCN	acetonitrile
MIC	Minimum inhibitory concentration
MeOH	Methanol
NBD	Nitrobenzoxadiazole
NMR	Nuclear Magnetic Resonance spectroscopy
PEG	Polyethylene glycol
PI	Propidium iodide
PEI	Polyethylenimine
PDGFRB	platelet-derived growth factor receptor beta
PBS	Phosphate buffered saline
PDI	Polydispersity Index
SNARE	Soluble N-ethylmaleimide-sensitive factor activating protein receptor
SRb	Sulforhodamine B
SNAP-25	Synaptosomal-Associated Protein-25
TMD	Transmembrane Domain
Trp	Tryptophan
TFA	Trifluoroacetic acid
TEM	Transmission Electron Microscope
VAMP	Vesicle Associated Membrane Protein

LIST OF PUBLICATIONS

1. **Shen, M. J.**; Olsthoorn, R. C. L.; Zeng, Y.; Bakkum, T.; Kros, A.; Boyle, A. L. Magnetic-Activated Cell Sorting Using Coiled-Coil Peptides: An Alternative Strategy for Isolating Cells with High Efficiency and Specificity. *ACS Appl Mater Interfaces* **2021,** *13*, 11621.
2. **Shen, M. J.**; Liang, T.-L.; Song, Y.-Q.; Xu, L.-J.; Hao, X.; Gong, H.-Y. Substrate-induced adjustment of "slipped" π–π stacking: en route to obtain 1D sandwich chain and higher order self-assembly supramolecular structures in solid state. *Supramolecular Chemistry* **2016,** *29*, 24.
3. Guan, A. J.; **Shen, M. J.**; Xiang, J. F.; Zhang, E. X.; Li, Q.; Sun, H. X.; Wang, L. X.; Xu, G. Z.; Tang, Y. L.; Xu, L. J.; Gong, H. Y. G-quadruplex induced chirality of methylazacalix[6]pyridine via unprecedented binding stoichiometry: en route to multiplex controlled molecular switch. *Sci Rep* **2015,** *5*, 10479.
4. Guan, A. J.; **Shen, M. J.**; Zhang, E. X.; Li, Q.; Wang, L. X.; Xu, L. J.; Xiang, J. F.; Tang, Y. L. Stabilizing G-quadruplex DNA by methylazacalix[n]pyridine through shape-complementary interaction. *Bioorg Med Chem Lett* **2016,** *26*, 609.
5. Zhang, Q.; Gimeno, A.; Santana, D.; Wang, Z.; Valdes-Balbin, Y.; Rodriguez-Noda, L. M.; Hansen, T.; Kong, L.; **Shen, M. J.**; Overkleeft, H. S.; Verez-Bencomo, V.; van der Marel, G. A.; Jimenez-Barbero, J.; Chiodo, F.; Codee, J. D. C. Synthetic, Zwitterionic Sp1 Oligosaccharides Adopt a Helical Structure Crucial for Antibody Interaction. *ACS Cent Sci* **2019,** *5*, 1407.
6. Ding, C.-J.; **Shen, M. J.**; Xu, L.-J.; Gong, H.-Y. The complexation between 'Texas sized' molecular box and linear n-aliphate dianion: en route to supramolecular organic frameworks (SOFs) for selectively CO2 absorption. *Tetrahedron* **2016,** *72*, 431.
7. **Shen, M. J.**; Zeng, Y.; Singhal, A.; Sevink, A.; Boyle, A. L.; Kros, A. Enhanced Liposomal Drug Delivery via membrane fusion triggered by Dimeric Coiled-coil Peptides. **Manuscript in preparation.**
8. **Shen, M. J.**; Boyle, A. L.; Kros, A. Investigating the Effect of Peptide Length on Coiled-Coil Stability, Self-Assembly, and Fusogenicity. **Manuscript in preparation.**
9. Shitut, S.; **Shen, M. J.**; Claushuis, B.; Derks, R. J. E; Giera, M.; Rozen, D.; Claessen, D.; Kros, A. Increased membrane fluidity facilitates bacterial cell-cell fusion. **Manuscript in preparation.**
10. Daudey, G. G. A.; **Shen, M. J.**; Singhal, A.; Van der Est, P.; Sevink, A.; Boyle, A. L.; Kros, A. Liposome fusion with orthogonal coiled-coil peptides as fusogens: The efficacy of roleplaying peptides. *Chem. Sci*. **2021**. **Accepted**

CURRICULUM VITAE

Mengjie Shen was born on July 14, 1988, in Linqu, Weifang city, Shandong province, R.P. China. Linqu is a small city named after an extinct volcano whose name is Mount Qu. Weifang is one of the biggest cities in Shandong province and the alternate name of Weifang in ancient times is “YuanDu (鸢都)”, which means “the Capital of Kites”.

In 2009, Mengjie started his bachelor study at Qingdao University of Science & Technology, where he obtained his bachelor's degree in chemistry four years later. In 2013, he continued his study in organic chemistry as a master student at Renmin University of China. In the following three years, he worked with Prof. Han-Yuan Gong from Beijing Normal University studying of Host-Guest interaction between the macrocyclic compound and small aromatic molecules. Also, he worked with Prof. Ya-Lin Tang from the Institute of Chemistry Chinese Academic of Science in researching the DNA G-quadruplex based “molecular switch”. After graduation in 2016, he moved to the Netherlands to start his PhD at Leiden University in the research group of Supramolecular & Biomaterials Chemistry. During his PhD, he was interested in coiled-coil based biomaterials and designed different E/K coiled-coil variants for various biological applications, such as membrane fusion and cell sorting.

ACKNOWLEDGEMENTS

“I’ve had my ups and downs. My fair share of bumpy roads and heavy winds. That’s what made me what I am today.” It’s a tough journey along with challenges and some accomplishments. Looking back to the past five years, I met lots of people and experienced lots of things, which helped me grow up. I appreciate those who helped and supported me during this journey.

Firstly, I would like to thank Alexander Kros for offering me the chance to join SBC group and doing research at Leiden University. You are always kind, patient and wisdom. I really appreciate your guide and inspiration. Also, I would like to extend my sincere gratitude to Aimee Boyle, who is not only my copromotor but also a role model and very good friend to me. Thank you for teaching me everything in scientific research and also life. Without your help and encouragement, I cannot finish my PhD and this thesis. Besides, I would like to thank René Olsthoorn who helped me a lot in the first year of my PhD. At that time, I can't communicate with people in English fluently. Thank you for your patience and kindness. I improved a lot in communication and biological experimental skills during that time, which has a strong influence on the next four years of my PhD.

I would like to thank all the lab cooperators from IBL. They are Dennis Claessen, Shraddha Shitut, Daniel Rozen, Renée Kapteijn and Thomas van Dijk. I learned a lot from all our discussions and I enjoyed a lot when performing experiments in the microbiology lab together. Special thanks to Shraddha who share lots of biological knowledge with me and help me a lot with thesis writing.

Then, I would like to express my heartfelt gratitude to my colleagues. They are Roy, Niek.C, Elena, Dimitris, Niek.H, Jeroen, Fred, Thom.S, Nicola, Lily, Tingxian, Ciqing, Jolinde, Panagiota, Bart Jan, Willem, Weizhe, Winant, Viorica, Michelle, Dinghao, Xuecheng, Ye, Dennis, Oscar, Lin, Wangyang, Xue, Nol, Ying, Wei, Jaco, Wessel, Stephen, Sandeepa, Joyal, Suchismita, Jasper, Jorn, Indigo, David, Gabriela, Thomas, Max, Batuhan, Grégory, Sander, Roxanne and all other SBCers. Having all of you around during the past five years is a great honour for me. I would also like to thank Gerda Lamers for training me TEM and confocal microscopy and Thomas Bakkum for training me FACS.

One of the best accomplishments at Leiden is that I made a lot of good friends. I would like to thank all my friends who make my life colourful in these years. They are Yang Shao, Xuequan Zhou, Shengxiang Yang, Mingchuan Luo, Diyu Zhang, Xiaoting Chen, Zhen Wang, Qingju Zhang, Junfei He, Hui Jin, Jing Zhang, Qi Zhang, Xinglin Jin, Na Zhou and Xuezi Tian. I will always remember the moments when we go travelling, cycling, fishing, hiking and many more things together. I am really happy to have all of you around in the past five years.

Then I would like to thank all my tennis friends, Chenguang Gao, Yu Wei, Yuchen Lian,

Xuequan Zhou, Ye Zeng and Deyi Wang. Playing tennis with you especially during the pandemic lockdown helped me release lots of pressure. I enjoyed the moments very much when we are running on the clay court regardless of rain and sunshine.

Also, I would like to thank my parents who always support me and encourage me in my life. I am very lucky to have parents like you. Since I was born, you suffered a lot to bring me up and you always give me the best you have. I hope I didn’t and won’t let you down in the past and future.

Last but not least, I would like to thank myself in the past. It’s not an easy journey for ‘you’. Lost, self-distrust, lonely, helpless, all of these feelings were around ‘you’ from time to time during your PhD. Thank you for your perseverance in all the struggling days and sleepless nights. “What doesn't kill you, makes you stronger.” After all these, I hope ‘you’ can face the future with brave and confidence while smiling.

I wish everyone has good luck and a bright future. Hope to see you again somewhere in the corner of world in the future.

Mengjie Shen
16/09/2021